

# DEVELOPMENT OF PATHOBLOCKERS BY TARGETING SECRETED BACTERIAL PROTEASES

**Dissertation**

zur Erlangung des Grades  
des Doktors der Naturwissenschaften  
der Naturwissenschaftlich-Technischen Fakultät  
der Universität des Saarlandes

von

**Apotheker Andreas Martin Kany**

Saarbrücken

2018

Tag des Kolloquiums: 20.Juli 2018

Dekan: Prof. Dr. Guido Kickelbick

Berichterstatter: Prof. Dr. Rolf W. Hartmann

Prof. Dr. Claus-M. Lehr

Akad. Mitglied: Dr. Jessica Hoppstädter

Vorsitz: Prof. Dr. Anna Hirsch

Die vorliegende Arbeit wurde von Januar 2015 bis März 2018 unter Anleitung von Herrn Univ.-Prof. Dr. Rolf W. Hartmann in der Fachrichtung Pharmazeutische und Medizinische Chemie der Naturwissenschaftlich-Technischen Fakultät der Universität des Saarlandes sowie am Helmholtz-Institut für Pharmazeutische Forschung Saarland (HIPS) in der Abteilung Drug Design and Optimization (DDOP) angefertigt.



*“Still round the corner there may wait  
A new road or a secret gate“*

J. R. R. Tolkien, *The Lord of the Rings, The Fellowship of the Rings*

## Acknowledgements

Ich möchte mich ganz herzlich bei all denjenigen bedanken, die zum Gelingen dieser Arbeit beigetragen haben:

Ein ganz besonderer Dank gilt Prof. Dr. Rolf W. Hartmann für die Möglichkeit der Promotion in diesen interessanten und vielseitigen Projekten, für die sehr gute Betreuung, die konstruktive Unterstützung und die Freiheiten, mich in verschiedenen Bereichen der Projekte zu verwirklichen.

Prof. Dr. Claus-Michael Lehr danke ich für die wissenschaftliche Begleitung und die Übernahme des Zweitgutachtens.

Ein großer Dank an Dr. Jörg Hauptenthal, für die Leitung der Protease-Projekte, seinen unerschütterlichen Optimismus und dafür, dass er mir immer mit Rat und Tat zur Seite stand. Ebenfalls ein großer Dank an Dr. Samir Yahiaoui für die Betreuung des chemischen Teils dieser Projekte und seine konstruktiven Beiträge, insbesondere in Bezug auf  $\beta$ -Laktamasen.

Des Weiteren gilt mein Dank unseren Kooperationspartnern, die wesentlich zum Gelingen dieser Arbeit beigetragen haben: Ich bedanke mich herzlich bei Prof. Dr. Hans Brandstetter aus Salzburg und besonders bei Dr. Esther Schönauer für die unkomplizierte, sympathische und überaus fruchtbare Kommunikation. Dies gilt nicht minder für Dr. Jesko Köhnke und Asfandyar Sikandar von HIPS-SBBE. Ebenso herzlich bedanken möchte ich mich bei Prof. Dr. Christian Ducho und Katrin Voos von der Universität des Saarlandes sowie Prof. Dr. Eugen Proschak von der Goethe-Universität Frankfurt.

Den „guten Leuten“ möchte ich danken für die freundliche Aufnahme in die Gruppe, die zahlreichen Ratschläge in Bezug auf die Laborarbeit und für ihre hilfreichen Erfahrungswerte über den Doktorandenalltag. Ein besonderer Dank gilt hierbei meinen ersten Bürokollegen aus C2.3 Christian Brengel, Andreas Thomann und Michael Zender für die Aufnahme in das *Carré* und die lustige, abwechslungsreiche und lehrreiche Zeit. Gleiches gilt für das aktuelle Büroteam um Philine Kirsch, Isabell Walter, Alwin Hartmann und Bürohund Molly, sowie Valentin Jakob und Chris Schütz, die ja quasi zum Büro dazugehören. Vielen Dank an Dr. Benni Kirsch für die sehr unterhaltsame Zeit im Bio-Labor und die Hilfe bei biologischen Fragen. Gleichermäßen ein großes Dankeschön an Dr. Christine Maurer für die Einführung in die Welt der Gallerien und Ihre Unterstützung bei analytischen Problemen. Dies richtet sich ebenfalls an Dr. Jens Eberhard und Dr. Giuseppe Allegretta. Des Weiteren ein großes Dankeschön an Dr. Martin Empting für seine Hilfe

insbesondere bei Computer-basierten Methoden und die Bereitstellung diverser Abbildungen, Dr. Mostafa Hamed und Chris Schütz für ihre Hilfe bei chemischen Fragestellungen, Dr. Michael Zender und Dr. Roman Sommer für die Einführung in ITC und die technische Unterstützung, Dr. Teresa Röhrig und Dr. Jörg Hauptenthal für die Hilfe bei den Galleria-Experimenten und die kurzweiligen Tage im S2-Labor sowie Antonio de Mello Martins für die Durchführung von Biofilm-Assays. Zudem vielen Dank für die gute Zusammenarbeit an meine Nachfolgerinnen in den Protease-Projekten, Cansu Kaya und Isabell Walter.

Vielen Dank an unseren guten Seelen im TA-Team für die unermüdliche Unterstützung im Labor und ihre immerwährende gute Laune, insbesondere Jeannine Jung, Simone Amann, Tabea Schramm und Dirk Hauck. Ebenfalls bedanken möchte ich mich bei den Sekretärinnen Julia Mohr und May Sena Küffner für ihre Hilfe bei administrativen Fragen und den Teams der IT und des Facility Managements für ihre stete Hilfsbereitschaft.

Prof. Dr. Uli Kazmaier ein Dank für die Aufnahme in die Graduiertenschule Naturstoffforschung und die damit verbundene Möglichkeit zum wissenschaftlichen Austausch.

Zudem ein herzliches Dankeschön allen ehemaligen und aktuellen Mitgliedern der Arbeitskreise Hartmann, Hirsch, Titz und Ducho sowie der PharmBioTec für die gute Zusammenarbeit und die sehr schöne und abwechslungsreiche gemeinsame Zeit, auch abseits des Labors!

Last but not least möchte ich mich ganz herzlich bei meinen Freunden und meiner Familie bedanken für die notwendige Ablenkung und den unfassbar wertvollen Ausgleich zur Arbeit.

Dies gilt insbesondere meinen Eltern, ohne deren fortwährende Unterstützung ich das alles so niemals geschafft hätte. Danke!

## Summary

The alarming rise of antibiotic resistant pathogens poses a serious threat to public health and urgently necessitates the development of new antibiotics. In order to reduce the selection pressure on bacteria, this study aims at the development of ‘pathoblockers’ which target bacterial virulence instead of killing the pathogens. In this context, secreted bacterial collagenases represent highly attractive targets because of their pivotal roles in the infection process and their advantageous extracellular localization.

In this thesis, the development of inhibitors of ColH from *Clostridium histolyticum* and LasB from *Pseudomonas aeruginosa* is described. A class of *N*-aryl mercaptoacetamides displays promising activity on both targets, with distinct differences in structure-activity relationships and the binding mode to the respective protease. Synthetic efforts further led to the development of a hydroxamate derivative of the lead LasB inhibitor.

The inhibitors described herein share a high selectivity toward mammalian matrix metalloproteases, which was rationalized by combining the information obtained from the co-crystal structures with computational approaches. Further biological assays shed light on the impact of LasB inhibition on key resistance mechanisms of *P. aeruginosa* and demonstrate *in vivo* efficacy in a *Galleria mellonella* infection model.

## Zusammenfassung

Der alarmierende Anstieg von Antibiotika-resistenten Bakterien stellt eine ernstzunehmende Bedrohung für die menschliche Gesundheit dar. Aus diesem Grund ist Entwicklung neuer Antibiotika dringend notwendig. Um den Selektionsdruck auf Bakterien zu reduzieren, hat diese Arbeit zum Ziel, „Pathoblocker“ zu entwickeln, welche die bakterielle Virulenz hemmen anstatt die Pathogene zu töten. In diesem Kontext stellen sezernierte bakterielle Kollagenasen sehr attraktive Targets dar, da sie eine zentrale Rolle im Infektionsprozess spielen und den Vorteil mit sich bringen, dass die bakterielle Zellwand nicht überwunden werden muss.

In dieser Dissertation ist die Entwicklung von Inhibitoren der Enzyme ColH aus *Clostridium histolyticum* und LasB aus *Pseudomonas aeruginosa* beschrieben. Eine Klasse von *N*-Arylmercaptoacetamiden zeigt vielversprechende Aktivität an beiden Targets, allerdings mit klaren Unterschieden in den Struktur-Wirkungs-Beziehungen und im Bindungsmodus. Über chemische Synthese wurde weiterhin ein Hydroxamsäure-Derivat des besten LasB-Inhibitors entwickelt.

Die hier beschriebenen Inhibitoren haben eine hohe Selektivität gegenüber humanen Matrix-Metalloproteasen gemein, die über die Kristallstrukturen und Computer-basierte Methoden rational erklärt werden konnte. Weitere biologische Assays beleuchten die Auswirkung der LasB-Hemmung auf zentrale Resistenzmechanismen von *P. aeruginosa* und zeigen *in vivo*-Effekte in einem *Galleria mellonella*-Infektionsmodell.

## **Publications Included in This Thesis**

Publication A: Schönauer, E.<sup>⊥</sup>; Kany, A. M.<sup>⊥</sup>; Hauptenthal, J.; Hüsecken, K.; Hoppe, I. J.; Voos, K.; Yahiaoui, S.; Elsässer, B.; Ducho, C.; Brandstetter, H.; Hartmann, R. W. (2017) Discovery of a Potent Inhibitor Class with High Selectivity toward Clostridial Collagenases. *J. Am. Chem. Soc.* *139*, 12696–12703. DOI: 10.1021/jacs.7b06935.

Publication B: Kany, A. M.<sup>⊥</sup>; Sikandar, A.<sup>⊥</sup>; Hauptenthal, J.; Yahiaoui, S.; Maurer, C. K.; Proschak, E.; Köhnke, J.; Hartmann, R. W. (2018) Binding Mode Characterization and Early *in Vivo* Evaluation of Fragment-Like Thiols as Inhibitors of the Virulence Factor LasB from *Pseudomonas aeruginosa*. *ACS Infect. Dis.* DOI: 10.1021/acsinfecdis.8b00010.

<sup>⊥</sup> these authors contributed equally

## **Publications of the Author Which Are Not Included in This Thesis**

Zender, M.; Witzgall, F.; Kiefer, A.; Kirsch, B.; Maurer, C.; Kany, A. M.; Börger, C.; Blankenfeldt, W.; Empting, M.; Hartmann, R. W. Flexible-Fragment-Growing Boosts Potency of Quorum Sensing Inhibitors Against *Pseudomonas aeruginosa* Virulence. *Manuscript in preparation*

## Contribution Report

Publication A: The author selected the compounds for SAR evaluation and contributed to the interpretation of the SAR. He synthesized the thiols and selected thiocarbamates. Furthermore, he established and performed the LC-MS-based stability assay and performed the ITC measurements. The author conceived and wrote the manuscript together with E. Schönauer, who contributed equally.

Publication B: The author performed the functional screening, syntheses and IC<sub>50</sub> determinations. He interpreted the SAR and the co-crystal structure, performed the LC-MS-based assays and contributed to their establishment. He further grew the PA14 cultures for LasB purification, performed the *G. mellonella* experiments, the molecular modeling and computational pK<sub>a</sub> calculations. He conceived and wrote the manuscript.

## Abbreviations

ACE	angiotensin-converting enzyme
AIDS	acquired immune deficiency syndrome
AMP	antimicrobial peptide
CF	cystic fibrosis
CFU	colony forming unit
CYP	cytochrome P450 enzyme
Da	Dalton
DNA	deoxyribonucleic acid
DPhG	Deutsche Pharmazeutische Gesellschaft
ECM	extracellular matrix
eDNA	extracellular DNA
EDTA	ethylenediaminetetraacetic acid
FDA	Food and Drug Administration
FRET	Förster resonance energy transfer
GTP	guanosine triphosphate
LC	liquid chromatography
HDAC	histone deacetylase
HCV	hepatitis C virus
HIV	human immunodeficiency virus
Ig	immunoglobulin
IL	interleukin
LB	lysogeny broth
MMP	matrix metalloprotease
MS	mass spectrometry
NDK	nucleoside-diphosphate kinase
PAR	proteinase-activated receptor 2
PDB	Protein Data Bank
PQS	Pseudomonas quinolone signal
QS	quorum sensing
SAR	structure-activity relationship
SPR	surface plasmon resonance
TIMP	tissue inhibitor of metalloproteinase
US	United States
WHO	World Health Organization



## Table of Contents

Acknowledgements.....	VI
Summary.....	VIII
Zusammenfassung.....	IX
Publications Included in This Thesis.....	X
Publications of the Author Which Are Not Included in This Thesis.....	X
Contribution Report.....	XI
Abbreviations.....	XII
Table of Contents.....	XIV
1 Introduction.....	1
1.1 Proteases in Drug Discovery.....	1
1.2 Antibiotic Resistance.....	3
1.3 Developing Novel ‘Pathoblockers’ to Tackle Bacterial Virulence.....	5
1.4 Targeting LasB from <i>Pseudomonas aeruginosa</i> .....	6
1.4.1 <i>Pseudomonas aeruginosa</i> .....	6
1.4.2 Properties and Functions of LasB.....	7
1.4.3 LasB Inhibitors.....	9
1.5 Targeting Clostridial Collagenases.....	10
1.5.1 Clostridia.....	10
1.5.2 Properties and Function of <i>C. histolyticum</i> Collagenases.....	11
1.5.3 <i>C. histolyticum</i> Collagenase Inhibitors.....	12
1.6 Matrix Metalloproteases (MMPs).....	13
2 Aim of the Thesis.....	14
3 Results.....	16
3.1 Chapter A: Discovery of a Potent Inhibitor Class with High Selectivity toward Clostridial Collagenases <sup>187</sup> .....	16
3.2 Chapter B: Binding Mode Characterization and Early <i>in Vivo</i> Evaluation of Fragment-Like Thiols as Inhibitors of the Virulence Factor LasB from <i>Pseudomonas aeruginosa</i> <sup>188</sup> .....	44
3.3 Chapter C: Tackling <i>Pseudomonas aeruginosa</i> Virulence by a Hydroxamic Acid-Based LasB Inhibitor.....	76

4	Final Discussion .....	93
4.1	SAR and Binding Modes of <i>N</i> -Aryl Mercaptoacetamides .....	93
4.2	Prodrug Character of the Thiocarbamate Function .....	96
4.3	Changing the ‘Warhead’ to a Hydroxamic Acid .....	97
4.4	Selectivity toward Human MMPs .....	98
4.5	Biological Evaluation of the Impact of LasB Inhibition .....	99
4.5.1	LL-37 Rescue .....	99
4.5.2	Effects on Biofilm Formation and eDNA Release .....	100
4.5.3	<i>In Vivo</i> Efficacy in <i>Galleria mellonella</i> .....	100
4.6	Outlook.....	102
5	References .....	103
6	Appendix: Conference Contributions .....	114

The references in chapter 5 refer to chapter 1 and 4 of this work. References for chapter 3 are listed in each subchapter, referring to the main text and the supporting information, respectively.



# 1 Introduction

## 1.1 Proteases in Drug Discovery

Proteases are enzymes capable of hydrolyzing peptide bonds.<sup>1</sup> Based on the mechanism of hydrolysis, these enzymes are classified as serine, threonine or cysteine proteases, which covalently bind their substrates, and aspartic, glutamic or metalloproteases, which cleave peptides via non-covalent catalysis involving an activated water molecule.<sup>1,2</sup> Peptides are cleaved either at the N- or C-terminus (by exopeptidases) or in between (by endopeptidases).<sup>1,2</sup> Conventionally, the amino acid residues of a substrate are labelled P1-Pn toward its N terminus and P1'-Pn' toward the C terminus, starting from the scissile bond (Figure 1).<sup>3</sup> Accordingly, the protease subsites which bind the respective amino acids are labelled S1-Sn (non-primed sites) and S1'-Sn' (primed sites).<sup>3</sup> Based on their sequence homology, proteases are grouped into different families in a peptidase database named MEROPS.<sup>4</sup>

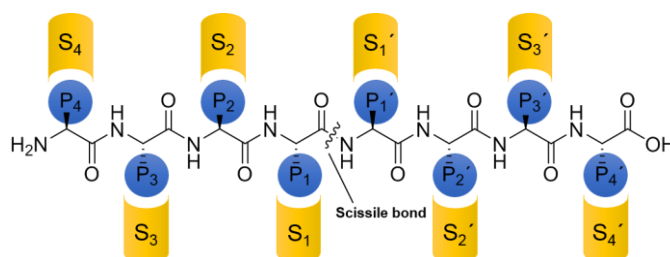


**Figure 1.** Schematic overview of substrate cleavage sites and their respective binding sites at the surface of a protease. Non-primed binding sites are located toward the N terminus of the substrates (S1-Sn), primed binding sites toward the C terminus (S1'-Sn'). Adapted from Schechter and Berger<sup>3</sup>

Proteases are important players in the regulation of human health and disease, since they control vital processes such as organ homeostasis, blood coagulation or tissue development, to name but a few.<sup>2,5,6</sup> Consequently, their inhibition represents an attractive approach toward the treatment of various diseases.<sup>2,5,6</sup>

A well-established method to develop protease inhibitors is to target the active site.<sup>6</sup> Different strategies to obtain access to active site-directed ligands are nicely reflected in the history of the renin inhibitor aliskiren (Figure 2): the first peptidic inhibitors (e.g. H-142, **1**) resembling the natural substrate angiotensinogen were modified to peptidomimetics serving as transition-state analogues (remikiren, **2**).<sup>7</sup> The idea of this approach is to generate an inhibitor which mimics the transition state of a substrate but binds with higher affinity and cannot be processed by the enzyme.<sup>8</sup> In this

context, knowledge about the substrate specificity of a protease is of vital benefit, granting access to compounds resembling preferred amino acids at the cleavage site.<sup>6</sup> In principle, this traces back to the lock and key model introduced by Fischer more than 120 years ago.<sup>9</sup> In case of the bacterial zinc-metalloprotease thermolysin, transition-state analogues are represented by compounds bearing tetrahedral phosphonamidate functions with activity in the nano- to picomolar range.<sup>10</sup> Since peptide-like inhibitors resemble protease substrates, resistance formation is believed to be reduced, because mutations would be disadvantageous when completely preventing the processing of natural substrates.<sup>11</sup>

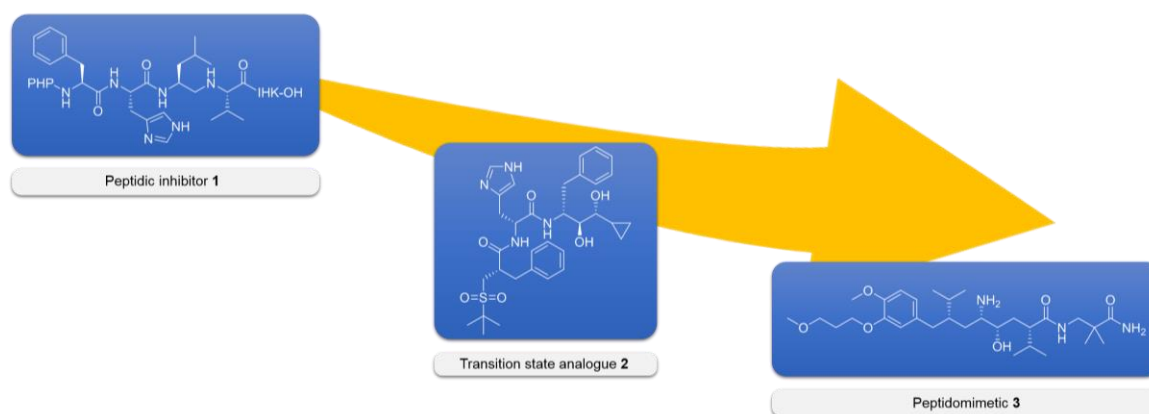


**Figure 2.** Schematic overview of the development cascade of renin inhibitors. Adapted from Drag, Salvesen<sup>6</sup> and Jensen et al.<sup>7</sup>

As an alternative to this ligand-based approach, structure-based methods have successfully been employed to discover specific protease inhibitors.<sup>2,5</sup> These efforts can be based on virtual screening campaigns or on the screening of focused or fragment libraries,<sup>2,12</sup> which can give rise to non-peptidic inhibitors.<sup>5,6</sup> A prominent example for a such an inhibitor is the approved drug aliskiren (**3**), which represents the latest step of the above mentioned development cascade for renin inhibitors.<sup>7</sup> An advantage of such non-peptidic inhibitors is their insensitivity to inactivation by endogenous proteases, which can increase bioavailability.<sup>2</sup>

With the aim of blocking the catalytic activity of a protease, it is well-established to equip inhibitors with so-called ‘warheads’ which directly interfere with the catalytic function of the enzyme.<sup>2,6</sup> In case of covalent catalysis this can lead to irreversible inhibition (e.g. by epoxides), which is viewed critically because of the high potential of unwanted side-effects.<sup>2,13</sup> In case of metalloprotease inhibition, compounds typically bear zinc-chelating moieties like thiols, hydroxamates or heterocycles.<sup>14</sup> There has been a special focus on hydroxamic acids as MMP inhibitors for cancer therapy,<sup>15–19</sup> which is outlined in more detail in chapter 1.6.

Apart from addressing the catalytic unit of a protease, the activity can also be diminished by targeting allosteric binding sites, as with allosteric caspase inhibitors introduced by Hardy et al.<sup>20</sup>

This approach can prove useful for boosting selectivity, as conserved active sites are not targeted directly.<sup>6</sup>

Several protease inhibitors are in clinical use (Figure 3), like ACE inhibitors for the reduction of blood pressure (e.g. captopril, **4**),<sup>5</sup> HDAC inhibitors for cancer treatment (e.g. vorinostat, **5**),<sup>21</sup> thrombin inhibitors as antiplatelet drugs (e.g. argatroban, **6**)<sup>5</sup> or the previously highlighted anti-hypertensive aliskiren (**3**, Figure 2).<sup>7</sup> In contrast to these endogenous human proteases, the disease state in case of an infection is substantially regulated by exogenous bacterial or viral proteases, which are responsible for tissue invasion, immune evasion or the development of a septic shock.<sup>22</sup> To date, protease inhibitors have been approved for the treatment of HIV (e.g. ritonavir, **7**, Figure 3) or HCV (e.g. simeprevir).<sup>23</sup> For bacterial infections however, no protease inhibitor is in clinical use yet.<sup>23,24</sup>

Still, this class of enzymes offers promising drug targets to develop novel antibacterial agents, which has become a matter of utmost importance in a time when mankind is facing the threat imposed by antibiotic resistant bacteria.<sup>23–27</sup>

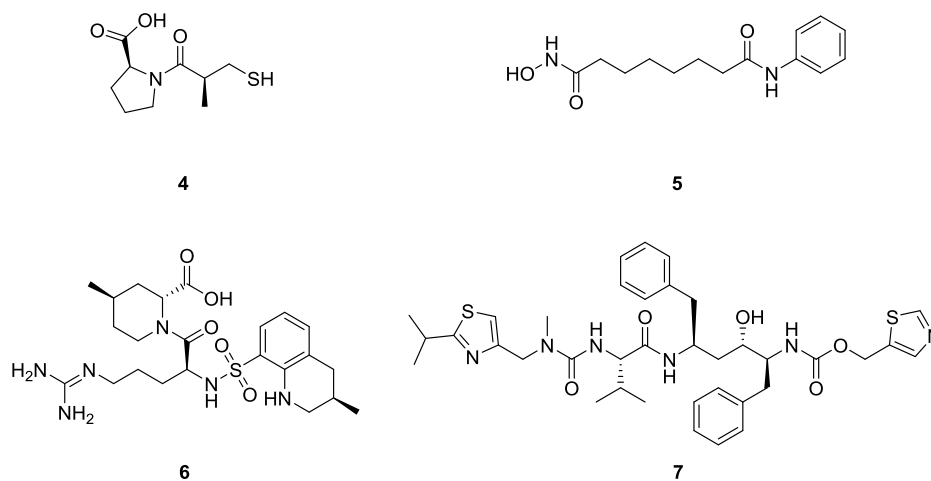


**Figure 3.** Structures of protease inhibitors in clinical use: captopril (**4**),<sup>5</sup> vorinostat (**5**),<sup>21</sup> argatroban (**6**),<sup>5</sup> ritonavir (**7**)<sup>23</sup>

## 1.2 Antibiotic Resistance

The introduction of antibiotics for the treatment of bacterial infections is one of the most tremendous achievements of modern medicine.<sup>28</sup> Starting with the discovery of penicillin and the sulfonamides in the late 1920s and 1930s, a “golden era” evolved, when most of the currently used antibiotics were developed.<sup>28,29</sup> These developments led to the assumption that “It is time to close the book on infectious diseases”, a much-quoted misconception attributed to Dr. William H. Stewart, US Surgeon General in the late 1960s.<sup>30</sup> Despite the lack of evidence that Dr. Stewart ever

made this statement,<sup>31</sup> this urban legend excellently sums up the underestimation of a serious medical problem: antibiotic treatment is becoming ineffective due to the development of resistance.<sup>32</sup> Remarkably, resistance toward sulfonamides was already reported in the late 1930s<sup>28,33</sup> and penicillinases were first described in 1940.<sup>34</sup>

In his Nobel lecture in 1945, Sir Alexander Fleming even mentioned the possibility of resistance development by underdosage of antibiotics.<sup>35</sup> Further reasons for the increasing ineffectiveness of antibiotics include their excessive use in animal husbandry, their misuse for the treatment of non-bacterial infections or poor patient compliance.<sup>36,37</sup> This has led to the selection of bacteria insensitive to multiple drugs like the so-called “ESKAPE” bugs.<sup>38</sup> More recently, the WHO has addressed highly critical pathogens creating a list of priority pathogens, with a special focus on Gram-negative bacteria like *Pseudomonas aeruginosa* or *Acinetobacter baumannii*.<sup>39</sup> Since permeation of the Gram-negative cell wall proves extremely challenging, these bacteria are particularly problematic to treat.<sup>40</sup> Clearly, efforts to decelerate resistance formation must include a reduction of antibiotic use in livestock and stewardship strategies.<sup>37,39</sup> On top of that, there is a dramatic need for the development of novel drugs against bacterial infections.<sup>37,39,41,42</sup>

Paradoxically, the increasing emergence of resistant bacteria is accompanied by decreased industrial efforts to develop novel antibiotics.<sup>41–43</sup> This is partly due to the reduced profit prospects of novel antibacterial drugs, given the relatively short time of administration compared to the treatment of chronic diseases, and the fact that novel antibiotics are likely to be used as reserve drugs.<sup>42,43</sup>

Most of the newly approved antibacterial agents of the last decades were derivatives of existing classes, with only two new classes being applied for systemic treatment.<sup>44</sup> The currently used antibiotics target essential processes in the bacterial life cycle, such as cell wall synthesis, DNA replication or protein biosynthesis.<sup>29</sup> This leads to a high selection pressure on the bacteria and consequently favors the formation of resistance.<sup>45</sup> In order to avert a “post-antibiotic era”<sup>32</sup> where routine infections cannot be treated anymore, the development of novel treatment options is a matter of utmost urgency.<sup>39,41</sup> Notably, teixobactin<sup>46</sup> and griselimycin<sup>47</sup> represent two examples of recently reported anti-bacterial compounds with the promise of low resistance formation.

To the end of increasing the effectiveness of novel antibiotics as well as reducing resistance formation by a different mechanism of action, there has been a recent paradigm shift toward the development of anti-infectives targeting bacterial virulence.<sup>33</sup>

### 1.3 Developing Novel ‘Pathoblockers’ to Tackle Bacterial Virulence

The term ‘virulence’ is a relative measure for the capacity of a pathogen to harm its host.<sup>48</sup> Upon infection with bacteria, disease progression and evasion of the host immune response is promoted by virulence factors such as toxins, proteases, adhesins, secretion systems or siderophores.<sup>49</sup> In order to develop new anti-infective drugs combating bacterial pathogenicity, these virulence factors are considered to be attractive targets.<sup>33,50–52</sup>

The pathoblocker approach largely extends the number of potential drug targets, since these are no longer limited to factors essential for the bacterial life-cycle.<sup>33,50,52</sup> In addition to directly interfering with virulence factors, it is also possible to inhibit their formation by blocking e.g. bacterial quorum sensing networks<sup>53</sup> or oxidative protein folding.<sup>50</sup> Since bacteria are ‘disarmed’ rather than impaired in their viability and growth (Figure 4), there is lower selection pressure which should reduce the formation of resistance.<sup>33,50–52</sup> Besides, the absence of growth-inhibiting properties would make these drugs less attractive for the use in animal husbandry, which eliminates another important factor contributing to the formation of resistance.<sup>52</sup> Targeting pathogen-specific pathways, anti-virulence agents also hold the promise of reduced side-effects since human signaling pathways are not affected.<sup>51</sup> Pathogen-specificity further limits the transmission of resistance genes to other bacteria via horizontal gene transfer.<sup>52</sup> Additionally, these agents would not harm the human microbiome, contrary to conventional antibiotics which can lead to severe complications by damaging the commensal flora.<sup>54</sup> Once their pathogenicity is reduced, the bacteria could then be cleared from the host either by the immune system or by conventional antibiotics.<sup>33,51</sup>

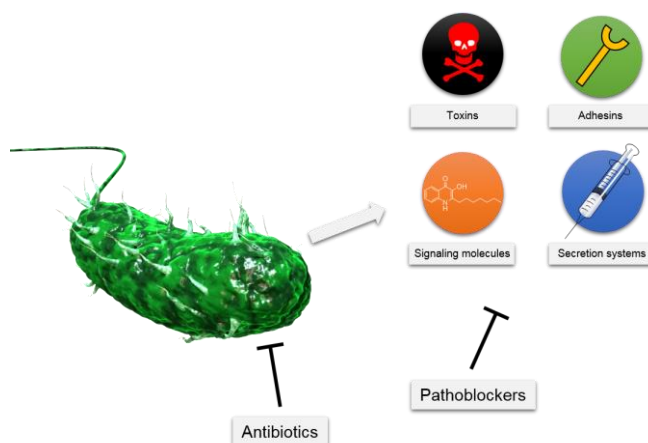


**Figure 4.** Schematic comparison of the action of conventional antibiotics to the inhibition of bacterial virulence. Adapted from Heras et al.<sup>50</sup> The structure of the PQS molecule was taken from Wagner et al.<sup>55</sup> and the image of *P. aeruginosa* was created by M. Empting.

The hypothesis that these drugs are less likely to cause resistance has been critically questioned by Allen et al.<sup>56</sup> In fact, resistance toward anti-virulence drugs has been observed, even in clinical isolates.<sup>57,58</sup> Allen et al. suggest that resistance development toward anti-virulence agents depends on whether the respective virulence factor is beneficial for the bacteria or not.<sup>56</sup> They argue that

addressing beneficial virulence factors could select for resistance, as for example a mutation in the target of virstatin led to better colonization of mice by *Vibrio cholerae*.<sup>57</sup> However, if this protein is only expressed at the site of infection, resistance formation will be reduced due to the minor selection pressure on the commensal population.<sup>56</sup> Consequently, the development of ‘evolution-proof’ drugs is possible, but depends on the selection of the target and the environment of antibacterial treatment.<sup>56</sup>

To date, several anti-virulence drugs are in development, with the only FDA-approved drugs being immunoglobulins that target extracellular virulence factors.<sup>52</sup> Several small-molecule inhibitors are in preclinical development, like for example antagonists for *P. aeruginosa* RhlR<sup>59</sup> or LasR,<sup>60</sup> but none of them has been approved for clinical use yet.<sup>52</sup>

## 1.4 Targeting LasB from *Pseudomonas aeruginosa*

### 1.4.1 *Pseudomonas aeruginosa*

*Pseudomonas aeruginosa* is a Gram-negative, aerobic nosocomial human pathogen.<sup>61</sup> It is a leading cause for infections of cystic fibrosis patients, often with fatal outcome.<sup>62,63</sup> According to the Cystic Fibrosis Foundation, in 2016 nearly every second CF patient was infected with *P. aeruginosa*, with 17.7% of the strains showing multi-drug resistance.<sup>64</sup> This pathogen is further responsible for urinary tract infections, keratitis and wound infections, especially in individuals suffering from burn wounds.<sup>65</sup> As resistant strains are emerging while new treatment options are missing, the WHO has recently classified *P. aeruginosa* as one of the three most critical pathogens on its priority list for global research and development.<sup>39</sup>

Several resistance mechanisms have been reported, including target mutations, inactivation of  $\beta$ -lactams by  $\beta$ -lactamases or compound efflux.<sup>66,67</sup> Another major cause for antibiotic resistance of *P. aeruginosa* is the formation of biofilms.<sup>66</sup> The bacterial biofilm is a matrix of extracellular polymeric substances such as polysaccharides, proteins, lipids or extracellular DNA (eDNA), which embeds the bacteria.<sup>68</sup> Surrounded by the biofilm matrix, these are significantly less sensitive to antibiotic treatment and to host defense mechanisms like phagocytosis.<sup>69</sup> Extracellular DNA, which is a major component of the *P. aeruginosa* biofilm,<sup>70</sup> leads to reduced permeability of the outer membrane and to acidification of the biofilm, causing resistance toward human antimicrobial peptides (AMPs)<sup>71</sup> and to aminoglycosides.<sup>72</sup> Biofilm formation further favors adherence to medical devices such as urethral or central venous catheters, thereby contributing to the establishment of hospital-acquired infections.<sup>73,74</sup>

In order to combat the threat posed by resistant *P. aeruginosa*, there is a special focus on virulence factors as potential drug targets.<sup>55,75</sup> *P. aeruginosa* produces numerous virulence factors contributing to disease progression.<sup>76</sup> On the one hand these can be cell-associated, like for example

pili, lipopolysaccharides or lectins which play important roles for adhesion and colonization.<sup>76,77</sup> Accordingly, lectin inhibitors have been shown to inhibit host cell invasion<sup>78</sup> and biofilm formation.<sup>79</sup> On the other hand, there are secreted toxins including proteases, hemolysins, HCN or the pigment pyocyanin.<sup>76,80</sup> Playing pivotal roles in the establishment of an acute infection by tissue invasion and dissemination,<sup>77</sup> extracellular factors represent attractive targets.<sup>55</sup> Virulence factor expression in *P. aeruginosa* is controlled by a network of population-dependent signaling cascades, known as quorum sensing.<sup>81</sup> Key players of this network have been addressed in drug discovery campaigns, including the multiple virulence factor regulator PqsR,<sup>82,83</sup> or PqsD, an enzyme crucial for signal molecule biosynthesis.<sup>84</sup> Compounds targeting these enzymes need to be cell-wall permeable, due to the intracellular location of the QS circuit.<sup>81</sup> A substantial advantage of addressing secreted targets is the fact that there is no need to cross the Gram-negative cell wall, which is very challenging due to the presence of two membranes.<sup>67,85</sup>

A key element of this work is the extracellular virulence factor elastase (LasB), which plays a pivotal role in host colonization and evasion of the host immune response and thereby significantly contributes to disease progression upon infection with *P. aeruginosa*.<sup>86</sup>

#### 1.4.2 Properties and Functions of LasB

LasB is a zinc-metalloprotease secreted by *P. aeruginosa*.<sup>87</sup> It is encoded by the *lasB* gene as a 53.4 kDa preproenzyme, whose signal sequence (2.4 kDa) is cleaved upon membrane passage into the periplasm, where the 18 kDa propeptide is removed to yield mature LasB (33 kDa).<sup>88,89</sup> The propeptide stays non-covalently attached to the mature protease during secretion into the extracellular space, where it is degraded.<sup>88,90</sup> The N-terminal domain of the protease is formed mainly by antiparallel  $\beta$ -strands, while the C-terminal domain is predominantly  $\alpha$ -helical with the active site being located in between these domains (Figure 5).<sup>91</sup> The resulting tertiary structure of LasB is highly similar to thermolysin from *Bacillus thermoproteolyticus*, why it belongs to the thermolysin (M4) family of 'Glu-zincin' enzymes.<sup>91,92</sup> Accordingly, conserved amino acid residues are the zinc-coordinating His-140, His-144 and Glu-164, as well as Glu-141, Tyr-155 and His-223 which are essential for catalysis.<sup>91</sup> LasB is active against a variety of substrates, including the connective tissue components collagen and elastin or laminin.<sup>87,93,94</sup> Generally, bulky hydrophobic amino acids at the N-terminal cleavage site of the protease are preferred.<sup>95</sup>

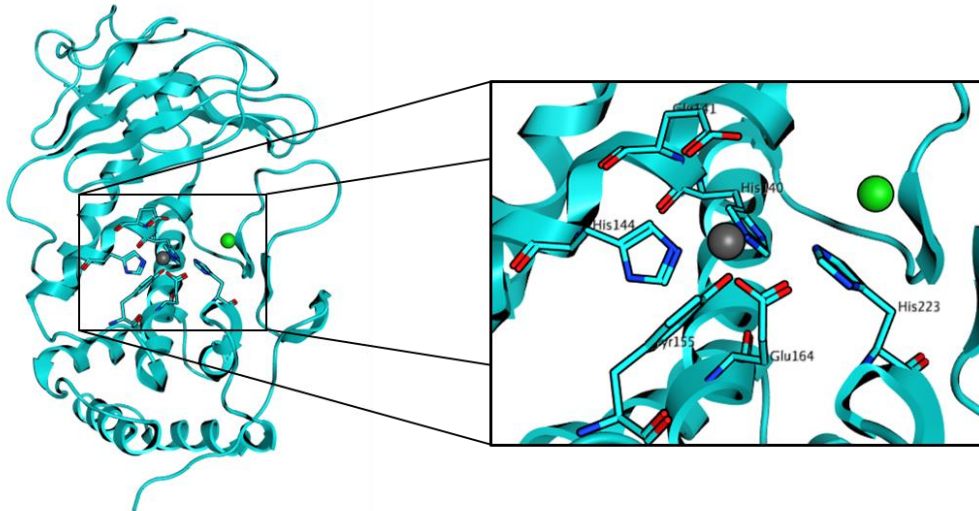


**Figure 5.** Apo structure of LasB (PDB Code 1EZM) visualized in standard orientation.<sup>96</sup> The N-terminal domain consisting mainly of  $\beta$ -strands is shown at the top, the  $\alpha$ -helical C-terminal domain at the bottom. Conserved residues are highlighted in a zoom in view. Zinc is depicted as a gray sphere, calcium as green one.

Apart from LasB (also known as pseudolysin), *P. aeruginosa* produces and secretes several other proteases.<sup>97</sup> Aeruginolysin (alkaline protease) can also contribute to tissue degradation in the infection process, but its proteolytic potency is low compared to LasB.<sup>97,98</sup> LasA (staphylolysin) is a zinc-metalloprotease capable of lysing staphylococci.<sup>99,100</sup> It has low elastolytic activity but makes elastin more susceptible to cleavage by LasB by breaking Gly-Gly bonds.<sup>99</sup> LasA itself is processed extracellularly by the action of LasB.<sup>88</sup> Furthermore, *P. aeruginosa* expresses lysyl endopeptidase (protease IV), a serine protease involved in immune evasion.<sup>101</sup> Out of these proteases, LasB is the most abundant one and possesses the highest endopeptidase activity.<sup>97</sup>

LasB is of crucial importance for the colonization and invasion of the host upon infection with *P. aeruginosa*.<sup>86,102</sup> This is due to its tissue-damaging properties which can lead to dermonecrosis,<sup>103</sup> airway<sup>104</sup> and cornea damage<sup>105</sup> or disruption of cell junctions.<sup>106,107</sup> It further plays a substantial role in the evasion of human response mechanisms by cleaving numerous components such as cytokines,<sup>108</sup> complement factors,<sup>109</sup> the immunoglobulin IgG<sup>110</sup> or surfactant proteins.<sup>111</sup> Using an *in vivo* model, Kuang et al. demonstrated LasB to reduce phagocytosis of *P. aeruginosa* by degrading surfactant protein-A in mice lungs.<sup>112</sup> LasB is further known to downregulate IL-6<sup>113</sup> and to disarm pulmonary defense receptor PAR2.<sup>114</sup> Additionally, it impairs wound healing by inhibiting the growth of fibroblasts.<sup>115</sup> Saint-Criq et al. have recently reported LasB to target a receptor mutated in CF patients, making lung epithelia more susceptible for infections.<sup>113</sup> LasB also degrades flagellin, thereby preventing it from inducing an immune response.<sup>116</sup> It further evades the host response by cleaving a peptide from thrombin which eventually inhibits pro-inflammatory processes.<sup>117</sup> The human AMP LL-37 has been found to be cleaved and thereby inactivated by LasB as well.<sup>118</sup>

On top of that, swarming motility as well as biofilm formation of *P. aeruginosa* were shown to depend on LasB.<sup>119</sup> Regarding the involvement of LasB in biofilm formation, two possible mechanisms have been reported: Kamath et al. have found LasB to proteolytically activate nucleoside diphosphate kinase (NDK), an enzyme generating GTP for the formation of alginate, which is an important constituent of the biofilm.<sup>120,121</sup> This has been related to retention of LasB in the periplasm, where NDK activation takes place.<sup>121</sup> Yu et al. have linked biofilm formation to the regulation of rhamnolipids, which is associated to the *lasB* gene.<sup>122</sup>

Taken together, these versatile, harmful functions in the infection process of *P. aeruginosa* make LasB an attractive anti-infective drug target.<sup>104,113,123</sup>

### 1.4.3 LasB Inhibitors

Since LasB is a zinc-metalloprotease, it is inhibited by zinc chelators like EDTA or phenanthroline.<sup>87</sup> Inhibitor development has further been based on zinc-chelating moieties like thiols or hydroxamates, which is a common strategy in protease drug discovery.<sup>14</sup> This approach has led to thiol-containing peptides with protective effects on keratitis in rabbits.<sup>105,124</sup> Kessler et al. have also demonstrated thiol and hydroxamate-based compounds to inhibit elastin and cartilage cleavage.<sup>125</sup> In line with the high structural similarity, several peptide hydroxamates are potent inhibitors of LasB and thermolysin alike.<sup>126</sup> Cathcart et al. have presented preference of nonpolar aliphatic and aromatic amino acids at the P<sub>1</sub>' position of metal-chelating dipeptides for inhibition of LasB, which is in agreement with the substrate specificity of LasB.<sup>127</sup> They have demonstrated thiol **8** (Figure 6) to significantly reduce *P. aeruginosa* biofilm formation and to completely eradicate biofilms in combination with antibiotics.<sup>128</sup> The first nonpeptidic LasB inhibitors have been introduced by Garner et al.<sup>129</sup> These heterocyclic zinc chelators, as well as a tropolone derivative (**9**)<sup>130</sup> impair swarming of *P. aeruginosa*. Besides, heterocyclic inhibitors developed as analogs of the *Pseudomonas* quinolone signal (PQS) are also active on LasB with low micromolar IC<sub>50</sub>s.<sup>131</sup> Alternative nonpeptidic inhibitors are the mercaptoacetamides described by Zhu et al. to increase the survival time of *Caenorhabditis elegans* in an early *in vivo* assay (**10**).<sup>132</sup> In addition to these small molecules, monoclonal antibodies also serve as LasB inhibitors.<sup>133</sup>

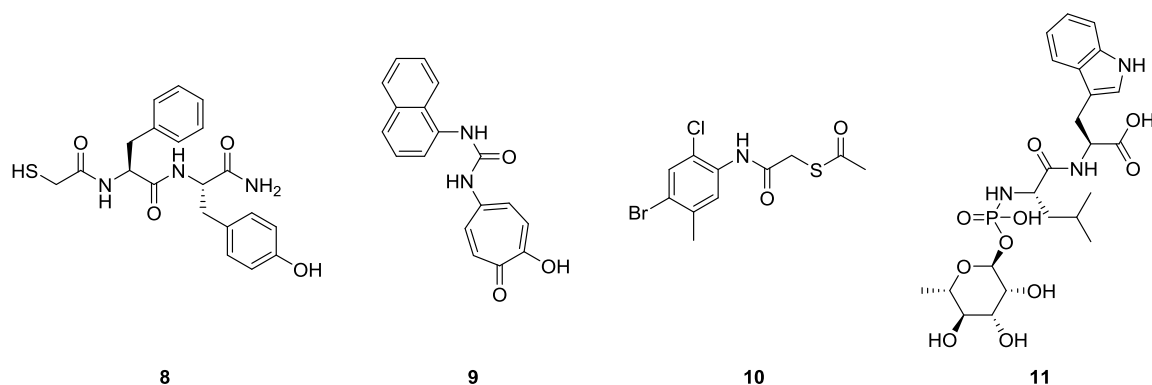


**Figure 6.** Structures of selected LasB inhibitors: peptidic mercaptoacetamide **8**,<sup>128</sup> tropolone **9**,<sup>130</sup> *N*-aryl mercaptoacetamide **10**<sup>132</sup> and phosphoramidon (**11**).<sup>134</sup>

The mentioned nonpeptidic compounds have low micromolar *in vitro* activities on LasB,<sup>129,130,132</sup> while some peptide-based compounds are active in the submicromolar range.<sup>105,128</sup> This holds true for the thermolysin-inhibitor phosphoramidon (**11**) as well.<sup>134,135</sup> Regarding selectivity, the mercaptoacetamides were shown to be selective toward individual human proteases (MMP-2 and HDAC),<sup>132</sup> while the thiol-based peptides did not impair the activity of MMP-2,-8, and -9.<sup>128</sup> The non-peptidic inhibitors introduced by Fullagar, Garner et al. are not selective against MMP-2 and -9, except for the tropolone scaffold.<sup>130</sup> A series of hydroxamate-based peptides presented by Adekoya et al. have been derived from MMP inhibitors, consequently lacking selectivity.<sup>136,137</sup>

## 1.5 Targeting Clostridial Collagenases

### 1.5.1 Clostridia

Clostridia are Gram-positive, obligate anaerobic bacteria which are ubiquitously present in soil or wastewater and form also part of the human commensal flora.<sup>138,139</sup> Several clostridial species can cause severe diseases like tetanus (*C. tetani*), botulism (*C. botulinum*), foodborne illness (*C. perfringens*) or gas gangrene (*C. perfringens*, *C. histolyticum*).<sup>139</sup> The incidence of gas gangrene is perilously increased in cases of natural disasters or during times of war.<sup>140</sup> Due to its rapid progress, which can also result in shock or organ failure, amputation is often necessary despite antibiotic treatment.<sup>141</sup> The strain *C. difficile* is a cause for severe nosocomial diarrhea as well as pseudomembranous colitis, which can be a consequence of antibiotic treatment.<sup>54,139,142</sup> Resistance toward multiple antibiotics, mainly caused by target mutations,<sup>143</sup> seriously hamper the treatment of *C. difficile* infections and make the development of novel treatment options an urgent necessity.<sup>54,142</sup> Antibiotic resistance has been observed in other *Clostridium* species as well.<sup>144</sup> Clostridial pathogenicity is based on the production and secretion of numerous toxins.<sup>145</sup> A few of these toxins are classified as biological warfare agents, including botulinum neurotoxin from

*C. botulinum*, which is the most toxic substance known.<sup>146</sup> Collagenases which are expressed and secreted by pathogenic clostridia have hydrolytic activity on components of the connective tissues and represent crucial virulence factors.<sup>139,145,147</sup> In addition to invasion of the host, they are also important for the acquisition of nutrients and toxin diffusion.<sup>145</sup> Based on a mouse myonecrosis model, Awad et al. concluded that collagenase is not crucial for the establishment of an infection by *C. perfringens*, but rather the production of  $\alpha$ -toxin.<sup>148</sup> In contrast, the invasiveness of *L. interrogans* was clearly related to the *in vivo* expression of extracellular collagenase, highlighting the significance of these harmful proteases for bacterial pathogenicity.<sup>149</sup>

### 1.5.2 Properties and Function of *C. histolyticum* Collagenases

For the degradation of connective tissue, one of the most efficient systems that is known are the collagenases secreted by *C. histolyticum*.<sup>150</sup> This bacterium produces two classes of these proteases, which are encoded by the *colH* or *colG* gene, respectively.<sup>151</sup> Contrary to mammalian MMPs, which cleave collagen at a single cleavage site, clostridial collagenases are capable of attacking it at multiple sites and cleaving it to small peptides.<sup>152</sup> This specificity is due to a high selectivity of the active site of these enzymes for the GPX sequence,<sup>153</sup> which is a characteristic motif of the collagen triple helix.<sup>154</sup>

ColH and ColG are classified into the M9 family of metallopeptidases.<sup>155</sup> Similar to LasB and thermolysin, they are ‘Glu-zincins’, harboring the characteristic zinc-binding motif ‘HEXXH’ with a downstream glutamate as third zinc ligand.<sup>156</sup> These two metalloproteases of ~115 kDa are composed of a saddle-shaped, N-terminal collagenase unit and a collagen recruitment unit, which is composed of one to two collagen binding and polycystic kidney disease-like domains (Figure 7).<sup>151,157–160</sup> The catalytic subdomain of ColG adopts a thermolysin-like fold, including a five-stranded  $\beta$ -sheet with the edge strand involved in substrate recognition.<sup>159</sup> The collagenase unit comprises an activator domain and a peptidase domain which is, unlike the full collagenase unit, not capable of degrading collagen.<sup>159</sup> In proximity to the catalytic zinc, a calcium binding site was discovered which is necessary for full collagenase activity.<sup>158</sup> Another important structural feature of these proteases is a double Gly-motif 28 amino acids downstream of the active site, forming a secondary S1’ oxyanion pocket.<sup>159,160</sup> The peptidase domain of ColG displays structural similarity to the ColH peptidase domain, but interestingly an even higher similarity to the one of ColT from *C. tetani*.<sup>158</sup> Furthermore, ColG and ColA from *C. perfringens* share the same domain architecture and have high sequential similarity.<sup>151</sup>

Interestingly, ColH from *C. histolyticum* is used as a therapeutic for Dupuytren’s Disease<sup>161</sup> which is characterized by a pathologic overproduction of collagen in hands,<sup>162</sup> and is also approved for the reduction of penile plaque in Peyronie’s disease.<sup>163</sup> Further applications are wound debridement<sup>164</sup> or human cell islet isolation.<sup>165</sup>

Given their detrimental role in the establishment of infections, clostridial collagenases represent prime targets for the development of novel anti-infective agents.<sup>27,160</sup>

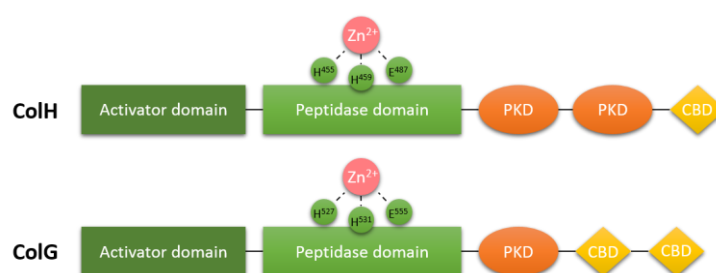


**Figure 7.** Domain organization of ColH and ColG. PKD: polycystic kidney disease like-domain, CBD: collagen binding domain. Adapted from Eckhard et al.<sup>158</sup>

### 1.5.3 *C. histolyticum* Collagenase Inhibitors

Similar to LasB inhibitors (chapter 1.4.3), several collagenase inhibitors are based on small peptides containing different zinc-binding groups such as thiols,<sup>166</sup> phosphoramides<sup>167,168</sup> or phosphonic amides like isoamyl-PO<sub>2</sub>-GPA (**12**, Figure 8),<sup>167</sup> with low micromolar to nanomolar activities. Aldehyde and ketone substrate analogs are less active with three-digit micromolar IC<sub>50</sub>s.<sup>169</sup> As expected, zinc chelation by phenanthroline leads to collagenase inhibition, too.<sup>170</sup> The thermolysin and LasB inhibitor phosphoramidon is also active on ColH, with an IC<sub>50</sub> of 16 μM.<sup>171</sup> Modification of natural coumarin derivatives isolated from *Viola yedoensis* have led to nanomolar collagenase inhibitors like compound **13**.<sup>171</sup> Supuran and Scozzafava have introduced hydroxamate derivatives of valin,<sup>172</sup> glycine<sup>173</sup> or alanine<sup>174</sup> with nanomolar activities (for a selected example see **14**). Similar inhibitors contain dibenzo-suber(en)yl moieties,<sup>175</sup> thiadiazole rings,<sup>176</sup> or succinate/iminodiacetic acid.<sup>177</sup>

Being partly derived from known MMP inhibitors, these compounds lack selectivity and are rather potent inhibitors of several MMPs alike.<sup>172–177</sup>

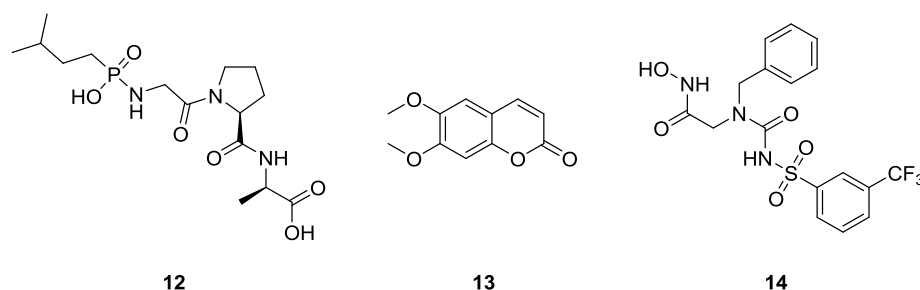


**Figure 8.** Structures of selected ColH inhibitors: isoamyl-PO<sub>2</sub>-GPA (**12**),<sup>167</sup> coumarin derivative **13**,<sup>171</sup> and succinyl hydroxamate **14**.<sup>173</sup>

## 1.6 Matrix Metalloproteases (MMPs)

MMPs are zinc-metalloproteases belonging to the M10 family of peptidases.<sup>4</sup> An important function of MMPs is the degradation and turnover of extracellular matrix (ECM) components, but they are also heavily involved in the regulation of inflammatory processes, apoptosis, cell differentiation and growth.<sup>178,179</sup> More recently, there has been insight into further intracellular functions of MMPs, like transcription factor activity.<sup>180</sup> The expression of MMPs is induced by e.g. components of the immune system or hormones and their activity is further regulated by tissue inhibitors of metalloproteinases (TIMPs) or  $\alpha_2$ -macroglobulin.<sup>179,181</sup> Dysregulation of MMP function can be the reason for various diseases like arthritis, cardiovascular diseases, inflammation and cancer.<sup>178,179,182</sup> Therefore, these proteases were considered promising targets for cancer therapy.<sup>2,19,183</sup>

Generally, MMPs are formed by a propeptide, a catalytic domain containing the active site zinc, the linking 'hinge region' and a hemopexin domain important for substrate recognition.<sup>178,179</sup> Presence and multiplicity of these domains vary, depending on the function of the respective enzyme.<sup>178,179</sup> In humans, more than 20 different MMPs are present, which are classified based on their function as collagenases (MMP-1, -8, -13), gelatinases (MMP-2, -9), as well as stromelysins, matrilysins and membrane-type MMPs.<sup>178</sup> With regard to the depth of their S<sub>1</sub>' binding pocket, MMPs are further divided into deep (e.g. MMP-3, -12, -14), intermediate (e.g. MMP-2, -8, -9) and shallow pocket MMPs (e.g. MMP-1, -7).<sup>184</sup> The structural differences in the S<sub>1</sub>' site are believed to grant access to inhibitors specifically targeting individual MMPs.<sup>16</sup> Similar to the bacterial collagenases described above, MMPs share the 'HEXXH' motif, yet the third zinc ligand is a histidine instead of a glutamate.<sup>178</sup>

In the last decades, MMP inhibitors like batimastat largely failed in clinical trials, partly because of poor oral bioavailability but mainly because of unwanted side effects, which were due to the unselective inhibition of various MMPs or other metalloproteases.<sup>2,15-19</sup> Given that many MMP inhibitors contain zinc chelating moieties, poor selectivity can to some extent be attributed to the disproportionate contribution of the zinc chelating moiety to compound binding.<sup>16</sup> Therefore, there is also considerable interest in targeting less conserved binding sites, like the hemopexin domain.<sup>19</sup> It has now become clear that the physiological function of MMPs can be extremely versatile, making them in part targets and anti-targets at the same time.<sup>185</sup> Along with partially poor trial design,<sup>15,17</sup> the heterogeneity of MMP function is another reason for the failure of MMP inhibitors in clinical studies.<sup>186</sup> As a consequence, selectivity toward other proteolytic enzymes is of high importance in protease drug discovery, with a special emphasis on MMPs as far as zinc metalloprotease inhibitors are considered.<sup>5,15,185</sup>

## 2 Aim of the Thesis

Because of their essential role in numerous processes regulating human health and disease, proteases are regarded as attractive drug targets and many protease inhibitors have been approved for clinical use. However, several drug discovery campaigns toward novel protease inhibitors failed i.a. for the reason of poor selectivity of the drug candidates toward other proteolytic antitargets. Developing selective inhibitors proves challenging, especially in case of active site-directed compounds. Yet, this approach is particularly attractive for the development of novel antibacterial drugs. In a time when humankind is facing the increasing emergence of bacteria which are resistant to commonly used antibiotics, this is a matter of utmost importance. In the search of new antibiotics with novel modes of action, the concept of targeting bacterial virulence has gained significant attraction. Since these ‘pathoblockers’ are supposed to reduce selection pressure on bacteria, they are considered as a promising new weapon to combat the threat imposed by these resistant pathogens. In this context, extracellular proteases represent conceptually attractive drug targets. They contribute essentially to host colonization and immune evasion and prove particularly advantageous due to their extracellular localization, which allows circumvention of potential permeability issues.

The objective of this thesis was the development of inhibitors targeting two bacterial collagenases: ColH from the Gram-positive *C. histolyticum* and LasB from the Gram-negative *P. aeruginosa*. These pathogens cause severe diseases like gas gangrene (*C. histolyticum*) and fatal lung infections in immunocompromised or CF patients (*P. aeruginosa*). Considering the lack of selectivity of many known inhibitors of ColH and LasB, there was a special focus on selectivity toward mammalian MMPs.

In previous work at HIPS-DDOP, an SPR screening of a focused protease inhibitor library was performed, which was followed by a functional assay of the binding hits in collaboration with the University of Salzburg. The aim of this work was the establishment of an SAR of the most promising class of hits, along with their biophysical and biological characterization. These efforts also included resynthesis of the most promising hits. The results regarding ColH are outlined in chapter 3.1.

The second part of this work aimed at the discovery of LasB inhibitors (chapter 3.2). To this end, a reported FRET-based assay was used to perform a functional screening of the aforementioned library and a fragment library. In order to overcome the problem of quenching compounds causing false-positive results, an LC-MS based counterscreen was developed. Further work aimed at SAR establishment, X-ray structure-based optimization and the biological evaluation of lead inhibitors including selectivity toward human MMPs and *in vivo* efficacy in *G. mellonella*.

The third part of this thesis describes synthetic efforts to replace the thiol function of the lead LasB inhibitor (chapter 3.3). This chemical work was again accompanied by further biological analysis of LasB inhibition. Here, the objective was to analyze effects on key resistance mechanisms of *P. aeruginosa*, such as biofilm formation, eDNA release and the cleavage of the human AMP LL-37.

### 3 Results

#### 3.1 Chapter A: Discovery of a Potent Inhibitor Class with High Selectivity toward Clostridial Collagenases<sup>187</sup>

Schönauer, E.<sup>⊥</sup>; Kany, A. M. <sup>⊥</sup>; Hauptenthal, J.; Hüsecken, K.; Hoppe, I. J.; Voos, K.; Yahiaoui, S.; Elsässer, B.; Ducho, C.; Brandstetter, H.; Hartmann, R. W.

<sup>⊥</sup> these authors contributed equally

Reprinted with permission from *J. Am. Chem. Soc.* **2017**, *139*, 12696–12703.

DOI:10.1021/jacs.7b06935

Copyright (2017) American Chemical Society



## Discovery of a Potent Inhibitor Class with High Selectivity toward Clostridial Collagenases

Esther Schönauer,<sup>†,‡,§</sup> Andreas M. Kany,<sup>†,‡,§</sup> Jörg Haupenthal,<sup>‡,§</sup> Kristina Hüsecken,<sup>‡</sup> Isabel J. Hoppe,<sup>†,§</sup> Katrin Voos,<sup>§</sup> Samir Yahiaoui,<sup>‡,§</sup> Brigitta Elsässer,<sup>†,§</sup> Christian Ducho,<sup>§</sup> Hans Brandstetter,<sup>\*,†,§</sup> and Rolf W. Hartmann<sup>\*,‡,§</sup>

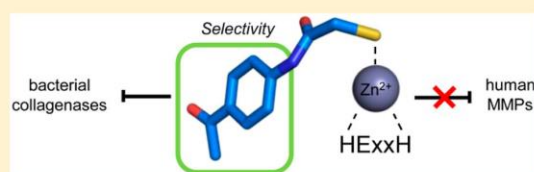
<sup>†</sup>Division of Structural Biology, Department of Molecular Biology, University of Salzburg, Billrothstrasse 11, 5020 Salzburg, Austria

<sup>‡</sup>Department of Drug Design and Optimization, Helmholtz Institute for Pharmaceutical Research Saarland (HIPS), Campus E8.1, 66123 Saarbrücken, Germany

<sup>§</sup>Department of Pharmacy, Pharmaceutical and Medicinal Chemistry, Saarland University, Campus C2.3, 66123 Saarbrücken, Germany

### Supporting Information

**ABSTRACT:** Secreted virulence factors like bacterial collagenases are conceptually attractive targets for fighting microbial infections. However, previous attempts to develop potent compounds against these metalloproteases failed to achieve selectivity against human matrix metalloproteinases (MMPs). Using a surface plasmon resonance-based screening complemented with enzyme inhibition assays, we discovered an *N*-aryl mercaptoacetamide-based inhibitor scaffold that showed sub-micromolar affinities toward collagenase H (ColH) from the human pathogen *Clostridium histolyticum*. Moreover, these inhibitors also efficiently blocked the homologous bacterial collagenases, ColG from *C. histolyticum*, ColT from *C. tetani*, and ColQI from the *Bacillus cereus* strain QI, while showing negligible activity toward human MMPs-1, -2, -3, -7, -8, and -14. The most active compound displayed a more than 1000-fold selectivity over human MMPs. This selectivity can be rationalized by the crystal structure of ColH with this compound, revealing a distinct non-primed binding mode to the active site. The non-primed binding mode presented here paves the way for the development of selective broad-spectrum bacterial collagenase inhibitors with potential therapeutic application in humans.



## INTRODUCTION

Clostridia represent a family of ubiquitously occurring Gram-positive bacteria comprising perilous pathogens that cause diseases such as botulism (*Clostridium botulinum*), gas gangrene (*C. perfringens*), tetanus (*C. tetani*), or pseudomembranous colitis (*C. difficile*).<sup>1,2</sup> These toxigenic clostridia still represent a threat to public health, as tetanus and clostridial myonecrosis have maintained high mortality rates and pseudomembranous colitis is a known severe complication of antibiotic therapy.<sup>3–6</sup> Furthermore, substantial amounts of pathogenic clostridia were cultured in the past 60 years for use as bioweapons.<sup>7</sup> Consequently, massive efforts have been aimed at unraveling the molecular basis of these life-threatening infections. Nevertheless, such infections remain a major challenge, as this knowledge did not yet lead to satisfactory treatment options.

The high lethality of these bacteria is related to collagenases which are crucial for clostridial virulence, given their critical role in colonization and evasion of host immune defense, acquisition of nutrients, facilitation of dissemination, or tissue damage during infection. Additionally, they might potentiate clostridial histotoxicity by facilitating toxin diffusion.<sup>2,8,9</sup>

The physiological substrate of clostridial collagenases is collagen, the main component of the extracellular matrix in mammals (up to 90%).<sup>10,11</sup> Its defining characteristic is the collagen triple-helix, which is perpetuated by the triplet repeat Gly-X-Y (X and Y positions are mostly occupied by proline (28%) and hydroxyproline (38%)).<sup>12</sup> The natively folded triple helix is highly resistant to proteolysis.<sup>13,14</sup> Even the most prominent human collagenases, the matrix metalloproteinases MMP-1, -2, -8, -13, -14, and -18, can cleave the triple helix only at a single site.<sup>15,16</sup> In contrast to that, clostridial collagenases can process collagen triple helices at multiple sites, as the active site displays a remarkable selectivity for the Gly-Pro-Y triplets,<sup>17</sup> and they can decompose collagen completely into small peptides.<sup>18,19</sup>

The inhibition of these extracellular collagenases is conceptually attractive, as it does not attack the pathogen directly but rather blocks the colonization and infiltration of the host by the clostridia. Thereby reducing the Darwinian selection pressure, targeting bacterial virulence is considered a promising approach to combat the emerging threat of drug-

Received: July 4, 2017

Published: August 18, 2017

resistant bacteria.<sup>20–22</sup> To date, several anti-virulence targets have been validated, demonstrating the potential of this approach.<sup>23–28</sup> Kassegne et al. showed, for example, that a collagenase knock-out strain from *Leptospira interrogans* displayed reduced virulence in an *in vivo* model.<sup>28</sup>

Targeting extracellular enzymes provides a substantial benefit because inhibitors do not need to cross the bacterial cell wall, which has turned out to be challenging in many cases.<sup>29–31</sup> Consequently, bacterial collagenases represent prime targets for an effective therapy against clostridial and bacillary infections.<sup>6,9,32,33</sup>

Clostridial collagenases are zinc metalloproteinases of ~115 kDa with a multi-domain organization, homologues of which are also found in many bacilli. The mature protein harbors an N-terminal collagenase unit of ~78 kDa, which is the minimal collagenolytic entity, followed by a varying composition of two to three accessory domains, which are thought to be involved in collagen swelling and binding to fibrillar collagen.<sup>34–38</sup> The collagenase unit is composed of the activator domain and the peptidase domain.<sup>34</sup> The peptidase domain harbors the catalytic zinc ion, which is coordinated by the two histidines of the canonical zinc-binding HEXXH motif, and a downstream glutamate.<sup>4,34,35,39–41</sup> The glutamate residue in the HEXXH motif acts as the general acid/base, which polarizes the catalytic water essential for catalysis. This polarized water molecule performs the nucleophilic attack, while the zinc ion serves as an oxyanion hole to the carbonyl oxygen of the scissile peptide bond.<sup>42</sup>

Several groups have been working on the development of clostridial collagenase inhibitors in the past, focusing on the collagenases G (ColG) and H (ColH) from *C. histolyticum*. In this context, besides the identification of active compounds from *Viola yedoensis*,<sup>43</sup> inhibitors based on sulfonylated derivatives of L-valine hydroxamate<sup>44</sup> have been synthesized as well as sulfonyl aminoacyl hydroxamates.<sup>45</sup> Furthermore, compounds incorporating 5-amino-2-mercapto-1,3,4-thiadiazole zinc binding functions,<sup>46</sup> arylsulfonyl-ureido and 5-dibenzo-suberonyl/suberyl,<sup>47</sup> or succinyl hydroxamate and iminodiacetic acid hydroxamate moieties<sup>48</sup> have been described. These inhibitors follow the classic architecture of metalloprotease inhibitors with a backbone that mimics the natural substrate, which is connected via a linker to a zinc-binding group that chelates the catalytic zinc ion and, thereby, expels the essential catalytic water molecule from the active site.<sup>49,50</sup> These inhibitors were developed as substrate analogues and/or designed on the basis of inhibitors for other metalloproteases that share the HEXXH motif,<sup>51</sup> like thermolysin or MMPs.<sup>44,47,52–58</sup> Unfortunately, the synthetic clostridial collagenase inhibitors are not selective, inhibiting clostridial collagenases and MMPs alike.<sup>44,45,47,48,55–57,59–61</sup> Therefore, they are not suitable for antibacterial therapy in humans. Consequently, novel and more effective drug candidates are urgently needed.

Efforts to design selective inhibitors were hampered by the lack of high-resolution structural data on clostridial collagenases until 2011. The first crystal structures revealed that, although there is no significant sequence homology between the peptidolytic domains of clostridial collagenases and MMPs, their active sites share a similar catalytic zinc ion-binding geometry and the canonical non-prime-site substrate-recognition motif, the edge strand.<sup>17</sup>

In this study, we wanted to capitalize on the recent crystal structures of the peptidase domains of three clostridial

collagenases<sup>34,41</sup> with the aim to rationally develop small organic molecules targeting collagenase ColH from *C. histolyticum*. In the following we describe the discovery of inhibitors which are highly active and selective for clostridial collagenases over MMPs and have the potential to be further optimized for a future therapeutic application in humans. Their selectivity can be rationalized on the basis of a co-crystal structure of the peptidase domain of ColH in complex with an inhibitor, revealing a distinct non-primed mode of binding of the inhibitor to the active site.

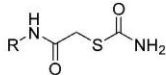
## ■ RESULTS AND DISCUSSION

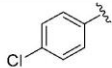
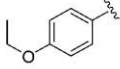
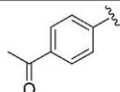
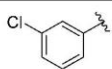
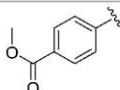
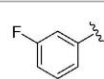
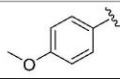
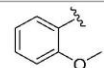
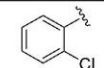
**Discovery of New Inhibitory Scaffold.** To discover new low-molecular-weight inhibitory compounds, a focused protease inhibitor library was screened with a surface plasmon resonance (SPR)-based binding assay using the amine-coupled peptidase domain of ColH (ColH-PD) as ligand. To ensure the integrity of ColH-PD after immobilization, the collagenase-specific peptidic substrate *N*-(3-[2-furyl]acryloyl)-L-leucylglycyl-L-prolyl-L-alanine (FALGPA)<sup>62</sup> was used as positive control (Figure S1a). A total of 1520 structurally diverse small molecules with an average molecular weight (MW) of  $389 \pm 78$  Da were screened at  $100 \mu\text{M}$ . Compounds showing a MW-normalized response higher than that of  $500 \mu\text{M}$  FALGPA (i.e., 35  $\mu$ -refractive index units) were classified as hits. The SPR screen resulted in 202 primary hits. Nineteen compounds were excluded from the subsequent testing as known promiscuous inhibitors,<sup>63</sup> resulting in a hit rate of 12.0% (Figure S2).

The secondary functional screening assessed the potential of the 183 SPR hits to inhibit the peptidolytic activity of ColH-PD using a custom-made fluorescence resonance energy transfer (FRET) substrate. Typically, the FALGPA<sup>62</sup> and Wünsch<sup>64</sup> assays are used to characterize the activity of clostridial collagenases due to their easy setup and commercial availability next to their specificity for these enzymes.<sup>62,65,66</sup> However, the low binding affinity of these peptides together with their low signal-to-noise ratios severely limits the sensitivity of these assays. Consequently, substantial amounts of enzyme and substrate are needed in characterization studies (e.g.,  $K_M$  values for FALGPA are in the mM range<sup>62,67</sup>). To facilitate our screening process, we designed and synthesized a decapeptide (Mca-Ala-Gly-Pro-Pro-Gly-Pro-Dpa-Gly-Arg-NH<sub>2</sub>) to be used as a substrate for a FRET-based assay. Its sequence was based on the detailed profile of the primed and non-primed cleavage site specificity of clostridial collagenases as determined by Proteomic Identification of protease Cleavage Sites (PICS) recently.<sup>17,68</sup> The assay sensitivity was increased by several orders of magnitude compared to the FALGPA assay by the application of the FRET technology.<sup>69,70</sup> The  $K_M$  value of this substrate is  $62 \pm 8 \mu\text{M}$  for ColH-PD. The 183 SPR binders were screened at a final concentration of  $40 \mu\text{M}$ . The inhibitor isoamylphosphonyl-Gly-Pro-Ala (Figure S1b) was used as positive control in the assay.<sup>58</sup> In sum, the SPR-based and activity-based screenings led to six functional hits (>25% inhibition) with MWs ranging from ~210 to ~385 Da (Figure S3). The two most active inhibitors in this assay were mercaptoacetamides 1 and 2 (Table 1). Compound 2 led to an inhibition of ColH-PD *in vitro* similar to that of isoamylphosphonyl-Gly-Pro-Ala, both at  $40 \mu\text{M}$ , i.e.,  $82 \pm 3\%$  and  $81 \pm 1\%$ , respectively.

Dose-response studies revealed an  $\text{IC}_{50}$  value of  $1.9 \pm 0.3 \mu\text{M}$  for this compound, while the non-substituted aniline

Table 1. IC<sub>50</sub> Values of Mercaptoacetamide Compounds for ColH-PD



Compound	R	IC <sub>50</sub> (μM)	Compound	R	IC <sub>50</sub> (μM)
1		25 ± 6	7		0.19 ± 0.02
2		1.9 ± 0.3	8		0.19 ± 0.03
3		0.010 ± 0.002	9		19 ± 3
4		0.044 ± 0.007	10		23 ± 3
5		0.071 ± 0.009	11		26 ± 4
6		0.12 ± 0.01	12		31 ± 7

derivative 1 showed lower activity toward ColH-PD ( $IC_{50} = 25 \pm 6 \mu M$ ). Our further hits showed considerably weaker inhibition and, in one case, proved to be incompatible with the FRET assay at high concentration. The high potency of the *N*-aryl mercaptoacetamides combined with their relatively low molecular weight encouraged us to investigate this promising compound class further in order to improve the inhibitory activity.

**Characterization of Mercaptoacetamide Hits.** A total of 36 derivatives of this compound class were purchased (see Tables 1, 3, and S1). Six derivatives showed improved inhibition compared to 2 (3–8). Generally, the introduction of functional groups in *para*-position to the aniline turned out to be favorable, considering the striking loss of activity of *ortho*-methoxy-substituted compound 11 compared to its *para*-analogue 5 (*ortho*-effect), and *ortho*-chloro-substituted compound 12 compared to its *para*-analogue 7. The superior performance of *para*-derivatives was also evident regarding the 100-fold decrease in  $IC_{50}$  of 7 compared to its *meta*-chloro-substituted counterpart 9. In comparison to the unsubstituted compound 1, *meta*-substituted compounds 9 and 10 showed no significant improvement in  $IC_{50}$ . Removal of the 3-methyl-group of compound 2 even led to a 16-fold decreased  $IC_{50}$  (compound 6), suggesting that the *meta*-substitution is not beneficial for ColH inhibition.

Regarding electronic properties of our hits it becomes apparent that the best compounds 3–5, displaying  $IC_{50}$  values in the two-digit nanomolar range, bear oxygen-containing groups with hydrogen bond accepting properties.

**Selectivity against MMPs and Broad-Spectrum Inhibition of Other Bacterial Collagenases.** To determine the selectivity of our compounds toward clostridial and bacillial collagenases on the one hand, and MMPs on the other, selected compounds (3 and 7, Figure 1) were tested using *in vitro*

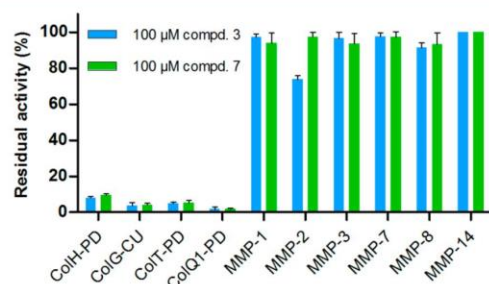
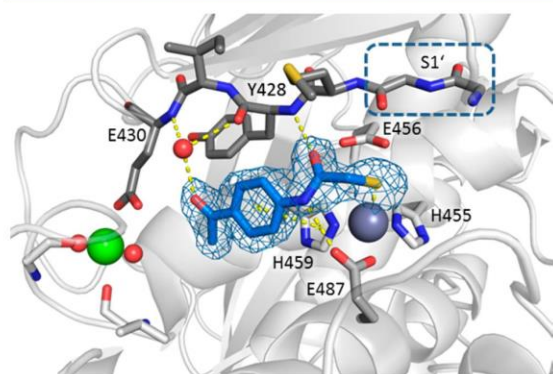


Figure 1. Inhibition of selected MMPs and bacterial collagenases by *N*-aryl mercaptoacetamide compounds 3 and 7.

inhibition assays with ColH-PD and the peptidase domains of ColT (ColT-PD), the collagenase units of ColG (ColG-CU) and of ColQ1 (ColQ1-CU), as well as the catalytic domains of MMP-1, -2, -3, -7, -8, and -14. The hydroxamate-based peptidomimetic batimastat (Figure S1c) is a highly potent and unselective inhibitor of MMPs<sup>71</sup> and was used as a positive control. MMPs are highly similar to each other in their active-site topology, which has made the development of selective active-site directed MMP inhibitors a challenging task.<sup>72,73</sup> The S1' binding site is the major specificity determinant in MMPs. Based on the S1' site, the MMPs are typically divided into deep, intermediate and shallow S1' binding pocket groups (e.g., deep: MMP-3, -12, and -14; intermediate: MMP-2, -8, and -9; shallow: MMP-1 and -7).<sup>74</sup> Therefore, we chose a panel of MMPs to investigate the binding of our compounds to all three S1' pocket types. In line with published results,<sup>71</sup> batimastat displayed  $IC_{50}$  values below 10 nM for all of these MMPs (Table S2). As expected from this broad-spectrum zinc metalloproteinase inhibitor, batimastat also inhibited ColH-

PD, ColT-PD, ColG-CU and ColQ1-CU (Figure S4). Intriguingly, compounds 3 and 7 resulted in no or negligible inhibition of the tested MMPs (Figure 1 and Figure S5). Only in case of MMP-2, we observed 25% inhibition at 100  $\mu$ M compound 3, while ColH-PD was efficiently inhibited, showing less than 10% residual activity. Thus, we observed a more than 1000-fold selectivity of these two compounds for ColH over MMPs. Strikingly, the clostridial collagenase homologues ColG and ColT, and the bacillial collagenase ColQ1, were even more efficiently inhibited, showing 5% or less residual activity when treated with 100  $\mu$ M compound 3 or 7. A similar compound scaffold had been reported by Zhu et al. to inhibit LasB, an extracellular elastase from *Pseudomonas aeruginosa*.<sup>75</sup> In sum, these findings showed that the *N*-aryl mercaptoacetamide-based inhibitors are not only selective against MMPs, but are also potent broad-spectrum inhibitors of bacterial collagenases.

**Crystal Structure of the Peptidase Domain of ColH in Complex with Compound 3.** To rationalize the binding mode of the *N*-aryl mercaptoacetamide-based inhibitors, we aimed to solve the crystal structure of ColH-PD in complex with compound 3. The structure was determined at 1.87 Å resolution with all residues being defined in the electron density at excellent geometric and crystallographic parameters (Table S3). The overall topology of the peptidase domain showed the expected thermolysin-like fold. The average root-mean-square displacements (RMSDs) of backbone atoms between the structure of the apo-peptidase domain and the peptidase domain in complex with isoamylphosphonyl-Gly-Pro-Ala were 0.133 and 0.123 Å, respectively. The peptidase domain of ColH is divided horizontally by the active-site cleft into an upper N-terminal and a lower C-terminal subdomain (CSD). Substrates can bind to the active-site cleft from the left (non-primed side) to the right (primed side) when viewed in standard orientation.<sup>76</sup> Central elements of the N-terminal subdomain (NSD) are the active-site helix and a mixed five-strand  $\beta$ -sheet. The zinc-binding motif HEXXH, which provides the two zinc-coordinating histidines and the general acid/base glutamate, is located in the active-site helix (Figure 2). The lowermost  $\beta$ -strand of the mixed  $\beta$ -sheet shapes the upper perimeter of the



**Figure 2.** Peptidase domain of ColH in complex with the hydrolysis product of compound 3. Close-up view of the active site in ball-and-stick representation. The inhibitor (blue) is shown in sticks with the maximum likelihood weighted  $2F_o - F_c$  electron density map contoured at  $1\sigma$ . The catalytic zinc ion (dark gray), calcium ion (green), and water molecule (red) are shown as spheres. The S1' site formed by Gly425 and Gly426 in the edge strand (shown in dark gray sticks) is indicated.

active-site cleft, the edge strand. The edge strand interacts in an antiparallel manner with the substrate predominantly on the non-primed side.<sup>34,77,78</sup> The third zinc ligand is a glutamate residue, located on the glutamate helix of the CSD. The insertion of 30 residues between the HEXXH motif and this glutamate residue shapes (i) the non-primed side of the active-site cleft and (ii) a calcium-binding site crucial for enzymatic activity.<sup>34,41,77</sup>

A well-defined electron density was observed for the ligand bound in the active site. The structure of compound 3 could be clearly modeled into the density (Figure 2), except for the carbonyl unit of the thiocarbamate moiety. Instead, the electron density showed the sulfur atom coordinating the catalytic zinc ion, suggesting that the thioester group had been hydrolyzed in the co-crystallization process. This result prompted an investigation of our newly discovered class of inhibitors with particular emphasis on the stability of the thiocarbamate function in aqueous buffers such as the buffer system of the functional assay and the crystallization buffer.

**Stability of the Thiocarbamate Unit.** Two inhibitors with major differences in potency (7, 12) were selected and the hydrolytic formation of the corresponding free thiol was analyzed by liquid chromatography–mass spectrometry (LC-MS). Free thiols were synthesized as references for the stability assay. The conversions of compounds 7 and 12 into compounds 14 and 15, respectively, proceeded rapidly in 10 mM HEPES, pH 7.5 at 22.5 °C, with thiocarbamate half-lives of  $26.8 \pm 1.4$  min (7) and  $20.6 \pm 0.9$  min (12, Figure 3). These results corroborated that the inhibition of thiocarbamates 1–12 was predominantly due to the respective free thiols. Considering the preparation time and the pre-incubation time of 1 h for each compound with ColH-PD before the functional assay was started by addition of the substrate the

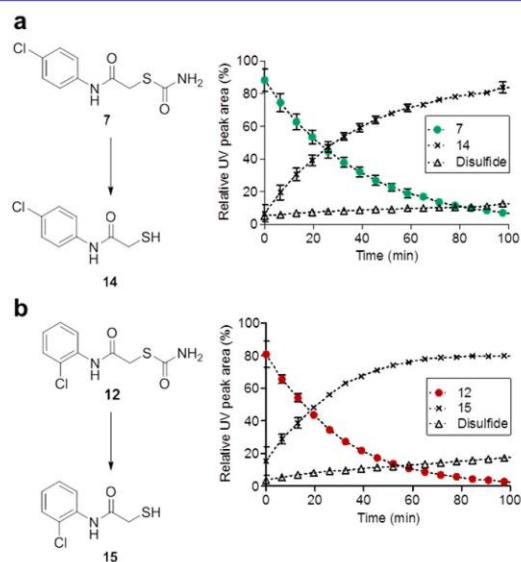


**Figure 3.** Conversion of thiocarbamates 7 and 12 into the respective corresponding free thiols: (a) compound 7 into 14 and (b) compound 12 into 15. Time course of hydrolysis in 10 mM HEPES, pH 7.4 (10% methanol), at 22.5 °C was monitored by LC-MS, showing conversion into corresponding thiol and to minor extent into another compound which is most likely the disulfide oxidation product.<sup>79</sup>

thiocarbamates were quantitatively converted within the time frame of the experiment. Thiol formation was also demonstrated at pH 6.4, corresponding to the buffer used for co-crystallization (Figure S6).

**Confirmation of Thiol as Active Compound.** To further substantiate these findings, we followed two different strategies. First, we studied the inhibitory activities of the free thiols 13–15. Thus, we determined the  $IC_{50}$  values of the free thiols 13–15 with ColH-PD in the presence of the reducing agent TCEP. The resulting  $IC_{50}$  values of 0.017, 0.21, and 40  $\mu$ M corresponded well with 0.010, 0.19, and 31  $\mu$ M of the thiocarbamate analogues (Tables 1 and 2).

**Table 2. Inhibition of ColH-PD by Thiol Compounds in the Presence of 5 mM TCEP**

Compound	R	$IC_{50}$ ( $\mu$ M)
13		0.017 $\pm$ 0.002
14		0.21 $\pm$ 0.01
15		40 $\pm$ 9

The results of the MMP and bacterial collagenase inhibition assays could also be reproduced using the thiol compounds, with 13 and 14 demonstrating a similarly high selectivity against MMPs and a broad-spectrum inhibition of bacterial collagenases (Figure 4).

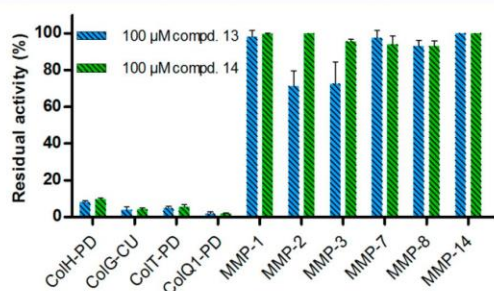


**Figure 4.** Inhibition of selected MMPs and bacterial collagenases by thiol compounds 13 and 14.

As a second strategy, we aimed to synthesize a structural analogue of compound 1 lacking the hydrolytically unstable thioester motif. The formal replacement of the sulfur atom with a methylene group led to the carboxamide analogue 16, which was prepared and tested for its inhibitory activity toward ColH-PD (Figure 5). Compound 16 was devoid of any activity even at 1000  $\mu$ M. This demonstrated that the carbamoyl moiety in 1 does not contribute to target binding, but is just part of a

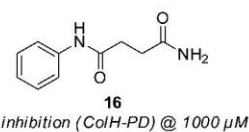


**Figure 5.** Structure and inhibitory activity of the non-hydrolyzable carboxamide analogue 16.

prodrug-like structure which furnishes the corresponding bioactive thiol by chemical hydrolysis.

Further in line with our findings, dithiocarbamates 17–21 (Table 3) were inactive toward ColH-PD. LC-MS experiments

**Table 3. Structure and Activity of Dithiocarbamates**

Compound	R	Inhibition at 100 $\mu$ M (%)
17		no inhibition
18		no inhibition
19		no inhibition
20		no inhibition
21		12 $\pm$ 3

with the dithiocarbamate analogue of our best hit 3 showed no formation of free thiol 13 within the time frame of our assay, explaining the inactivity of these derivatives by stability toward hydrolysis (Figure S7).

In addition, the thermodynamic profile of the interaction between compounds 7 and 14 and ColH-PD was determined. As expected, isothermal titration calorimetry (ITC) measurements resulted in very similar affinities and free energy values, resulting from the hydrolysis of 7 to furnish thiol 14 (Table 4). Compound binding to ColH-PD turned out to be enthalpy-driven. In sum, the findings from the stability assay, the *in vitro* assay and the ITC data confirmed the thiols as active compounds in our enzyme inhibition assay.

**Cytotoxicity Test.** Regarding the potential therapeutic use of our compounds in humans, we investigated the cytotoxic properties of selected *N*-aryl mercaptoacetamides. Cytotoxicity tests using HEP G2 cells showed compounds 13 and 14 to display low cytotoxicity, comparable to that of the marketed antibiotic rifampicin (Table 5), while doxorubicin as control showed the expected cytotoxic effect. These findings underline

**Table 4.** ITC and IC<sub>50</sub> Results of the Thiocarbamate–Thiol Pair 7 and 14

	7	14
IC <sub>50</sub> (μM) <sup>a</sup>	0.19 ± 0.02	0.21 ± 0.01
K <sub>D</sub> (μM) <sup>b</sup>	0.309 ± 0.045	0.360 ± 0.038
ΔG (kcal mol <sup>-1</sup> ) <sup>b</sup>	-8.9 ± 0.1	-8.8 ± 0.1
ΔH (kcal mol <sup>-1</sup> ) <sup>b</sup>	-12.7 ± 1.2	-15.4 ± 0.3
-TΔS (kcal mol <sup>-1</sup> ) <sup>b</sup>	3.8 ± 1.3	6.6 ± 0.4
N <sup>b,c</sup>	0.54 ± 0.05	0.48 ± 0.03

<sup>a</sup>IC<sub>50</sub> refers to the functional FRET assay. <sup>b</sup>Results are from at least two independent measurements. <sup>c</sup>The low stoichiometry could be explained by incomplete zinc occupation of the active sites.<sup>41</sup>

the potential of our compounds for the development of novel anti-infectives.

**Table 5.** Cytotoxicity of 13, 14, and Three Reference Compounds in HEP G2 Cells

compound	concn (μM)	reduction of viability (%)
13	100	17 ± 12
14	100	28 ± 12
rifampicin	100	29 ± 5
doxorubicin	1	50 ± 5
batimastat	100	13 ± 7

**Zinc Coordination by a Thiolate.** The identification of the thiol as active compound in our functional assays was in excellent agreement with the crystal structure analysis which demonstrated that only a sulfur atom, to be precise a thiolate, was coordinating the catalytic zinc ion. To validate our conclusions on the protonation state of the sulfur atom, we calculated the pK<sub>a</sub> values for the thiol group resulting from the hydrolysis of thiocarbamate 3 in solution and when bound to the active site using the Molecular Operating Environment (MOE) software.<sup>80</sup> The pK<sub>a</sub> of the thiol group was strongly lowered from 9.0 in the solvent to 3.1 by the direct coordination to the zinc ion. This suggests that the thiol is fully ionized to the thiolate form in both the activity assay and the crystallization experiment upon binding to the active site.

**Binding Mode of the *N*-Aryl Mercaptoacetamide Compound to the Active Site of ColH-PD.** The hydrolysis product of compound 3 binds to the S3 to S1 substrate binding pockets (Figure 2). The thiolate coordinates the zinc ion with a sulfur-to-zinc distance of 2.27 Å. In the S1 pocket, the amide oxygen of compound 3 forms a hydrogen bond with the main-chain amide nitrogen of Tyr428 (3.11 Å) of the NSD, while the amide nitrogen of compound 3 hydrogen-bonds with the carbonyl oxygen (OE2) of Glu487 (2.97 Å) of the CSD. In addition, the benzene ring of the ligand is involved in a π–π-stacking interaction with the imidazole ring of His459 (centroid-centroid distance of 3.80 Å). The oxygen of the acetyl group of 3 interacts via a bridging water molecule (3.07 Å) with the main-chain oxygen of Tyr428 in S1 (3.11 Å) and with the main-chain nitrogen of Glu430 in S3 (2.84 Å). Thus, the inhibitor is well-braced in-between the NSD and the CSD of the peptidase domain.

Importantly, the binding mode of the inhibitor is not directed toward the primed substrate-binding sites, but toward the non-primed recognition sites in-between the calcium-binding site and the catalytic zinc ion. Thus, this complex of ColH-PD with the thiol derived from compound 3 is the first to

describe non-primed interactions between a clostridial collagenase and an active site-directed ligand.

**Identification of Selectivity Determinant.** The thiol derived from compound 3 interacts with two central elements of the active site: (i) the zinc ion and its liganding sphere (His455, Glu456, His459, and Glu487), and (ii) the edge strand (Gly425–Glu430). These two central elements are also present in MMPs.<sup>17</sup> A structurally, but not sequentially, homologous edge strand frames the upper rim of the active site in MMPs, and the zinc-liganding sphere composed of the HEXXH motif and a third proteinaceous ligand is nearly identical between the MMPs and the clostridial collagenases. The geometry of the zinc-liganding sphere is almost perfectly superimposable in clostridial collagenases and MMPs (RMSD = 0.060 Å between ColH and MMP-1). Only the third zinc-binding residue differs. While in MMPs, this position is occupied by a histidine; in clostridial collagenases, this ligand is a glutamate provided by the gluzincin-specific glutamate helix. Given this high similarity in the active site between clostridial collagenases and MMPs, this triggered the question of how we can rationalize the observed differences in selectivity of the *N*-aryl mercaptoacetamide compounds toward the two enzyme families. A first *in silico* structural analysis of the active sites of MMP-1, -2, -3, -8, -12, and -13 suggested that (i) these enzymes could accommodate the mercaptoacetamide compounds in their non-primed substrate pockets, and that (ii) the residues on the edge strand and the zinc ion are positioned as such as to allow productive interactions with the thiolate. Yet, the MMPs, lacking the zinc-binding glutamate, cannot provide the hydrogen-bonding partner for the amide nitrogen of the mercaptoacetamide inhibitor. Hence, is the interaction with the gluzincin-specific Glu487 crucial for selectivity? To test this hypothesis, we mimicked the zinc-liganding sphere of MMPs in ColH-PD by mutating Glu487 into a histidine. A comparison of the apparent inhibition constant  $K_{i(\text{app})}$  of compound 11 toward wild-type ColH-PD and the mutant E487H, 92 ± 8 and 166 ± 23 μM, respectively, showed that the mutation did not result in a drastic change in the inhibitory potency. This suggests that the interaction with the edge strand on the non-primed site, mediated via main-chain contacts, is the main structural selectivity determinant. This hypothesis is further supported by a structural analysis of the edge-strand conformations in MMPs and clostridial collagenases in the ligand-bound state. Within each family, the ligand-bound edge-strand conformation is highly conserved (Figure 6). Compared to the clostridial situation, the edge strand in MMPs is tilted by 27–29°. This tilted orientation could explain the inefficient binding of the *N*-aryl mercaptoacetamide compounds to the MMPs, suggesting that the interactions with the non-primed edge strand (S1–S3) are the crucial selectivity determinants.

It was also interesting to see that related mercaptoacetamide derivatives were shown to inhibit LasB from *P. aeruginosa*.<sup>75</sup> Analysis of our best compound 13 in an *in vitro* LasB inhibition assay revealed a more than 1000-fold lower activity compared to ColH (data not shown). This is likely due to the distinct binding mode of compound 13 to the non-primed binding site of ColH (Figure 2) in contrast to the proposed primed binding mode of the related compounds in LasB by Zhu et al.<sup>75</sup>

With regard to future inhibitor design, these findings suggest that by (i) amplification of the interactions with the edge strand and (ii) extension of the inhibitor scaffold in *para*, i.e., by developing the compound further into the non-primed substrate recognition pockets, even more potent and selective

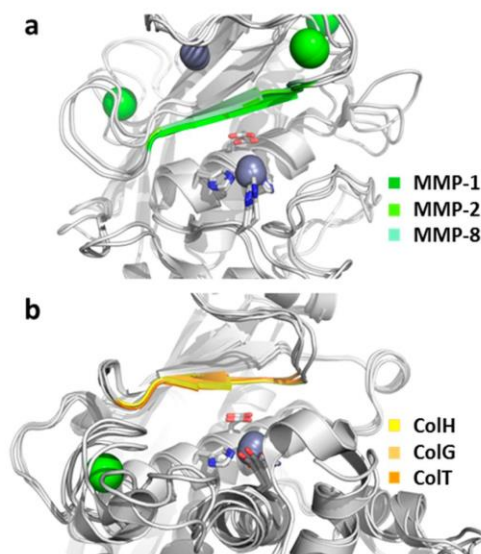


**Figure 6.** Close-up on the superpositioned active sites of three MMPs (a) and of three clostridial collagenases (b) in the ligand-bound state. The ligands have been removed for better visualization. The HEXXH motif is shown in sticks, and the zinc ions (gray) and calcium ions (green) are shown as spheres. The edge strand on top of the catalytic zinc is highlighted in color.

compounds could be developed. In compounds with optimized affinity to the edge strand and the non-primed substrate binding pockets, we plan to investigate the replacement of the thiol moiety by a less reactive ZBG. Such lead compounds hold the promise of higher efficacy and therefore higher safety in potential therapeutic applications in humans.

## CONCLUSION

We identified a novel compound scaffold for the selective inhibition of clostridial collagenases. Starting with an SPR-based primary screening of a focused library, we validated the SPR-hits in a secondary enzyme inhibition assay using a custom-tailored FRET peptide substrate for clostridial collagenases. Two mercaptoacetamide derivatives were the most potent functional hits in this assay. Further derivatization of these initial hits, in particular the introduction of oxygen-containing groups in *para*-position to the aniline, led to the generation of highly potent *N*-aryl mercaptoacetamide-based clostridial collagenase inhibitors with  $IC_{50}$  values in the two-digit nanomolar range. These compounds showed unprecedented selectivity against MMPs, while at the same time they displayed a broad-spectrum inhibition of bacterial collagenases. The selectivity of these compounds could be rationalized on the basis of a co-crystal structure of ColH-PD with the most active compound, revealing a distinct non-primed binding mode of the inhibitor to the active site. The mercaptoacetamides were also shown to display no cytotoxicity toward human cells. These insights pave the way for the development of selective broad-spectrum bacterial collagenase inhibitors with potential therapeutic application in humans.

## ASSOCIATED CONTENT

### Supporting Information

The Supporting Information is available free of charge on the ACS Publications website at DOI: 10.1021/jacs.7b06935.

Supporting Figures S1–S7 and Tables S1–S3, giving molecular structures of positive controls, SPR and functional screening hits, inhibition of the selected MMPs and bacterial collagenases by batimastat, MMP inhibition assay, LC-MS analyses of **3** and **21**, structure and activity of additional thiocarbamates and related compounds, and data collection and refinement statistics (PDF)

## AUTHOR INFORMATION

### Corresponding Authors

\*hans.brandstetter@sbg.ac.at

\*rolf.hartmann@helmholtz-hzi.de

### ORCID

Esther Schönauer: 0000-0002-2625-9446

Andreas M. Kany: 0000-0001-7580-3658

Jörg Haupenthal: 0000-0003-3991-2800

Isabel J. Hoppe: 0000-0001-9050-1260

Samir Yahiaoui: 0000-0001-5134-5007

Brigitta Elsässer: 0000-0002-9087-243X

Hans Brandstetter: 0000-0002-6089-3045

Rolf W. Hartmann: 0000-0002-5871-5231

### Author Contributions

<sup>†</sup>E.S. and A.M.K. contributed equally.

### Notes

The authors declare no competing financial interest.

## ACKNOWLEDGMENTS

This work was supported by grants from the Austrian Science Fund (project W\_01213 & M\_1901). We thank Dr. Elfriede Dall for X-ray data collection, Dr. Werner Tegge for peptide synthesis, and Dr. Christine Maurer and Jeannine Jung for technical support.

## REFERENCES

- (1) Cato, E.; George, W.; Finegold, S. *Bergey's Manual of Systematic Bacteriology*; Williams & Wilkins: Baltimore, 1986; pp 1141–1200.
- (2) Hatheway, C. L. *Clin. Microbiol. Rev.* **1990**, *3*, 66–98.
- (3) Burke, M. P.; Opekin, K. *Am. J. Forensic Med. Pathol.* **1999**, *20*, 158–162.
- (4) Bruggemann, H.; Baumer, S.; Fricke, W. F.; Wiezer, A.; Liesegang, H.; Decker, I.; Herzberg, C.; Martinez-Arias, R.; Merkl, R.; Henne, A.; Gottschalk, G. *Proc. Natl. Acad. Sci. U. S. A.* **2003**, *100*, 1316–1321.
- (5) Taubes, G. *Science* **2008**, *321*, 360.
- (6) Taubes, G. *Science* **2008**, *321*, 356–361.
- (7) Arnon, S. S.; Schechter, R.; Inglesby, T. V.; Henderson, D. A.; Bartlett, J. G.; Ascher, M. S.; Eitzen, E.; Fine, A. D.; Hauer, J.; Layton, M.; Lillibridge, S.; Osterholm, M. T.; O'Toole, T.; Parker, G.; Perl, T. M.; Russell, P. K.; Swerdlow, D. L.; Tonat, K.; Working Group on Civilian Biodefense. *JAMA* **2001**, *285*, 1059–1070.
- (8) Matsushita, O.; Okabe, A. *Toxicol.* **2001**, *39*, 1769–1780.
- (9) Popoff, M. R.; Bouvet, P. *Future Microbiol.* **2009**, *4*, 1021–1064.
- (10) Burgeson, R. E.; Nimni, M. E. *Clin. Orthop. Relat. Res.* **1992**, *282*, 250–272.
- (11) Brozek, J.; Grande, F.; Anderson, J. T.; Keys, A. *Ann. N. Y. Acad. Sci.* **1963**, *110*, 113–140.

- (12) Ramshaw, J. A.; Shah, N. K.; Brodsky, B. J. *Struct. Biol.* **1998**, *122*, 86–91.
- (13) Bruckner, P.; Prockop, D. J. *Anal. Biochem.* **1981**, *110*, 360–368.
- (14) Bächinger, H. P.; Bruckner, P.; Timpl, R.; Prockop, D. J.; Engel, J. *Eur. J. Biochem.* **1980**, *106*, 619–632.
- (15) Nagase, H.; Visse, R.; Murphy, G. *Cardiovasc. Res.* **2006**, *69*, 562–573.
- (16) Fields, G. B. *J. Biol. Chem.* **2013**, *288*, 8785–8793.
- (17) Eckhard, U.; Huesgen, P. F.; Brandstetter, H.; Overall, C. M. *J. Proteomics* **2014**, *100*, 102–114.
- (18) Seifter, S.; Harper, E. In *The Enzymes*; Boyer, P. D.; Academic Press: New York, 1971; pp 649–697.
- (19) Mookhtiar, K. A.; Van Wart, H. E. *Matrix Suppl.* **1992**, *1*, 116–126.
- (20) Rasko, D. A.; Sperandio, V. *Nat. Rev. Drug Discovery* **2010**, *9*, 117–128.
- (21) Heras, B.; Scanlon, M. J.; Martin, J. L. *Br. J. Clin. Pharmacol.* **2015**, *79*, 208–215.
- (22) Clatworthy, A. E.; Pierson, E.; Hung, D. T. *Nat. Chem. Biol.* **2007**, *3*, 541–548.
- (23) Storz, M. P.; Maurer, C. K.; Zimmer, C.; Wagner, N.; Brengel, C.; de Jong, C.; Lucas, S.; Müsken, M.; Häussler, S.; Steinbach, A.; Hartmann, R. W. *J. Am. Chem. Soc.* **2012**, *134*, 16143–16146.
- (24) Lu, C.; Maurer, C. K.; Kirsch, B.; Steinbach, A.; Hartmann, R. W. *Angew. Chem., Int. Ed.* **2014**, *53*, 1109–1112.
- (25) Hung, D. T.; Shakhnovich, E. A.; Pierson, E.; Mekalanos, J. J. *Science* **2005**, *310*, 670–674.
- (26) Wagner, S.; Sommer, R.; Hinsberger, S.; Lu, C.; Hartmann, R. W.; Empting, M.; Titz, A. *J. Med. Chem.* **2016**, *59*, 5929–5969.
- (27) Böttcher, T.; Sieber, S. A. *J. Am. Chem. Soc.* **2008**, *130*, 14400–14401.
- (28) Kassegne, K.; Hu, W.; Ojcius, D. M.; Sun, D.; Ge, Y.; Zhao, J.; Yang, X. F.; Li, L.; Yan, J. *J. Infect. Dis.* **2014**, *209*, 1105–1115.
- (29) Lewis, K. *Nat. Rev. Drug Discovery* **2013**, *12*, 371–387.
- (30) Payne, D. J.; Gwynn, M. N.; Holmes, D. J.; Pompliano, D. L. *Nat. Rev. Drug Discovery* **2007**, *6*, 29–40.
- (31) Graef, F.; Vukosavljevic, B.; Michel, J.-P.; Wirth, M.; Ries, O.; De Rossi, C.; Windbergs, M.; Rosilio, V.; Ducho, C.; Gordon, S.; Lehr, C.-M. *J. Controlled Release* **2016**, *243*, 214–224.
- (32) Peterkofsky, B. *Methods Enzymol.* **1982**, *82*, 453–471.
- (33) Supuran, C. T.; Scozzafava, A.; Mastrolorenzo, A. *Expert Opin. Ther. Pat.* **2001**, *11*, 221–259.
- (34) Eckhard, U.; Schönauer, E.; Nüss, D.; Brandstetter, H. *Nat. Struct. Mol. Biol.* **2011**, *18*, 1109–1114.
- (35) Matsushita, O.; Jung, C. M.; Katayama, S.; Minami, J.; Takahashi, Y.; Okabe, A. *J. Bacteriol.* **1999**, *181*, 923–933.
- (36) Matsushita, O.; Jung, C. M.; Minami, J.; Katayama, S.; Nishi, N.; Okabe, A. *J. Biol. Chem.* **1998**, *273*, 3643–3648.
- (37) Matsushita, O.; Koide, T.; Kobayashi, R.; Nagata, K.; Okabe, A. *J. Biol. Chem.* **2001**, *276*, 8761–8770.
- (38) Wang, Y.-K.; Zhao, G.-Y.; Li, Y.; Chen, X.-L.; Xie, B.-B.; Su, H.-N.; Lv, Y.-H.; He, H.-L.; Liu, H.; Hu, J.; Zhou, B.-C.; Zhang, Y.-Z. *J. Biol. Chem.* **2010**, *285*, 14285–14291.
- (39) Jung, C. M.; Matsushita, O.; Katayama, S.; Minami, J.; Sakurai, J.; Okabe, A. *J. Bacteriol.* **1999**, *181*, 2816–2822.
- (40) Bond, M. D.; Van Wart, H. E. *Biochemistry* **1984**, *23*, 3085–3091.
- (41) Eckhard, U.; Schönauer, E.; Brandstetter, H. *J. Biol. Chem.* **2013**, *288*, 20184–20194.
- (42) Matthews, B. W. *Acc. Chem. Res.* **1988**, *21*, 333–340.
- (43) Oshima, N.; Narukawa, Y.; Takeda, T.; Kiuchi, F. *J. Nat. Med.* **2013**, *67*, 240–245.
- (44) Supuran, C. T.; Scozzafava, A. *Eur. J. Pharm. Sci.* **2000**, *10*, 67–76.
- (45) Clare, B. W.; Scozzafava, A.; Supuran, C. T. *J. Med. Chem.* **2001**, *44*, 2253–2258.
- (46) Scozzafava, A.; Supuran, C. T. *Bioorg. Med. Chem. Lett.* **2002**, *12*, 2667–2672.
- (47) Ilies, M. A. M.; Banciu, M. D.; Scozzafava, A.; Ilies, M. A. M.; Caproiu, M. T.; Supuran, C. T. *Bioorg. Med. Chem.* **2003**, *11*, 2227–2239.
- (48) Santos, M. A.; Marques, S.; Gil, M.; Tegoni, M.; Scozzafava, A.; Supuran, C. T. *J. Enzyme Inhib. Med. Chem.* **2003**, *18*, 233–242.
- (49) Jacobsen, F. E.; Lewis, J. A.; Cohen, S. M. *ChemMedChem* **2007**, *2*, 152–171.
- (50) Rouffet, M.; Cohen, S. M. *Dalton Trans.* **2011**, *40*, 3445–3454.
- (51) Hooper, N. M. *FEBS Lett.* **1994**, *354*, 1–6.
- (52) Grobelny, D.; Galardy, R. E. *Biochemistry* **1985**, *24*, 6145–6152.
- (53) Vencill, C. F.; Rasnick, D.; Crumley, K. V.; Nishino, N.; Powers, J. C. *Biochemistry* **1985**, *24*, 3149–3157.
- (54) Dive, V.; Yiotakis, A.; Nicolaou, A.; Toma, F. *Eur. J. Biochem.* **1990**, *191*, 685–693.
- (55) Scozzafava, A.; Supuran, C. T. *Bioorg. Med. Chem.* **2000**, *8*, 637–645.
- (56) Scozzafava, A.; Ilies, M. A.; Manole, G.; Supuran, C. T. *Eur. J. Pharm. Sci.* **2000**, *11*, 69–79.
- (57) Supuran, C. T.; Briganti, F.; Mincione, G.; Scozzafava, A. *J. Enzyme Inhib.* **2000**, *15*, 111–128.
- (58) Galardy, R. E.; Grobelny, D. *Biochemistry* **1983**, *22*, 4556–4561.
- (59) Scozzafava, A.; Supuran, C. T. *J. Med. Chem.* **2000**, *43*, 3677–3687.
- (60) Scozzafava, A.; Supuran, C. T. *Eur. J. Med. Chem.* **2000**, *35*, 299–307.
- (61) Supuran, C. T. In *Drug Design of Zinc-Enzyme Inhibitors*; Supuran, C. T., Winum, J.-Y., Eds.; John Wiley & Sons, Inc.: Hoboken, NJ, 2009; pp 721–729.
- (62) Van Wart, H. E.; Steinbrink, D. R. *Anal. Biochem.* **1981**, *113*, 356–365.
- (63) Baell, J. B.; Holloway, G. A. *J. Med. Chem.* **2010**, *53*, 2719–2740.
- (64) Wünsch, E.; Heidrich, H. H.-G. *Hoppe-Seyler's Z. Physiol. Chem.* **1963**, *333*, 149–151.
- (65) Komsa-Penkova, R. S.; Rashap, R. K.; Yomtova, V. M. *J. Biochem. Biophys. Methods* **1997**, *34*, 237–249.
- (66) Watanabe, K. *Appl. Microbiol. Biotechnol.* **2004**, *63*, 520–526.
- (67) Eckhard, U.; Schönauer, E.; Ducka, P.; Briza, P.; Nüss, D.; Brandstetter, H. *Biol. Chem.* **2009**, *390*, 11–18.
- (68) Schilling, O.; Overall, C. M. *Nat. Biotechnol.* **2008**, *26*, 685–694.
- (69) Fields, G. B. *Methods Mol. Biol.* **2010**, *622*, 393–433.
- (70) Knight, C. G. *Methods Enzymol.* **1995**, *248*, 18–34.
- (71) Rasmussen, H. S.; McCann, P. P. *Pharmacol. Ther.* **1997**, *75*, 69–75.
- (72) Cathcart, J.; Pulkoski-Gross, A.; Cao, J. *Genes Dis.* **2015**, *2*, 26–34.
- (73) Overall, C. M.; López-Otín, C. *Nat. Rev. Cancer* **2002**, *2*, 657–672.
- (74) Park, H. I.; Jin, Y.; Hurst, D. R.; Monroe, C. A.; Lee, S.; Schwartz, M. A.; Sang, Q.-X. *J. Biol. Chem.* **2003**, *278*, 51646–51653.
- (75) Zhu, J.; Cai, X.; Harris, T. L.; Gooyit, M.; Wood, M.; Lardy, M.; Janda, K. D. *Chem. Biol.* **2015**, *22*, 483–491.
- (76) Gomis-Rüth, F. X.; Botelho, T. O.; Bode, W. *Biochim. Biophys. Acta, Proteins Proteomics* **2012**, *1824*, 157–163.
- (77) Cerdà-Costa, N.; Xavier Gomis-Rüth, F. *Protein Sci.* **2014**, *23*, 123–144.
- (78) Gomis-Rüth, F. X. *J. Biol. Chem.* **2009**, *284*, 15353–15357.
- (79) Pramari, Y.; Das Gupta, V.; Bethea, C. J. *Clin. Pharm. Ther.* **1992**, *17*, 185–189.
- (80) Labute, P. *Proteins: Struct., Funct., Genet.* **2009**, *75*, 187–205.

SUPPORTING INFORMATION OF THE PUBLICATION

## **Discovery of a potent inhibitor class with high selectivity towards clostridial collagenases**

Esther Schönauer†‡, Andreas M. Kany†‡, Jörg Haupenthal‡, Kristina Hüsecken‡, Isabel J. Hoppe†, Katrin Voos§, Samir Yahiaoui‡, Brigitta Elsässer†, Christian Ducho§, Hans Brandstetter†\*, Rolf W. Hartmann‡§\*

† Division of Structural Biology, Department of Molecular Biology, University of Salzburg, Billrothstr. 11, 5020 Salzburg, Austria

‡ Helmholtz Institute for Pharmaceutical Research Saarland (HIPS), Department of Drug Design and Optimization, Campus E8.1, 66123, Saarbrücken, Germany

§ Department of Pharmacy, Pharmaceutical and Medicinal Chemistry, Saarland University, Campus C2.3, 66123 Saarbrücken, Germany

## Table of Contents

1. Supporting Figures and Tables	S2
2. Experimental Section	S10
3. References	S19

## 1. Supporting Figures and Tables

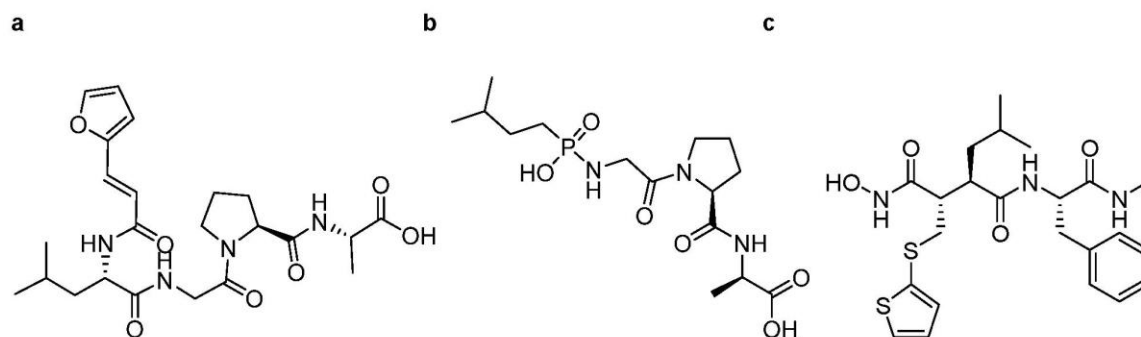


**Figure S1.** Molecular structures of the positive-control compounds (a) FALGPA, (b) isoamylphosphonyl-Gly-Pro-Ala and (c) batimastat.

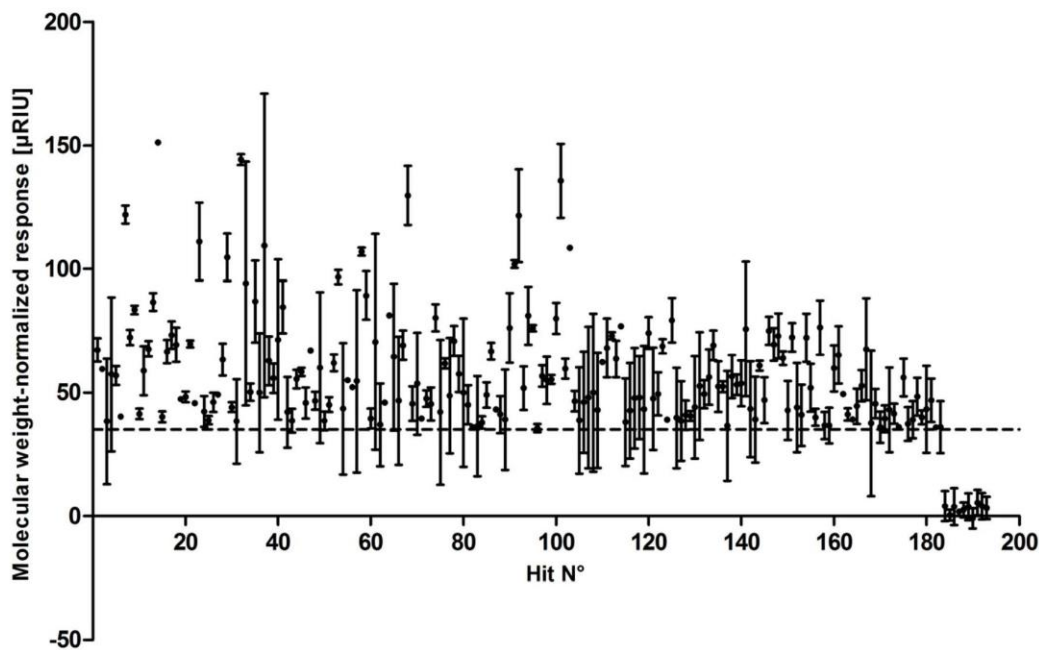


**Figure S2.** SPR screening for ColH inhibitor discovery. Screening data for 183 hits and 10 selected non-hits of the TimTec Acti-Targ-P library are shown. Compounds at 100  $\mu\text{M}$  that showed a higher response than 500  $\mu\text{M}$  FALGPA (35  $\mu\text{RIU}$ ; line) were designated as hits.

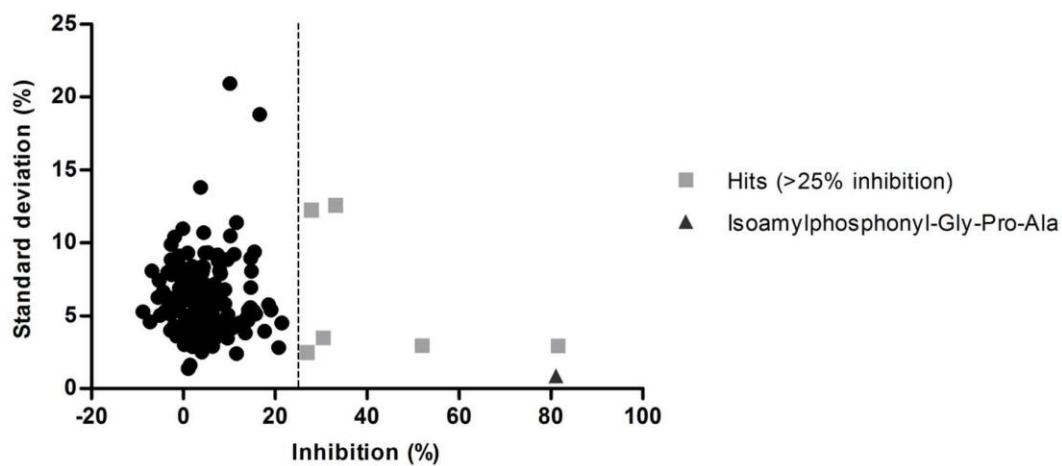


**Figure S3.** Functional screening hits of the peptidolytic activity of ColH-PD. Compounds were screened at 40  $\mu\text{M}$ .

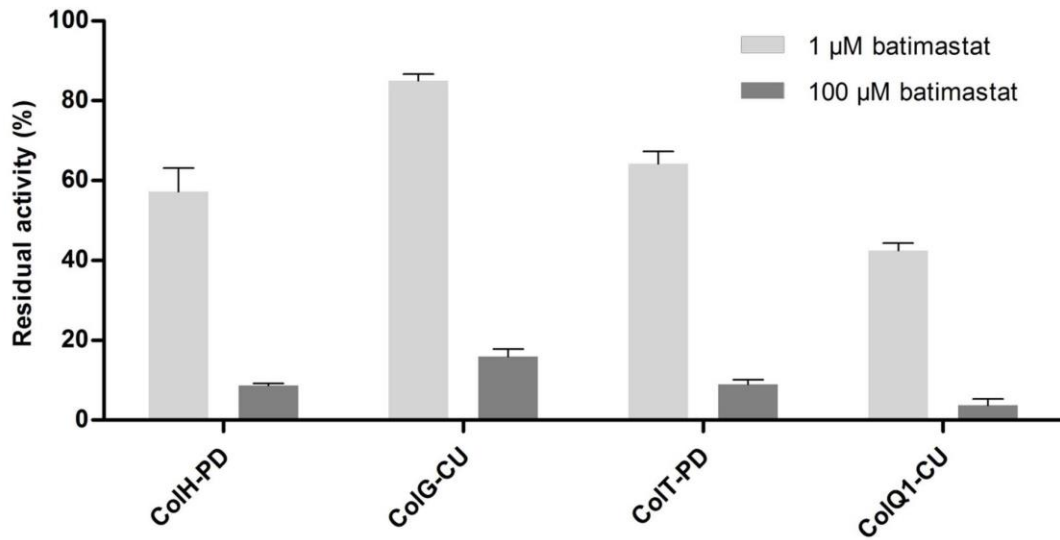


Figure S4. Inhibition of bacterial collagenases by batimastat.

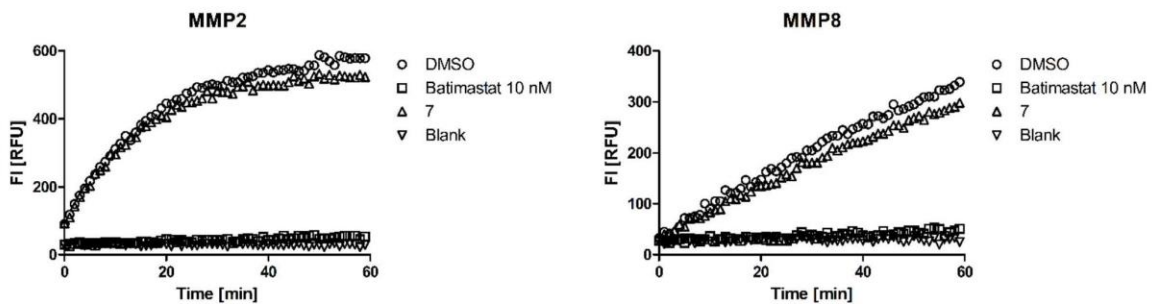


Figure S5. MMP inhibition assay. Exemplary representation of fluorescence intensity curves indicating protease activity of MMP-2 and -8. The influence of selected compounds on MMP activity is shown. The fluorescence intensity at 520 nm was determined every 60 s for a period of one hour.

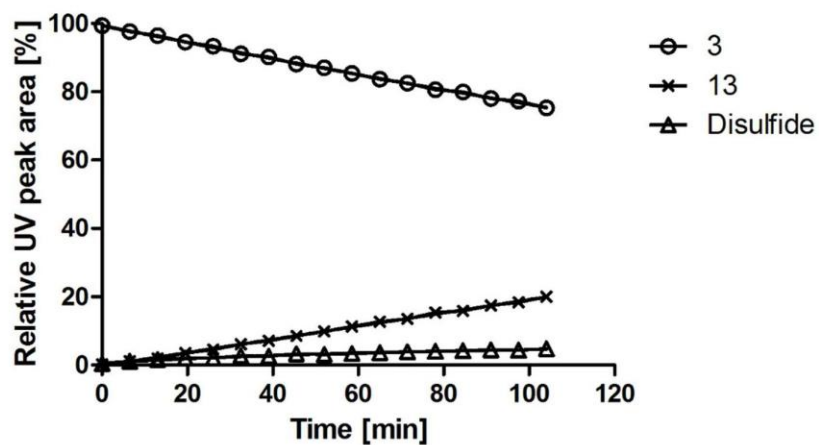


Figure S6. LC-MS stability assay of cp. 3 in 10 mM MES pH 7.4 (10% methanol) at 22.5°C.

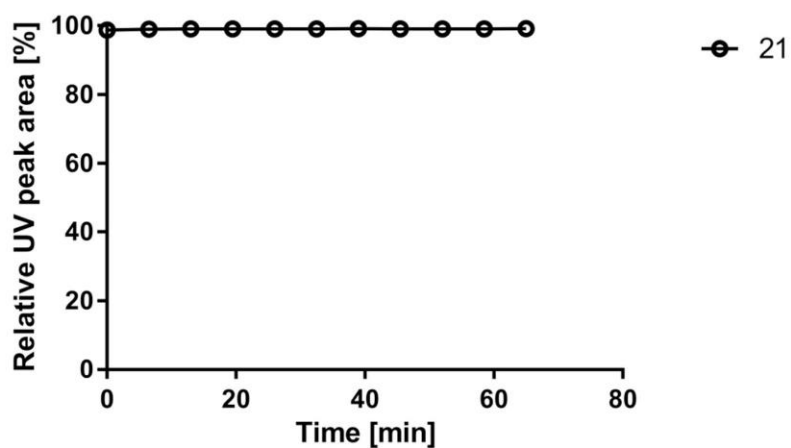
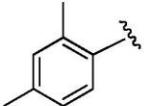
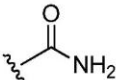
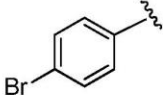
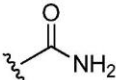
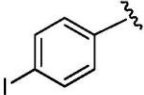
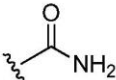
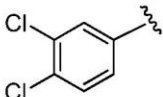
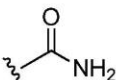
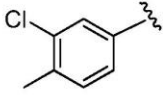
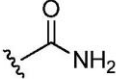
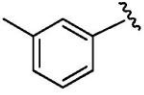
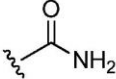
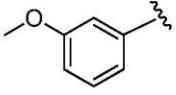
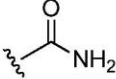
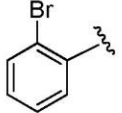
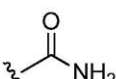
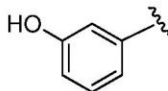
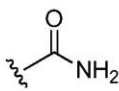
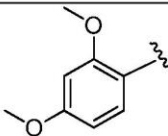
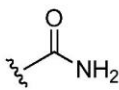
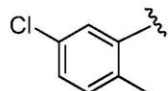
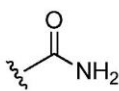
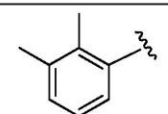
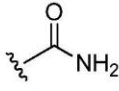
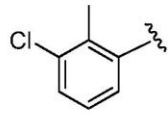
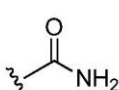
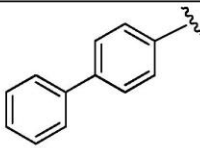
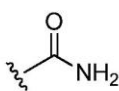
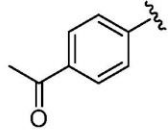
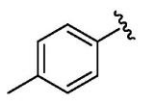
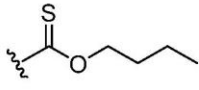


Figure S7. LC-MS stability assay of dithiocarbamate 21 in 10 mM HEPES pH 7.4 (10% methanol) at 22.5°C, illustrating that the dithiocarbamates are stable within the experimental time frame as no hydrolysis to the corresponding free thiol 13 occurs.

**Table S1.** Structure and activity of thiocarbamates and related compounds.

$\text{R}_1\text{-N}(\text{H})\text{-C(=O)-CH}_2\text{-S-R}_2$			
Compound	R <sub>1</sub>	R <sub>2</sub>	Inhibition at 100 μM (%)
22			90 ± 3
23			89 ± 5
24			89 ± 2
25			86 ± 2
26			85 ± 2
27			75 ± 1
28			72 ± 1
29			71 ± 4

30			$69 \pm 2$
31			$68 \pm 6$
32			$49 \pm 6$
33			$44 \pm 6$
34			$39 \pm 9$
35			$28 \pm 10$
36			$13 \pm 3$
37			no inhibition

**Table S2.** IC<sub>50</sub> values of batimastat towards MMP-1, -2, -3, -7, -8 and -14

	IC <sub>50</sub> (nM)
MMP-1	2.2 ± 0.1
MMP-2	1.8 ± 0.1
MMP-3	5.6 ± 0.9
MMP-7	7.0 ± 0.2
MMP-8	0.7 ± 0.2
MMP-14	2.8 ± 0.2

**Table S3.** Data collection and refinement statistics for ColH-PD in complex with compound **3**.

Data collection	
<b>Space Group</b>	<b>P 1 2<sub>1</sub> 1</b>
<b>Cell dimensions</b>	
<b>a (Å)</b>	<b>51.3</b>
<b>b (Å)</b>	<b>79.7</b>
<b>c (Å)</b>	<b>57.0</b>
<b>α (°)</b>	<b>90.0</b>
<b>β (°)</b>	<b>91.2</b>
<b>γ (°)</b>	<b>90.0</b>
<b>Wavelength (Å)</b>	<b>0.97623</b>
<b>Resolution range (Å)</b>	<b>46.33 - 1.87 (1.937 - 1.87)<sup>a</sup></b>
<b>R<sub>merge</sub></b>	<b>0.083 (0.636)</b>
<b>Mean I/sigma(I)</b>	<b>8.7 (1.9)</b>
<b>Completeness (%)</b>	<b>99.6 (99.8)</b>
<b>Multiplicity</b>	<b>3.5 (3.6)</b>
<b>CC1/2</b>	<b>0.998 (0.771)</b>
<b>CC*</b>	<b>0.999 (0.933)</b>
<b>Wilson B-factor</b>	<b>21.73</b>

Refinement	
Resolution range (Å)	46.33 - 1.87 (1.937 - 1.87)
No. of unique reflections	37834 (3810)
R <sub>work</sub> /R <sub>free</sub>	0.1903/0.2264
No. of non-hydrogen atoms	3258
Protein	3129
Ligand	16
Solvent	113
B factors	
Protein	25.70
Ligand	29.00
Solvent	23.80
RMSD	
Bond lengths (Å)	0.005
Bond angles (°)	0.82
Ramachandran favoured (%)	99.5
Ramachandran allowed (%)	0.5
Ramachandran outliers (%)	0.0

<sup>a</sup> Statistics for the highest-resolution shell are shown in parentheses.

## 2. Experimental Section

**Protein Expression and Purification of ColH-PD.** The peptidase domain of ColH (Uniprot: Q46085; Leu331-Gly721) was expressed and purified as published previously<sup>1</sup>. The homogeneous protein, as judged by SDS-PAGE and size-exclusion chromatography, was flash-frozen in thin-walled PCR tubes at 12.3 mg/mL concentration in 10  $\mu$ L aliquots in 10 mM Hepes pH 7.5, 100 mM NaCl, 1 mM CaCl<sub>2</sub>, 3% (v/v) glycerol, and 3 mM NaN<sub>3</sub>. For functional assays, the protein samples were prepared immediately before usage. After thawing, the protein solution was clarified by centrifugation at 13,000 g at 4°C for 30 min and protein concentrations were determined by UV<sub>280</sub> measurements using the molar extinction coefficient calculated by ProtParam ( $\epsilon = 77130 \text{ M}^{-1} \text{ cm}^{-1}$ )<sup>2</sup>.

**Screening Library.** The screening library comprising 1,520 low-molecular weight compounds was purchased from TimTec (Newark, DE, USA). The compounds had an average molecular weight (MW) of 390 Da and were provided as 10 mM stock solutions in DMSO.

**SPR-based Primary Screening.** The surface plasmon resonance experiments were performed using a Reichert SR 7500DC equipped with CMD500m sensor chip (Xantec Bioanalytics, Düsseldorf, Germany). For immobilization, standard amine coupling chemistry was applied. Both channels were activated for 7 min with a mixture of 0.1 M NHS (*N*-hydroxysuccinimide) and 0.1 M EDC (3-(Ethyl-iminomethyleneamino)-*N,N*-dimethylpropan-1-amine) at a flow rate of 10  $\mu$ L/min. The peptidase domain of ColH (1 mg/mL; 45.8 kDa; crystallization grade) was diluted 1:20 in 10 mM sodium acetate buffer pH 4.0 and coupled to the sensor surface via standard amine coupling chemistry on one of the channels to 15-20,000  $\mu$ RIU. Flow cell 2 was left blank to serve as a reference surface. Both channels were blocked with a 3 min injection of 1 M ethanolamine, pH 8.0. The 1,520 analytes were diluted in running buffer (10 mM Hepes pH 7.4, 150 mM NaCl, 0.005 % (v/v) Tween 20, 5 % (v/v) DMSO) to a final concentration of 100  $\mu$ M. The screening was run at 18 °C and a flow rate of 50  $\mu$ L/min. An initial series of buffer injections was carried out on both flow cells to equilibrate the system. Each cycle consisted of a 60 s injection of 100  $\mu$ M analyte, followed by a 120 s dissociation phase. Every 12 injections included 500  $\mu$ M FALGPA (*N*-[3-(2-furyl)acryloyl]-Leu-Gly-Pro-Ala) as positive and 100  $\mu$ M ampicillin as negative control. All screening experiments comprised two seven-point DMSO injections, to produce a DMSO calibration curve in order to correct differences in solvent effects on empty and target surface. They consisted of 60 s injections ranging from 4.25 to 5.75 % (v/v) DMSO. Data were zeroed, referenced, and calibrated using Scrubber 2.0 software. SPR responses, expressed in refractive index units [ $\mu$ RIU] that were used for analysis correspond to the corrected response recorded 45 s after start of the injection.

**Determination of Kinetic Parameters.** Steady state measurements were used to determine  $K_M$  for the custom-made FRET substrate Mca-Ala-Gly-Pro-Pro-Gly-Pro-Dpa-Gly-Arg-NH<sub>2</sub> (FS1-1) (Mca = (7-Methoxycoumarin-4-yl)acetyl; Dpa = *N*-3-(2,4-dinitrophenyl)-L-2,3-diaminopropionyl). The substrate was dissolved in DMSO. The enzymatic reaction was started by adding

ColH-PD to a final concentration of 2, 4, and 6 nM. The final reaction buffer contained 250 mM Hepes pH 7.5, 400 mM NaCl, 10 mM CaCl<sub>2</sub>, 10 μM ZnCl<sub>2</sub>, 2% DMSO, and 2.5 – 120 μM substrate. Cleavage of the substrate was followed by measuring the fluorescence signal every 5 s for 2 min (Excitation: 328 nm, Emission: 392 nm) in an Infinite M200 plate reader (Tecan, Grödig, Austria) at 25°C. The initial velocity was determined from the progress curves (<10% substrate conversion) using regression analysis<sup>3</sup> and inner filter effect-correction<sup>4</sup>. The  $\epsilon_{\text{ex}328}$  and  $\epsilon_{\text{em}392}$  were estimated in the buffer used for the kinetic assays to be 21794 M<sup>-1</sup> cm<sup>-1</sup> and 9561 M<sup>-1</sup> cm<sup>-1</sup>.  $K_M$  and  $k_{\text{cat}}$  were calculated by non-linear regression from the resulting Michaelis – Menten plot using GraphPad Prism 5 (Graph Pad Software, San Diego, CA, USA).

**FRET-Based Inhibition Assay.** In the secondary screening, ColH-PD was pretreated with the compounds for 1 h at room temperature. The reaction was initiated by the addition of 5 μM FS1-1. The increase in fluorescence was monitored for 2 min (Excitation: 328 nm, Emission: 392 nm) at 25°C. The final concentrations were 50 nM ColH-PD, 40 μM compound or isoamylphosphonyl-Gly-Pro-Ala, 250 mM Hepes pH 7.5, 400 mM NaCl, 10 mM CaCl<sub>2</sub>, 10 μM ZnCl<sub>2</sub>, and 2% DMSO. In case of poor compound solubility, the DMSO concentration was increased, but never exceeded 4.8%. The percentage of enzyme inhibition was calculated in relation to a reference without a compound added, only plus buffer control. For IC<sub>50</sub> measurements, the experiments were performed as described above, but using 10 nM ColH-PD, 2 μM FS1-1, 2% DMSO and employing 8 different compound concentrations. The compound concentrations were chosen to be evenly distributed above and below the estimated IC<sub>50</sub>. All experiments were performed in triplicates and repeated at least three times. IC<sub>50</sub> values were determined using non-linear regression with a constant Hill slope of -1. In case of tight binding conditions ( $E_T \approx K_{i(\text{app})}$ ), the initial velocities were fit to the Morrison equation<sup>5</sup>. Enzyme concentration was held at a constant value  $E_T = 10$  nM (when  $K_{i(\text{app})} > E_T$ ), whereas  $v_0$  and  $K_{i(\text{app})}$  were treated as adjustable parameters<sup>6</sup>. IC<sub>50</sub> values are given as mean values of three independent experiments ± standard deviation. Reported apparent inhibition constants ( $K_{i(\text{app})}$ ) were measured under first-order conditions ( $S_0 \ll K_M$ ) and with  $K_{i(\text{app})}/E_T > 10^7$  and in the presence of 3.5% DMSO. Measurements under reducing conditions were performed in the presence of 5 mM TCEP. Regression analysis was performed using GraphPad Prism 5 (Graph Pad Software, San Diego, CA, USA) and DYNAFIT (BioKin, Ltd., Madison, WI, USA).

**Bacterial Collagenase Inhibition Assay.** These assays were performed as described above for the IC<sub>50</sub> measurements using 100 μM of the indicated compounds. The final enzyme concentrations used were 10 nM ColH-PD, 30 nM ColT-PD, 40 nM ColG-CU, and 2 nM ColQ1-CU, respectively.

**Human matrix metalloproteinases (MMP) inhibition assay.** The catalytic domains of MMP-1, -2, -3, -7, -8 and -14 along with the Sensolyte 520 Generic MMP Activity Kit were purchased from AnaSpec (Fremont, CA, USA). The assay was performed according to the guidelines of the manufacturer. Fluorescence signals were measured in a CLARIOstar plate reader (BMG LABTECH, Ortenberg, Germany) every 60 s for a period of 1 h. Compounds synthesized by us were tested at 100 μM. IC<sub>50</sub> values

were determined for the hydroxamate-based peptidomimetic batimastat which was used as a positive control. The calculation of the  $IC_{50}$  value was performed by plotting the percent inhibition vs. the different inhibitor concentrations on a semi-log plot. At least three independent measurements were performed for each compound.

**Isothermal Titration Calorimetry (ITC).** ITC experiments were carried out using an ITC200 instrument (Microcal Inc., GE Healthcare). Final ligand concentrations were obtained by dilution 1:20 (v/v) in the experimental buffer resulting in a final DMSO concentration of 5% (v/v). Protein concentration was determined by measuring the absorbance at 280 nm using the molar extinction coefficient calculated by ProtParam ( $\epsilon = 77130 \text{ M}^{-1} \text{ cm}^{-1}$ )<sup>2</sup> DMSO concentration in the protein solution was adjusted to 5% (v/v). ITC measurements were routinely performed at 25 °C in 10 mM Hepes pH 7.5, 100 mM NaCl, 1 mM  $\text{CaCl}_2$ , 3% (v/v) glycerol, and 3 mM  $\text{NaN}_3$ . Titrations were performed on 40-50  $\mu\text{M}$  ColH peptidase domain in the 200  $\mu\text{L}$  sample cell using 2  $\mu\text{L}$  injections of 250-500  $\mu\text{M}$  ligand solution every 180 s. Raw data was collected and the area under each peak was integrated. To correct for heats of dilution and mixing, the final baseline consisting of small peaks of the same size at the end of the experiment was subtracted.

Experimental data was fitted to a theoretical titration curve (one site binding model) using MicroCal Origin 7 software, with  $\Delta H$  (enthalpy change in kcal mol<sup>-1</sup>),  $K_A$  (association constant in M<sup>-1</sup>), and N (number of binding sites) as adjustable parameters. Thermodynamic parameters were calculated from equation  $\Delta G = \Delta H - T\Delta S = RT \ln K_A = -RT \ln K_D$  where  $\Delta G$ ,  $\Delta H$ , and  $\Delta S$  are the changes in Gibbs free energy, enthalpy, and entropy of binding, respectively. T is the absolute temperature, and R = 1.98 cal mol<sup>-1</sup> K<sup>-1</sup>. For every sample, at least two independent measurements were performed.

**LC-MS method.** The stability assay was performed measuring the UV254 chromatogram of 20  $\mu\text{M}$  thiocarbamate compound in 10 mM HEPES pH 7.5 or in 10 mM MES pH 6.4 in presence of 20  $\mu\text{M}$  caffeine as internal standard. Injections were performed every 6.5 minutes during 104 minutes in total. Samples of the respective free thiols to determine the retention time were analyzed before thiocarbamate injection using the same method. Compounds and ISTD were dissolved in MeOH and diluted 1:20 in assay buffer, respectively, giving a final volume of 200  $\mu\text{L}$  with a methanol concentration of 10% (v/v). The solution of internal standard in assay buffer was incubated at 22.5°C for at least 10 min before adding thiocarbamates. Measurements were started directly after compound addition.

The analyses were performed using a TF UltiMate 3000 binary RSLC UHPLC (Thermo Fisher, Dreieich, Germany) equipped with a degasser, a binary pump, an autosampler and a thermostated column compartment and a MWD, coupled to a TF TSQ Quantum Access Max mass spectrometer with heated electrospray ionization source (HESI-II). For gradient elution, a NUCLEODUR C18 Pyramid column (150 × 2 mm, 3  $\mu\text{m}$ , Macherey-Nagel, Düren, Germany) was used with a mobile phase consisting of acetonitrile containing 1‰ formic acid (FA; v/v; eluent A) and water containing 1‰ FA (v/v; eluent B) and a flow rate of 600  $\mu\text{L}/\text{min}$  under the following conditions: 0 – 0.5 min 10% A, 0.5 – 4 min 10 – 95% A, 4 – 5 min hold, 5 – 5.5 min 10% A for column equilibra-

tion giving a total run time of 5.5 min. The injection volume was 5  $\mu$ L. The divert valve was set to 1.5 min. Before injecting samples the column was equilibrated with 10% methanol (v/v) in assay buffer using this method.

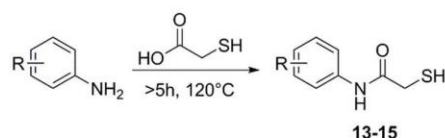
For UV detection we monitored the following wavelengths: 254 nm, 272 nm and 290 nm. The following MS conditions were used: electrospray ionization (ESI), positive mode, sheath gas, nitrogen at a flow rate of 60 arbitrary units; auxiliary gas, nitrogen at flow rate of 20 arbitrary units; vaporizer temperature, 300 °C; ion transfer capillary temperature, 350 °C; capillary offset, 15 V; spray voltage, 3500 V. The mass spectrometer was operated in the SIM mode with the following masses: caffeine  $m/z$  194.0 (tube lens offset 100 V), cp. 3  $m/z$  252.1, cp. 7/12  $m/z$  245.0 (tube lens offset 88 V), cp. 13  $m/z$  252.1, cp. 14/15  $m/z$  202.1 (tube lens offset 129 V) with a scan width of  $m/z$  2.0 and a scan time of 0.1 s, respectively. Three independent measurements were performed.

Observed retention times were as follows: caffeine 2.29 min, cp. 3 2.68, cp. 12 3.08 min, cp. 7 3.22 min, cp. 13 3.00 min, cp. 14 3.57 min, cp. 15 3.52 min. Additional peaks were found at 3.51 min, 4.32 min and 4.19 min for cp. 13, 14 and 15, respectively, hinting at disulfide formation. Peak areas were determined using TF Xcalibur Software. Peak areas were normalized by ISTD peak area and divided by total peak area. Half-life was determined using a one-phase decay model (GraphPad Prism 5 software).

**Cytotoxicity assay.** Hep G2 cells ( $2 \times 10^5$  cells per well) were seeded in 24-well, flat-bottomed plates. Culturing of cells, incubations and OD measurements were performed as described previously<sup>8</sup> with small modifications. 24 h after seeding the cells the incubation was started by the addition of compounds in a final DMSO concentration of 1%. The living cell mass was determined after 48 h. At least two independent measurements were performed for each compound.

**Co-Crystallization, X-ray Data Collection and Analysis.** Prior to crystallization, 4 mg/mL ColH-PD were preincubated with 260  $\mu$ M compound 3 in 8 mM Hepes pH 7.5, 33 mM NaCl, 0.33 mM CaCl<sub>2</sub>, and 2% DMSO for 1 h on ice and then clarified by centrifugation for 30 min at 13,000 g at 4°C. The co-crystal was grown by the sitting drop vapour diffusion method by mixing 1  $\mu$ L protein-inhibitor solution with 1  $\mu$ L reservoir solution. The reservoir contained 0.1 M MES pH 6.4, 25% w/v polyethylene glycol methyl ether 2000, and 50 mM NaCl. The drop was streak-seeded from crystals of unliganded ColH-PD<sup>9</sup>. Crystals appeared within several days. The crystals were cryoprotected with MiTeGen LV Cryo-oil (MiTeGen, Ithaca, NY) and immediately flash-frozen in liquid nitrogen. X-ray diffraction data were collected on beamline ID29 at the European Synchrotron Radiation Facility (ESRF) in Grenoble, France. The data set was processed using XDS<sup>10</sup> and AIMLESS<sup>11</sup>. The phase problem was solved by molecular replacement with PHASER<sup>12</sup> using a ColH-PD structure as search model (PDB code 4arf; ligand deleted). Final structures were obtained by several refinement cycles using PHENIX<sup>13</sup> interspersed with model building in WinCoot<sup>14</sup>. The PyMOL Molecular Graphics System, version 1.7.6.0, Schrodinger, LLC, was used for (i) figure generation, (ii) calculation of RMSD values (apo ColH-PD: 4ar1, MMP1: 3shi) and (iii) for comparison of ligand-bound edge strand conformations (MMP-1: 1hfc, MMP-2: 3ayu, MMP-3: 1b8y, MMP8: 1i76, MMP-12: 1jiz, MMP-13: 4jpp4, ColT: 4ar8, ColG: 2y6i)<sup>15</sup>. The final refined structure of ColH-PD in complex with compound 3 was deposited in the Protein Data Bank (PDB) as entry 5O7E.

**Chemistry. General Procedures.** Compounds **2-12** and **21-37** were commercially available (ChemBridge, San Diego, CA, USA). Synthesis of free thiols **13-15** was achieved by treating the respective anilines with thioglycolic acid in a neat reaction (see Scheme S1).<sup>16</sup> Selected thiocarbamates were synthesized according to the procedures described below.

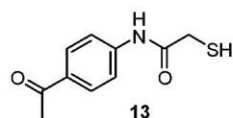


**Scheme S1.** Synthesis of free thiol compounds **13-15**.

All reagents were used from commercial suppliers without further purification. Procedures were not optimized regarding yield. NMR spectra were recorded on a Bruker Fourier 300 (300 MHz) spectrometer. Chemical shifts are given in parts per million (ppm) and referenced against the residual proton, <sup>1</sup>H, or carbon, <sup>13</sup>C, resonances of the >99% deuterated solvents as internal reference. Coupling constants (J) are given in Hertz. Data are reported as follows: chemical shift, multiplicity (s = singlet, d = doublet, t = triplet, m = multiplet, br = broad and combinations of these) coupling constants and integration. Mass spectrometry was performed on a SpectraSystems-MSQ LCMS system (Thermo Fisher, Dreieich, Germany). Flash chromatography was performed on silica gel 60 M, 0.04 - 0.063 mm (Machery-Nagel, Düren, Germany) or using the automated flash chromatography system CombiFlash Rf+ (Teledyne Isco, Lincoln, NE, USA) equipped with RediSepRf silica columns (Axel Semrau, Sprockhövel Germany) or Chromabond Flash C<sub>18</sub> columns (Macherey-Nagel, Düren, Germany). Purity of compounds synthesized by us was determined by LCMS using the area percentage method on the UV trace recorded at a wavelength of 254 nm and found to be >95%.

### Thiol synthesis

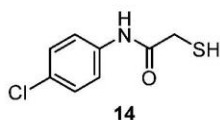
*N*-(4-acetylphenyl)-2-mercaptoacetamide (**13**)



4'-Aminoacetophenone (300 mg, 2.21 mmol) was placed in a crimp vial. The vial was evacuated and flushed with nitrogen three times, followed by addition of thioglycolic acid (160  $\mu$ L, 2.3 mmol). The vial was flushed with argon and heated to 120°C for 18 hours. The crude was purified by automated flash chromatography (petroleum ether:ethyl acetate 70:30 to 0:100) to yield the

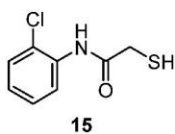
title compound as a white powder (50 mg, 11%).  $^1\text{H}$  NMR (300 MHz, Methanol- $d_4$ )  $\delta$  ppm 2.58 (s, 3 H), 3.34 (s, 2 H), 7.69 - 7.77 (m, 2 H), 7.95 - 8.03 (m, 2 H);  $^{13}\text{C}$  NMR (75 MHz, Methanol- $d_4$ )  $\delta$  ppm 26.61, 29.55, 120.32, 130.89, 134.09, 144.75, 172.04, 199.56; MS (ESI $^+$ )  $m/z$  210 (M+H) $^+$

*N*-(4-chlorophenyl)-2-mercaptoacetamide (**14**)



4-chloroaniline (200 mg, 1.57 mmol) was placed in a crimp vial. The vial was evacuated and flushed with nitrogen three times, followed by addition of thioglycolic acid (120  $\mu\text{L}$ , 1.72 mmol). The vial was flushed with argon and heated to 120°C for 5 hours. The crude was purified by flash chromatography (petroleum ether:ethyl acetate 90:10 to 70:30) to yield the title compound as a white powder (187 mg, 59%).  $^1\text{H}$  NMR (300 MHz, DMSO- $d_6$ )  $\delta$  ppm 2.97 (br s, 1 H) 3.29 (s, 2 H) 7.30 - 7.42 (m, 2 H) 7.53 - 7.68 (m, 2 H) 10.21 (s, 1 H);  $^{13}\text{C}$  NMR (75 MHz, DMSO- $d_6$ )  $\delta$  ppm 28.24, 120.61, 126.92, 128.67, 137.92, 168.72; MS (ESI $^+$ )  $m/z$  202 (M+H) $^+$

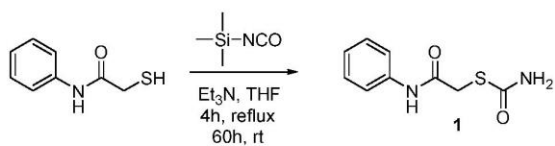
*N*-(2-chlorophenyl)-2-mercaptoacetamide (**15**)



2-chloroaniline (164  $\mu\text{L}$ , 1.57 mmol) was placed in a crimp vial. The vial was evacuated and flushed with nitrogen three times, followed by addition of thioglycolic acid (120  $\mu\text{L}$ , 1.72 mmol). The vial was flushed with argon and heated to 120°C for 5 hours. The crude was purified by automated flash chromatography (petroleum ether:ethyl acetate 70:30 to 50:50) to yield the title compound as a white powder (160 mg, 51%).  $^1\text{H}$  NMR (300 MHz, DMSO- $d_6$ )  $\delta$  ppm 3.02 (s, 1 H), 7.19 (dt,  $J$  = 7.6, 1.7 Hz, 1 H), 7.33 (dt,  $J$  = 7.6, 1.4 Hz, 1 H), 7.50 (dd,  $J$  = 8.0, 1.5 Hz, 1 H), 7.80 (dd,  $J$  = 8.1, 1.4 Hz, 1 H), 9.66 (br. s., 1 H),  $^{13}\text{C}$  NMR (75 MHz, DMSO- $d_6$ )  $\delta$  ppm 27.79, 125.23, 125.81, 126.20, 127.48, 129.45, 134.62, 168.93; MS (ESI $^+$ )  $m/z$  202 (M+H) $^+$

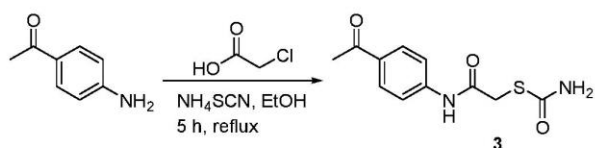
### Thiocarbamate synthesis

*S*-(2-oxo-2-(phenylamino)ethyl) carbamothioate (**1**)



Under nitrogen atmosphere, *N*-phenyl-2-mercaptoacetamide (209 mg, 1.25 mmol) was dissolved in 20 mL dry THF and triethylamine (200  $\mu$ L, 1.44 mmol) and trimethylsilyl isocyanate (200  $\mu$ L, 1.48 mmol) were added. The reaction mixture was refluxed for 4 hours and then stirred at room temperature for 60 hours. After that, the reaction was quenched for 30 min with methanol. The crude was purified using flash chromatography (petroleum ether:ethyl acetate 7:3) to yield the title compound as a white powder (50 mg, 19 %).  $^1\text{H}$  NMR (500 MHz,  $\text{DMSO-d}_6$ )  $\delta$  ppm 3.69 (s, 2H), 7.04 (t,  $J = 7.4$  Hz, 1H), 7.30 (t,  $J = 7.1$  Hz, 2H), 7.57 (dd,  $J = 8.4, 0.8$  Hz, 2H), 7.40-7.90 (b, 2H), 10.09 (s, 1H);  $^{13}\text{C}$  NMR (126 MHz,  $\text{DMSO-d}_6$ )  $\delta$  ppm 34.10, 119.03, 123.31, 128.75, 139.02, 166.24, 166.89; MS (ESI $^+$ )  $m/z$  211 (M+H) $^+$

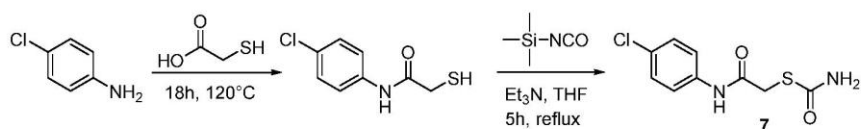
*S*-(2-((4-acetylphenyl)amino)-2-oxoethyl) carbamothioate (3)



Following the procedure described by Koulberg<sup>17</sup> 4'-Aminoacetophenone (200 mg, 1.5 mmol) was added to a solution of chloroacetic acid (140 mg, 1.5 mmol) and ammonium thiocyanate (90 mg, 1.5 mmol) in 5 mL absolute ethanol. The reaction was refluxed for 5 hours and then stirred at room temperature for 14 hours. Addition of water, followed by extraction with ethyl acetate gave the crude which was purified using automated flash chromatography (acetonitrile + 0.1% formic acid:water + 0.1% formic acid 5:95 to 70:30) to yield the title compound as a white powder (39 mg, 10%).

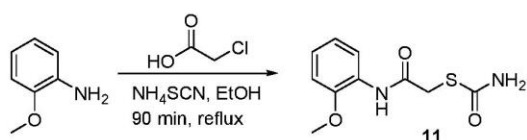
$^1\text{H}$  NMR (300 MHz,  $\text{DMSO-d}_6$ )  $\delta$  ppm 2.52 (s, 3 H), 3.74 (s, 2 H), 7.50 - 7.87 (br s, 2H), 7.67 - 7.74 (m, 2 H), 7.89 - 7.97 (m, 2 H), 10.46 (s, 1 H);  $^{13}\text{C}$  NMR (75 MHz,  $\text{DMSO-d}_6$ )  $\delta$  ppm 26.39, 34.19, 118.27, 129.48, 131.74, 143.28, 166.08, 167.52, 196.46; MS (ESI $^+$ )  $m/z$  253 (M+H) $^+$

*S*-(2-((4-chlorophenyl)amino)-2-oxoethyl) carbamothioate (7)



*N*-(4-chlorophenyl)-2-mercaptoacetamide (**14**) was prepared according to the described procedure and the crude was taken in 6 mL THF without further workup or purification. Triethylamine (260  $\mu$ L, 1.9 mmol) was added, followed by trimethylsilyl isocyanate (250  $\mu$ L, 1.9 mmol). The reaction mixture was kept under argon atmosphere and refluxed for 5 hours. After cooling to room temperature the reaction was quenched for 10 min with methanol. The crude was purified by flash chromatography (petroleum ether:ethyl acetate 75:25 to 50:50) to yield the title compound as a white powder (70 mg, 18% over two steps).  $^1\text{H}$  NMR (300 MHz, DMSO- $d_6$ )  $\delta$  ppm 3.69 (s, 2 H), 7.30 – 8.00 (br s, 2 H), 7.32 – 7.40 (m, 2 H), 7.57 – 7.65 (m, 2 H), 10.25 (s, 1 H);  $^{13}\text{C}$  NMR (75 MHz, DMSO- $d_6$ )  $\delta$  ppm 34.05, 120.57, 126.82, 128.63, 137.94, 166.10, 167.06; MS (ESI $^+$ )  $m/z$  245 (M+H) $^+$

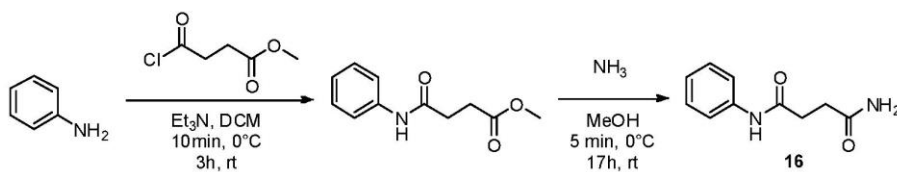
*S*-2-((2-methoxyphenyl)amino)-2-oxoethyl carbamothioate (**11**)



*O*-anisidine (380  $\mu$ L, 3.4 mmol) was added to a solution of chloroacetic acid (318 mg, 3.4 mmol) and ammonium thiocyanate (205 mg, 2.7 mmol) in 6 mL absolute ethanol. The reaction was refluxed for 1.5 hours until formation of a precipitate. Addition of water, followed by filtration gave the crude which was purified using automated flash chromatography (petroleum ether:ethyl acetate 80:20 to 0:100) to yield the title compound as a white powder (140 mg, 22%).

$^1\text{H}$  NMR (300 MHz, DMSO- $d_6$ )  $\delta$  ppm 3.69 (s, 2 H), 3.83 (s, 3 H), 6.84 – 6.95 (m, 1 H), 6.98 – 7.11 (m, 2 H), 7.59 – 8.00 (br s, 2 H), 8.04 (d,  $J = 7.5$  Hz, 1 H), 9.25 (s, 1 H);  $^{13}\text{C}$  NMR (75 MHz, DMSO- $d_6$ )  $\delta$  ppm 33.79, 55.80, 111.08, 120.34, 124.10, 127.28, 148.76, 166.29, 167.16; MS (ESI $^+$ )  $m/z$  240 (M+H) $^+$

*N*-phenylsuccinamide (**16**)



Methyl succinyl chloride (170  $\mu$ L, 1.4 mmol) was added dropwise over 5 min to a solution of aniline (100  $\mu$ L, 1.1 mmol) and triethylamine (300  $\mu$ L, 2.2 mmol) in dry dichloromethane at 0°C. After another 5 min, the reaction was allowed to warm up to room temperature and was stirred for 3 hours. Washing with sodium bicarbonate solution and evaporation of the solvent gave the crude which was purified using radial thin-layer chromatography (dichloromethane) to yield methyl-4-oxo-4-(phenylamino)butanoate as a white powder (222 mg, 98%).

$^1\text{H}$  NMR (500 MHz,  $\text{CDCl}_3$ )  $\delta$  ppm 2.66 (t,  $J = 6.5$  Hz, 2H), 2.75 (t,  $J = 6.5$  Hz, 2H), 3.70 (s, 3H), 7.09 (t,  $J = 7.4$  Hz, 1H), 7.30 (t,  $J = 7.9$  Hz, 2H), 7.50 (d,  $J = 7.9$  Hz, 2H), 7.71 (s, 1H);  $^{13}\text{C}$  NMR (126 MHz,  $\text{CDCl}_3$ )  $\delta$  ppm 29.37, 32.21, 52.13, 119.91, 124.36, 129.08, 137.98, 169.86, 173.80; MS (ESI $^+$ )  $m/z$  208 (M+H) $^+$

Methyl-4-oxo-4-(phenylamino)butanoate (26 mg, 0.13 mmol) was added to a 10% ammonia solution in methanol (9 mL) at 0°C. After addition, the reaction was allowed to warm up to room temperature and was stirred for 17 h. The reaction mixture was concentrated in air stream and the crude was purified using flash chromatography (dichloromethane:methanol:triethylamine 97:2:1) to give the title compound (29 mg, quant.).

$^1\text{H}$  NMR (500 MHz,  $\text{DMSO-d}_6$ )  $\delta$  ppm 2.38 (t,  $J = 7.2$  Hz, 2H), 2.38 (t,  $J = 7.2$  Hz, 2H), 6.76 (s, 1H), 7.00 (t,  $J = 7.4$  Hz, 1H), 7.27 (t,  $J = 7.9$  Hz, 2H), 7.33 (s, 1H), 7.58 (d,  $J = 7.7$  Hz, 2H), 9.92 (s, 1H);  $^{13}\text{C}$  NMR (126 MHz,  $\text{DMSO-d}_6$ )  $\delta$  ppm 29.96, 31.51, 118.87, 122.83, 128.63, 139.38, 170.55, 173.33; MS (ESI $^+$ )  $m/z$  215 (M+Na) $^+$

### Peptide synthesis

Solid-phase synthesis of the peptide Mca-Ala-Gly-Pro-Pro-Gly-Pro-Dpa-Gly-Arg-amide (with Mca = 7-methoxycoumarin-4-acetyl and Dpa = Dap(Dnp) = N-beta-2,4-dinitrophenyl-L-2,3-diaminopropionyl) was carried out on a scale of 100  $\mu\text{mol}$  with a Syro Multiple Peptide Synthesizer (MultiSynTech, Witten, Germany) on Rapp S RAM resin (Rapp Polymere, Tübingen, Germany) for the generation of the C-terminal amide. Fmoc chemistry with TBTU / diisopropylethyl amine activation with tenfold excess was employed for the coupling of the amino acids. Coupling time was 1 hour. Side chain protection of arginine was Pbf. After assembly of the peptide chain Mca was coupled in a threefold excess with activation by TBTU / diisopropylethyl amine in DMF over 3 hours at room temperature. The crude peptide was cleaved from the resin and deprotected by a 3 hour treatment with TFA containing 3% triisopropylsilane and 2% water (10 mL/g resin). After precipitation with *t*-butylmethyl ether, the resulting crude peptide was purified by preparative HPLC on C18 material with water/acetonitrile gradients containing 0.1% TFA and characterized by analytical HPLC and MALDI-MS. The final product was lyophilized from water. For the calculation of the concentration of stock solutions of the peptide one counter ion of trifluoroacetic acid (mol. weight 114.02) was taken into account. Yield: 56 mg (44.6  $\mu\text{mol}$ ).

### 3. References

- (1) Eckhard, U.; Schönauer, E.; Brandstetter, H. *J. Biol. Chem.* **2013**, *288*, 20184–20194.
- (2) Gasteiger, E.; Hoogland, C. In *The Proteomics Protocols Handbook*; Humana Press Inc: Totowa, NJ, 2005; pp 571–607.
- (3) Briers, Y.; Lavigne, R.; Volckaert, G.; Hertveldt, K. *J. Biochem. Biophys. Methods* **2007**, *70*, 531–533.
- (4) Liu, Y.; Kati, W.; Chen, C.-M.; Tripathi, R.; Molla, A.; Kohlbrenner, W. *Anal. Biochem.* **1999**, *267*, 331–335.
- (5) Williams, J.; Morrison, J. *Methods Enzymol.* **1979**, *63*, 437–467.
- (6) Kuzmic, P.; Elrod, K. C.; Cregar, L. M.; Sideris, S.; Rai, R.; Janc, J. W. *Anal. Biochem.* **2000**, *286*, 45–50.
- (7) Copeland, R. A. *Methods Biochem. Anal.* **2005**, *46*, 1–265.
- (8) Hauptenthal, J.; Baehr, C.; Zeuzem, S.; Piiper, A. *Int. J. Cancer* **2007**, *121*, 206–210.
- (9) Stura, E. A.; Wilson, I. A. *J. Cryst. Growth* **1991**, *110*, 270–282.
- (10) Kabsch, W. *Acta Crystallogr. D. Biol. Crystallogr.* **2010**, *66*, 125–132.
- (11) Evans, P. R.; Murshudov, G. N. *Acta Crystallogr. Sect. D Biol. Crystallogr.* **2013**, *69*, 1204–1214.
- (12) McCoy, A. J. *Acta Crystallogr. D. Biol. Crystallogr.* **2007**, *63*, 32–41.
- (13) Adams, P. D.; Afonine, P. V.; Bunkóczi, G.; Chen, V. B.; Davis, I. W.; Echols, N.; Headd, J. J.; Hung, L.-W.; Kapral, G. J.; Grosse-Kunstleve, R. W.; McCoy, A. J.; Moriarty, N. W.; Oeffner, R.; Read, R. J.; Richardson, D. C.; Richardson, J. S.; Terwilliger, T. C.; Zwart, P. H. *Acta Crystallogr. Sect. D, Biol. Crystallogr.* **2010**, *66*, 213–221.
- (14) Emsley, P.; Lohkamp, B.; Scott, W. G.; Cowtan, K. *Acta Crystallogr. Sect. D, Biological Crystallogr.* **2010**, *66*, 486–501.
- (15) DeLano, W. L. The PyMOL Molecular Graphics System, Version-1.3r1, 2010.
- (16) Shaitanov, P. V.; Lukashov, S. S.; Turov, O. V.; Yarmoluk, S. M. *Ukr. Bioorganica Acta* **2007**, *5*, 56–61.

**3.2 Chapter B: Binding Mode Characterization and Early *in Vivo* Evaluation of Fragment-Like Thiols as Inhibitors of the Virulence Factor LasB from *Pseudomonas aeruginosa*<sup>188</sup>**

Kany, A. M. †; Sikandar, A. †; Hauptenthal, J.; Yahiaoui, S.; Maurer, C. K.; Proschak, E.; Köhnke, J.; Hartmann, R. W.

† these authors contributed equally

Reprinted with permission from *ACS Infect. Dis.* **2018**, DOI:10.1021/acsinfecdis.8b00010.  
[Epub ahead of print]

Copyright (2018) American Chemical Society

## Binding Mode Characterization and Early *in Vivo* Evaluation of Fragment-Like Thiols as Inhibitors of the Virulence Factor LasB from *Pseudomonas aeruginosa*

Andreas M. Kany,<sup>†,‡,⊥</sup> Asfandyar Sikandar,<sup>‡,⊥</sup> Jörg Haupenthal,<sup>†,⊥</sup> Samir Yahiaoui,<sup>†,⊥</sup> Christine K. Maurer,<sup>†</sup> Ewgenij Proschak,<sup>||,⊥</sup> Jesko Köhnke,<sup>‡,⊥</sup> and Rolf W. Hartmann<sup>\*,†,§,⊥</sup>

<sup>†</sup>Department of Drug Design and Optimization, Helmholtz Institute for Pharmaceutical Research Saarland (HIPS), Campus E8.1, 66123, Saarbrücken, Germany

<sup>‡</sup>Workgroup Structural Biology of Biosynthetic Enzymes, Helmholtz Institute for Pharmaceutical Research Saarland (HIPS), Campus E8.1, 66123, Saarbrücken, Germany

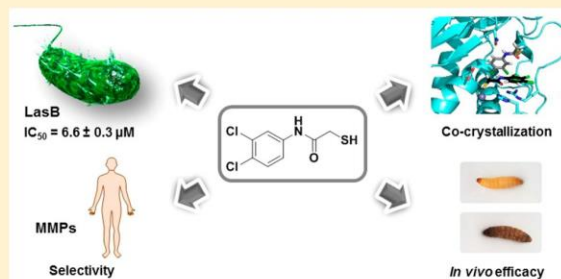
<sup>§</sup>Department of Pharmacy, Pharmaceutical and Medicinal Chemistry, Saarland University, Campus E8.1, 66123, Saarbrücken, Germany

<sup>||</sup>Institute of Pharmaceutical Chemistry, Goethe University Frankfurt, Max-von-Laue-Straße 9, 60438, Frankfurt, Germany

### Supporting Information

**ABSTRACT:** The increasing emergence of antibiotic resistance necessitates the development of anti-infectives with novel modes of action. Targeting bacterial virulence is considered a promising approach to develop novel antibiotics with reduced selection pressure. The extracellular collagenase elastase (LasB) plays a pivotal role in the infection process of *Pseudomonas aeruginosa* and therefore represents an attractive antivirulence target. Mercaptoacetamide-based thiols have been reported to inhibit LasB as well as collagenases from clostridia and bacillus species. The present work provides an insight into the structure–activity relationship (SAR) of these fragment-like LasB inhibitors, demonstrating an inverse activity profile compared to similar inhibitors of clostridial collagenase H (ColH). An X-ray cocrystal structure is presented, revealing distinct binding of two compounds to the active site of LasB, which unexpectedly maintains an open conformation. We further demonstrate *in vivo* efficacy in a *Galleria mellonella* infection model and high selectivity of the LasB inhibitors toward human matrix metalloproteinases (MMPs).

**KEYWORDS:** antibiotic resistance, antivirulence agent, elastase, LasB, binding mode, selectivity, *Galleria mellonella*



The increasing emergence of resistant bacteria poses a threat to public health, especially in the case of Gram-negative species.<sup>1,2</sup> *Pseudomonas aeruginosa* is one of the three most problematic pathogens on the WHO priority list.<sup>1</sup> It is the reason for many hospital-acquired infections as well as fatal lung infections in cystic fibrosis and bronchiectasis patients.<sup>3,4</sup> To combat the rise of antibiotic-resistant *Pseudomonas aeruginosa* infections, novel treatment options are urgently needed.<sup>5,6</sup>

A promising new approach to reduce selection pressure is to target bacterial virulence in order to disarm pathogens rather than to kill them.<sup>7–10</sup> *Pseudomonas aeruginosa* produces numerous virulence factors contributing to disease progression, which provide attractive anti-infective targets.<sup>11–14</sup> The extracellular collagenase elastase (LasB) is a major virulence factor, playing a crucial role for the pathogenicity of *P. aeruginosa*.<sup>15</sup> The enzyme is a zinc–metalloprotease with high structural similarity to thermolysin.<sup>16,17</sup> One of its main functions is the cleavage of components of the connective tissue

like elastin<sup>15</sup> or collagen<sup>18</sup> to allow the bacteria to colonize a niche in the host. Tissue damage is further caused by disruption of cell-to-cell junctions.<sup>19,20</sup> Additionally, LasB enables *P. aeruginosa* to evade the human immune response by cleaving, i.e., IgG,<sup>21</sup> cytokines,<sup>22</sup> surfactant proteins A and D,<sup>23</sup> complement factor C3,<sup>24</sup> or pulmonary defense receptor PAR2.<sup>25</sup> Consequently, this protease represents an attractive anti-infective target and its extracellular localization facilitates drug discovery as permeation of the Gram-negative cell wall is not needed.<sup>9,26</sup>

LasB belongs to the thermolysin (M4) family of enzymes.<sup>27</sup> For this class, it has been reported that the rather open active site cleft of the protease adopts a more closed conformation upon inhibitor binding.<sup>28</sup> To date, several zinc-chelating inhibitors of LasB have been described,<sup>29–32</sup> including

Received: January 8, 2018

Published: February 27, 2018

compounds bearing a mercaptoacetamide motif attached either to small peptides<sup>33</sup> or to aniline.<sup>34</sup> Crystallographic data shedding light on the binding mode of these thiols to the protease has not been available yet. We have recently described *N*-aryl mercaptoacetamide-based compounds as very potent clostridial collagenase inhibitors with high selectivity toward human matrix metalloproteinases (MMPs).<sup>35</sup> The compounds contain a prodrug-like thiocarbamate-motif, which liberates free thiols as the active form after hydrolysis in buffer. The best collagenase H (ColH) inhibitor **1** (Figure 1) was also found to inhibit LasB.

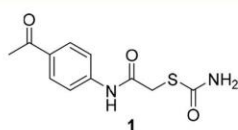


Figure 1. Structure of most potent ColH inhibitor **1**.

In this work, we report a functional screening followed by LC-MS validation for LasB inhibition of the focused TimTec ActiTarget-P library previously used to discover the ColH inhibitors. The only inhibitor resulting from the screening was an *N*-aryl mercaptoacetamide. Encouraged by the promising inhibitory activity and selectivity, we wanted to gain further insight into LasB inhibition by this compound class. We describe the activity and selectivity profiles of a broad range of *N*-aryl mercaptoacetamides. An X-ray crystal structure of a mercaptoacetamide-based inhibitor in complex with LasB is presented revealing an unprecedented open conformation of the active site, which harbors two inhibitor molecules. To the best of our knowledge, this is the first description of inhibitor binding to LasB which does not lead to a closure of the active site cleft.

## RESULTS AND DISCUSSION

**Screening for Novel LasB Inhibitors.** In order to expand the chemical space of LasB inhibitors, we performed a functional screening based on the FRET-based *in vitro* assay developed by Nishino and Powers.<sup>36</sup> We used a protease inhibitor-enriched library which, after removing structures known as PAINS,<sup>37</sup> comprised 1192 low molecular weight compounds. In addition, we included 330 fragments (Maybridge Fragment Library) into the screening. The only compound showing more than 50% inhibition when tested at 100  $\mu$ M was mercaptoacetamide **2** (Figure 2). Several false-positive hits had to be excluded because of quenching of substrate fluorescence.

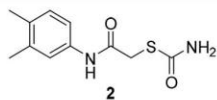


Figure 2. Structure of screening hit **2**.

**Development of an LC-MS-Based Readout for the FRET Assay.** In the FRET-based proteolytic assay, active LasB cleaves a quenched substrate, which results in an increase of fluorescence.<sup>36</sup> Enzyme inhibition leads to reduced substrate cleavage and consequently to reduced fluorescence. However, compounds interfering with the fluorophore by quenching effects<sup>38</sup> can pretend enzyme inhibition, resulting in false-

positive hits.<sup>39,40</sup> Several quenching compounds were found, especially among fragments. To clarify if reduced fluorescence was caused by protease inhibition or to quenching effects, we developed an LC-MS-based readout for the FRET Assay. Elastase cleaves the synthetic substrate Abz-Ala-Gly-Leu-Ala-Nba (**3**) at the Gly-Leu bond,<sup>36,41</sup> forming cleavage products **4** and **5** (Figure 3A) which could be separated chromatographically. Using the published LasB inhibitor phosphoramidon<sup>42</sup> as a positive control, the FRET assay results were excellently reproduced using an LC-MS-based readout which was based on the mass peak of cleavage product **5** (Figure S1). Applying this technology, we could detect several false positives whose apparent inhibition in the FRET assay was only due to quenching. Two examples are shown in Figure 3B.

**Structure–Activity Relationship of *N*-Aryl Mercaptoacetamides.** To elucidate the structure–activity relationship (SAR) of *N*-aryl mercaptoacetamides, 35 derivatives were purchased or synthesized (for further information, see the Supporting Information) and tested for LasB inhibition applying the FRET-based *in vitro* assay (Tables 1 and S1). Nonpolar aromatic substituents, especially halogens, turned out to be favorable for activity while polar hydrogen-bond accepting moieties led to significantly reduced inhibition. For the *o*-, *m*-, and *p*-Cl derivatives **9**, **12**, and **17** as well as *m*- and *p*-CH<sub>3</sub> derivatives **13** and **21**, no substantial effect of the substitution position on activity was found. The same holds true for the methoxy (**11**, **15**, **23**) and *o*- and *p*-phenyl (**10**, **18**) analogues. Introduction of a second substituent improved the IC<sub>50</sub> at least 2-fold. Addition of methyl or chlorine substituents to **17** resulted in the best compounds **26**, **27**, and **28**, displaying IC<sub>50</sub> values in the one-digit micromolar range. An exception is dimethoxy derivative **32**, which showed an activity similar to the monomethoxy analogues **11**, **15**, and **23**. In comparison to the initial screening hit **2**, the activity could be improved by more than 2.5-fold. Two examples showed that the introduction of a third substituent was not beneficial for inhibition: Introduction of a methyl group to compound **26** led to a 2-fold drop in activity (**34**), while no difference was observed between di- and trimethyl derivatives **29** and **33**.

**Comparison to the SAR for ColH Inhibition.** Interestingly, the here reported SAR shows an inverse activity profile of the *N*-aryl mercaptoacetamides compared to ColH. We previously reported polar, hydrogen bond-accepting substituents, especially in *para*-position to the aniline function, to be most potent for ColH inhibition.<sup>35</sup> Contrary to that, oxygen-containing compounds like, e.g., the methoxy-derivatives **11**, **15**, **23**, and **32** showed considerably weaker LasB inhibition compared to their halogen-substituted analogs. Strikingly, our best ColH inhibitor **1** is one of the weakest inhibitors described in this study. The position of the substituent substantially affects inhibition of ColH but not of LasB.

**Confirmation of Thiols as Active Compounds.** As previously described,<sup>35</sup> thiocarbamates are rapidly cleaved to the corresponding free thiols in aqueous buffers (Figure 4A). Consequently, to confirm that the observed weaker activity on LasB compared to clostridial collagenases was not due to slower hydrolysis in LasB assay buffer, we performed the recently reported LC-MS-based stability test. Fast hydrolysis of **17** in 50 mM Tris, pH 7.2, was observed with a thiocarbamate half-life of  $3.7 \pm 0.1$  min (Figure 4B). A third component was formed which is most likely the disulfide oxidation product. Compound hydrolysis proceeded faster than described for the ColH assay

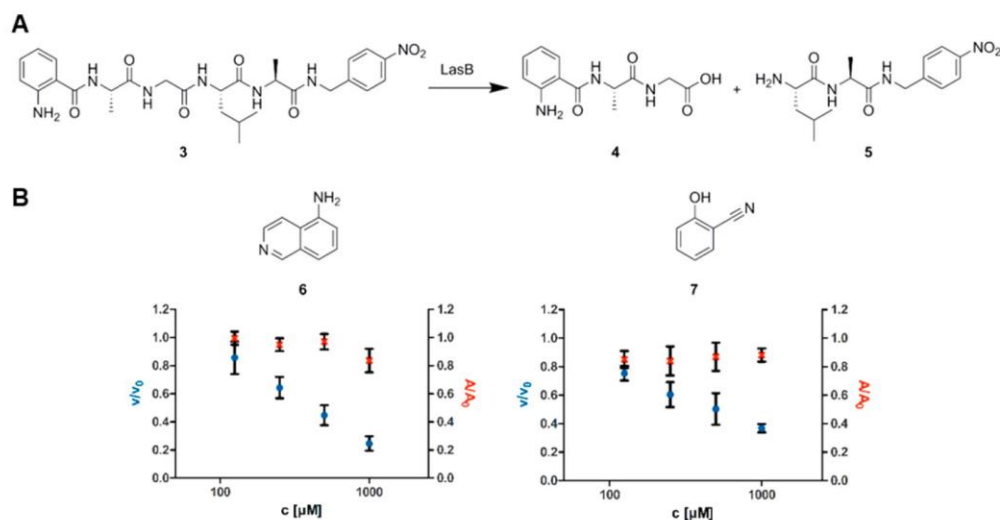


**Figure 3.** (A) Cleavage of FRET substrate Abz–Ala–Gly–Leu–Ala–Nba (3) into products 4 and 5 by LasB. Abz = 2-aminobenzoyl; Nba = 4-nitrobenzylamide. (B) Structure and comparison of FRET (blue,  $v/v_0$ ) vs LC-MS results (red,  $A/A_0$ ) for fragments 6 and 7.

**Table 1. Chemical Structures and LasB Inhibition of a Series of *N*-aryl Mercaptoacetamides**

Cp.	R	IC <sub>50</sub> (μM)	Cp.	R	IC <sub>50</sub> (μM)	Cp.	R	IC <sub>50</sub> (μM)
8	2-Br	11.4 ± 0.2	17	4-Cl	15.7 ± 0.4	26	2-CH <sub>3</sub> -3-Cl	5.9 ± 0.3
9	2-Cl	14.1 ± 0.5	18	4-Ph	19.8 ± 1.4	27	3,4-di-Cl	6.2 ± 0.3
10	2-Ph	25.0 ± 0.8	19	4-Br	22.8 ± 1.1	28	2-CH <sub>3</sub> -5-Cl	7.2 ± 0.2
11	2-OCH <sub>3</sub>	51.7 ± 4.0	20	4-I	32.9 ± 1.3	29	2,4-di-CH <sub>3</sub>	12.1 ± 0.4
12	3-Cl	19.4 ± 0.5	21	4-CH <sub>3</sub>	36.1 ± 0.7	30	2,3-di-CH <sub>3</sub>	12.3 ± 0.4
13	3-CH <sub>3</sub>	47.5 ± 1.4	22	4-OC <sub>2</sub> H <sub>5</sub>	47.6 ± 1.1	2	3,4-di-CH <sub>3</sub>	16.0 ± 1.9
14	3-F	59.2 ± 0.9	23	4-OCH <sub>3</sub>	47.7 ± 1.0	31	3-Cl-4-CH <sub>3</sub>	16.3 ± 1.0
15	3-OCH <sub>3</sub>	61.7 ± 2.1	1	4-COCH <sub>3</sub>	73.1 ± 2.5	32	2,4-di-OCH <sub>3</sub>	54.0 ± 2.7
16	3-NHSO <sub>2</sub> CH <sub>3</sub>	127.2 ± 3.5	24	4-COOCH <sub>3</sub>	81.5 ± 2.5	33 <sup>a</sup>	2,4,6-tri-CH <sub>3</sub>	11.9 ± 0.4
			25	4-(CH <sub>2</sub> -1,2,4-triazole)	85.6 ± 2.3	34 <sup>a</sup>	3-Cl-2,6-di-CH <sub>3</sub>	11.9 ± 0.4

<sup>a</sup>Compounds 33 and 34 were synthesized as free thiols.

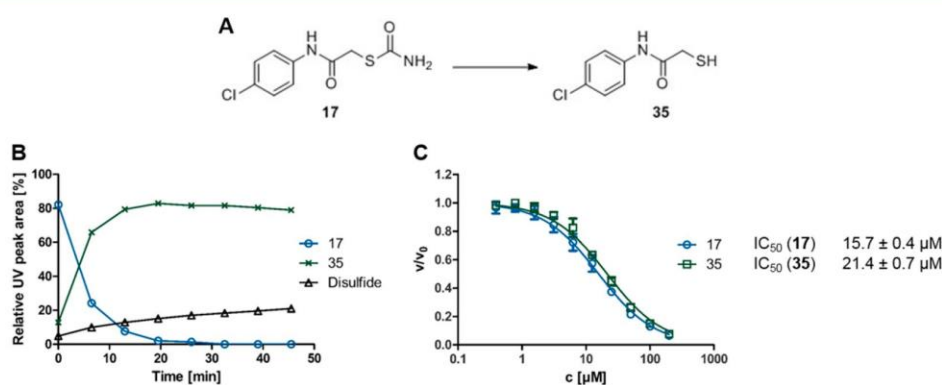


**Figure 4.** (A) Conversion of thiocarbamate 17 into corresponding free thiol 35. (B) LC-MS stability assay showing fast hydrolysis of 17 into 35 in 50 mM Tris, pH 7.2 (10% methanol), at 37 °C. (C) *In vitro* results for 17 and 35 are in accordance with the LC-MS results.

at 22.5 °C,<sup>35</sup> indicating temperature dependence of hydrolysis. Additionally, we found the same *in vitro* activity of selected thiols compared to their prodrugs, confirming the results from

the LC-MS assay that compound activation occurs within the preincubation time of our assay (Figures 4C and 5). Unlike thiols, which can be oxidized to disulfides,<sup>43</sup> these thiocarbamate

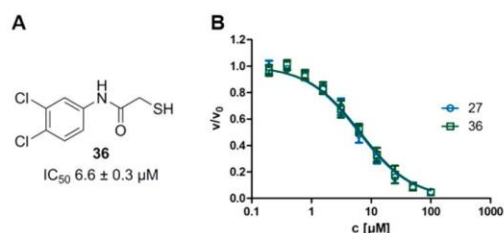


**Figure 5.** (A) Structure of thiol **36**. (B) FRET assay results for **36** and prodrug **27**. Nonlinear regression was performed with the Hill Slope constrained to 1.

mate prodrugs have the advantage of being stable toward oxidation. As expected, the inactivity of dithiocarbamates **75–82** (Table S1) could be explained by their stability toward hydrolysis (Figure S2).

**Binding Mode of Compound **36** to LasB.** To elucidate the binding mode of the *N*-aryl mercaptoacetamides to LasB, we cocrystallized compound **27** with LasB purified from *Pseudomonas aeruginosa* PA14 culture supernatant. The putative LasB–**27** complex crystallized in space group *P2*<sub>1</sub>, and crystals diffracted to 1.3 Å resolution (Figure 6). The structure was

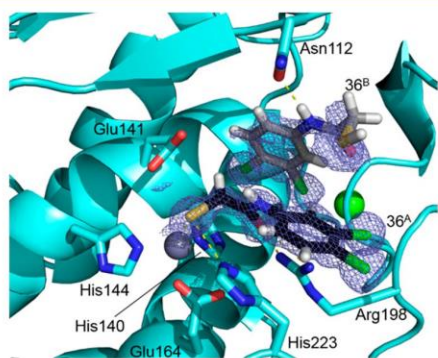


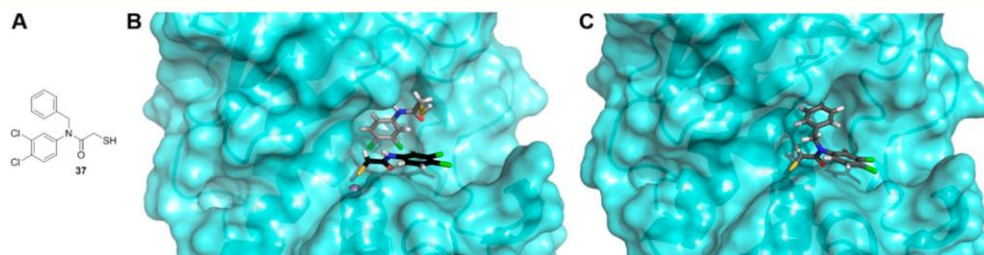
**Figure 6.** Structure of LasB in complex with **36**. Cartoon representations of LasB (cyan) in complex with **36** (black, gray). The difference electron density ( $F_o - F_c$ ) contoured to  $3\sigma$  with phases calculated from a model that was refined in the absence of **36** is shown as a yellow isomesh. The active-site zinc ion is shown as a gray sphere and calcium ion, as a green sphere. Residues involved in binding of  $36^A$  and  $36^B$  are shown as sticks.

solved by molecular replacement using the published LasB apo structure (PDB ID 1EZM) as a search model. Full details of the

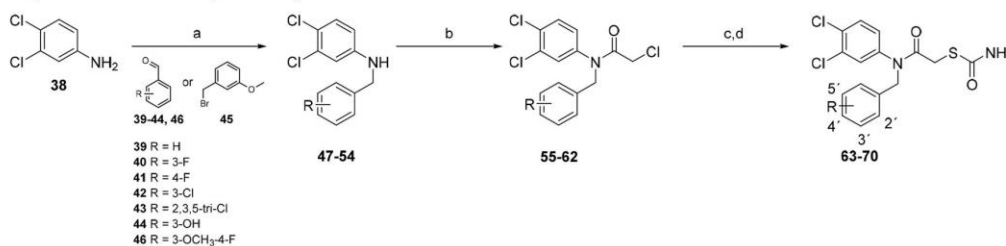
data collection and refinement statistics can be found in Table S2.

Hydrolysis of **27** to **36** was expected from the stability tests and from the *in vitro* assay using the corresponding thiol **36**, and indeed, there was no electron density for the thiocarbamate group observed. These observations confirm that the prodrug moiety does not contribute to the inhibitory activity. To our surprise, instead of one molecule, the active site of LasB contained unambiguous electron density for two molecules of **36**, arranged in an antiparallel fashion (hereafter, referred to as  $36^A$  and  $36^B$ ). In the LasB apo structure, the active-site zinc ion is coordinated by the side chains of His140, His144, and Glu164 as well as one water molecule. The free thiol of  $36^A$  displaces the water molecule to complete the tetrahedral coordination sphere (sulfur–zinc distance of 2.3 Å). The carbonyl oxygen of  $36^A$  forms a bidentate hydrogen bond with Arg198 in the S1' binding site (2.2 Å/2.3 Å), while the side chain of His223 forms a hydrogen bond with the thiol and amide nitrogen (2.4 Å/3.5 Å). The amide nitrogen of the second molecule hydrogen bonds with Asn112 in the edge strand (2.0 Å), while its aromatic core lies in the lipophilic S2' binding pocket. The tolerance of substitution at different positions without crucial changes in activity can be explained by the relatively large size of the binding site in comparison to the rather narrow binding pocket of ColH. Calculations performed with Molecular Operating Environment (MOE) software<sup>44</sup> enabled us to determine differences in the acidity of the thiol groups: Zinc coordination significantly increased thiol acidity, reducing the  $pK_a$  value from 9.0 in solution to 4.0. These results indicate full ionization of this sulfur atom when bound to the active site. In contrast, no significant change in the acidity of the nonzinc bound thiol could be determined, indicating a protonated state of this sulfur atom. It appears probable that binding of  $36^A$  is required for  $36^B$  to bind to the protein by providing a hydrophobic surface anchored to the active-site zinc ion  $36^B$  with which it can interact. Regarding the Hill Slope of 1 in the *in vitro* assay for **36** (Figure 5B), it seems that only one binding event is necessary for full inhibition. This indicates that a second molecule might not be required for the activity of the compound and its absence in solution cannot be excluded.

Elastase belongs to the M4 family of peptidases, showing high similarity to thermolysin from *Bacillus thermoproteolyticus*.<sup>27</sup> Its C-terminal domain is composed mostly of  $\alpha$ -helices, while the N-terminal domain is formed predominantly by antiparallel  $\beta$ -sheets. The active site cleft is positioned within the hinge region in between the two domains.<sup>17</sup> Interestingly, binding of  $36^A$  and  $36^B$  does not lead to a closure of the active site cleft as it has been reported after binding of phosphoramidon<sup>45</sup> and another peptidic inhibitor.<sup>46</sup> In fact,



**Figure 7.** (A) Structure of **37**, the *N*-benzyl derivative of active thiol **36**. (B) Surface representation of LasB bound to two molecules of **27**. (C) Modeling of **37**, the *N*-benzyl derivative of the active thiol **36** based on the X-ray crystal structure.

Scheme 1. Synthesis of *N*-Benzyl Mercaptoacetamides<sup>a</sup>

<sup>a</sup>Reagents and conditions: (a) sodium triacetoxyborohydride, DCM, RT, 20 h (47–52, 54), or 3-methoxybenzylbromide, K<sub>2</sub>CO<sub>3</sub>, DMF, 120 °C, 20 h (53); (b) chloroacetyl chloride, acetone, 0 °C to r.t., 1.5 h; (c) ammonium thiocyanate, ethanol, 80 °C, 2 h; (d) sulfuric acid, acetic acid, 0 °C, 30 min.

the open conformation observed in the apo structure is virtually unperturbed ( $C_{\alpha}$  rmsd of just 0.24 over 290 residues, Figure S3). It seems likely that the antiparallel binding of two molecules of **36** prevents the active site from closing and thus allows the enzyme to be addressed in an open conformation. This offers a completely new avenue for the design of LasB inhibitors.

In the work of Zhu et al., a primed binding mode of *N*-aryl mercaptoacetamides to the LasB active site was proposed on the basis of docking studies.<sup>34</sup> We experimentally confirmed the inhibitor to be placed in the primed binding pocket. However, there are substantial differences in the orientation of the inhibitor, mainly owing to the presence of two molecules. The reported docking studies suggested additional chelation of the zinc atom by the carbonyl group of the inhibitor, which we demonstrated to hydrogen bond with Arg198. The proposed hydrogen bond between Asn112 and the amide nitrogen of the inhibitor is indeed present, yet it is formed by **36<sup>B</sup>** and not by the zinc chelating **36<sup>A</sup>**.

**Structure-Based Optimization.** Binding of a single molecule to the binding site instead of two might have an entropic benefit resulting in improved inhibition. Hence, we tried to replace the second, nonzinc chelating molecule and to grow the zinc-binding molecule deeper into the binding pocket, using the crystal structure of the LasB–**36** complex. Modeling approaches showed a benzyl group to be appropriate to fill the part of the binding pocket occupied by the aromatic core of the nonzinc binding molecule (Figure 7).

A straightforward approach was used to synthesize *N*-benzyl derivatives of compound **27** (Scheme 1): *N*-benzyl substituted anilines **47–54** were obtained via reductive amination, using aniline **38** and a variety of benzaldehydes (**39–44,46**). Amide coupling with chloroacetyl chloride led to intermediates **55–62**. Replacement of the  $\alpha$ -chlorine by a thiocyanate group was followed by hydrolysis to the respective thiocarbamates **63–70** using a mixture of concentrated sulfuric acid and acetic acid.<sup>47</sup>

Introduction of a benzylic group at the position of the amide nitrogen of **27** led to an active compound with an IC<sub>50</sub> of 20.4 ± 0.9  $\mu$ M (**63**, Table 2). The activity was approximately 3-fold lower compared to the nonbenzylated compound (Table 1). We introduced halogens at several positions of the benzyl group (**64–67**) to improve hydrophobic interactions with the lipophilic part of the binding pocket. The activity was slightly increased compared to **63**; however, with IC<sub>50</sub>'s in the two-digit micromolar range, our compounds were still less active than **27**. The polar phenol and methoxyphenol derivatives **68** and **69** inhibited LasB in the same range as the halogenated compounds **64–67**, indicating that the lipophilic part of the

Table 2. Structure and LasB Inhibition of *N*-Substituted Derivatives **63–74**

Cp.	R	IC <sub>50</sub> ( $\mu$ M)
63	Ph	20.4 ± 0.9
64	3'-F-Ph	12.6 ± 0.4
65	4'-F-Ph	15.3 ± 0.6
66	3'-Cl-Ph	17.3 ± 0.8
67	2',3',5'-tri-Cl-Ph	15.9 ± 0.9
68	3'-OH-Ph	17.6 ± 0.6
69	3'-OCH <sub>3</sub> -Ph	14.3 ± 0.6
70	3'-OCH <sub>3</sub> -4'-F-Ph	18.3 ± 0.9
71	H	15.9 ± 0.7
72	<i>m</i> -C <sub>4</sub> H <sub>9</sub>	15.0 ± 0.5
73	<i>t</i> -C <sub>4</sub> H <sub>9</sub>	54.5 ± 2.3
74	C <sub>6</sub> H <sub>11</sub>	27.6 ± 1.4

binding pocket might not be reached. Combination of the 4'-fluorine of **65** and the 3'-methoxy group of **69** did not lead to an additive effect (**70**).

Given that the activity could not be improved by introducing rigid aromatic functions, we investigated conformationally more flexible alkyl substituents. Synthesis was achieved following the same procedure (Scheme 1) using the respective alkyl aldehydes, giving compounds **71–74** (Table 2). Similar to the benzyl compounds **63–70**, introduction of alkyl substituents at the amide nitrogen led to a loss of activity, especially in case of the rather bulky neopentyl and cyclohexylmethyl substituents (**73** and **74**). Considering that replacement of the amide hydrogen by the methyl group already resulted in a more than 2-fold loss of activity (**71**), we concluded that the hydrogen bond formed between Asn112 and the second molecule in the binding pocket plays an important role for compound binding.

To assess the impact of *N*-substitution on thiocarbamate half-life, the stability of **68** and **74** was analyzed. Again, we proved that thiocarbamates were cleaved rapidly; thus, the reduced activity was not caused by slower compound activation in assay buffer (Figure S4).

**Selectivity toward Further Proteases.** MMPs are ubiquitously present in the human body, playing pivotal roles in the progress of various diseases but also exerting beneficial effects on human health. The unselective inhibition of various MMPs was the reason for the failure of several protease

inhibitors, while selectively inhibiting specific MMPs remains a challenging task in protease drug discovery.<sup>48–53</sup> Several bacterial protease inhibitors lacking MMP selectivity have been reported.<sup>54–56</sup> Thiol-based LasB inhibitors have been tested toward selected MMPs.<sup>33,34</sup> In this context, the inhibition of range of six MMPs with structural variation in their S1' binding pocket<sup>57</sup> (deep: MMP-3 and -14; intermediate: MMP-2 and -8; shallow: MMP-1 and -7) was analyzed for 27. As we previously demonstrated for other *N*-aryl mercaptoacetamides,<sup>35</sup> 27 did not inhibit this broad range of MMPs at concentrations up to 100  $\mu$ M either (Figure S5).

In contrast to these antitargets, bacterial metallo- $\beta$ -lactamases represent attractive additional targets, since cleavage of  $\beta$ -lactam antibiotics by these proteases is a crucial mechanism of antibiotic resistance.<sup>58</sup> Inhibition of metallo- $\beta$ -lactamases by thiol-based inhibitors has been reported to restore the activity of  $\beta$ -lactam antibiotics.<sup>59–62</sup> To this end, we tested IMP-7, a metallo- $\beta$ -lactamase present in clinical isolates of *P. aeruginosa* for *in vitro* inhibition by prodrug 27 and thiol 36. Interestingly, the enzyme was found to be inhibited by 27 ( $1.16 \pm 0.07 \mu$ M) as well as 36 ( $0.86 \pm 0.06 \mu$ M).

**Cytotoxicity Assays.** For a potential therapeutic application in humans, we analyzed the cytotoxicity of thiocarbamate 17 as well as thiols 35 and 36 toward two different human cell lines (Table 3). As described previously,<sup>35</sup> the mercaptoaceta-

**Table 3. Cytotoxicity of 17, 35, and 36 in HEP G2 and HEK293 Cells**

Cp.	concn [ $\mu$ M]	reduction of viability [%]	
		HEP G2	HEK293
17	100	26 $\pm$ 16	51 $\pm$ 12
35	100	28 $\pm$ 12 <sup>a</sup>	51 $\pm$ 4
36	100	25 $\pm$ 3	22 $\pm$ 5
doxorubicin	1	50 $\pm$ 5 <sup>a</sup>	49 $\pm$ 7
rifampicin	100	29 $\pm$ 5 <sup>a</sup>	19 $\pm$ 3
batimastat	100	13 $\pm$ 7 <sup>a</sup>	2 $\pm$ 2

<sup>a</sup>Values taken from Schönauer et al.<sup>35</sup>

mides had only a low cytotoxic effect on HEP G2 cells at a concentration as high as 100  $\mu$ M. Likewise, the cytotoxic effect on HEK293 cells was also low at this high concentration.

***Galleria mellonella* Infection Model.** Stimulated by the promising *in vitro* results, the *in vivo* efficacy of our compounds was investigated. Infection models with *Galleria mellonella* larvae have previously been employed by us to assess novel treatment options for *Pseudomonas aeruginosa*-induced infections<sup>63,64</sup> and were reported to highly correlate with mouse models.<sup>65</sup> We analyzed the effect of prodrug 27 and active thiol 36 by coinjecting them with PA14. The larvae were challenged with PA14 concentrations corresponding to two times the LD<sub>50</sub>.<sup>65</sup> Compared to PA14-infected larvae receiving no treatment, 2.5 nmol of 36 significantly increased the survival of *G. mellonella* from 43% to 72% after 65 h (Figure 8). Notably, not only the survival time was increased, as reported for LasB inhibitors in a *C. elegans* model,<sup>34</sup> but also the survival rate. However, administering the same concentration of thiocarbamate prodrug did not lead to a significant effect, indicating an insufficient release of the thiol in *G. mellonella* hemolymph. These findings prove the potential of LasB inhibition to effectively reduce *P. aeruginosa* pathogenicity.

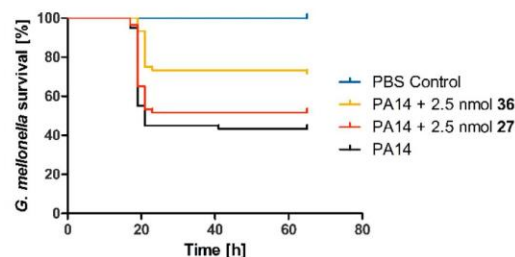


**Figure 8.** Survival curves for PA14-challenged *Galleria mellonella* larvae receiving treatment with 2.5 nmol 27 or 36 in comparison to larvae receiving treatment with PBS only. Curves represent results from at least three independent measurements. The survival rate was significantly higher for larvae treated with 36 ( $p = 0.0003$ , log-rank test) but not with 27. The survival rate for larvae treated with the compounds in PBS was 100%.

## CONCLUSION

In this study, a functional screening of a protease-inhibitor enriched library and a fragment library was performed using a well-established FRET assay, with the aim to expand the chemical space of LasB inhibitors. An LC-MS-based counter-screen was developed, allowing identification of false-positives. Only one real screening hit was identified, an *N*-aryl mercaptoacetamide. Compounds of this class are known to be inhibitors of LasB as well as of ColH from *C. histolyticum*. We analyzed the inhibition of a further 35 derivatives of this class of fragment-like molecules. Interestingly, the SAR was inverse to the activity profile we discovered for ColH, allowing rational optimization of the compound class to selectively inhibit either LasB or ColH. The X-ray crystal structure of a LasB–inhibitor complex was solved, revealing a primed binding mode of two thiol molecules to the active site of the protease. Importantly, our results show that inhibitor binding does not necessarily lead to a closure of the binding pocket, as it has been described for thermolysin-like proteases. These findings pave the way for the development of novel LasB inhibitors targeting the open conformation of the enzyme, providing an important starting point for lead optimization. The structural information obtained by X-ray crystallography was used to grow the fragments by introducing benzyl or alkyl groups. These compounds indeed inhibited LasB, yet the activity was not improved. Supposably, the conformation of the *N*-substituted compounds is not ideal to replace the second inhibitor molecule in the binding pocket. With the  $\beta$ -lactamase IMP-7, we discovered an additional target of the *N*-aryl mercaptoacetamides, which is attractive for the development of novel anti-infectives. Furthermore, *in vivo* efficacy was demonstrated using a *Galleria mellonella* infection model. The survival rate of PA14-infected larvae was increased significantly when treated with our best thiol. Considering the fragment-like character of our inhibitors and the fact that they represent antivirulence agents instead of traditional antibiotics, this is a remarkable effect. These results underline the potential of reducing bacterial pathogenicity to develop novel antibacterial drugs, which are urgently needed to combat antibiotic resistance. *N*-aryl mercaptoacetamides prove particularly interesting for the development of such drugs, since they display high selectivity toward human MMPs.

## ■ EXPERIMENTAL SECTION

**Expression and Purification of LasB.** *Pseudomonas aeruginosa* PA14 were grown in lysogeny broth medium for 72 h at 37 °C. Cells were removed by centrifugation (5000 rpm, 4 °C, 60 min), and the supernatant was filtered through a bottle-top-filter (0.20 μm). Purification was performed according to the method described by Morihara et al.<sup>66</sup> with few modifications. The precipitate formed by acetone treatment was dissolved in water and dialyzed against buffer A (20 mM Tris, pH 8.0). The dialyzed sample was then loaded onto a Hitrap Q HP column (GE Healthcare, Little Chalfont, UK) and washed back to baseline in buffer A, before being eluted with a gradient from buffer A into buffer A2 (20 mM Tris, pH 8.0, 1 M NaCl). The fractions with the strongest activity were pooled together (*in vitro* assay described below) and loaded onto a Superdex 200 gel filtration column (GE Healthcare) that was pre-equilibrated with buffer B (20 mM Tris, pH 8.0, 2 mM CaCl<sub>2</sub>). Protein purity and activity was assessed by SDS-PAGE and the *in vitro* inhibition assay.

**In Vitro Inhibition Assay.** For the initial screening, Elastase was purchased from Elastin Products Company (Owensville, MO, USA) or Merck (Darmstadt, Germany). Later, purified elastase prepared according to the procedure described above was used. The fluorogenic substrate 2-Aminobenzoyl-Ala-Gly-Leu-Ala-4-Nitrobenzylamide<sup>36</sup> was purchased from Peptides International (Louisville, KY, USA). Fluorescence intensity was measured for 60 min at 37 °C in black 384-well microtiter plates (Greiner BioOne, Kremsmünster, Austria) using a CLARIOstar microplate reader (BMG Labtech, Ortenberg, Germany) with an excitation wavelength of 340 ± 15 nm and an emission wavelength of 415 ± 20 nm. The assay was performed in a final volume of 50 μL of assay buffer (50 mM Tris, pH 7.2, 2.5 mM CaCl<sub>2</sub>, 0.075% Pluronic F-127, 5% DMSO) containing LasB at a final concentration of 10 nM (commercial batch) or 0.3 nM (purified batch) and the substrate at 150 μM. Before substrate addition, compounds were preincubated with the enzyme for 15 min at 37 °C. Experiments were performed in duplicates and repeated for at least two times. Blank controls without enzyme were performed. After blank subtraction, the slope of samples containing inhibitors (*v*) was divided by the slope of a simultaneously started uninhibited enzymatic reaction (*v*<sub>0</sub>). IC<sub>50</sub> values were determined with nonlinear regression using GraphPad Prism 5 (Graph Pad Software, San Diego, CA, USA) and are given as mean values ± standard deviation (SD). The slope factor was constrained to 1.

**LC-MS-Based Readout for the FRET Assay.** The FRET-based fluorescence assay was performed according to the procedure described above using 50 mM Tris, pH 7.2. At the end of the measurement, the enzymatic reaction was stopped by adding formic acid at a final concentration of 2%. Simultaneously, amitryptiline was added as internal standard. The resulting mixture was diluted 1:10 in a mixture of 10% acetonitrile in Milli-Q water containing 2% formic acid, resulting in a 10 μM amitryptiline concentration. The analyses were performed using a TF UltiMate 3000 binary RSLC UHPLC (Thermo Fisher, Dreieich, Germany) equipped with a degasser, a binary pump, an autosampler, and a thermostated column compartment and a MWD, coupled to a TF TSQ Quantum Access Max mass spectrometer with heated electrospray ionization source (HESI-II). For gradient elution, an Accucore RP-MS column (150 × 2.1 mm, 2.6 μm, Thermo

Fisher, Dreieich, Germany) was used with a mobile phase consisting of acetonitrile containing 1% formic acid (FA; v/v; eluent A) and water containing 1% FA (v/v; eluent B) at a flow rate of 400 μL/min under the following conditions: 0–0.9 min 10% A, 0.9–2.5 min 10–50% A, 2.5–5.5 min 50–70% A, 5.5–6 min hold, and 6–6.5 min 10% A, giving a total run time of 6.5 min. The injection volume was 10 μL. The divert valve was set to 1.6 min. The autosampler temperature was set to 6 °C. The following MS conditions were used: electrospray ionization (ESI), positive mode, sheath gas, nitrogen at a flow rate of 35 arbitrary units; auxiliary gas, nitrogen at flow rate of 10 arbitrary units; vaporizer temperature, 50 °C; ion transfer capillary temperature, 270 °C; capillary offset, 15 V; spray voltage, 3000 V. The mass spectrometer was operated in the SIM mode with the following masses: 4, *m/z* 266.1 (tube lens offset 120 V); amitryptiline, *m/z* 278.1 (tube lens offset 90 V); 5, *m/z* 337.0 (tube lens offset 120 V); 3, *m/z* 584.1 (tube lens offset 120 V) with a scan width of *m/z* 2.0 and a scan time of 0.1 s, respectively. Measurements were performed in duplicates and repeated for at least two times. Observed retention times were as follows: 4, 2.00 min; 5, 3.52 min; amitryptiline, 4.02 min; 3, 4.37 min. MS-peak areas were determined using TF Xcalibur Software. Peak areas were normalized by ISTD peak area (giving *A*) and divided by the peak area of the respective ISTD normalized sample without inhibitor (*A*<sub>0</sub>). IC<sub>50</sub> values were determined using the method described above (GraphPad Prism 5 software).

**LC-MS-Based Stability Assay.** The assay was performed as described previously<sup>35</sup> using 50 mM Tris, pH 7.2, and a temperature of 37 °C.

**Screening Library.** The protease inhibitor enriched screening library (ActiTarg-P) was purchased from TimTec (Newark, DE, USA). Fragments were obtained from the Maybridge Fragment Library (Maybridge, Altrincham, UK). Compounds were stored as DMSO stock solutions.

**Chemistry.** All reagents were used from commercial suppliers without further purification. Procedures were not optimized regarding yield. NMR spectra were recorded on a Bruker Fourier 300 (300 MHz) spectrometer. Chemical shifts are given in parts per million (ppm) and referenced against the residual proton, <sup>1</sup>H, or carbon, <sup>13</sup>C, resonances of the >99% deuterated solvents as internal reference. Coupling constants (*J*) are given in Hertz. Data are reported as follows: chemical shift, multiplicity (*s* = singlet, *d* = doublet, *t* = triplet, *m* = multiplet, *br* = broad and combinations of these) coupling constants, and integration. Mass spectrometry was performed on a SpectraSystems-MSQ LCMS system (Thermo Fisher, Dreieich, Germany). Flash chromatography was performed using the automated flash chromatography system CombiFlash Rf+ (Teledyne Isco, Lincoln, NE, USA) equipped with RediSepRf silica columns (Axel Semrau, Sprockhövel Germany) or Chromabond Flash C18 columns (Macherey-Nagel, Düren, Germany). Purity of compounds synthesized by us was determined by LCMS using the area percentage method on the UV trace recorded at a wavelength of 254 nm and found to be >95%. Thiols and thiocarbamates were synthesized according to the procedures described previously.<sup>35</sup> *N*-benzyl and *N*-aryl mercaptoacetamides were synthesized according to Schemes S1 and S2 using General Procedures 1–3 as described in more detail in the Supporting Information.

**Human MMP Inhibition Assay.** The catalytic domains of MMP-1, -2, -3, -7, -8, and -14 along with the SensoLyte S20 Generic MMP Activity Kit were purchased from AnaSpec

(Fremont, CA, USA). The assay was performed as described previously using Batimastat as a positive control,<sup>35</sup> according to the guidelines of the manufacturer.

**$\beta$ -Lactamase Inhibition Assay.** Activity assays for IMP-7 were carried out, as described by Klingler et al.<sup>60</sup> Final protein concentrations of 0.1 nM in a 50 mM HEPES buffer (pH 7.5, 0.01% Triton X-100). Substrate (Fluorocillin (Invitrogen, Darmstadt, Germany)) was dissolved in assay buffer to a final concentration of 888 nM. Test compounds were dissolved and prediluted in DMSO (final concentration: 1%). In a black polystyrol 96-well plate (Corning), an amount of 1  $\mu$ L of the respective inhibitor solution at different concentrations was incubated with 89  $\mu$ L of IMP-7 containing buffer for 30 min at room temperature. Ten  $\mu$ L of substrate solution was added. The readout of the emitted fluorescence was started immediately (45 s for 30 cycles) using a Tecan Infinite F200Pro (Tecan Group Ltd.; excitation at 495 nm and emission at 525 nm). Blank controls were performed without enzyme. Positive controls were performed with enzyme but without inhibitor. The inhibitory activity of each test compound was measured in three independent experiments. For calculation of IC<sub>50</sub> values, data obtained from measurements with eight different inhibitor concentrations were used. For the evaluation of the sigmoidal dose response equation (variable slope with four parameters), GraphPad Prism 5 (GraphPad Software, La Jolla, CA, USA) was used.

**Cytotoxicity Assays.** Hep G2 or HEK293 cells ( $2 \times 10^5$  cells per well) were seeded in 24-well, flat-bottomed plates. Culturing of cells, incubations, and OD measurements were performed as described previously<sup>67</sup> with small modifications. Twenty-four hours after seeding the cells, the incubation was started by the addition of compounds in a final DMSO concentration of 1%. The living cell mass was determined after 48 h. At least two independent measurements were performed for each compound.

**Galleria mellonella Virulence Assay.** The virulence assay was performed as described by Lu et al.<sup>63</sup> with some modifications: *Galleria mellonella* larvae (TruLarv) were purchased from BioSystems Technology (Exeter, United Kingdom). Injections were performed using a LA120 syringe pump (Landgraf Laborsysteme, Langenhagen, Germany) equipped with 1 mL Injekt-F tuberculin syringes (B. Braun, Melsungen, Germany) and Sterican 0.30  $\times$  12 mm, 30G  $\times$  1.5 needles (B. Braun). The following treatment conditions were applied: (a) sterile PBS solution, (b) PA14 suspension, (c) 2.5 nmol of 27 in "b", (d) 2.5 nmol of 36 in "b", (e) 2.5 nmol of 27 in "a", and (f) 1.25 nmol of 36 in "a". Samples a–e contained 1% DMSO and f, 0.5%. For each treatment, data from at least three independent measurements were combined.

**X-ray Crystallography.** LasB was concentrated to 10–12 mg/mL and mixed with inhibitor 27 at a final concentration of 1 mM. Complex crystals were grown by the sitting drop method using a reservoir solution containing 0.2 M magnesium chloride and 30% (w/v) PEG 3350. Crystals were cryoprotected in glycerol, and diffraction data was collected from single crystals at 100 K at beamline ID23-2 (ESRF) at a wavelength of 0.873 Å. Data was processed using Xia2,<sup>68</sup> and the structure was solved using PHASER<sup>69</sup> molecular replacement with *Pseudomonas aeruginosa* elastase (PAE, PDB ID 1EZM) as a search model. The solution was manually rebuilt with COOT<sup>70</sup> and refined using PHENIX<sup>71</sup> and Refmac5.<sup>72</sup> The final refined structure of LasB in complex with compound 27 was deposited in the Protein Data Bank (PDB) as entry 6F8B.

**Molecular Modeling.** Molecular modeling was performed with Molecular Operating Environment 2015.10 (MOE) software (Chemical Computing Group, Montreal, Canada) using standard parameters. In the cocrystal structure of LasB and 36, inhibitor molecule 36<sup>B</sup> was removed and 36<sup>A</sup> was grown using the Builder function. The final structure was energy-minimized using the QuickPrep function. AMBER10:EHT was used as a force field.

## ■ ASSOCIATED CONTENT

### ● Supporting Information

The Supporting Information is available free of charge on the ACS Publications website at DOI: 10.1021/acsinfecdis.8b00010.

Supporting Tables S1 and S2, Schemes 1 and 2, and Figures S1–S5, giving structures and stability data of inactive compounds, X-ray data collection and refinement statistics, FRET and LC-MS results for phosphoramidon, stability data for 68 and 74, MMP inhibition assay, experimental procedures, and spectral data for synthetic compounds (PDF)

## ■ AUTHOR INFORMATION

### Corresponding Author

\*E-mail: Rolf.Hartmann@helmholtz-hzi.de.

### ORCID

Andreas M. Kany: 0000-0001-7580-3658

Jörg Haupenthal: 0000-0003-3991-2800

Samir Yahiaoui: 0000-0001-5134-5007

Ewgenij Proschak: 0000-0003-1961-1859

Jesko Köhnke: 0000-0002-7153-1365

Rolf W. Hartmann: 0000-0002-5871-5231

### Author Contributions

<sup>†</sup>A.M.K. and A.S. contributed equally.

### Notes

The authors declare no competing financial interest.

## ■ ACKNOWLEDGMENTS

We thank Jeannine Jung, Simone Amann, Tabea Schramm, and Lilia Weizel for technical support, Dr. Jens Eberhard and Dr. Giuseppe Allegretta for help with the establishment of the LC-MS assay, Dr. Teresa Röhrig for support with the *G. mellonella* assay, and Dr. Martin Empting for help with molecular modeling. E.P. thanks German Research Foundation (DFG, Heisenberg-Professur PR1405/4-1) for financial support.

## ■ REFERENCES

- (1) World Health Organization. (2017) Antibacterial Agents in Clinical Development. In *An analysis of the antibacterial clinical development pipeline, including tuberculosis*, World Health Organization, Geneva.
- (2) Taubes, G. (2008) The bacteria fight back. *Science* 321, 356–361.
- (3) Hancock, R. E. W., and Speert, D. P. (2000) Antibiotic resistance in *Pseudomonas aeruginosa*. Mechanisms and impact on treatment. *Drug Resist. Updates* 3, 247–255.
- (4) Sordé, R., Pahissa, A., and Rello, J. (2011) Management of refractory *Pseudomonas aeruginosa* infection in cystic fibrosis. *Infect. Drug Resist.* 4, 31–41.
- (5) Mesaros, N., Nordmann, P., Plésiat, P., Roussel-Delvallez, M., van Eldere, J., Glupczynski, Y., van Laethem, Y., Jacobs, F., Lebecque, P., Malfroot, A., Tulkens, P. M., and van Bambeke, F. (2007)

- Pseudomonas aeruginosa*. Resistance and therapeutic options at the turn of the new millennium. *Clin. Microbiol. Infect.* 13, 560–578.
- (6) Cooper, M. A., and Shlaes, D. (2011) Fix the antibiotics pipeline. *Nature* 472, 32.
- (7) Dickey, S. W., Cheung, G. Y. C., and Otto, M. (2017) Different drugs for bad bugs. Antivirulence strategies in the age of antibiotic resistance. *Nat. Rev. Drug Discovery* 16, 457–471.
- (8) Heras, B., Scanlon, M. J., and Martin, J. L. (2015) Targeting virulence not viability in the search for future antibacterials. *Br. J. Clin. Pharmacol.* 79, 208–215.
- (9) Lewis, K. (2013) Platforms for antibiotic discovery. *Nat. Rev. Drug Discovery* 12, 371–387.
- (10) Rasko, D. A., and Sperandio, V. (2010) Anti-virulence strategies to combat bacteria-mediated disease. *Nat. Rev. Drug Discovery* 9, 117–128.
- (11) Strateva, T., and Mitov, I. (2011) Contribution of an arsenal of virulence factors to pathogenesis of *Pseudomonas aeruginosa* infections. *Ann. Microbiol.* 61, 717–732.
- (12) Wagner, S., Sommer, R., Hinsberger, S., Lu, C., Hartmann, R. W., Empting, M., and Titz, A. (2016) Novel Strategies for the Treatment of *Pseudomonas aeruginosa* Infections. *J. Med. Chem.* 59, 5929–5969.
- (13) Storz, M. P., Maurer, C. K., Zimmer, C., Wagner, N., Brengel, C., de Jong, J. C., Lucas, S., Müsken, M., Häussler, S., Steinbach, A., and Hartmann, R. W. (2012) Validation of PqsD as an anti-biofilm target in *Pseudomonas aeruginosa* by development of small-molecule inhibitors. *J. Am. Chem. Soc.* 134, 16143–16146.
- (14) Kamal, A. A. M., Maurer, C. K., Allegretta, G., Hauptenthal, J., Empting, M., and Hartmann, R. W. (2017) Quorum Sensing Inhibitors as Pathoblockers for *Pseudomonas aeruginosa* Infections: A New Concept in Anti-Infective Drug Discovery. In *Topics in Medicinal Chemistry*, pp 1–26, Springer, Berlin, Heidelberg.
- (15) Wretling, B., and Pavlovskis, O. R. (1983) *Pseudomonas aeruginosa* elastase and its role in *Pseudomonas* infections. *Clin. Infect. Dis.* 5 (Suppl 5), S998–S1004.
- (16) Morihara, K. (1964) Production of elastase and proteinase by *Pseudomonas aeruginosa*. *J. Bacteriol.* 88, 745–757.
- (17) Thayer, M. M., Flaherty, K. M., and McKay, D. B. (1991) Three-dimensional structure of the elastase of *Pseudomonas aeruginosa* at 1.5-Å resolution. *J. Biol. Chem.* 266, 2864–2871.
- (18) Heck, L. W., Morihara, K., McRae, W. B., and Miller, E. J. (1986) Specific cleavage of human type III and IV collagens by *Pseudomonas aeruginosa* elastase. *Infect. Immun.* 51, 115–118.
- (19) Golovkine, G., Faudry, E., Bouillot, S., Voulhoux, R., Attrée, I., and Huber, P. (2014) VE-cadherin cleavage by LasB protease from *Pseudomonas aeruginosa* facilitates type III secretion system toxicity in endothelial cells. *PLoS Pathog.* 10, e1003939.
- (20) Azghani, A. O. (1996) *Pseudomonas aeruginosa* and epithelial permeability. Role of virulence factors elastase and exotoxin A. *Am. J. Respir. Cell Mol. Biol.* 15, 132–140.
- (21) Holder, I. A., and Wheeler, R. (1984) Experimental studies of the pathogenesis of infections owing to *Pseudomonas aeruginosa*. Elastase, an IgG protease. *Can. J. Microbiol.* 30, 1118–1124.
- (22) Parmely, M., Gale, A., Clabaugh, M., Horvat, R., and Zhou, W. W. (1990) Proteolytic inactivation of cytokines by *Pseudomonas aeruginosa*. *Infect. Immun.* 58, 3009–3014.
- (23) Mariencheck, W. L., Alcorn, J. F., Palmer, S. M., and Wright, J. R. (2003) *Pseudomonas aeruginosa* elastase degrades surfactant proteins A and D. *Am. J. Respir. Cell Mol. Biol.* 28, 528–537.
- (24) Schmidtchen, A., Holst, E., Tapper, H., and Björck, L. (2003) Elastase-producing *Pseudomonas aeruginosa* degrade plasma proteins and extracellular products of human skin and fibroblasts, and inhibit fibroblast growth. *Microb. Pathog.* 34, 47–55.
- (25) Dulon, S., Leduc, D., Cottrell, G. S., D'Alayer, J., Hansen, K. K., Bunnnett, N. W., Hollenberg, M. D., Pidard, D., and Chignard, M. (2005) *Pseudomonas aeruginosa* elastase disables proteinase-activated receptor 2 in respiratory epithelial cells. *Am. J. Respir. Cell Mol. Biol.* 32, 411–419.
- (26) Graef, F., Vukosavljevic, B., Michel, J.-P., Wirth, M., Ries, O., De Rossi, C., Windbergs, M., Rosilio, V., Ducho, C., Gordon, S., and Lehr, C.-M. (2016) The bacterial cell envelope as delimiter of anti-infective bacterial inner membrane - An in vitro permeation model of the Gram-negative bioavailability - An in vitro permeation model of the Gram-negative bacterial inner membrane. *J. Controlled Release* 243, 214–224.
- (27) Adekoya, O. A., and Sylte, I. (2009) The thermolysin family (M4) of enzymes. Therapeutic and biotechnological potential. *Chem. Biol. Drug Des.* 73, 7–16.
- (28) Holland, D. R., Tronrud, D. E., Pley, H. W., Flaherty, K. M., Stark, W., Jansonius, J. N., McKay, D. B., and Matthews, B. W. (1992) Structural comparison suggests that thermolysin and related neutral proteases undergo hinge-bending motion during catalysis. *Biochemistry* 31, 11310–11316.
- (29) Adekoya, O. A., Sjöli, S., Wuxiuer, Y., Bilot, I., Marques, S. M., Santos, M. A., Nuti, E., Cercignani, G., Rossello, A., Winberg, J.-O., and Sylte, I. (2015) Inhibition of pseudolysin and thermolysin by hydroxamate-based MMP inhibitors. *Eur. J. Med. Chem.* 89, 340–348.
- (30) Fullagar, J. L., Garner, A. L., Struss, A. K., Day, J. A., Martin, D. P., Yu, J., Cai, X., Janda, K. D., and Cohen, S. M. (2013) Antagonism of a zinc metalloprotease using a unique metal-chelating scaffold. Tropolones as inhibitors of *P. aeruginosa* elastase. *Chem. Commun. (Cambridge, U. K.)* 49, 3197–3199.
- (31) Burns, F. R., Paterson, C. A., Gray, R. D., and Wells, J. T. (1990) Inhibition of *Pseudomonas aeruginosa* elastase and *Pseudomonas keratitis* using a thiol-based peptide. *Antimicrob. Agents Chemother.* 34, 2065–2069.
- (32) Kessler, E., Israel, M., Landshman, N., Chechick, A., and Blumberg, S. (1982) In vitro inhibition of *Pseudomonas aeruginosa* elastase by metal-chelating peptide derivatives. *Infect. Immun.* 38, 716–723.
- (33) Cathcart, G. R. A., Quinn, D., Greer, B., Harriott, P., Lynas, J. F., Gilmore, B. F., and Walker, B. (2011) Novel inhibitors of the *Pseudomonas aeruginosa* virulence factor LasB. A potential therapeutic approach for the attenuation of virulence mechanisms in pseudomonal infection. *Antimicrob. Agents Chemother.* 55, 2670–2678.
- (34) Zhu, J., Cai, X., Harris, T. L., Gooyit, M., Wood, M., Lardy, M., and Janda, K. D. (2015) Disarming *Pseudomonas aeruginosa* virulence factor LasB by leveraging a *Caenorhabditis elegans* infection model. *Chem. Biol.* 22, 483–491.
- (35) Schönauer, E., Kany, A. M., Hauptenthal, J., Hüsecken, K., Hoppe, I. J., Voos, K., Yahiaoui, S., Elsässer, B., Ducho, C., Brandstetter, H., and Hartmann, R. W. (2017) Discovery of a Potent Inhibitor Class with High Selectivity toward Clostridial Collagenases. *J. Am. Chem. Soc.* 139, 12696–12703.
- (36) Nishino, N., and Powers, J. C. (1980) *Pseudomonas aeruginosa* elastase. Development of a new substrate, inhibitors, and an affinity ligand. *J. Biol. Chem.* 255, 3482–3486.
- (37) Baell, J. B., and Holloway, G. A. (2010) New substructure filters for removal of pan assay interference compounds (PAINS) from screening libraries and for their exclusion in bioassays. *J. Med. Chem.* 53, 2719–2740.
- (38) Lakowicz, J. R. (2010) *Principles of Fluorescence Spectroscopy*, 3rd ed., Springer, New York, NY.
- (39) Kongkamnerd, J., Milani, A., Cattoli, G., Terregino, C., Capua, I., Beneduce, L., Gallotta, A., Pengo, P., Fassina, G., Monthakantirat, O., Umehara, K., De-Eknamkul, W., and Miertus, S. (2011) The quenching effect of flavonoids on 4-methylumbelliferone, a potential pitfall in fluorimetric neuraminidase inhibition assays. *J. Biomol. Screening* 16, 755–764.
- (40) Shapiro, A. B., Walkup, G. K., and Keating, T. A. (2009) Correction for interference by test samples in high-throughput assays. *J. Biomol. Screening* 14, 1008–1016.
- (41) Morihara, K., and Hiroshige, T. (1971) Comparative study of various neutral proteinases from microorganisms. Specificity with oligopeptides. *Arch. Biochem. Biophys.* 146, 291–296.
- (42) Morihara, K., and Tsuzuki, H. (1978) Phosphoramidon as an inhibitor of elastase from *Pseudomonas aeruginosa*. *Jpn. J. Exp. Med.* 48, 81–84.

- (43) Pramara, Y., Das Gupta, V., and Bethea, C. (1992) Stability of captopril in some aqueous systems. *J. Clin. Pharm. Ther.* 17, 185–189.
- (44) Labute, P. (2009) Protonate3D. Assignment of ionization states and hydrogen coordinates to macromolecular structures. *Proteins: Struct., Funct., Genet.* 75, 187–205.
- (45) McKay, D. B., and Overgaard, M. T. (2009) *Pseudomonas aeruginosa elastase with phosphoramidon*; <https://www.rcsb.org/structure/3DBK>.
- (46) Bitto, E., and McKay, D. B. (2004) *Elastase of Pseudomonas aeruginosa with an inhibitor*; <https://www.rcsb.org/structure/1u4g>.
- (47) Kim, Y.-G., Lim, H. N., and Lee, K.-J. (2009) A new route to allyl thiols and allyl thiocarbamates from Baylis-Hillman adducts. *J. Heterocycl. Chem.* 46, 23–27.
- (48) Cathcart, J., Pulkoski-Gross, A., and Cao, J. (2015) Targeting Matrix Metalloproteinases in Cancer. *Bringing New Life to Old Ideas. Genes Dis* 2, 26–34.
- (49) Dufour, A., and Overall, C. M. (2013) Missing the target. Matrix metalloproteinase antitargets in inflammation and cancer. *Trends Pharmacol. Sci.* 34, 233–242.
- (50) Overall, C. M., and López-Otín, C. (2002) Strategies for MMP inhibition in cancer. Innovations for the post-trial era. *Nat. Rev. Cancer* 2, 657–672.
- (51) Sbardella, D., Fasciglione, G. F., Gioia, M., Ciaccio, C., Tundo, G. R., Marini, S., and Coletta, M. (2012) Human matrix metalloproteinases. An ubiquitous class of enzymes involved in several pathological processes. *Mol. Aspects Med.* 33, 119–208.
- (52) Turk, B. (2006) Targeting proteases. Successes, failures and future prospects. *Nat. Rev. Drug Discovery* 5, 785–799.
- (53) Vandenbroucke, R. E., and Libert, C. (2014) Is there new hope for therapeutic matrix metalloproteinase inhibition? *Nat. Rev. Drug Discovery* 13, 904–927.
- (54) Ilies, M., Banciu, M. D., Scozzafava, A., Ilies, M. A., Caproiu, M. T., and Supuran, C. T. (2003) Protease inhibitors. Synthesis of bacterial collagenase and matrix metalloproteinase inhibitors incorporating arylsulfonyleureido and 5-dibenzo-suberenyl/suberyl moieties. *Bioorg. Med. Chem.* 11, 2227–2239.
- (55) Scozzafava, A., and Supuran, C. T. (2002) Protease inhibitors. Synthesis of matrix metalloproteinase and bacterial collagenase inhibitors incorporating 5-amino-2-mercapto-1,3,4-thiadiazole zinc binding functions. *Bioorg. Med. Chem. Lett.* 12, 2667–2672.
- (56) Sjøli, S., Nuti, E., Camodeca, C., Bilot, L., Rossello, A., Winberg, J.-O., Sylte, I., and Adekoya, O. A. (2016) Synthesis, experimental evaluation and molecular modelling of hydroxamate derivatives as zinc metalloproteinase inhibitors. *Eur. J. Med. Chem.* 108, 141–153.
- (57) Park, H. I., Jin, Y., Hurst, D. R., Monroe, C. A., Lee, S., Schwartz, M. A., and Sang, Q.-X. A. (2003) The intermediate S1' pocket of the endometase/matrixlysin-2 active site revealed by enzyme inhibition kinetic studies, protein sequence analyses, and homology modeling. *J. Biol. Chem.* 278, 51646–51653.
- (58) Bush, K., and Fisher, J. F. (2011) Epidemiological expansion, structural studies, and clinical challenges of new  $\beta$ -lactamases from gram-negative bacteria. *Annu. Rev. Microbiol.* 65, 455–478.
- (59) Buynak, J. D., Chen, H., Vogeti, L., Gadachanda, V. R., Buchanan, C. A., Palzkill, T., Shaw, R. W., Spencer, J., and Walsh, T. R. (2004) Penicillin-derived inhibitors that simultaneously target both metallo- and serine-beta-lactamases. *Bioorg. Med. Chem. Lett.* 14, 1299–1304.
- (60) Klingler, F.-M., Wichelhaus, T. A., Frank, D., Cuesta-Bernal, J., El-Delik, J., Müller, H. F., Sjuets, H., Göttig, S., Koenigs, A., Pos, K. M., Pogoryelov, D., and Proschak, E. (2015) Approved Drugs Containing Thiols as Inhibitors of Metallo- $\beta$ -lactamases. Strategy To Combat Multidrug-Resistant Bacteria. *J. Med. Chem.* 58, 3626–3630.
- (61) Tehrani, K. H. M. E., and Martin, N. I. (2017) Thiol-Containing Metallo- $\beta$ -Lactamase Inhibitors Resensitize Resistant Gram-Negative Bacteria to Meropenem. *ACS Infect. Dis.* 3, 711–717.
- (62) Büttner, D., Kramer, J. S., Klingler, F.-M., Wittmann, S. K., Hartmann, M. R., Kurz, C. G., Kohnhäuser, D., Weizel, L., Brüggerhoff, A., Frank, D., Steinhilber, D., Wichelhaus, T. A., Pogoryelov, D., and Proschak, E. (2017) Challenges in the Development of a Thiol-Based Broad-Spectrum Inhibitor for Metallo- $\beta$ -Lactamases. *ACS Infect. Dis.*, DOI: 10.1021/acscinfecdis.7b00129.
- (63) Lu, C., Maurer, C. K., Kirsch, B., Steinbach, A., and Hartmann, R. W. (2014) Overcoming the unexpected functional inversion of a PqsR antagonist in *Pseudomonas aeruginosa*. An in vivo potent antivirulence agent targeting pqs quorum sensing. *Angew. Chem., Int. Ed.* 53, 1109–1112.
- (64) Thomann, A., de Mello Martins, A. G. G., Brengel, C., Empting, M., and Hartmann, R. W. (2016) Application of Dual Inhibition Concept within Looped Autoregulatory Systems toward Antivirulence Agents against *Pseudomonas aeruginosa* Infections. *ACS Chem. Biol.* 11, 1279–1286.
- (65) Jander, G., Rahme, L. G., and Ausubel, F. M. (2000) Positive correlation between virulence of *Pseudomonas aeruginosa* mutants in mice and insects. *J. Bacteriol.* 182, 3843–3845.
- (66) Morihara, K., Tsuzuki, H., Oka, T., Inoue, H., and Ebata, M. (1965) *Pseudomonas aeruginosa* elastase: isolation, crystallization, and preliminary characterization. *J. Biol. Chem.* 240, 3295–3304.
- (67) Hauptenthal, J., Baehr, C., Zeuzem, S., and Piiper, A. (2007) RNase A-like enzymes in serum inhibit the anti-neoplastic activity of siRNA targeting polo-like kinase 1. *Int. J. Cancer* 121, 206–210.
- (68) Winter, G. (2010) xia2. An expert system for macromolecular crystallography data reduction. *J. Appl. Crystallogr.* 43, 186–190.
- (69) McCoy, A. J., Grosse-Kunstleve, R. W., Adams, P. D., Winn, M. D., Storoni, L. C., and Read, R. J. (2007) Phaser crystallographic software. *J. Appl. Crystallogr.* 40, 658–674.
- (70) Emsley, P., Lohkamp, B., Scott, W. G., and Cowtan, K. (2010) Features and development of Coot. *Acta Crystallogr., Sect. D: Biol. Crystallogr.* 66, 486–501.
- (71) Adams, P. D., Afonine, P. V., Bunkóczi, G., Chen, V. B., Davis, I. W., Echols, N., Headd, J. J., Hung, L.-W., Kapral, G. J., Grosse-Kunstleve, R. W., McCoy, A. J., Moriarty, N. W., Oeffner, R., Read, R. J., Richardson, D. C., Richardson, J. S., Terwilliger, T. C., and Zwart, P. H. (2010) PHENIX. A comprehensive Python-based system for macromolecular structure solution. *Acta Crystallogr., Sect. D: Biol. Crystallogr.* 66, 213–221.
- (72) Skubák, P., Murshudov, G. N., and Pannu, N. S. (2004) Direct incorporation of experimental phase information in model refinement. *Acta Crystallogr., Sect. D: Biol. Crystallogr.* 60, 2196–2201.

**SUPPORTING INFORMATION TO THE PUBLICATION****Binding Mode Characterization and Early *in Vivo* Evaluation of Fragment-Like Thiols as Inhibitors of the Virulence Factor LasB from *Pseudomonas aeruginosa***

Andreas M. Kany<sup>†,‡</sup>, Asfandyar Sikandar<sup>‡,‡</sup>, Jörg Haupenthal<sup>†</sup>, Samir Yahiaoui<sup>†</sup>, Christine K. Maurer<sup>†</sup>, Ewgenij Proschak<sup>‡</sup>, Jesko Köhnke<sup>‡</sup>, Rolf W. Hartmann<sup>\*,†,§</sup>

<sup>†</sup> Department of Drug Design and Optimization, Helmholtz Institute for Pharmaceutical Research Saarland (HIPS), Campus E8.1, 66123, Saarbrücken, Germany

<sup>‡</sup> Workgroup Structural Biology of Biosynthetic Enzymes, Helmholtz Institute for Pharmaceutical Research Saarland (HIPS), Campus E8.1, 66123, Saarbrücken, Germany

<sup>§</sup> Department of Pharmacy, Pharmaceutical and Medicinal Chemistry, Saarland University, Campus E8.1, 66123 Saarbrücken, Germany

<sup>‡</sup> Institute of Pharmaceutical Chemistry, Goethe University Frankfurt, Max-von-Laue-Straße 9, 60438 Frankfurt, Germany

\* Rolf.Hartmann@helmholtz-hzi.de

**Table of Contents**

1	Supporting Tables and Figures .....	S3
2	Synthetic Procedures .....	S7
2.1	Thiol synthesis.....	S7
2.2	Thiocarbamate synthesis .....	S9
2.3	Synthesis of <i>N</i> -benzyl and <i>N</i> -alkyl mercaptoacetamides .....	S11

## 1 Supporting Tables and Figures

Table S1. Structures of compounds showing no activity in the *in vitro* LasB inhibition assay.

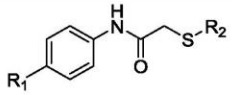
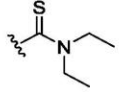
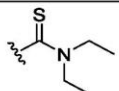
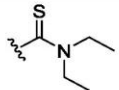
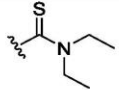
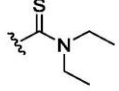
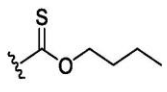
		
Compound	R <sub>1</sub>	R <sub>2</sub>
75		
76		
77		
78		
79		
80		
81		
82		

Table S2. Data collection and refinement statistics.

<b>LasB-27</b>	
Resolution range	38.22 - 1.3 (1.346 - 1.3)
Space group	P 1 21 1
Unit cell	40.3 90.0 41.9 90 114.1 90
Total reflections	128214 (12304)
Unique reflections	64739 (6304)
Multiplicity	2.0 (2.0)
Completeness (%)	96.96 (94.56)
Mean I/sigma(I)	17.78 (3.97)
R-merge	0.02876 (0.1924)
R-work	0.1421 (0.1982)
R-free	0.1557 (0.2238)
Number of non-hydrogen atoms	2736
macromolecules	2285
ligands	28
solvent	423
Protein residues	298
RMS(bonds)	0.008
RMS(angles)	0.99
Ramachandran favored (%)	96.28
Ramachandran allowed (%)	3.38
Ramachandran outliers (%)	0.34
Rotamer outliers (%)	0.43
Clashscore	2.50
Average B-factor	13.78
macromolecules	11.34
ligands	16.93
solvent	26.79

Statistics for the highest-resolution shell are shown in parentheses.

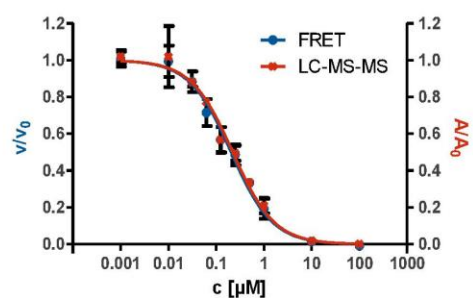


Figure S1. Comparison of FRET-assay results (blue,  $v/v_0$ ) with results from the LC-MS-based counterassay (red,  $A/A_0$ ) using the positive control phosphoramidon.  $IC_{50}$  values:  $207 \pm 13$  nM (FRET);  $223 \pm 15$  nM (LC-MS)

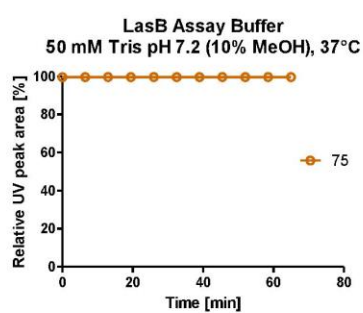


Figure S2. LC-MS stability assay of dithiocarbamate **75** in 50 mM Hepes pH 7.2 (10% methanol) at 37°C, confirming dithiocarbamates to be stable toward hydrolysis within the experimental timeframe of the assay.

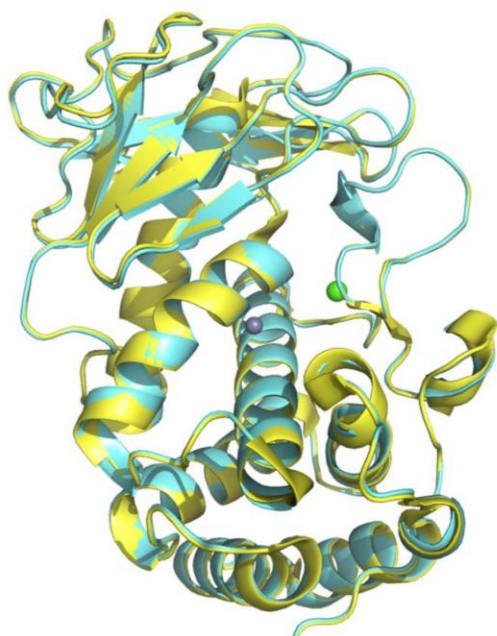


Figure S3. Superposition of LasB apo (yellow) with LasB-27 (cyan). Binding of the inhibitor does not trigger LasB to adopt a closed conformation.

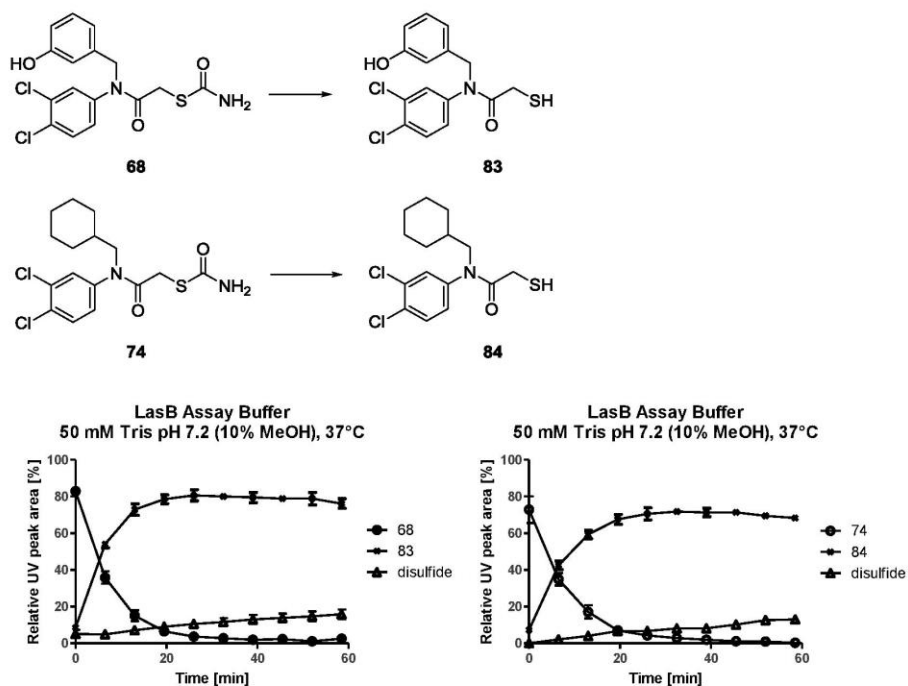


Figure S4. LC-MS stability assay of compounds 68 and 74, showing *N*-substitution not to affect thiocarbamate half-life.

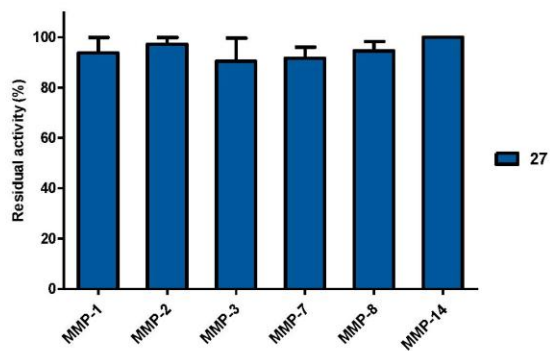
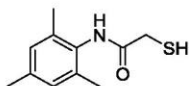


Figure S5. Inhibition of selected MMPs by 27. Values are means of at least three independent determinations at 100  $\mu$ M (50  $\mu$ M on MMP-8).

## 2 Synthetic Procedures

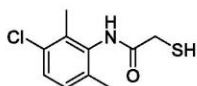
### 2.1 Thiol synthesis

#### 2-mercapto-*N*-mesitylacetamide (**33**)

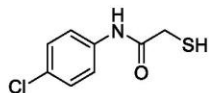


2,4,6-trimethylaniline (208  $\mu\text{L}$ , 1.48 mmol) was placed in a crimp vial. The vial was evacuated and flushed with nitrogen three times, followed by addition of thioglycolic acid (114  $\mu\text{L}$ , 1.62 mmol). The vial was flushed with argon and heated to 120°C for 6 hours. The crude was purified using automated flash chromatography (reversed-phase: acetonitrile + 0.1% formic acid:water + 0.1% formic acid 5:95 to 100:0) to yield the title compound as a white powder (43 mg, 14%).  $^1\text{H}$  NMR (300 MHz,  $\text{DMSO-d}_6$ )  $\delta$  ppm 2.10 (s, 6 H), 2.21 (s, 3 H), 2.93 (br. s, 1 H), 3.28 (s, 2 H), 6.86 (s, 2 H), 9.30 (s, 1 H);  $^{13}\text{C}$  NMR (75 MHz,  $\text{DMSO-d}_6$ )  $\delta$  ppm 17.9, 18.1, 20.5, 27.2, 128.2, 132.1, 134.8, 135.4, 168.5; MS (ESI<sup>+</sup>)  $m/z$  210 (M+H)<sup>+</sup>

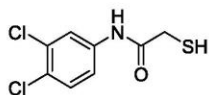
#### *N*-(3-chloro-2,6-dimethylphenyl)-2-mercaptoacetamide (**34**)



3-chloro-2,6-dimethylaniline (170 mg, 1.09 mmol) was placed in a crimp vial. The vial was evacuated and flushed with nitrogen three times, followed by addition of thioglycolic acid (91  $\mu\text{L}$ , 1.30 mmol). The vial was flushed with argon and heated to 120°C for 40 hours. The crude was purified using automated flash chromatography (reversed-phase: acetonitrile + 0.1% formic acid:water + 0.1% formic acid 30:70 to 80:20) to yield the title compound as a white powder (33 mg, 13%).  $^1\text{H}$  NMR (300 MHz,  $\text{DMSO-d}_6$ )  $\delta$  ppm 2.14 (s, 3 H), 2.18 (s, 3 H), 2.99 (br. s., 1 H), 3.32 (s, 2 H), 7.11 (d,  $J = 8.2$  Hz, 1 H), 7.27 (d,  $J = 8.3$  Hz, 1 H), 9.61 (s, 1 H);  $^{13}\text{C}$  NMR (75 MHz,  $\text{DMSO-d}_6$ )  $\delta$  ppm 15.3, 17.8, 27.1, 127.1, 128.4, 130.8, 133.3, 134.5, 136.2, 168.7; MS (ESI<sup>+</sup>)  $m/z$  230 (M+H)<sup>+</sup>

*N*-(4-chlorophenyl)-2-mercaptoacetamide (**35**)

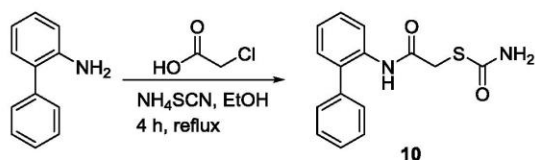
4-chloroaniline (200 mg, 1.57 mmol) was placed in a crimp vial. The vial was evacuated and flushed with nitrogen three times, followed by addition of thioglycolic acid (120  $\mu$ L, 1.72 mmol). The vial was flushed with argon and heated to 120°C for 5 hours. The crude was purified by automated flash chromatography (petroleum ether:ethyl acetate 90:10 to 70:30) to yield the title compound as a white powder (187 mg, 59%).  $^1\text{H}$  NMR (300 MHz, DMSO- $d_6$ )  $\delta$  ppm 2.97 (br. s., 1 H) 3.29 (s, 2 H) 7.30 - 7.42 (m, 2 H) 7.53 - 7.68 (m, 2 H) 10.21 (s, 1 H);  $^{13}\text{C}$  NMR (75 MHz, DMSO- $d_6$ )  $\delta$  ppm 28.2, 120.6, 126.9, 128.7, 137.9, 168.7; MS (ESI $^+$ )  $m/z$  202 (M+H) $^+$

*N*-(3,4-dichlorophenyl)-2-mercaptoacetamide (**36**)

3,4-dichloroaniline (800 mg, 4.94 mmol) was placed in a crimp vial. The vial was evacuated and flushed with nitrogen three times, followed by addition of thioglycolic acid (350  $\mu$ L, 5.02 mmol). The vial was flushed with argon and heated to 120°C for 5 hours. The crude was purified by automated flash chromatography (petroleum ether:ethyl acetate 90:10 to 55:45) to yield the title compound as a white powder (792 mg, 68%).  $^1\text{H}$  NMR (300 MHz, DMSO- $d_6$ )  $\delta$  ppm 3.00 (s, 1 H), 3.31 (s, 2 H), 7.47 (dd,  $J$  = 8.9, 2.4 Hz, 1 H), 7.58 (d,  $J$  = 8.8 Hz, 1 H), 7.97 (d,  $J$  = 2.4 Hz, 1 H), 10.38 (s, 1 H);  $^{13}\text{C}$  NMR (75 MHz, DMSO- $d_6$ )  $\delta$  ppm 28.3, 119.1, 120.2, 124.8, 130.7, 131.0, 139.0, 169.1; MS (ESI $^+$ )  $m/z$  236 (M+H) $^+$

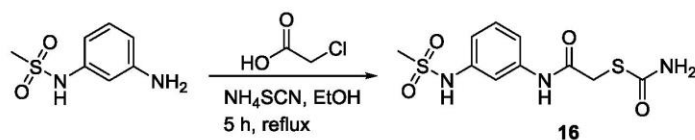
## 2.2 Thiocarbamate synthesis

*S*-(2-([1,1'-biphenyl]-2-ylamino)-2-oxoethyl) carbamothioate (**10**)

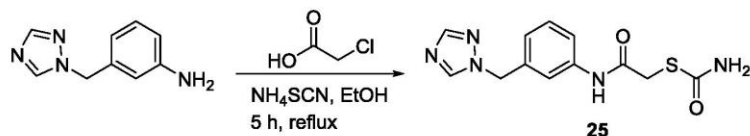


2-Aminobiphenyl (100 mg, 0.59 mmol) was added to a solution of chloroacetic acid (56 mg, 0.59 mmol) and ammonium thiocyanate (45 mg, 0.59 mmol) in 5 mL absolute ethanol. The reaction was refluxed for 4 hours. Water was added and the mixture extracted with ethyl acetate. The combined organic phases were washed with brine, dried over sodium sulfate and concentrated under reduced pressure to give the crude which was purified using automated flash chromatography (reversed-phase: acetonitrile + 0.1% formic acid:water + 0.1% formic acid 20:80 to 80:20) to yield the title compound as a white powder (44 mg, 26%). <sup>1</sup>H NMR (300 MHz, DMSO-*d*<sub>6</sub>) δ ppm 3.53 (s, 2 H), 7.20 - 8.00 (br. s., 2 H), 7.22 - 7.50 (m, 8 H), 7.65 (d, *J* = 7.8 Hz, 2 H), 9.25 (s, 1 H); <sup>13</sup>C NMR (75 MHz, DMSO-*d*<sub>6</sub>) δ ppm 33.4, 125.4, 125.6, 127.4, 127.8, 128.6, 128.8, 130.3, 134.5, 135.2, 138.3, 166.0, 167.3; MS (ESI<sup>+</sup>) *m/z* 287 (M+H)<sup>+</sup>

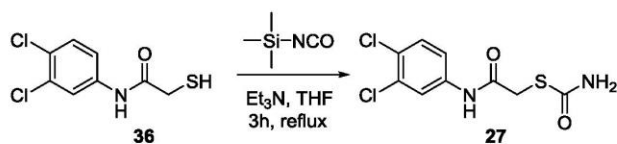
*S*-(2-((3-(methylsulfonamido)phenyl)amino)-2-oxoethyl) carbamothioate (**16**)



*N*-(3-Aminophenyl)methanesulfonamide (100 mg, 0.54 mmol) was added to a solution of chloroacetic acid (51 mg, 0.54 mmol) and ammonium thiocyanate (41 mg, 0.54 mmol) in 5 mL absolute ethanol. The reaction was refluxed for 5 hours. Water was added and the mixture extracted with ethyl acetate. The combined organic phases were washed with brine, dried over sodium sulfate and concentrated under reduced pressure to give the crude which was purified using automated flash chromatography (reversed-phase: acetonitrile + 0.1% formic acid:water + 0.1% formic acid 5:95 to 30:70) to yield the title compound as a white powder (33 mg, 20%). <sup>1</sup>H NMR (300 MHz, DMSO-*d*<sub>6</sub>) δ ppm 2.97 (s, 3 H), 3.68 (s, 2 H), 6.88 (m, 1 H), 7.24 (t, *J* = 8.1 Hz, 1 H), 7.34 (m, 1 H), 7.40 - 7.89 (br. s., 2 H), 7.50 (t, *J* = 2.0 Hz, 1 H), 9.75 (s, 1 H), 10.17 (s, 1 H); <sup>13</sup>C NMR (75 MHz, DMSO-*d*<sub>6</sub>) δ ppm 34.1, 110.3, 114.5, 114.6, 129.5, 138.8, 139.8, 166.2, 167.0; MS (ESI<sup>+</sup>) *m/z* 304 (M+H)<sup>+</sup>

*S*-2-((3-((1*H*-1,2,4-triazol-1-yl)methyl)phenyl)amino)-2-oxoethyl carbamothioate (**25**)

4-((1*H*-1,2,4-triazol-1-yl)methyl)aniline (100 mg, 0.57 mmol) was added to a solution of chloroacetic acid (54 mg, 0.57 mmol) and ammonium thiocyanate (44 mg, 0.57 mmol) in 7.5 mL absolute ethanol. The reaction was refluxed for 5 hours. Water was added and the mixture extracted with ethyl acetate. The combined organic phases were washed with brine, dried over sodium sulfate and concentrated under reduced pressure to give the crude which was purified using automated flash chromatography (reversed-phase: acetonitrile + 0.1% formic acid:water + 0.1% formic acid 10:90 to 30:70) to yield the title compound as a white powder (10 mg, 6%). <sup>1</sup>H NMR (300 MHz, DMSO-*d*<sub>6</sub>) δ ppm 3.68 (s, 2 H), 5.34 (s, 2 H), 7.23 (m, 2 H), 7.54 (m, 2 H), 7.39 - 7.89 (br. s., 2 H), 7.96 (s, 1 H), 8.61 (s, 1 H), 10.15 (s, 1 H); <sup>13</sup>C NMR (75 MHz, DMSO-*d*<sub>6</sub>) δ ppm 34.0, 48.6, 51.7, 119.1, 128.5, 131.0, 138.7, 144.0, 151.6, 166.2, 166.9; MS (ESI<sup>+</sup>) *m/z* 292 (M+H)<sup>+</sup>

*S*-2-((3,4-dichlorophenyl)amino)-2-oxoethyl carbamothioate (**27**)

**36** was prepared according to the procedure described above and used without further purification starting from 200 mg 3,4-dichloroaniline (1.23 mmol). The crude was dissolved in 4 mL dry THF and triethylamine (170 μL, 1.23 mmol) and trimethylsilyl isocyanate (170 μL, 1.26 mmol) were added. The reaction mixture was refluxed under argon atmosphere for 3 hours. The reaction was quenched for 30 min with methanol. The crude was purified using automated flash chromatography (petroleum ether:ethyl acetate 80:20 to 90:10) to yield the title compound as a white powder (160 mg, 47% over two steps). <sup>1</sup>H NMR (300 MHz, DMSO-*d*<sub>6</sub>) δ ppm 3.70 (s, 2 H), 7.47 (dd, *J* = 8.9, 2.4 Hz, 1 H), 7.55 (d, *J* = 8.8 Hz, 1 H), 7.39-7.87, (br. s., 2 H), 7.97 (d, *J* = 2.3 Hz, 1 H), 10.42 (s, 1H); <sup>13</sup>C NMR (75 MHz, DMSO-*d*<sub>6</sub>) δ ppm 34.1, 119.1, 120.2, 124.7, 130.7, 131.0, 139.1, 166.0, 167.5; MS (ESI<sup>+</sup>) *m/z* 279 (M+H)<sup>+</sup>

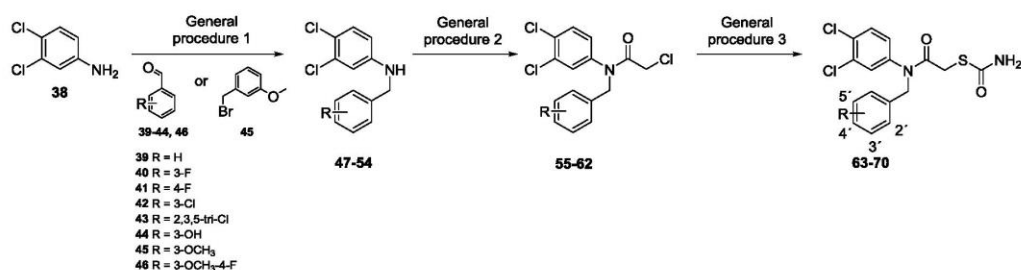
### 2.3 Synthesis of *N*-benzyl and *N*-alkyl mercaptoacetamides

*Preparation of N-benzylanilines 47-54 and N-alkylanilines 85-88 (General procedure 1).* To a solution of 3,4-dichloroaniline **38** (1 equiv.) in DCM (10 mL) in a crimp reaction vial was added the appropriate aldehyde (1.0 – 1.2 equiv.), followed by acetic acid (0.1 equiv). Sodium triacetoxyborohydride (1.5 – 2.0 equiv) was added stepwise. The vial was flushed with argon and the reaction was stirred for 20 hours at room temperature. The mixture was quenched 10% NaOH (5 mL) under cooling and extracted using DCM. The combined organic phases were washed with brine, dried over sodium sulfate and concentrated under reduced pressure to afford crude product.

*Preparation of N-benzyl-N-(3,4-dichlorophenyl)acetamides 55-62 and N-alkyl-N-(3,4-dichlorophenyl)-acetamides 89-92 (General procedure 2).* The appropriate *N*-benzylaniline or *N*-alkylaniline was dissolved in 10 mL of acetone. Chloroacetyl chloride (1.0 – 1.4 equiv.) was added dropwise under cooling on ice. After 30 min the reaction was allowed to warm at room temperature for 1 hour. The reaction was quenched by addition of saturated NaHCO<sub>3</sub> solution (5 mL) and stirring for 10 min. The mixture was extracted with ethyl acetate. The combined organic phases were washed with brine, dried over sodium sulfate and concentrated under reduced pressure to afford crude product.

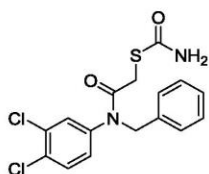
*Preparation of S-(2-((3,4-dichlorophenyl)(arylamino)-2-oxoethyl) carbamothioates 63-70 and S-(2-((3,4-dichlorophenyl)(alkylamino)-2-oxoethyl) carbamothioates 71-74 (General procedure 3).* The appropriate *N*-benzyl-*N*-(3,4-dichlorophenyl)acetamide or *N*-alkyl-*N*-(3,4-dichlorophenyl)-acetamide was dissolved in 4 mL ethanol and placed in a crimp vial, followed by addition ammonium thiocyanate (1 – 1.1 equiv.). The reaction was heated to 80°C for 2 hours. Water was added and the mixture was extracted with ethyl acetate. The combined organic phases were washed with brine, dried over sodium sulfate and concentrated under reduced pressure to give crude intermediate. The crude was dissolved in 2 mL ethanol and added dropwise to a pre-cooled mixture of 3 mL 90% sulfuric acid and 10% acetic acid. After stirring on ice for 30 min, the reaction mixture was diluted in water and extracted with ethyl acetate. Washing with brine, followed by drying over sodium sulfate and concentration under reduced pressure gave the crude.

### Synthesis of *S*-(2-((3,4-dichlorophenyl)(arylamino)-2-oxoethyl) carbamothioates 63-70



Scheme S1. Synthesis of *N*-benzyl mercaptoacetamides.

#### *S*-(2-(benzyl(3,4-dichlorophenyl)amino)-2-oxoethyl) carbamothioate (**63**)

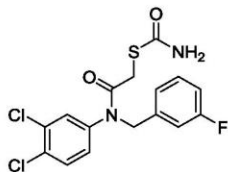


**47** was prepared according to general procedure 1 using 3,4-dichloroaniline (250 mg, 1.54 mmol), benzaldehyde (156  $\mu$ L, 1.54 mmol), acetic acid (8.8  $\mu$ L, 0.15 mmol) and sodium triacetoxyborohydride (491 mg, 2.32 mmol). The obtained brown oil (352 mg) was used without further purification. MS (ESI<sup>+</sup>)  $m/z$  252 (M+H)<sup>+</sup>

**55** was prepared according to general procedure 2 using **47** (352 mg, 1.40 mmol) and chloroacetyl chloride (111  $\mu$ L, 1.54 mmol). After 5 hours at room temperature, additional chloroacetyl chloride was added (37  $\mu$ L, 0.51 mmol) and the reaction stirred at room temperature for 17 hours. The obtained crude was purified using automated flash chromatography (reversed-phase: acetonitrile + 0.1% formic acid:water + 0.1% formic acid 30:70 to 50:50) to yield the title compound as a white powder (282 mg, 56% over two steps). MS (ESI<sup>+</sup>)  $m/z$  328 (M+H)<sup>+</sup>

**63** was prepared according to general procedure 3 using **55** (44 mg, 0.13 mmol) and ammonium thiocyanate (10 mg, 0.13 mmol). The crude was purified using automated flash chromatography (reversed-phase: acetonitrile + 0.1% formic acid:water + 0.1% formic acid 50:50 to 100:0) to yield the title compound as a white powder after freeze-drying (20 mg, 40%). <sup>1</sup>H NMR (300 MHz, DMSO-d<sub>6</sub>)  $\delta$  ppm 3.56 (br. s, 2 H), 4.89 (s, 2 H), 7.14 - 7.34 (m, 6 H), 7.39 - 7.84 (br. s, 2 H), 7.61 (d,  $J$  = 2.2 Hz, 1 H), 7.64 (d,  $J$  = 8.6 Hz, 1 H); <sup>13</sup>C NMR (75 MHz, DMSO-d<sub>6</sub>)  $\delta$  ppm 32.7, 52.2, 127.3, 127.8, 128.4, 128.7, 130.3, 130.6, 131.1, 131.5, 136.8, 141.5, 165.9, 167.8; MS (ESI<sup>+</sup>)  $m/z$  369 (M+H)<sup>+</sup>

*S*-2-((3,4-dichlorophenyl)(3-fluorobenzyl)amino)-2-oxoethyl carbamothioate (**64**)

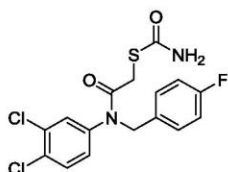


**48** was prepared according to general procedure 1 using 3,4-dichloroaniline (250 mg, 1.54 mmol), 3-fluorobenzaldehyde (196  $\mu$ L, 1.85 mmol), acetic acid (8.8  $\mu$ L, 0.15 mmol) and sodium triacetoxyborohydride (654 mg, 3.09 mmol). The obtained brown oil (401 mg) was used without further purification. MS (ESI<sup>+</sup>)  $m/z$  270 (M+H)<sup>+</sup>

**56** was prepared according to general procedure 2 using **48** (200 mg, 0.74 mmol) and chloroacetyl chloride (82  $\mu$ L, 1.04 mmol). The obtained crude (258 mg) was used without further purification. MS (ESI<sup>+</sup>)  $m/z$  346 (M+H)<sup>+</sup>

**64** was prepared according to general procedure 3 using **56** (258 mg, 0.74 mmol) and ammonium thiocyanate (56 mg, 0.74 mmol). The crude was purified using automated flash chromatography (reversed-phase: acetonitrile + 0.1% formic acid:water + 0.1% formic acid 30:70 to 100:0) to yield the title compound as a white powder after freeze-drying (117 mg, 39% over three steps). <sup>1</sup>H NMR (300 MHz, DMSO-*d*<sub>6</sub>)  $\delta$  ppm 3.57 (br. s, 2 H), 4.90 (s, 2 H), 7.01- 7.11 (m, 3 H), 7.28 (dd,  $J$  = 8.6, 1 H), 7.30- 7.38 (m, 1 H), 7.66 (m, 1 H), 7.40- 7.80 (br. s, 2 H), 7.67 (d,  $J$  = 1.0, 1 H); <sup>13</sup>C NMR (75 MHz, DMSO-*d*<sub>6</sub>)  $\delta$  ppm 32.8, 51.9, 114.2 (d,  $J_{C-F}$  = 20.9 Hz), 114.6 (d,  $J_{C-F}$  = 21.6 Hz), 123.9 (d,  $J_{C-F}$  = 2.24 Hz), 128.7, 130.4, 130.5 (d,  $J_{C-F}$  = 8.2 Hz), 130.8, 131.3, 131.7, 139.9 (d,  $J_{C-F}$  = 7.5 Hz), 141.6, 162.3 (d,  $J_{C-F}$  = 243.6 Hz), 166.1, 168.1; MS (ESI<sup>+</sup>)  $m/z$  387 (M+H)<sup>+</sup>

*S*-2-((3,4-dichlorophenyl)(4-fluorobenzyl)amino)-2-oxoethyl carbamothioate (**65**)



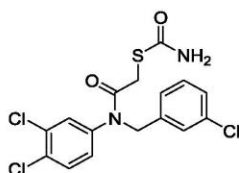
**49** was prepared according to general procedure 1 using 3,4-dichloroaniline (250 mg, 1.54 mmol), 4-fluorobenzaldehyde (199  $\mu$ L, 1.85 mmol), acetic acid (8.8  $\mu$ L, 0.15 mmol) and sodium triacetoxyborohydride (653 mg, 3.09 mmol). The obtained brown oil (398 mg) was used without further purification. MS (ESI<sup>+</sup>)  $m/z$  270 (M+H)<sup>+</sup>

**57** was prepared according to general procedure 2 using **49** (185 mg, 0.68 mmol) and chloroacetyl chloride (54  $\mu$ L, 0.68 mmol). After 3 hours at room temperature, additional chloroacetyl chloride was

added (27  $\mu\text{L}$ , 0.34 mmol) and the reaction stirred at room temperature for 2 hours. The obtained crude (226 mg) was used without further purification. MS (ESI<sup>+</sup>)  $m/z$  346 (M+H)<sup>+</sup>

**65** was prepared according to general procedure **3** using **57** (266 mg, 0.65 mmol) and ammonium thiocyanate (50 mg, 0.66 mmol). The crude was purified using automated flash chromatography (reversed-phase: acetonitrile + 0.1% formic acid:water + 0.1% formic acid 40:60 to 100:0) to yield the title compound as a white powder after freeze-drying (109 mg, 37% over three steps). <sup>1</sup>H NMR (300 MHz, DMSO-*d*<sub>6</sub>)  $\delta$  ppm 3.54 (br. s, 2 H), 4.86 (s, 2 H), 7.06 - 7.16 (m, 2 H), 7.17 - 7.27 (m, 3 H), 7.37-7.96 (br. s, 2 H), 7.61 (d,  $J$  = 2.4 Hz, 1 H), 7.65 (d,  $J$  = 8.6 Hz, 1 H); <sup>13</sup>C NMR (75 MHz, DMSO-*d*<sub>6</sub>)  $\delta$  ppm 32.7, 51.5, 115.2 (d,  $J_{\text{C-F}}$  = 20.9 Hz), 128.8, 130.0 (d,  $J_{\text{C-F}}$  = 8.2 Hz), 130.4, 130.6, 131.2, 131.6, 133.0 (d,  $J_{\text{C-F}}$  = 3.0 Hz), 141.4, 161.4 (d,  $J_{\text{C-F}}$  = 243.6 Hz), 165.9, 167.8; MS (ESI<sup>+</sup>)  $m/z$  387 (M+H)<sup>+</sup>

*S*-(2-((3,4-dichlorophenyl)(3-chlorobenzyl)amino)-2-oxoethyl) carbamothioate (**66**)

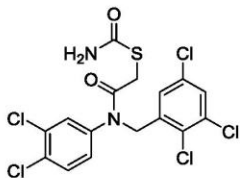


**50** was prepared according to general procedure 1 using 3,4-dichloroaniline (250 mg, 1.54 mmol), 3-chlorobenzaldehyde (210  $\mu\text{L}$ , 1.85 mmol), acetic acid (8.8  $\mu\text{L}$ , 0.15 mmol) and sodium triacetoxyborohydride (654 mg, 3.09 mmol). The obtained brown oil (458 mg) was used without further purification. MS (ESI<sup>+</sup>)  $m/z$  286 (M+H)<sup>+</sup>

**58** was prepared according to general procedure 2 using **50** (229 mg, 0.80 mmol) and chloroacetyl chloride (70  $\mu\text{L}$ , 0.88 mmol). After 1 hour at room temperature, additional chloroacetyl chloride was added (35  $\mu\text{L}$ , 0.44 mmol) and the reaction stirred at room temperature for 2 hours. The obtained crude (255 mg) was used without further purification. MS (ESI<sup>+</sup>)  $m/z$  362 (M+H)<sup>+</sup>

**66** was prepared according to general procedure **3** using **58** (255 mg, 0.70 mmol) and ammonium thiocyanate (53 mg, 0.70 mmol). The crude was purified using automated flash chromatography (reversed-phase: acetonitrile + 0.1% formic acid:water + 0.1% formic acid 30:70 to 100:0) to yield the title compound as a white powder after freeze-drying (150 mg, 49% over three steps). <sup>1</sup>H NMR (300 MHz, DMSO-*d*<sub>6</sub>)  $\delta$  ppm 3.57 (br. s, 2 H), 4.89 (s, 2 H), 7.13- 7.21 (m, 1 H), 7.23- 7.36 (m, 4 H), 7.45- 7.85 (br. s, 2 H), 7.66 (dd,  $J$  = 8.6, 2 H); <sup>13</sup>C NMR (75 MHz, DMSO-*d*<sub>6</sub>)  $\delta$  ppm 32.7, 51.7, 126.5, 127.3, 127.7, 128.7, 130.2, 130.7, 131.2, 131.6, 133.1, 139.4, 141.4, 165.9, 168.0; MS (ESI<sup>+</sup>)  $m/z$  403 (M+H)<sup>+</sup>

*S*-(2-((3,4-dichlorophenyl)(3-chlorobenzyl)amino)-2-oxoethyl) carbamothioate (**67**)

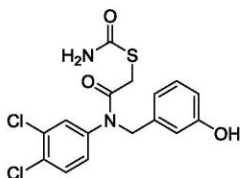


**51** was prepared according to general procedure 1 using 3,4-dichloroaniline (250 mg, 1.54 mmol), 2,3,5-trichlorobenzaldehyde (386 mg, 1.85 mmol), acetic acid (8.8  $\mu$ L, 0.15 mmol) and sodium triacetoxyborohydride (654 mg, 3.09 mmol). The obtained crude was purified using automated flash chromatography (petroleum ether:ethyl acetate 100:0 to 30:70) to yield the title compound as a white powder (300 mg, 55%). MS (ESI<sup>+</sup>) *m/z* 403 (M+H)<sup>+</sup>

**59** was prepared according to general procedure 2 using **51** (150 mg, 0.42 mmol) and chloroacetyl chloride (48  $\mu$ L, 0.59 mmol). After 1 hour at room temperature, additional chloroacetyl chloride was added (48  $\mu$ L, 0.59 mmol) and the reaction stirred at room temperature for 2 hours. The obtained crude was purified using automated flash chromatography (reversed-phase: acetonitrile + 0.1% formic acid:water + 0.1% formic acid 30:70 to 100:0) to yield the title compound as a white powder (116 mg, 64%). MS (ESI<sup>+</sup>) *m/z* 430 (M+H)<sup>+</sup>

**67** was prepared according to general procedure 3 using **59** (116 mg, 0.27 mmol) and ammonium thiocyanate (21 mg, 0.27 mmol). The crude was purified using automated flash chromatography (reversed-phase: acetonitrile + 0.1% formic acid:water + 0.1% formic acid 40:60 to 100:0) to yield the title compound as a white powder after freeze-drying (88 mg, 43% over three steps). <sup>1</sup>H NMR (300 MHz, DMSO-*d*<sub>6</sub>)  $\delta$  ppm 3.60 (br. s, 2 H), 4.97 (br. s, 2 H), 7.33-7.90 (br. s, 2 H) 7.40 (d, *J* = 8.4, 1 H), 7.50 (br. s, 1 H), 7.69 (d, *J* = 8.6, 1 H), 7.72-7.78 (m, 1 H), 7.81 (br. s, 1 H); <sup>13</sup>C NMR (75 MHz, DMSO-*d*<sub>6</sub>)  $\delta$  ppm 32.7, 51.0, 127.9, 128.5, 128.9, 129.2, 130.2, 130.9, 131.3, 131.7, 132.3, 132.9, 138.3, 141.3, 165.9, 168.3; MS (ESI<sup>+</sup>) *m/z* 473 (M+H)<sup>+</sup>

*S*-(2-((3,4-dichlorophenyl)(3-hydroxybenzyl)amino)-2-oxoethyl) carbamothioate (**68**)



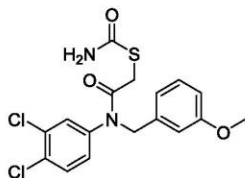
**52** was prepared according to general procedure 1 using 3,4-dichloroaniline (250 mg, 1.54 mmol), 3-hydroxybenzaldehyde (226 mg, 1.85 mmol), acetic acid (8.8  $\mu$ L, 0.15 mmol) and sodium

triacetoxyborohydride (654 mg, 3.09 mmol). The obtained pale oil (344 mg) was used without further purification. MS (ESI<sup>+</sup>)  $m/z$  268 (M+H)<sup>+</sup>

**60** was prepared according to general procedure 2 using **52** (172 mg, 0.64 mmol) and chloroacetyl chloride (51  $\mu$ L, 0.64 mmol). After 1 hour at room temperature, additional chloroacetyl chloride was added (26  $\mu$ L, 0.32 mmol) and the reaction stirred at room temperature for 2 hours. The obtained pale oil (220 mg) was used without further purification. MS (ESI<sup>+</sup>)  $m/z$  344 (M+H)<sup>+</sup>

**68** was prepared according to general procedure 3 using **60** (220 mg, 0.64 mmol) and ammonium thiocyanate (49 mg, 0.64 mmol). The crude was purified using automated flash chromatography (reversed-phase: acetonitrile + 0.1% formic acid:water + 0.1% formic acid 25:75 to 100:0) to yield the title compound as a white powder after freeze-drying (61 mg, 21% over three steps). <sup>1</sup>H NMR (300 MHz, DMSO-*d*<sub>6</sub>)  $\delta$  ppm 2.07 (s, 1 H), 3.55 (br. s, 2 H), 4.79 (br. s, 2 H), 6.50 - 6.66 (m, 3 H), 7.07 (t,  $J$  = 8.0 Hz, 1 H), 7.22 (dd,  $J$  = 8.6, 2.4 Hz, 1 H), 7.32 - 7.88 (br. s, 2 H), 7.59 (d,  $J$  = 2.4 Hz, 1 H), 7.65 (d,  $J$  = 8.6 Hz, 1 H), 9.35 (s, 1 H); <sup>13</sup>C NMR (75 MHz, DMSO-*d*<sub>6</sub>)  $\delta$  ppm 32.7, 52.2, 114.3, 114.8, 118.4, 128.7, 129.4, 130.3, 130.4, 131.1, 131.4, 138.2, 141.5, 157.4, 165.8, 167.7; MS (ESI<sup>+</sup>)  $m/z$  385 (M+H)<sup>+</sup>

*S*-(2-((3,4-dichlorophenyl)(3-methoxybenzyl)amino)-2-oxoethyl) carbamothioate (**69**)

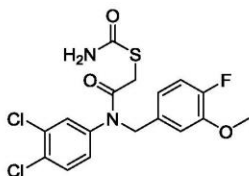


3,4-dichloroaniline (300 mg, 1.85 mmol), 3-methoxybenzyl bromide (260  $\mu$ L, 1.85 mmol) and potassium carbonate (511 mg, 3.7 mmol) were placed in a crimp vial and dissolved in 5 mL DMF. The reaction was heated to 120°C for 20 hours. Water (5 mL) was added and the mixture extracted with ethyl acetate. The combined organic phases were washed with brine, dried over sodium sulfate and concentrated under reduced pressure. The crude was purified using automated flash chromatography (petroleum ether:ethyl acetate 100:0 to 80:20) to yield the title compound as a pale oil (342 mg, 66%). MS (ESI<sup>+</sup>)  $m/z$  282 (M+H)<sup>+</sup>

**61** was prepared according to general procedure 2 using **53** (150 mg, 0.53 mmol) and chloroacetyl chloride (44  $\mu$ L, 0.56 mmol). After 1 hour at room temperature, additional chloroacetyl chloride was added (20  $\mu$ L, 0.25 mmol) and the reaction stirred at room temperature for 2 hours. The obtained pale oil (140 mg) was used without further purification. MS (ESI<sup>+</sup>)  $m/z$  358 (M+H)<sup>+</sup>

**69** was prepared according to general procedure 3 using **61** (140 mg, 0.39 mmol) and ammonium thiocyanate (30 mg, 0.39 mmol). The crude was purified using automated flash chromatography (reversed-phase: acetonitrile + 0.1% formic acid:water + 0.1% formic acid 40:60 to 100:0) to yield the title compound as a white powder after freeze-drying (45 mg, 21% over two steps). <sup>1</sup>H NMR (300 MHz, DMSO-d<sub>6</sub>) δ ppm 3.56 (br. s, 2 H), 3.71 (s, 3 H), 4.86 (s, 2 H), 6.71 - 6.84 (m, 3 H), 7.20 (t, *J* = 8.0 Hz, 1 H), 7.25 (dd, *J* = 8.5, 2.5 Hz, 1 H), 7.36-7.85 (br. s, 2 H), 7.61 - 7.68 (m, 2 H); <sup>13</sup>C NMR (75 MHz, DMSO-d<sub>6</sub>) δ ppm 32.7, 52.1, 55.0, 112.8, 113.2, 119.9, 128.7, 129.4, 130.2, 130.5, 131.1, 131.5, 138.4, 141.6, 159.3, 165.9, 167.8; MS (ESI<sup>+</sup>) *m/z* 399 (M+H)<sup>+</sup>

*S*-(2-((3,4-dichlorophenyl)(4-fluoro-3-methoxybenzyl)amino)-2-oxoethyl) carbamothioate (**70**)

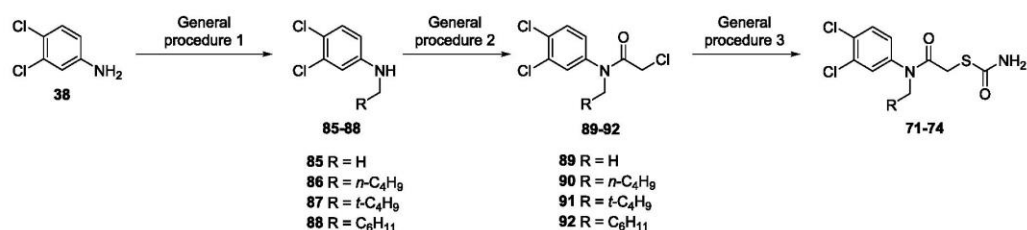


**54** was prepared according to general procedure 1 using 3,4-dichloroaniline (300 mg, 1.85 mmol), 4-fluoro-3-methoxybenzaldehyde (343 mg, 2.22 mmol), acetic acid (10.6 μL, 0.19 mmol) and sodium triacetoxyborohydride (785 mg, 3.70 mmol). The obtained oil (550 mg) was used without further purification. MS (ESI<sup>+</sup>) *m/z* 300 (M+H)<sup>+</sup>

**62** was prepared according to general procedure 2 using **54** (200 mg, 0.67 mmol) and chloroacetyl chloride (64 μL, 0.80 mmol). The obtained pale oil (162 mg) was used without further purification. MS (ESI<sup>+</sup>) *m/z* 376 (M+H)<sup>+</sup>

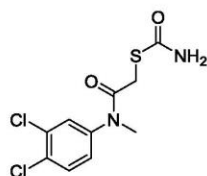
**70** was prepared according to general procedure 3 using **62** (162 mg, 0.43 mmol) and ammonium thiocyanate (36 mg, 0.47 mmol). The crude was purified using automated flash chromatography (reversed-phase: acetonitrile + 0.1% formic acid:water + 0.1% formic acid 30:70 to 100:0) to yield the title compound as a white powder after freeze-drying (38 mg, 14% over three steps). <sup>1</sup>H NMR (300 MHz, DMSO-d<sub>6</sub>) δ ppm 3.54 (br. s, 2 H), 3.73 - 3.82 (s, 3 H), 4.85 (s, 2 H), 6.68 - 6.78 (m, 1 H), 6.98 (d, *J* = 8.0 Hz, 1 H), 7.09 (dd, *J* = 11.6, 8.3 Hz, 1 H), 7.25 (dd, *J* = 8.6, 2.4 Hz, 1 H), 7.36 - 7.98 (br. s, 2 H), 7.62 - 7.68 (m, 2 H); <sup>13</sup>C NMR (75 MHz, DMSO-d<sub>6</sub>) δ ppm 32.7, 51.8, 55.9, 113.3, 115.7 (d, *J*<sub>C-F</sub> = 17.9 Hz, 1 C), 120.2 (d, *J*<sub>C-F</sub> = 6.7 Hz, 1 C), 128.8, 130.4, 130.6, 131.2, 131.5, 133.6 (d, *J*<sub>C-F</sub> = 3.7 Hz, 1 C), 141.5, 147.0 (d, *J*<sub>C-F</sub> = 10.4 Hz, 1 C), 150.7 (d, *J*<sub>C-F</sub> = 242.9 Hz, 1 C), 166.0, 167.9; MS (ESI<sup>+</sup>) *m/z* 417 (M+H)<sup>+</sup>

### Synthesis of *S*-(2-((3,4-dichlorophenyl)(alkylamino)-2-oxoethyl) carbamothioates 71-74



Scheme S2. Synthesis of *N*-alkyl mercaptoacetamides.

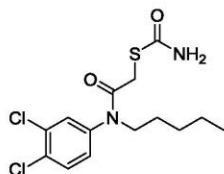
### *S*-(2-((3,4-dichlorophenyl)(methyl)amino)-2-oxoethyl) carbamothioate (71)



**85** was prepared according to general procedure 1 using 3,4-dichloroaniline (300 mg, 1.85 mmol), formaldehyde (81  $\mu$ L, 2.22 mmol), acetic acid (10.6  $\mu$ L, 0.19 mmol) and sodium triacetoxyborohydride (785 mg, 3.70 mmol). The obtained crude was purified using automated flash chromatography (petroleum ether:ethyl acetate 100:0 to 30:70) to yield the title compound as a pale powder (80 mg, 25%). MS (ESI<sup>+</sup>)  $m/z$  217 (M+H)<sup>+</sup>

**89** was prepared according to general procedure 2 using **85** (80 mg, 0.45 mmol) and chloroacetyl chloride (44  $\mu$ L, 0.55 mmol). The obtained pale oil (107 mg) was used without further purification. MS (ESI<sup>+</sup>)  $m/z$  252 (M+H)<sup>+</sup>

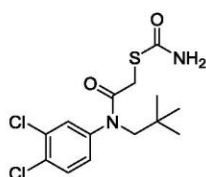
**71** was prepared according to general procedure 3 using **89** (107 mg, 0.42 mmol) and ammonium thiocyanate (36 mg, 0.47 mmol). The crude was purified using automated flash chromatography (reversed-phase: acetonitrile + 0.1% formic acid:water + 0.1% formic acid 30:70 to 100:0) to yield the title compound as a white powder after freeze-drying (41 mg, 32% over three steps). <sup>1</sup>H NMR (300 MHz, DMSO-*d*<sub>6</sub>)  $\delta$  ppm 3.19 (br. s, 3 H), 3.55 (br. s, 2 H), 7.28 - 7.88 (br. s, 2H), 7.42 (dd,  $J$  = 8.6 Hz,  $J$  = 2.1 Hz, 1 H), 7.72 (d,  $J$  = 8.7 Hz, 1 H), 7.75 (br. s, 1 H); <sup>13</sup>C NMR (75 MHz, DMSO-*d*<sub>6</sub>)  $\delta$  ppm 32.6, 37.3, 127.7, 129.4, 131.2, 131.6, 143.4, 165.9, 167.5; MS (ESI<sup>+</sup>)  $m/z$  293 (M+H)<sup>+</sup>

*S*-(2-((3,4-dichlorophenyl)(pentyl)amino)-2-oxoethyl) carbamothioate (**72**)

**86** was prepared according to general procedure 1 using 3,4-dichloroaniline (300 mg, 1.85 mmol), valeraldehyde (217  $\mu$ L, 2.04 mmol), acetic acid (10.6  $\mu$ L, 0.19 mmol) and sodium triacetoxyborohydride (785 mg, 3.70 mmol). The obtained oil (360 mg) was used without further purification. MS (ESI<sup>+</sup>)  $m/z$  232 (M+H)<sup>+</sup>

**90** was prepared according to general procedure 2 using **86** (180 mg, 0.78 mmol) and chloroacetyl chloride (74  $\mu$ L, 0.93 mmol). The obtained pale oil (240 mg) was used without further purification. MS (ESI<sup>+</sup>)  $m/z$  308 (M+H)<sup>+</sup>

**72** was prepared according to general procedure 3 using **90** (240 mg, 0.78 mmol) and ammonium thiocyanate (65 mg, 0.86 mmol). The crude was purified using automated flash chromatography (reversed-phase: acetonitrile + 0.1% formic acid:water + 0.1% formic acid 50:50 to 100:0) to yield the title compound as a white powder after freeze-drying (110 mg, 34% over three steps). <sup>1</sup>H NMR (300 MHz, DMSO-*d*<sub>6</sub>)  $\delta$  ppm 0.77 - 0.87 (m, 3 H), 1.10 - 1.30 (m, 4 H), 1.36 (m, 2 H), 3.45 (br. s, 2 H), 3.61 (t,  $J$  = 7.3 Hz, 2 H), 7.21 - 7.90 (br. s, 2 H), 7.39 (m, 1 H), 7.72 (s, 1 H), 7.75 (s, 1 H); <sup>13</sup>C NMR (75 MHz, DMSO-*d*<sub>6</sub>)  $\delta$  ppm 13.8, 21.7, 26.7, 28.1, 32.8, 38.7, 39.0, 39.2, 39.8, 40.1, 40.4, 48.7, 128.9, 130.4, 131.2, 131.7, 141.8, 165.9, 167.1; MS (ESI<sup>+</sup>)  $m/z$  349 (M+H)<sup>+</sup>

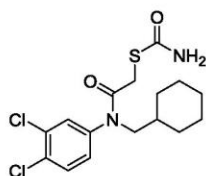
*S*-(2-((3,4-dichlorophenyl)(neopentyl)amino)-2-oxoethyl) carbamothioate (**73**)

**87** was prepared according to general procedure 1 using 3,4-dichloroaniline (300 mg, 1.85 mmol), pivaldehyde (221  $\mu$ L, 2.04 mmol), acetic acid (10.6  $\mu$ L, 0.19 mmol) and sodium triacetoxyborohydride (785 mg, 3.70 mmol). The obtained oil (360 mg) was used without further purification. MS (ESI<sup>+</sup>)  $m/z$  232 (M+H)<sup>+</sup>

**91** was prepared according to general procedure 2 using **87** (180 mg, 0.78 mmol) and chloroacetyl chloride (74  $\mu$ L, 0.93 mmol). The obtained pale oil (240 mg) was used without further purification. MS (ESI<sup>+</sup>)  $m/z$  308 (M+H)<sup>+</sup>

**73** was prepared according to general procedure 3 using **91** (240 mg, 0.78 mmol) and ammonium thiocyanate (65 mg, 0.86 mmol). The crude was purified using automated flash chromatography (reversed-phase: acetonitrile + 0.1% formic acid:water + 0.1% formic acid 30:70 to 100:0) to yield the title compound as a white powder after freeze-drying (20 mg, 6% over three steps). <sup>1</sup>H NMR (300 MHz, DMSO-d<sub>6</sub>) δ ppm 0.77 (s, 9 H), 3.54 (br. s, 2 H), 3.61 (s, 2 H), 7.28 - 7.79 (br. s, 2 H), 7.45 - 7.55 (dd, *J* = 2.0, *J* = 8.5, 1 H), 7.70 (d, *J* = 8.7 Hz, 1 H), 7.85 (br. s, 1 H); <sup>13</sup>C NMR (75 MHz, DMSO-d<sub>6</sub>) δ ppm 28.1, 33.0, 33.8, 59.7, 128.8, 130.2, 131.0, 131.5, 143.9, 166.0, 168.1; MS (ESI<sup>+</sup>) *m/z* 349 (M+H)<sup>+</sup>

*S*-(2-((cyclohexylmethyl)(3,4-dichlorophenyl)amino)-2-oxoethyl) carbamothioate (**74**)



**88** was prepared according to general procedure 1 using 3,4-dichloroaniline (300 mg, 1.85 mmol), cyclohexanecarboxaldehyde (224 μL, 1.85 mmol), acetic acid (10.6 μL, 0.19 mmol) and sodium triacetoxyborohydride (654 mg, 3.09 mmol). The obtained oil (400 mg) was used without further purification. MS (ESI<sup>+</sup>) *m/z* 258 (M+H)<sup>+</sup>

**92** was prepared according to general procedure 2 using **88** (200 mg, 0.78 mmol) and chloroacetyl chloride (86 μL, 1.08 mmol). The obtained pale oil (215 mg) was used without further purification. MS (ESI<sup>+</sup>) *m/z* 334 (M+H)<sup>+</sup>

**74** was prepared according to general procedure 3 using **92** (215 mg, 0.64 mmol) and ammonium thiocyanate (49 mg, 0.64 mmol). The crude was purified using automated flash chromatography (reversed-phase: acetonitrile + 0.1% formic acid:water + 0.1% formic acid 40:60 to 100:0) to yield the title compound as a white powder after freeze-drying (71 mg, 25% over three steps). <sup>1</sup>H NMR (300 MHz, Chloroform-d) δ ppm 0.84 - 1.07 (m, 2 H), 1.07 - 1.29 (m, 3 H), 1.30 - 1.62 (m, 6 H), 3.47 (s, 2 H), 3.55 (d, *J* = 7.3 Hz, 2 H), 6.03 (br. s, 2 H), 7.15 (d, *J* = 7.8 Hz, 1 H), 7.38 (br. s, 1 H), 7.52 (d, *J* = 8.4 Hz, 1 H); <sup>13</sup>C NMR (75 MHz, Chloroform-d) δ ppm 32.7, 51.0, 127.9, 128.5, 128.9, 129.2, 130.2, 130.9, 131.3, 131.7, 132.3, 132.9, 138.3, 141.3, 165.9, 168.3; MS (ESI<sup>+</sup>) *m/z* 377 (M+H)<sup>+</sup>



### 3.3 Chapter C: Tackling *Pseudomonas aeruginosa* Virulence by a Hydroxamic Acid-Based LasB Inhibitor

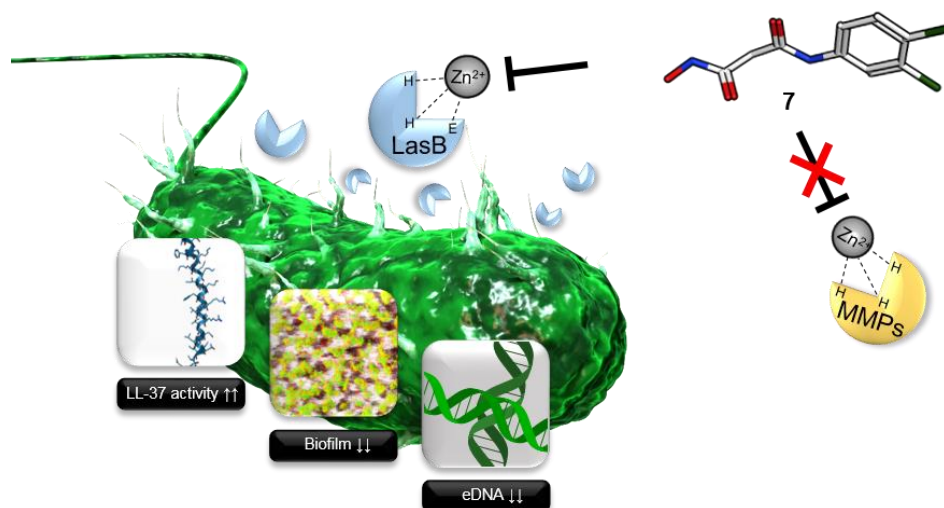
The following persons contributed experimentally to this chapter:

Andreas M. Kany: performed syntheses and the *in vitro* inhibition assay, established and performed the LL-37 assay, planned Biofilm/eDNA assays

Asfandyar Sikandar: purified LasB and modified the protocol, performed LasB crystallization experiments and structure determination

Dr. Martin Empting: performed structural superimposition of LasB with MMP structures and image preparation

This part of the thesis has been submitted to *ACS Chem. Biol.*



Proteases have proven to be attractive targets for the treatment of various diseases, including infections.<sup>1</sup> While antiviral protease inhibitors are in clinical use for the treatment of e.g. HIV or HCV, no bacterial protease inhibitors have been approved as anti-infective drugs yet.<sup>2,3</sup> However, in order to combat the spread of antibiotic resistance, new antibacterial agents with novel modes of action are urgently needed.<sup>4-6</sup> This applies especially for Gram-negative pathogens which are challenging to treat as their cell wall is difficult to permeate.<sup>7</sup> Due to their reduced selection pressure, anti-virulence agents are of great interest in anti-infective drug discovery.<sup>8-11</sup> In this context, bacterial proteases represent attractive targets.<sup>2,3,12</sup> Notably, the only FDA-approved anti-virulence drugs are immunoglobulins that target secreted virulence factors, highlighting the potential of extracellular targets to circumvent cell wall permeation problems.<sup>8</sup> The highly problematic Gram-negative pathogen *Pseudomonas aeruginosa* has been assigned critical priority by the WHO<sup>13</sup> and urgently requires novel treatment options because of increasing resistance.<sup>14,15</sup> *P. aeruginosa* is i.a. responsible for fatal lung infections in cystic fibrosis patients.<sup>16</sup> Among its numerous virulence factors displaying potential drug targets,<sup>15,17-20</sup> the zinc-metalloprotease elastase (LasB) is of specific interest, given its extracellular location.<sup>21</sup> LasB substantially contributes to disease progression in *P. aeruginosa* infected individuals by facilitating host invasion and immune evasion.<sup>22</sup> It was for example found to degrade and thereby inactivate the endogenous antimicrobial peptide (AMP) LL-37.<sup>23</sup> Furthermore, LasB was reported to be involved in the formation of *P. aeruginosa* biofilms either by periplasmic activation of nucleoside diphosphate kinase (NDK) required for alginate synthesis<sup>24</sup>, or by upregulation of rhamnolipids.<sup>25</sup> The aggregation of bacteria in the biofilm matrix seriously impedes successful antibiotic treatment and blocks host defense mechanisms.<sup>26,27</sup>

Several thiol-based inhibitors with promising activity on LasB have been described.<sup>28-32</sup> A class of *N*-aryl mercaptoacetamides turned out to be particularly attractive since these thiols display high selectivity toward a range of human matrix metalloproteinases (MMPs).<sup>32,33</sup> Thiol-containing compounds are in clinical use for the treatment of various diseases.<sup>34-36</sup> However, a disadvantage of this class compared to other zinc-chelating inhibitors is the possible oxidation to the respective disulfides, resulting in inactivation of the compounds.<sup>37</sup>

In this study, we describe the synthetic replacement of the sulfhydryl function of LasB inhibitor **1**<sup>32</sup> (IC<sub>50</sub> 6.6 ± 0.3 μM, Figure 1) by zinc-binding groups insensitive to oxidation. Among the compounds tested, a hydroxamic acid derivative was found to inhibit LasB in the low micromolar range as well. Hydroxamates have been reported as LasB inhibitors, but the described compounds lack selectivity toward human MMPs.<sup>38,39</sup> In contrast, the inhibitor described in this work maintained the remarkable selectivity of thiol **1**, despite a binding mode equivalent to described hydroxamate-MMP complexes. The new compound was further able to reduce biofilm formation and eDNA release by *P. aeruginosa* and to restore the antimicrobial effect of LL-37.

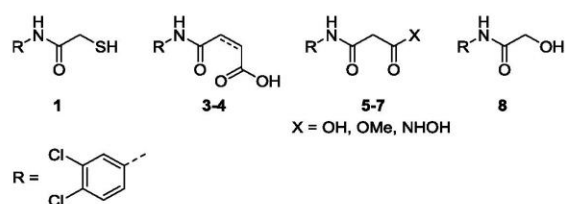
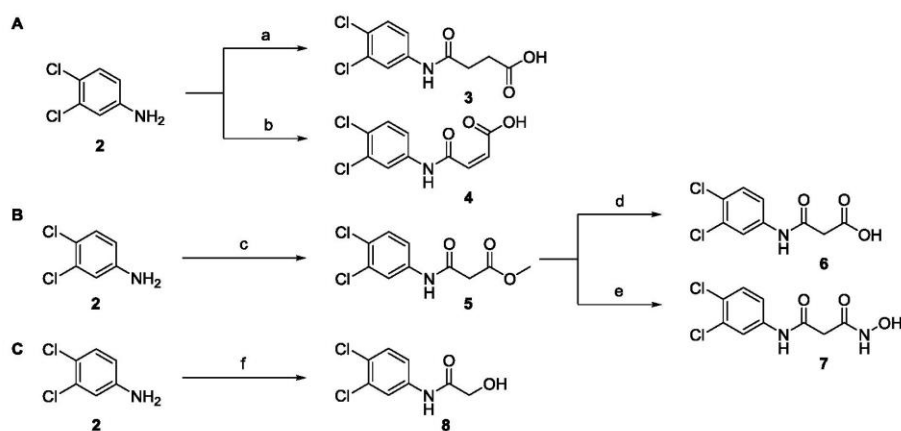


Figure 1. Structures of lead LasB inhibitor **1** and compounds **3-8** synthesized in this article.

## RESULTS AND DISCUSSION

### Synthesis of novel compounds **3-8**.

Among the variety of chemically diverse zinc binding groups in literature,<sup>40</sup> we focused on hydroxyl, carboxyl and hydroxamate functions. By introducing these relatively small zinc chelating groups, drastic changes in the size of the thiol function of **1** were avoided in order to allow the inhibitor backbone to preserve the previously observed binding mode. Carboxylic acid derivatives **3**, **4** and **6** were obtained either by reacting aniline **2** with succinic/maleic anhydride or via hydrolysis of methyl ester intermediate **5**. Similarly, **7** was synthesized by reacting **5** with hydroxylamine (Scheme 1, A-B). As an isosteric modification we further synthesized the alcohol derivative of **1**, compound **8**, using glycolic acid in a neat reaction (Scheme 1, C).



Scheme 1. Reagents and conditions: (a) succinic anhydride, dioxane, 70 °C, 6 h, (b) maleic anhydride, dioxane, 70 °C, 6 h; (c) methyl malonyl chloride, Et<sub>3</sub>N, DCM, RT, 4 h; (d) NaOH, THF, RT, 24 h; (e) H<sub>2</sub>NOH, DIPEA, MeOH, 8 h reflux, 16 h RT; (f) glycolic acid, 130°C, 24 h

### Identification of compound **7** as a potent LasB inhibitor

Using a FRET-based inhibition assay<sup>40</sup> it turned out that replacement of the thiol function of **1** by a hydroxy group led to a complete loss of activity when tested at 600 μM (**8**). Compounds bearing a carboxylic acid in γ- (**3,4**) or in β-position (**6**) to the carbonyl group were also inactive. Contrary to that, the β-hydroxamic acid derivative **7** displayed an IC<sub>50</sub> of 17.4 ± 0.8 μM.

### Binding Mode of 7 to LasB.

In order to rationalize whether the minor difference in activity compared to **1** was due to a different binding mode, the X-ray co-crystal structure of the LasB-7 complex was solved. The complex crystallized in space group  $P2_12_12_1$  and crystals diffracted to 2.1 Å resolution (Figure 2, A). The structure was solved by molecular replacement using the published LasB apo structure (PDB ID 1E2M) as a search model. Full details of the data collection and refinement statistics can be found in Table S1. Hydroxamate **7** was found to be orientated toward the primed binding site of the protease. As expected, the active site zinc atom is coordinated by both the carbonyl oxygen and the hydroxamide oxygen of **7**, leading to a distorted trigonal-bipyramidal geometry. The carbonyl oxygen further undergoes a weaker interaction with His223 (3.5 Å). Additionally, the hydroxamide oxygen forms a hydrogen bond with the adjacent Glu141 (2.5 Å), while the amide nitrogen interacts with the carbonyl group of Ala113 (3.0 Å). These observations are in excellent accordance with the reported binding of hydroxamate functions to MMP-7,<sup>41</sup> MMP-3<sup>42</sup> or to thermolysin.<sup>43</sup> Inhibitor binding to thermolysin-like proteases like LasB was described to lead to a closure of the binding pocket due to hinge-bending motion.<sup>44</sup> Intriguingly, thiol **1** has recently been discovered by us to keep the active site cleft in an open conformation due to the unexpected binding of two molecules to the primed binding site (Figure S1).<sup>32</sup> In contrast, only one molecule of the hydroxamate binds to the protease, which undergoes the characteristic hinge-bending. Unlike the zinc-chelating thiol, the hydroxamate directly interacts with the edge strand via a hydrogen bond with the main chain oxygen of Ala113. This interaction presumably promotes closure of the active site cleft, which is hampered in case of thiol **1** by the second molecule interacting with Asn112. Due to the twisted orientation of the aromatic core of **7** compared to **1**, a previously observed bidentate hydrogen bond with Arg198 in the S1' binding site is not possible. This observation could explain the slightly weaker activity of the hydroxamate compared to the thiol.

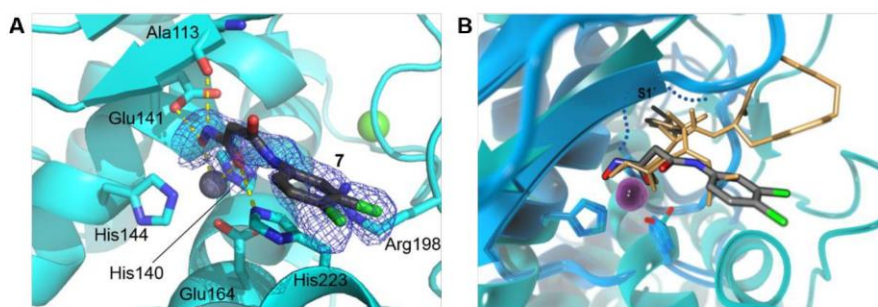


Figure 2. (A) Structure of LasB in complex with **7**. Cartoon representations of LasB (cyan) in complex with **7** (black). The difference electron density ( $F_o - F_c$ ) contoured to  $3\sigma$  with phases calculated from a model that was refined in the absence of **7** is shown as a blue isomesh. The active-site zinc ion is shown as a grey, calcium ion as a green sphere. Residues involved in binding of **7** are shown as sticks, their interactions depicted as yellow dashed lines. (B) Overlay of LasB (cyan) in complex with **7** (grey) and MMP-3/-7 (green) occupied by hydroxamate inhibitors **9** and **10** (brown, PDB codes 4G9L/1MMQ). Zinc ligands are highlighted.

### Selectivity Toward MMPs.

Strong zinc chelating groups like hydroxamic acids can be the reason for poor selectivity toward further metalloproteases, when compound binding is driven more by the chelating moiety than by the rest of the molecule.<sup>45</sup> In fact, the lack of selectivity toward MMP anti-targets has been one reason for the failure of various hydroxamate-based MMP inhibitors in clinical trials.<sup>46,47</sup> Considering the high similarity of zinc chelation by **7** to hydroxamate binding to MMP-3 or MMP-7, it was investigated whether the previously demonstrated selectivity of *N*-aryl mercaptoacetamides toward six human MMPs<sup>32,33</sup> could be maintained. Fortunately, **7** did not inhibit the activities of these MMPs with differing depth of the S1' binding site<sup>48</sup> including MMP-3 and -7 (Table 1). By contrast, the unselective inhibitor Batimastat<sup>49</sup> (Figure S3) inhibited all tested enzymes in the low nanomolar range.

Table 1. Residual activity of six MMPs in presence of 100  $\mu$ M **7** and IC<sub>50</sub> values of Batimastat<sup>33</sup>; Means and SD of at least three independent measurements are displayed.

	<b>7</b>	<b>Batimastat</b>
	<b>Residual activity at 100 <math>\mu</math>M [%]</b>	<b>IC<sub>50</sub> [nM]</b>
<b>MMP-1</b>	91 $\pm$ 9	2.2 $\pm$ 0.1
<b>MMP-2</b>	87 $\pm$ 3	1.8 $\pm$ 0.1
<b>MMP-3</b>	84 $\pm$ 5	5.6 $\pm$ 0.9
<b>MMP-7</b>	98 $\pm$ 3	7.0 $\pm$ 0.2
<b>MMP-8</b>	73 $\pm$ 6	0.7 $\pm$ 0.2
<b>MMP-14</b>	98 $\pm$ 4	2.8 $\pm$ 0.2

This of course prompted the question why, despite comparable interactions of the hydroxamate function, LasB was inhibited but not MMP-7. Logically, the selectivity might be related to differences in the positioning of the inhibitor backbone in the pocket. In order to investigate this, published X-ray structures of MMPs in complex with hydroxamates were overlaid with the LasB-**7** complex. The shallow S1' pocket of MMP-7 is occupied by an isobutyl moiety of inhibitor **9**<sup>41</sup> and the deep S1' pocket of MMP-3 by an aromatic core of inhibitor **10**<sup>42</sup> (for inhibitor structures see Figure S2). In contrast, the core of **7** does not bind to the respective pocket of LasB (Figure 2, B). The ability to bind the S1' pocket of the respective MMP is a common feature of reported hydroxamate-based MMP inhibitors, which can also be the cause for a lack of selectivity.<sup>45,50</sup> Consequently, the high selectivity toward various MMPs with differing depth of the S1' binding pocket could be explained by an inability of **7** to bind to this site of the protease.

### Cytotoxicity Assays.

In addition to selectivity, it was also investigated whether the cytotoxicity of **7** toward human cell lines was as low as described for thiol **1**.<sup>32</sup> This was of specific interest since cytotoxic properties are a known

drawback of hydroxamates.<sup>51</sup> Notably, **7** has only low effects on the viability of HEK293 cells at 100  $\mu\text{M}$ , comparable to thiol **1** and rifampicin (Table 2). The effect on HEP G2 cells was a little bit higher at this high concentration. Yet, compared to doxorubicin, a 100 times higher concentration is needed to achieve approximately 50% reduction of viability.

Table 2. Cytotoxicity of **1**, **7** and two reference compounds in HEP G2 and HEK293 cells.

Compound	Concn [ $\mu\text{M}$ ]	Reduction of viability [%]	
		HEP G2	HEK293
<b>1</b>	100	25 $\pm$ 3 <sup>a</sup>	22 $\pm$ 5 <sup>a</sup>
<b>7</b>	100	55 $\pm$ 18	29 $\pm$ 14
Rifampicin	100	34 $\pm$ 12	24 $\pm$ 10
Doxorubicin	1	50 $\pm$ 4	47 $\pm$ 8

<sup>a</sup>Values taken from<sup>52</sup>

#### Restoration of LL-37 antibacterial activity against *P. aeruginosa* PA14.

LL-37 is an  $\alpha$ -helical human cathelicidin peptide, which shows increased prevalence in cystic fibrosis patients.<sup>52</sup> Its effectiveness against *P. aeruginosa* is considerably reduced as it is susceptible toward cleavage by LasB.<sup>23</sup> In order to assess a potential restoration effect of **7** on the activity of LL-37, a bacterial growth assay with PA14 and LL-37 in presence/absence of **7** was performed (Figure 3). The antibacterial effect of LL-37 alone was only minor at 25  $\mu\text{g}/\text{mL}$  ( $p = 0.0211$ ). However, when combined with the LasB inhibitor, it recovered its ability to reduce bacterial growth in a dose-dependent way. Significant reduction of the OD<sub>600</sub> was observed starting from a hydroxamate concentration of 62.5  $\mu\text{M}$  ( $p = 0.0047$ ). At high concentrations, **7** itself slightly inhibited PA14 growth, yet to a much lower extent than in combination with LL-37 ( $p = 0.0255$  at 250  $\mu\text{M}$  **7**). These findings highlight the potential of LasB inhibitor **7** to restore a host defense mechanism which is otherwise hampered by LasB.

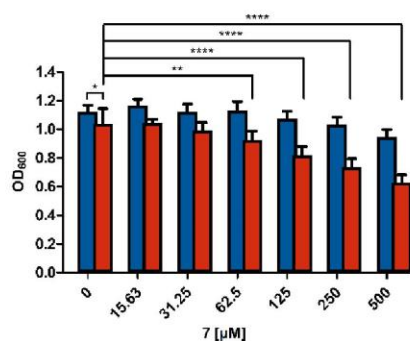


Figure 3. Growth of PA14 cultures incubated with **7** in absence (blue) and presence (red) of 25  $\mu\text{g}/\text{mL}$  LL-37. Means and SD of three independent measurements are depicted. \* =  $p < 0.05$ , \*\* =  $p < 0.01$ , \*\*\*\* =  $p < 0.0001$

### Biofilm volume and eDNA reduction

The biofilm matrix, a key element of *P. aeruginosa* resistance,<sup>26</sup> is composed of extracellular polysaccharides, lipids, proteins and, importantly, extracellular DNA (eDNA).<sup>53,54</sup> Inhibition of LasB was shown to inhibit biofilm formation.<sup>28</sup> Therefore, it was of great interest to investigate whether treatment of PA14 cultures with **7** would result in reduced biofilm formation as well. Indeed, the hydroxamate caused a concentration-dependent reduction eDNA release (Figure 4, A) and of the overall biofilm volume (Figure 4, B). Since significant inhibition was observed at concentrations lower than 250  $\mu\text{M}$ , these effects can be attributed to the on-target activity of the compound and are not due to a reduction of bacterial growth or lysis of cells. Hence, LasB inhibitor **7** has demonstrated important pathoblocker activity. It is able to interfere with crucial factors leading to bacterial resistance of *P. aeruginosa* toward antibiotics and host defense molecules.<sup>27,55</sup> Given the periplasmic localization of NDK<sup>24</sup> the inhibitor appears to be able to permeate at least the first membrane of the Gram-negative cell wall. To the best of our knowledge, no direct correlation between LasB inhibition and a reduction of eDNA release has been reported to date.

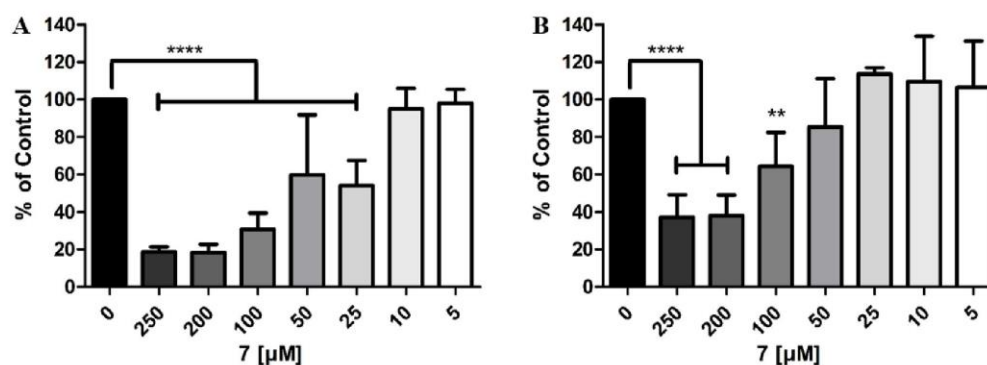


Figure 4. Reduction of eDNA release by treatment of PA14 cultures with **7**. (A) Reduction of overall PA14 biofilm volume by **7**. (B) Columns represent mean and SD of at least four independent measurements. \*\* =  $p < 0.01$ , \*\*\*\* =  $p < 0.0001$

### CONCLUSION

Based on our recent findings that *N*-aryl mercaptoacetamides are promising highly selective inhibitors of the virulence factor LasB from *P. aeruginosa*, the lead inhibitor was modified by changing the zinc-chelating moiety to a hydroxamate. Using X-ray crystallography, it was shown that similar to the thiol analogue **1**, hydroxamate **7** occupied the primed binding site. Contrary to our recent observations for **1**, only one inhibitor molecule was bound to the protease, which could undergo the characteristic hinge-bending motion resulting in a closed conformation of the enzyme. This was attributed to the ability of the inhibitor to interact with catalytic zinc and the edge strand alike. Despite the high similarity of zinc binding to hydroxamates inhibiting MMP-7, inhibitor **7** was unexpectedly able to maintain the

remarkable selectivity of **1** toward a range of MMPs. This could be rationalized by the fact that the S1' pocket was not occupied by **7**, unlike observed for MMP inhibitors. These findings show that despite the selectivity issues related to hydroxamic acids, selectivity can indeed be achieved by sparing the S1' pocket. Furthermore, low cytotoxicity toward HEK293 cells was observed as well as minor antibiotic effects at relatively high concentrations. Below an antibacterial concentration of 250  $\mu$ M, LasB was efficiently inhibited *in vitro*. This inhibition could be translated into more complex, cellular assays, highlighting this compound as a promising anti-virulence agent. After reduction of their pathogenicity by such an agent, bacteria are supposed to be cleared by host defense mechanisms or with the help of conventional antibiotics.<sup>10,11</sup> In this context, our results highlight a direct restoration effect of the antibacterial activity of the host defense peptide AMP LL-37 *in vitro*. Indirectly, the activity of host defense mechanisms might be further improved by the inhibition of biofilm formation and eDNA release also observed for **7**. The same holds true for the effectiveness of conventional antibiotics, which is seriously hampered by bacterial biofilms. Overall, these findings pave the way for the rational development of selective protease inhibitors as potential new antibiotics.

## METHODS.

**Chemistry.** All reagents were used from commercial suppliers without further purification. Procedures were not optimized regarding yield. NMR spectra were recorded on a Bruker Fourier 300 (300 MHz) spectrometer. Chemical shifts are given in parts per million (ppm) and referenced against the residual proton, <sup>1</sup>H, or carbon, <sup>13</sup>C, resonances of the >99% deuterated solvents as internal reference. Coupling constants (*J*) are given in Hertz. Data are reported as follows: chemical shift, multiplicity (s = singlet, d = doublet, t = triplet, m = multiplet, br = broad and combinations of these) coupling constants and integration. Mass spectrometry was performed on a SpectraSystems-MSQ LCMS system (Thermo Fisher, Dreieich, Germany). Flash chromatography was performed on silica gel 60 M, 0.04 - 0.063 mm (Machery-Nagel, Düren, Germany) or using the automated flash chromatography system CombiFlash Rf+ (Teledyne Isco, Lincoln, NE, USA) equipped with RediSepRf silica columns (Axel Semrau, Sprockhövel Germany) or Chromabond Flash C18 columns (Macherey-Nagel, Düren, Germany). Purity of compounds synthesized by us was determined by LCMS using the area percentage method on the UV trace recorded at a wavelength of 254 nm and found to be >95%.

**Expression and Purification of LasB.** LasB was expressed and purified as described previously.<sup>32</sup>

***In vitro* Inhibition Assays.** The LasB *in vitro* inhibition assay and the MMP assay were performed as described previously.<sup>32</sup>

**Cytotoxicity assays.** Hep G2 or HEK293 cells ( $2 \times 10^5$  cells per well) were seeded in 24-well, flat-bottomed plates. Culturing of cells, incubations and OD measurements were performed as described previously<sup>56</sup> with small modifications. 24 h after seeding the cells the incubation was started by the

addition of compounds in a final DMSO concentration of 1 %. The living cell mass was determined after 48 h. At least three independent measurements were performed for each compound.

**X-ray Crystallography and image preparation.** LasB was concentrated to 10-12 mg/mL and mixed with inhibitor 7 at a final concentration of 1mM. Complex crystals were grown by the sitting drop method using a reservoir solution containing 1.8 M AM<sub>4</sub>SO<sub>4</sub> and 0.1 M Tris-Cl, pH 8.8. Crystals were cryoprotected in glycerol and diffraction data was collected from single crystals at 100 K at beamline ID29 (ESRF) at a wavelength of 1.738 Å. Data was processed using Xia2<sup>57</sup> and the structure solved using PHASER<sup>58</sup> molecular replacement with *Pseudomonas aeruginosa* elastase (PAE, PDB ID 1EZM) as a search model. The solution was manually rebuilt with COOT<sup>59</sup> and refined using PHENIX<sup>60</sup> and Refmac<sup>61</sup>. The final refined structure of LasB in complex with compound 7 was deposited in the Protein Data Bank (PDB) as entry 6FZX. Structural superimposition of complex structures of human MMPs (1MMQ and 4G9L) and LasB (6FZX) was achieved through alignment of residues 201-205 of 4G9L (corresponds to residues 140-144 of 1MMQ) using the align atoms algorithm of YASARA structure (YASARA Biosciences GmbH).<sup>62</sup> Image was rendered using PovRay (<http://www.povray.org/>).

**Bacterial growth assay.** The assay was performed in 96 well plates (Greiner, Kremsmünster, Austria) with a final volume of 200 µL. LL-37 was purchased from AnaSpec (Fremont, CA, USA) and diluted to a final concentration of 25 µg/ml from 125 µg/mL stocks in 18MΩ H<sub>2</sub>O. Prior to culture addition 7 was serially diluted in DMSO. A pre-culture of PA14 was adjusted to the final start OD<sub>600</sub> 0.02 in lysogeny broth medium. All samples contained 1% DMSO and 40% of 18MΩ H<sub>2</sub>O. OD<sub>600</sub> was measured using a FLUOstar Omega (BMG labtech, Offenburg, Germany) after inoculation and after incubation for 16.5 h at 37°C with 200 rpm. Given OD<sub>600</sub> values were obtained after subtraction of the respective start OD<sub>600</sub> and represent three independent measurements with at least two replicates each. One-way ANOVA was performed using GraphPad Prism 6 software.

**Biofilm and eDNA assays.** The assays were performed as described previously.<sup>63</sup>

## REFERENCES.

- 1 Turk, B. (2006) Targeting proteases. Successes, failures and future prospects. *Nat. Rev. Drug Discovery*. 5, 785–799.
- 2 Agbowuro, A. A., Huston, W. M., Gamble, A. B., Tyndall, J. D. A. (2017) Proteases and protease inhibitors in infectious diseases. *Med. Res. Rev.*
- 3 Culp, E., Wright, G. D. (2017) Bacterial proteases, untapped antimicrobial drug targets. *J. Antibiot.* 70, 366–377.
- 4 Cooper, M. A., Shlaes, D. (2011) Fix the antibiotics pipeline. *Nature*. 472, 32.
- 5 Taubes, G. (2008) The bacteria fight back. *Science*. 321, 356–361.
- 6 Coates, A. R. M., Halls, G., Hu, Y. (2011) Novel classes of antibiotics or more of the same? *Br. J. Pharmacol.* 163, 184–194.
- 7 Payne, D. J., Gwynn, M. N., Holmes, D. J., Pompliano, D. L. (2007) Drugs for bad bugs. Confronting the challenges of antibacterial discovery. *Nat. Rev. Drug Discovery*. 6, 29–40.
- 8 Dickey, S. W., Cheung, G. Y. C., Otto, M. (2017) Different drugs for bad bugs. Antivirulence strategies in the age of antibiotic resistance. *Nat. Rev. Drug Discovery*. 16, 457–471.
- 9 Heras, B., Scanlon, M. J., Martin, J. L. (2015) Targeting virulence not viability in the search for future antibacterials. *Br. J. Clin. Pharmacol.* 79, 208–215.
- 10 Rasko, D. A., Sperandio, V. (2010) Anti-virulence strategies to combat bacteria-mediated disease. *Nat. Rev. Drug Discovery*. 9, 117–128.
- 11 Clatworthy, A. E., Pierson, E., Hung, D. T. (2007) Targeting virulence. A new paradigm for antimicrobial therapy. *Nat. Chem. Biol.* 3, 541–548.
- 12 Travis, J., Potempa, J. (2000) Bacterial proteinases as targets for the development of second-generation antibiotics. *Biochim. Biophys. Acta*. 1477, 35–50.
- 13 World Health Organization (2017) Antibacterial Agents in Clinical Development. *An analysis of the antibacterial clinical development pipeline, including tuberculosis*. World Health Organization, Geneva.
- 14 Aloush, V., Navon-Venezia, S., Seigman-Igra, Y., Cabili, S., Carmeli, Y. (2006) Multidrug-resistant *Pseudomonas aeruginosa*. Risk factors and clinical impact. *Antimicrob. Agents Chemother.* 50, 43–48.
- 15 Wagner, S., Sommer, R., Hinsberger, S., Lu, C., Hartmann, R. W., Empting, M., Titz, A. (2016) Novel Strategies for the Treatment of *Pseudomonas aeruginosa* Infections. *J. Med. Chem.* 59, 5929–5969.
- 16 Sordé, R., Pahissa, A., Rello, J. (2011) Management of refractory *Pseudomonas aeruginosa* infection in cystic fibrosis. *Infect Drug. Resist.* 4, 31–41.
- 17 Storz, M. P., Maurer, C. K., Zimmer, C., Wagner, N., Brengel, C., Jong, J. C. de, Lucas, S., Müsken, M., Häussler, S., Steinbach, A., Hartmann, R. W. (2012) Validation of PqsD as an anti-biofilm target in *Pseudomonas aeruginosa* by development of small-molecule inhibitors. *J. Am. Chem. Soc.* 134, 16143–16146.
- 18 Kamal, A. A. M., Maurer, C. K., Allegretta, G., Hauptenthal, J., Empting, M., Hartmann, R. W. (2017) Quorum Sensing Inhibitors as Pathoblockers for *Pseudomonas aeruginosa* Infections: A New Concept in Anti-Infective Drug Discovery. In *Topics in Medicinal Chemistry*, pp 1-26, Springer, Berlin, Heidelberg.
- 19 Strateva, T., Mitov, I. (2011) Contribution of an arsenal of virulence factors to pathogenesis of *Pseudomonas aeruginosa* infections. *Ann. Microbiol.* 61, 717–732.
- 20 Lu, C., Maurer, C. K., Kirsch, B., Steinbach, A., Hartmann, R. W. (2014) Overcoming the unexpected functional inversion of a PqsR antagonist in *Pseudomonas aeruginosa*. An in vivo potent antivirulence agent targeting pqs quorum sensing. *Angew. Chem. Int. Ed. Engl.* 53, 1109–1112.
- 21 Morihara, K., Tsuzuki, H., Oka, T., Inoue, H., Ebata, M. (1965) *Pseudomonas aeruginosa* elastase: isolation, crystallization, and preliminary characterization. *J. Biol. Chem.* 240, 3295–3304.
- 22 Wretling, B., Pavlovskis, O. R. (1983) *Pseudomonas aeruginosa* elastase and its role in *Pseudomonas* infections. *Rev. Infect. Dis.* 5 Suppl 5, S998-1004.
- 23 Schmidtchen, A., Frick, I.-M., Andersson, E., Tapper, H., Björck, L. (2002) Proteinases of common pathogenic bacteria degrade and inactivate the antibacterial peptide LL-37. *Mol. Microbiol.* 46, 157–168.
- 24 Kamath, S., Kapatral, V., Chakrabarty, A. M. (1998) Cellular function of elastase in *Pseudomonas aeruginosa*. Role in the cleavage of nucleoside diphosphate kinase and in alginate synthesis. *Mol. Microbiol.* 30, 933–941.
- 25 Yu, H., He, X., Xie, W., Xiong, J., Sheng, H., Guo, S., Huang, C., Di Zhang, Zhang, K. (2014) Elastase LasB of *Pseudomonas aeruginosa* promotes biofilm formation partly through rhamnolipid-mediated regulation. *Can. J. Microbiol.* 60, 227–235.

- 26 Hoiby, N., Bjamsholt, T., Givskov, M., Molin, S., Ciofu, O. (2010) Antibiotic resistance of bacterial biofilms. *Int. J. Antimicrob. Agents*. 35, 322–332.
- 27 Lambert, P. A. (2002) Mechanisms of antibiotic resistance in *Pseudomonas aeruginosa*. *J. R. Soc. Med.* 95 Suppl 41, 22–26.
- 28 Cathcart, G. R. A., Quinn, D., Greer, B., Harriott, P., Lynas, J. F., Gilmore, B. F., Walker, B. (2011) Novel inhibitors of the *Pseudomonas aeruginosa* virulence factor LasB. A potential therapeutic approach for the attenuation of virulence mechanisms in pseudomonal infection. *Antimicrob. Agents Chemother.* 55, 2670–2678.
- 29 Zhu, J., Cai, X., Harris, T. L., Gooyit, M., Wood, M., Lardy, M., Janda, K. D. (2015) Disarming *Pseudomonas aeruginosa* virulence factor LasB by leveraging a *Caenorhabditis elegans* infection model. *Chem. Biol.* 22, 483–491.
- 30 Burns, F. R., Paterson, C. A., Gray, R. D., Wells, J. T. (1990) Inhibition of *Pseudomonas aeruginosa* elastase and *Pseudomonas keratitis* using a thiol-based peptide. *Antimicrob. Agents Chemother.* 34, 2065–2069.
- 31 Kessler, E., Israel, M., Landshman, N., Chechick, A., Blumberg, S. (1982) In vitro inhibition of *Pseudomonas aeruginosa* elastase by metal-chelating peptide derivatives. *Infect. Immun.* 38, 716–723.
- 32 Kany, A. M., Sikandar, A., Hauptenthal, J., Yahiaoui, S., Maurer, C. K., Proschak, E., Koehnke, J., Hartmann, R. W. (2018) Binding Mode Characterization and Early in vivo Evaluation of Fragment-like Thiols as Inhibitors of the Virulence Factor LasB from *Pseudomonas aeruginosa*. *ACS Infect. Dis.*
- 33 Schönauer, E., Kany, A. M., Hauptenthal, J., Hüsecken, K., Hoppe, I. J., Voos, K., Yahiaoui, S., Elsässer, B., Ducho, C., Brandstetter, H., Hartmann, R. W. (2017) Discovery of a Potent Inhibitor Class with High Selectivity toward Clostridial Collagenases. *J. Am. Chem. Soc.* 139, 12696–12703.
- 34 Pereillo, J.-M., Maftouh, M., Andrieu, A., Uzabiaga, M.-F., Fedeli, O., Savi, P., Pascal, M., Herbert, J.-M., Maffrand, J.-P., Picard, C. (2002) Structure and stereochemistry of the active metabolite of clopidogrel. *Drug Metab. Dispos.* 30, 1288–1295.
- 35 Primi, M. P., Bueno, L., Baumer, P., Berard, H., Lecomte, J. M. (1999) Racecadotril demonstrates intestinal antisecretory activity in vivo. *Aliment. Pharmacol. Ther.* 13 Suppl 6, 3–7.
- 36 Cushman, D. W., Ondetti, M. A. (1991) History of the design of captopril and related inhibitors of angiotensin converting enzyme. *Hypertension*. 17, 589–592.
- 37 Prammar, Y., Das Gupta, V., Bethea, C. (1992) Stability of captopril in some aqueous systems. *J. Clin. Pharm. Ther.* 17, 185–189.
- 38 Adekoya, O. A., Sjöli, S., Wuxiuer, Y., Bילו, I., Marques, S. M., Santos, M. A., Nuti, E., Cercignani, G., Rossello, A., Winberg, J.-O., Sylte, I. (2015) Inhibition of pseudolysin and thermolysin by hydroxamate-based MMP inhibitors. *Eur. J. Med. Chem.* 89, 340–348.
- 39 Sjöli, S., Nuti, E., Camodeca, C., Bילו, I., Rossello, A., Winberg, J.-O., Sylte, I., Adekoya, O. A. (2016) Synthesis, experimental evaluation and molecular modelling of hydroxamate derivatives as zinc metalloproteinase inhibitors. *Eur. J. Med. Chem.* 108, 141–153.
- 40 Jacobsen, J. A., Major Jourden, J. L., Miller, M. T., Cohen, S. M. (2010) To bind zinc or not to bind zinc. An examination of innovative approaches to improved metalloproteinase inhibition. *Biochim. Biophys. Acta.* 1803, 72–94.
- 41 Browner, M. F., Smith, W. W., Castellano, A. L. (1995) Matrilysin-inhibitor complexes. Common themes among metalloproteases. *Biochemistry*. 34, 6602–6610.
- 42 Belviso, B. D., Caliandro, R., Siliqi, D., Calderone, V., Arnesano, F., Natile, G. (2013) Structure of matrix metalloproteinase-3 with a platinum-based inhibitor. *Chem. Commun. (Cambridge, U. K.)*. 49, 5492–5494.
- 43 Holmes, M. A., Matthews, B. W. (1981) Binding of hydroxamic acid inhibitors to crystalline thermolysin suggests a pentacoordinate zinc intermediate in catalysis. *Biochemistry*. 20, 6912–6920.
- 44 Holland, D. R., Tronrud, D. E., Pley, H. W., Flaherty, K. M., Stark, W., Jansonius, J. N., McKay, D. B., Matthews, B. W. (1992) Structural comparison suggests that thermolysin and related neutral proteases undergo hinge-bending motion during catalysis. *Biochemistry*. 31, 11310–11316.
- 45 Overall, C. M., Kleifeld, O. (2006) Towards third generation matrix metalloproteinase inhibitors for cancer therapy. *Br. J. Cancer*. 94, 941–946.
- 46 Fisher, J. F., Mobashery, S. (2006) Recent advances in MMP inhibitor design. *Cancer Metastasis Rev.* 25, 115–136.
- 47 Vandenbroucke, R. E., Libert, C. (2014) Is there new hope for therapeutic matrix metalloproteinase inhibition? *Nat. Rev. Drug Discovery*. 13, 904–927.
- 48 Park, H. I., Jin, Y., Hurst, D. R., Monroe, C. A., Lee, S., Schwartz, M. A., Sang, Q.-X. A. (2003) The intermediate S1' pocket of the endometase/matrilysin-2 active site revealed by enzyme inhibition kinetic studies, protein sequence analyses, and homology modeling. *J. Biol. Chem.* 278, 51646–51653.

- 49 Rasmussen, H. S., McCann, P. P. (1997) Matrix metalloproteinase inhibition as a novel anticancer strategy. A review with special focus on batimastat and marimastat. *Pharmacol. Ther.* 75, 69–75.
- 50 Overall, C. M., Kleinfeld, O. (2006) Tumour microenvironment - opinion. Validating matrix metalloproteinases as drug targets and anti-targets for cancer therapy. *Nat. Rev. Cancer.* 6, 227–239.
- 51 Shen, S., Kozikowski, A. P. (2016) Why Hydroxamates May Not Be the Best Histone Deacetylase Inhibitors--What Some May Have Forgotten or Would Rather Forget? *ChemMedChem.* 11, 15–21.
- 52 Chen, C. I.-U., Schaller-Bals, S., Paul, K. P., Wahn, U., Bals, R. (2004) Beta-defensins and LL-37 in bronchoalveolar lavage fluid of patients with cystic fibrosis. *J. Cyst. Fibros.* 3, 45–50.
- 53 Flemming, H.-C., Wingender, J. (2010) The biofilm matrix. *Nat. Rev. Microbiol.* 8, 623–633.
- 54 Whitchurch, C. B., Tolker-Nielsen, T., Ragas, P. C., Mattick, J. S. (2002) Extracellular DNA required for bacterial biofilm formation. *Science.* 295, 1487.
- 55 Lewenza, S. (2013) Extracellular DNA-induced antimicrobial peptide resistance mechanisms in *Pseudomonas aeruginosa*. *Front. Microbiol.* 4, 21.
- 56 Hauptenthal, J., Baehr, C., Zeuzem, S., Piiper, A. (2007) RNase A-like enzymes in serum inhibit the anti-neoplastic activity of siRNA targeting polo-like kinase 1. *Int. J. Cancer.* 121, 206–210.
- 57 Winter, G. (2010) xia2. An expert system for macromolecular crystallography data reduction. *J. Appl. Crystallogr.* 43, 186–190.
- 58 McCoy, A. J., Grosse-Kunstleve, R. W., Adams, P. D., Winn, M. D., Storoni, L. C., Read, R. J. (2007) Phaser crystallographic software. *J. Appl. Crystallogr.* 40, 658–674.
- 59 Emsley, P., Lohkamp, B., Scott, W. G., Cowtan, K. (2010) Features and development of Coot. *Acta Crystallogr., Sect. D: Biol. Crystallogr.* 66, 486–501.
- 60 Adams, P. D., Afonine, P. V., Bunkóczi, G., Chen, V. B., Davis, I. W., Echols, N., Headd, J. J., Hung, L.-W., Kapral, G. J., Grosse-Kunstleve, R. W., McCoy, A. J., Moriarty, N. W., Oeffner, R., Read, R. J., Richardson, D. C., Richardson, J. S., Terwilliger, T. C., Zwart, P. H. (2010) PHENIX. A comprehensive Python-based system for macromolecular structure solution. *Acta Crystallogr., Sect. D: Biol. Crystallogr.* 66, 213–221.
- 61 Skubák, P., Murshudov, G. N., Pannu, N. S. (2004) Direct incorporation of experimental phase information in model refinement. *Acta Crystallogr., Sect. D: Biol. Crystallogr.* 60, 2196–2201.
- 62 Krieger, E., Koraimann, G., Vriend, G. (2002) Increasing the precision of comparative models with YASARA NOVA--a self-parameterizing force field. *Proteins.* 47, 393–402.
- 63 Thomann, A., Mello Martins, A. G. G. de, Brengel, C., Empting, M., Hartmann, R. W. (2016) Application of Dual Inhibition Concept within Looped Autoregulatory Systems toward Antivirulence Agents against *Pseudomonas aeruginosa* Infections. *ACS Chem. Biol.* 11, 1279–1286.

## Supporting Information to Chapter C

Table S1. Data collection and refinement statistics.

<b>LasB-7</b>	
Resolution range	61.26 - 2.1 (2.175 - 2.1)
Space group	P 21 21 21
Unit cell	43.7 53.0 122.5 90 90 90
Total reflections	88777
Unique reflections	16581 (1575)
Multiplicity	5.3 (5.4)
Completeness (%)	95.88 (93.64)
Mean I/sigma(I)	4.3 (1.9)
R-merge	0.257 (0.689)
R-work	0.1828 (0.2210)
R-free	0.2102 (0.3084)
Number of non-hydrogen atoms	2641
macromolecules	2317
ligands	29
solvent	295
Protein residues	300
RMS(bonds)	0.004
RMS(angles)	0.94
Ramachandran favored (%)	95.27
Ramachandran allowed (%)	4.39
Ramachandran outliers (%)	0.34
Rotamer outliers (%)	0.00
Clashscore	2.00
Average B-factor	17.59
macromolecules	16.44
ligands	24.71
solvent	25.92

Statistics for the highest-resolution shell are shown in parentheses.

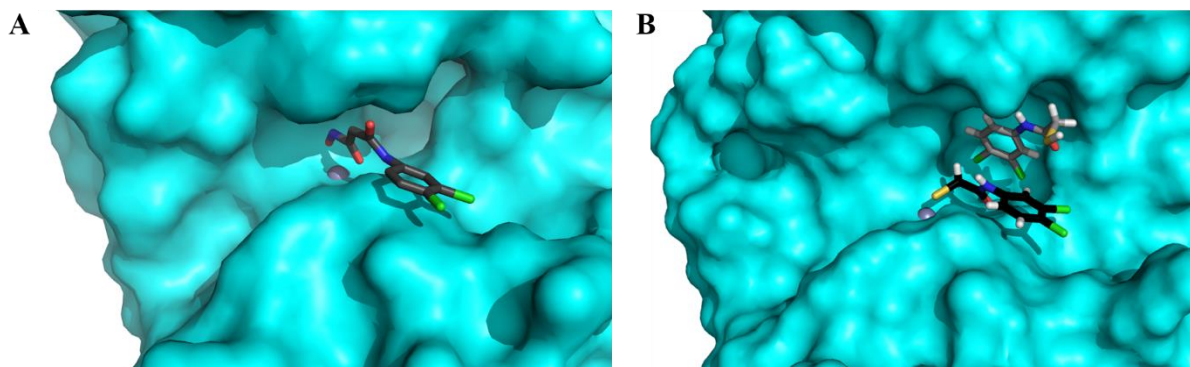


Figure S1. (A) Binding of the hydroxamate compound **7** leads to a closed conformation of the LasB active site. (B) In contrast, binding of the recently reported thiol inhibitor of LasB (**1**) arrests the enzyme in an open conformation. LasB is shown as a cyan surface representation, the active site zinc ion as a grey sphere and ligand molecules as grey/black sticks.

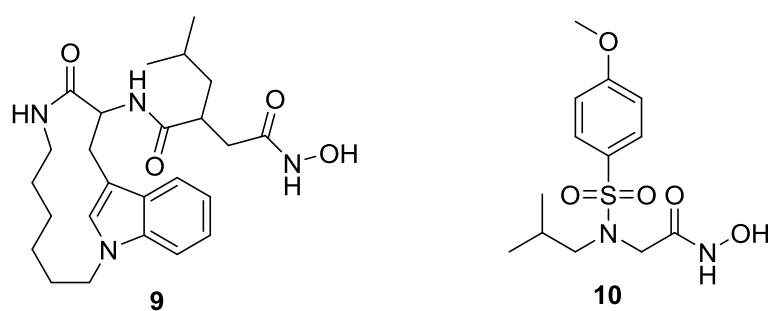


Figure S2. Structures of published hydroxamate-based MMP-7 inhibitor **9**<sup>1</sup> and MMP-3 inhibitor **10**.<sup>2</sup>

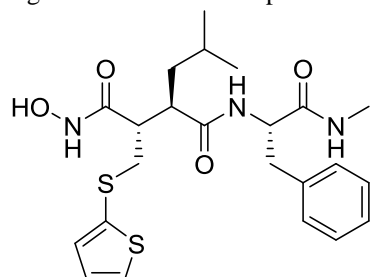


Figure S3. Structure of MMP inhibitor Batimastat.<sup>3</sup>

## Synthesis

*4-((3,4-dichlorophenyl)amino)-4-oxobutanoic acid (3)*. 3,4-dichloroaniline (160 mg, 0.99 mmol) was placed in a crimp vial and dissolved in 5 mL of dioxane at 70°C. Succinic anhydride (105 mg, 1.05 mmol) was added. The reaction was stirred at 70°C for 6 hours. Hydrochloric acid (2 M, 2 mL) was added and the aqueous phase was extracted with ethyl acetate, washed with brine and dried over magnesium sulfate and concentrated under reduced pressure. The crude was purified using automated flash chromatography (reversed-phase: acetonitrile + 0.1% formic acid:water + 0.1% formic acid 15:85 to 65:35) to yield the title compound as a white powder (152 mg, 59%). <sup>1</sup>H NMR (300 MHz, DMSO-d<sub>6</sub>) δ ppm 2.37 - 2.49 (m, 4 H), 7.36 - 7.44 (dd, *J* = 8.8, 2.3 Hz, 1 H), 7.48 (d, *J* = 8.8 Hz, 1 H), 7.93 (d, *J* = 2.2 Hz, 1 H), 10.21 (s, 1 H), 11.57 - 12.75 (br. s, 2 H); <sup>13</sup>C NMR (75 MHz, DMSO-d<sub>6</sub>) δ ppm 28.6, 31.1, 118.9, 120.1, 124.3, 130.6, 131.0, 139.3, 170.7, 173.7; MS (ESI<sup>+</sup>) *m/z* 262 (M+H)<sup>+</sup>

*(Z)-4-((3,4-dichlorophenyl)amino)-4-oxobut-2-enoic acid (4)*. 3,4-dichloroaniline (170 mg, 1.05 mmol) was placed in a crimp vial and dissolved in 5 mL of dioxane at 70°C. Maleic anhydride (103 mg, 1.05 mmol) was added. The reaction was stirred at 70°C for 6 hours. Filtration of the formed precipitate gave the title compound as a white powder (151 mg, 55%). <sup>1</sup>H NMR (300 MHz, DMSO-d<sub>6</sub>) δ ppm 6.32 (d, *J* = 11.9 Hz, 1 H), 6.48 (d, *J* = 11.9 Hz, 1 H), 7.50 (dd, *J* = 8.9, 2.4 Hz, 1 H), 7.59 (d, *J* = 8.8 Hz, 1 H), 8.01 (d, *J* = 2.3 Hz, 1 H), 10.6 (s, 1 H), 12.76 - 13.04 (br s., 1 H); <sup>13</sup>C NMR (75 MHz, DMSO-d<sub>6</sub>) δ ppm 119.4, 120.5, 125.1, 130.1, 130.7, 131.0, 131.6, 138.8, 163.7, 166.8; MS (ESI<sup>+</sup>) *m/z* 260 (M+H)<sup>+</sup>

*Methyl-3-((3,4-dichlorophenyl)amino)-3-oxopropanoate (5)*. 3,4-dichloroaniline (500 mg, 3.1 mmol) was dissolved in 10 mL of dichloromethane under cooling on ice. Triethylamine (850 μL, 6.2 mmol) were added, followed stepwise by methyl malonyl chloride (520 μL, 4.9 mmol). The mixture was warmed to room temperature and stirred for 4 hours. The organic phase was washed with saturated ammonium bicarbonate solution. The crude was purified automated flash chromatography (petroleum ether:ethyl acetate 80:20 to 5:95) to yield the title compound as a white powder (548 mg, 67%). <sup>1</sup>H NMR (300 MHz, DMSO-d<sub>6</sub>) δ ppm 3.49 (s, 2 H), 3.66 (s, 3 H), 7.45 (dd, *J* = 8.9, 2.4 Hz, 1 H), 7.58 (d, *J* = 8.8 Hz, 1 H), 7.96 (d, *J* = 2.4 Hz, 1 H), 10.49 (s, 1 H); <sup>13</sup>C NMR (75 MHz, DMSO-d<sub>6</sub>) δ ppm 43.5, 52.0, 119.1, 120.3, 125.0, 130.8, 131.0, 138.8, 164.5, 167.8; MS (ESI<sup>+</sup>) *m/z* 262 (M+H)<sup>+</sup>

*3-((3,4-dichlorophenyl)amino)-3-oxopropanoic acid (6)*. **5** (150 mg, 0.57 mmol) was dissolved in 4 mL of tetrahydrofuran. Sodium hydroxide solution (2 M, 570 μL) was added, followed stepwise by 1.43 mL of water. The mixture was stirred at room temperature for 24 hours. The aqueous phase was extracted with diethyl ether. After addition of 5 mL of water, the aqueous phase was extracted with ethyl acetate, dried over magnesium sulfate and concentrated under reduced pressure to yield the title compound as a white powder (115 mg, 81%). <sup>1</sup>H NMR (300 MHz, DMSO-d<sub>6</sub>) δ ppm 3.36 (s, 2 H), 7.46 (dd, *J* = 8.9, 2.4 Hz, 1 H), 7.58 (d, *J* = 8.8 Hz, 1 H), 7.98 (d, *J* = 2.3 Hz, 1 H), 10.43

(s, 1 H), 12.48 - 12.94 (br. s, 1 H);  $^{13}\text{C}$  NMR (75 MHz, DMSO- $d_6$ )  $\delta$  ppm 44.0, 119.1, 120.2, 124.8, 130.8, 131.0, 139.0, 165.1, 168.9; MS (ESI $^+$ )  $m/z$  248 (M+H) $^+$

*N*<sup>1</sup>-(3,4-dichlorophenyl)-*N*<sup>3</sup>-hydroxymalonamide (7). Hydroxylamine hydrochloride (106 mg, 1.52 mmol) was dissolved in 10 mL of methanol. *N,N*-Diisopropylethylamine (280  $\mu$ l, 1.68 mmol) was added. The mixture was stirred at room temperature for 30 minutes. **5** (100 mg, 0.84 mmol) was added and the reaction refluxed for 8 hours, followed by 16 hours at room temperature. The mixture was acidified with hydrochloric acid until pH 1 and extracted with ethyl acetate. The organic phase was washed with brine, dried over magnesium sulfate and concentrated under reduced pressure. The crude was purified using automated flash chromatography (reversed-phase: acetonitrile + 0.1% formic acid:water + 0.1% formic acid 20:80 to 100:0) to yield the title compound as a white powder (27 mg, 27%).  $^1\text{H}$  NMR (300 MHz, DMSO- $d_6$ )  $\delta$  ppm 3.12 (s, 2 H), 7.48 (dd,  $J$  = 8.9, 2.4 Hz, 1 H), 7.57 (d,  $J$  = 8.9 Hz, 1 H), 7.98 (d,  $J$  = 2.3 Hz, 1 H), 8.99 (s, 1 H), 10.42 (s, 1 H), 10.62 (s, 1 H);  $^{13}\text{C}$  NMR (75 MHz, DMSO- $d_6$ )  $\delta$  ppm 44.5, 119.6, 120.7, 125.3, 131.3, 131.5, 139.5, 165.6, 169.4; MS (ESI $^+$ )  $m/z$  263 (M+H) $^+$

*N*-(3,4-dichlorophenyl)-2-hydroxyacetamide (8). 3,4-dichloroaniline (200 mg, 1.23 mmol) and glycolic acid (94 mg, 1.24 mmol) were placed in a crimp vial. The vial was sealed and heated to 130°C for 24 hours. The crude was purified using flash chromatography (petroleum ether:ethyl acetate 70:30 to 60:40) to yield the title compound as a white powder (156 mg, 58%).  $^1\text{H}$  NMR (300 MHz, DMSO- $d_6$ )  $\delta$  ppm 4.00 (s, 2 H) 5.50 – 6.00 (br. s, 1 H) 7.56 (d,  $J$  = 8.9 Hz, 1 H) 7.70 (dd,  $J$  = 8.8, 2.5 Hz, 1 H) 8.11 (d,  $J$  = 2.4 Hz, 1 H) 9.76 – 10.23 (br. s, 1 H);  $^{13}\text{C}$  NMR (75 MHz, DMSO- $d_6$ )  $\delta$  ppm 61.9, 119.7, 120.8, 124.8, 130.5, 130.8, 138.7, 171.5; MS (ESI $^+$ )  $m/z$  220 (M+H) $^+$

## References

- 1 Browner, M. F., Smith, W. W., Castelhano, A. L. (1995) Matrilysin-inhibitor complexes. Common themes among metalloproteases. *Biochemistry*. 34, 6602–6610.
- 2 Belviso, B. D., Caliendo, R., Siliqi, D., Calderone, V., Arnesano, F., Natile, G. (2013) Structure of matrix metalloproteinase-3 with a platinum-based inhibitor. *Chem. Commun. (Cambridge, U. K.)*. 49, 5492–5494. DOI: 10.1039/c3cc41278d.
- 3 Rasmussen, H. S., McCann, P. P. (1997) Matrix metalloproteinase inhibition as a novel anticancer strategy. A review with special focus on batimastat and marimastat. *Pharmacol. Ther.* 75, 69–75.



## 4 Final Discussion

The goal of this thesis was the discovery of inhibitors of bacterial collagenases, precisely ColH from *C. histolyticum* and LasB from *P. aeruginosa*. As described in the introduction, these extracellular enzymes prove attractive targets for the development of new anti-infectives targeting bacterial virulence, since they play a key role in the infection process of these pathogenic bacteria. Since LasB and ColH are zinc-metalloproteases, the drug discovery strategy was based on a focused protease inhibitor library (ActiTarg-P, obtained from TimTec). For the discovery of LasB inhibitors, a functional screening was performed, using a FRET-based assay supplemented by an LC-MS-based readout to exclude false-positives. The development of ColH inhibitors was based on the results of an SPR binding assay complemented with a secondary functional FRET assay. Interestingly, both screening campaigns yielded *N*-aryl mercaptoacetamides as most promising inhibitors. Although not derived from a fragment library, these compounds do represent fragments, fulfilling the criteria presented for fragment-based lead discovery in the so-called ‘rule of three’ (molecular weight <300 Da, number of hydrogen bond donors/acceptors  $\leq 3$ , ClogP  $\leq 3$ ).<sup>189</sup> Their inverse Structure-Activity Relationships (SAR) toward the two targets, the unprecedented high selectivity toward human MMPs along with the prodrug character will be discussed and compared in the following chapters. This is followed by a discussion of synthetic modifications and the evaluation of LasB inhibition in more complex cellular systems and an *in vivo* model.

For the sake of clarity, compounds mentioned in this part of the thesis are denominated with the capital letter A, B or C referring to the respective manuscript, followed by an Arabic number corresponding to the numbering in each manuscript.

### 4.1 SAR and Binding Modes of *N*-Aryl Mercaptoacetamides

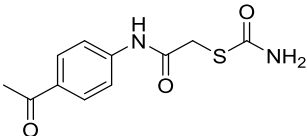
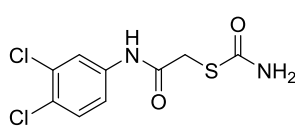
A central element of this work was the SAR elucidation of *N*-aryl mercaptoacetamides toward ColH and LasB. Interestingly, the functional assay results for a series of derivatives with varying substitution of the aromatic core revealed different structural properties to be favorable for the activity toward ColH (chapter A) and LasB (chapter B).

In case of ColH, substitution in *para*-position to the aniline moiety is highly beneficial for inhibition. There is, for example, a more than 300-fold difference in activity between *p*-methoxy derivative **A5** (IC<sub>50</sub> 0.071 ± 0.009 μM) and its *o*-analogue **A11** (IC<sub>50</sub> 26 ± 4 μM). Similarly, *p*-Cl substituted **A7** (IC<sub>50</sub> 0.19 ± 0.02 μM) is considerably more active than *o*-Cl derivative **A12** (IC<sub>50</sub> 31 ± 7 μM) or *m*-Cl derivative **A9** (IC<sub>50</sub> 19 ± 3 μM). The most potent ColH inhibitor is

*N*-(4-acetylphenyl)-2-mercaptoacetamide with an  $IC_{50}$  of  $0.017 \pm 0.002 \mu\text{M}$  (**A13**, or  $0.010 \pm 0.002 \mu\text{M}$  when its prodrug **A3** is concerned, Table 1). Two additional compounds with  $IC_{50}$  values in the two-digit nanomolar range bear methylester (**A4**) or methoxy (**A5**) groups para to the aniline moiety, demonstrating a strong preference for polar, hydrogen-bond accepting functions.

The observed SAR could be rationalized by the X-ray crystal structure of **A13** in complex with the ColH peptidase domain. The hydrolysis product of thiocarbamate prodrug **A3** was found to bind to the S1-S3 site of the protease, forming a hydrogen bond with the main-chain oxygen of Tyr428 in S1 and the main-chain nitrogen of Glu430 in S3 via the acetyl function and a bridging water molecule. This interaction explains the preference for hydrogen bond-accepting moieties in para-position to the aniline. Considering the tremendous drop in activity upon removal of the para-acetyl moiety (**A1**,  $IC_{50}$   $25 \pm 6 \mu\text{M}$ ), these hydrogen bonds seem to be of particular importance.

**Table 1.** Structure and inhibition of ColH and LasB by the respective lead inhibitors.

Cp.	<b>A3/B1</b>	<b>A25/B27</b>
Structure		
ColH $IC_{50}$ [ $\mu\text{M}$ ]	$0.010 \pm 0.002$	$86 \pm 2\%$ inhibition @ $100 \mu\text{M}$
LasB $IC_{50}$ [ $\mu\text{M}$ ]	$73.1 \pm 2.5$	$6.2 \pm 0.3$

As mentioned above, the SAR toward LasB showed a different activity profile of the *N*-aryl mercaptoacetamides. Notably, the best ColH inhibitor **A3** is one of the weakest LasB inhibitors described in chapter B (**B1**,  $IC_{50}$   $73.1 \pm 2.5 \mu\text{M}$ ). Likewise, the activity of the very potent ColH inhibitors **A4** and **A5** on LasB is in the high two-digit micromolar range (**B24**,  $IC_{50}$   $81.5 \pm 2.5 \mu\text{M}$  and **B23**,  $IC_{50}$   $47.7 \pm 1.0 \mu\text{M}$ ). Contrary to what was observed for ColH, nonpolar substituents, especially halogens, were advantageous for activity on LasB, which is exemplified by *o*-, *m*-, or *p*-Cl derivatives **B9**, **B12** and **B17**, with  $IC_{50}$  values between 14 and  $19 \mu\text{M}$ . This is one of several examples pointed out in the chapter, which highlights that the position of a substituent does not substantially affect the activity of the compound. Yet, addition of a second substituent to the aromatic core of **B17** ( $IC_{50}$   $15.7 \pm 0.4 \mu\text{M}$ ) generally improved the activity and led to the best LasB inhibitors **B26-B28** with one-digit micromolar  $IC_{50}$  values ( $5.9 - 7.2 \mu\text{M}$ ). These observations are in accordance with studies reporting LasB to prefer bulky, hydrophobic amino acids at the cleavage site of its substrates.<sup>95,127</sup>

As expected, the co-crystal structure of **B36** with LasB revealed the thiol function of the inhibitor to chelate the active site zinc. In contrast to the ColH-**A13** complex, a primed binding mode was discovered, with the unexpected binding of a second molecule in an antiparallel orientation toward

the zinc-chelating one (a more detailed binding mode analysis is subject of chapter 4.3). Actually, the presence of two molecules in the X-ray structure is in disagreement with the observed Hill slope of 1 in the *in vitro* assay. Apparently, for full inhibition only one binding event is necessary. Consequently, the second molecule appears to have no impact on inhibition and its absence in solution cannot be excluded.

Considering the notable difference in activity of the best hit toward the respective target, which is in the low nanomolar range for ColH but only in the low micromolar range for LasB, the question arises what causes this disparity. The SAR on ColH is sharp, given that several derivatives show only less than 50% inhibition at 100  $\mu\text{M}$  (**A32-A35**). The co-crystal structure with the best inhibitor revealed that literally all functional groups of **A13** undergo distinct interactions with active site amino acid residues. Accordingly, this small molecule represents a highly specific ‘key’ perfectly fitting into its ‘lock’, the protease binding site. This is remarkable for an inhibitor of that size, given that fragments are normally low-affinity ligands.<sup>190</sup> Clearly, this is related to the presence of a thiol moiety as a ‘warhead’ binding the catalytic zinc, which results, as determined using ITC, in enthalpy-driven binding of this compound class.

The SAR deduced for LasB is generally less sharp, with a much smaller difference in activity between the best (**B26**,  $\text{IC}_{50}$   $5.9 \pm 0.3 \mu\text{M}$ ) and the weakest *N*-aryl mercaptoacetamide (**B16**,  $\text{IC}_{50}$   $127.2 \pm 3.5 \mu\text{M}$ ). The X-ray co-crystal structure revealed several interactions between the inhibitor and the binding pocket, but not for the aromatic core or the amide nitrogen of the zinc-chelating molecule as in ColH-**A13**. Contrary to that complex, edge strand interactions are not achieved by the zinc-chelating **B36<sup>A</sup>**, but rather by the second thiol bound. Hence, in order to improve the activity on LasB, a more specific ‘key’ engaged in more interactions with the binding site would be needed. A rational strategy toward this end is the *N*-benzylation/-alkylation approach outlined in chapter B. The fact that all the resulting compounds were active on the target (**B63-B74**) indicates a high tolerance for different substitution patterns, which could be due to the comparatively large binding site of LasB. Presumably, these new inhibitors do not possess an optimal conformation for binding to LasB in the mode that was suggested by molecular modelling. An alternative approach toward a more specific (and hence more potent) ‘key’ could be the development of a thiol inhibitor that is capable of leading to a closure of the active site by combining the interactions of the two molecules present.

Regarding the distinct differences between the two targets, the herein discussed SAR and co-crystal structures clearly allow the rational, structure-based design of novel anti-infectives specifically targeting LasB or ColH.

## 4.2 Prodrug Character of the Thiocarbamate Function

Prodrugs are compounds which have to undergo transformation after they are administered, in order to yield the actual active drug.<sup>191</sup> This approach has proven useful for crossing biological barriers (like the blood-brain barrier), or when drug solubility needs to be altered, as for example in case of intravenous application of otherwise poorly water-soluble drugs.<sup>192,193</sup> Furthermore, prodrugs are used to enhance the chemical stability of drugs.<sup>192</sup> Mostly, they are converted enzymatically by e.g. esterases, phosphatases or hepatic CYP enzymes, but non-enzymatic hydrolysis can also take place.<sup>193</sup> Prominent protease inhibitors equipped with a prodrug moiety are ACE inhibitors like ramipril.<sup>2</sup> Examples for masked thiols are clopidogrel<sup>194</sup> or racecadotril, where the active metabolite thiorphan is equipped with an acetate function.<sup>195</sup> A similar approach has been used for *N*-aryl mercaptoacetamides.<sup>132</sup>

The sulfhydryl groups of the inhibitors presented in this study are protected with a carbamate function, which liberates free thiols after hydrolysis (Figure 9). Carbamates have been used to design prodrugs of phenolic compounds, mostly to overcome metabolic instability.<sup>196</sup> The somewhat fortuitous discovery of the prodrug character of our inhibitors prompted us to closely investigate their stability. Using an LC-MS-based assay it was shown that thiocarbamates hydrolyze rapidly in aqueous buffers, in absence of hydrolytic enzymes. On the contrary, carbamates are generally known to be stable.<sup>197</sup>

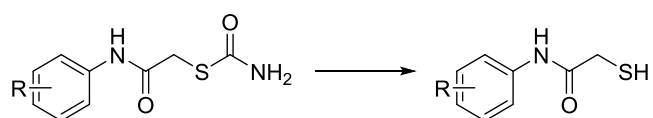


**Figure 9.** General scheme for the formation of active thiols from thiocarbamate prodrugs.

Comparison of the formation of *N*-(4-chlorophenyl)-2-mercaptoacetamide (**A14/B35**) in 10 mM HEPES pH 7.5 at 22.5°C (chapter A) to 50 mM Tris pH 7.2 at 37°C (chapter B) shows differences in thiocarbamate half-lives with  $26.8 \pm 1.4$  min for **A7** at 22.5°C and  $3.7 \pm 0.1$  min for **B17** at 37°C. The faster activation in Tris buffer is most likely caused by the difference in temperature. Considering the human body temperature of 37°C, the rapid activation in Tris buffer is presumably closer to a scenario of potential application in men. Certainly, thiocarbamate stability was not determined in human plasma, so differences in half-life cannot be excluded. Still, in terms of temperature and pH our assay conditions are close to the physiological state. Consequently, it can be assumed that the thiocarbamate function would be completely hydrolyzed after the prodrug was, for instance, exposed to human plasma after intravenous application. This would prevent reduced activity due to incomplete prodrug activation. Thiols like captopril were shown to form disulfides not only in aqueous systems;<sup>198</sup> in fact this is also possible for the dry substance as in a tablet.<sup>199</sup>

Hence, stability of the undissolved compound, which eventually affects shelf life, will also be enhanced by using this thiocarbamate protection group.

### 4.3 Changing the ‘Warhead’ to a Hydroxamic Acid

Several thiol-containing drugs are in clinical use, as for example the aforementioned antiplatelet drug clopidogrel,<sup>194</sup> the antidiarrheal racecadotril<sup>195</sup> or the ACE inhibitor captopril.<sup>200</sup> A drawback of thiols is their sensitivity to oxidation to the respective disulphides.<sup>198</sup> Consequently, newer ACE inhibitors like enalapril do not contain sulfhydryl groups and are less prone to oxidative metabolism.<sup>201</sup> As an alternative to the use of a thiocarbamate prodrug to avoid oxidation, the strategy of replacing the thiol ‘warhead’ was pursued in chapter C.

Among the newly synthesized compounds derived from lead thiol **B36**, which included several carboxylic acids (**C3-C6**) and an alcoholic isoster **C8**, hydroxamic acid **C7** is the only one with *in vitro* activity on LasB (IC<sub>50</sub> 17.4 ± 0.8 µM). This indicates that in combination with the phenylacetamide core a strong zinc binder is necessary for protease inhibition.

Even though **B36** and **C7** differ only by the zinc-chelating group, remarkable differences in their binding to LasB were found. In the past, the presence of inhibitors at the active site of LasB was related to a closure of the active site cleft due to hinge-bending motion.<sup>202</sup> Concrete examples for this phenomenon include a peptidic inhibitor<sup>203</sup> and phosphoramidon.<sup>204</sup> We also made this observation for hydroxamate **C7**. By contrast, the open conformation of the apo protein is virtually maintained upon binding of thiol **B36**. An explanation for the different conformation of the enzyme when occupied by these inhibitors was provided by the respective binding modes: The perpetuation of the open conformation is most likely caused by the unexpected presence of two molecules of **B36** in the protease. The second, antiparallely oriented thiol does not chelate the active site zinc, but rather occupies the lipophilic S2' pocket. It presumably prevents the protease from closing over the zinc-binding molecule, which therefore cannot undergo interactions with the edge strand. By contrast, only one molecule of hydroxamate **C7** was found in the pocket. The absence of a second molecule enabled **C7** to interact with the catalytic zinc and the edge strand alike, allowing the characteristic closure of the active site cleft.

Apart from the conformation of the enzyme and the number of ligands bound, the orientation of the inhibitor backbone was not equivalent either for this new compound. While the amide oxygen of **B36** is able to form a bidentate hydrogen bond with Arg198, the twisted orientation of the backbone of **C7** does not allow this interaction anymore. The 2.5-fold weaker activity of the hydroxamate toward the thiol might be originated from the lack of this interaction.

In all, these findings point out that replacement of the zinc-chelating group of a metalloprotease inhibitor, even if it does not cause a crucial difference in activity, can lead to substantial changes in

the binding mode. This does not only affect the orientation of the inhibitor in the pocket, but even the conformation of the entire protease.

#### 4.4 Selectivity toward Human MMPs

As outlined in the introduction, a critical requirement for protease inhibitors is selectivity toward other protease anti-targets. For zinc-metalloproteases these are in particular human MMPs, due to their versatile functions (see chapter 1.6). For this reason, it was a key goal of this study to develop inhibitors selectively targeting bacterial proteases. Therefore, we analyzed the potential activity of selected compounds on MMPs. In order to cover a broad range of these antitargets, six representative enzymes with differing depth of the S1' binding pocket were chosen, namely the following: MMP-1, -7 (shallow), MMP-2, -8 (intermediate) and MMP-3, -14 (deep).

For the *N*-aryl mercaptoacetamides high selectivity was not necessarily to be expected, considering the presence of a common zinc anchor and their small size. However, the compounds displayed an unprecedented selectivity with negligible inhibition of all anti-targets tested. This could be attributed to the interactions with the non-primed edge strand in ColH. This structural element is also present in MMPs, but since it is tilted by 27-29°, productive interactions with the *N*-aryl mercaptoacetamides are not possible. In line with these results, selected inhibitors showed promising activities on collagenases from other Gram-positive species like *C. tetani* or *B. cereus*. Mimicking the zinc-coordination sphere in MMPs by mutation of the glutamate ligand in ColH to histidine did not cause a tremendous drop in activity, thus this interaction could be excluded as alternative selectivity determinant.

The maintenance of the high selectivity of the thiols when changing the zinc-chelating group to a hydroxamate was equally surprising. This is especially true in view of the fact that the interactions of the hydroxamic acid function with LasB are highly similar to reported structures of hydroxamates in complex with MMP-7,<sup>205</sup> MMP-3<sup>206</sup> or with thermolysin,<sup>207</sup> leading to a commonly observed distorted trigonal-bipyramidal coordination geometry.<sup>208</sup> Consequently, the observed selectivity must be determined by the interactions of the backbone of the molecule. Comparing the orientation of the molecules in the binding pocket it becomes apparent that contrary to **C7**, the aforementioned inhibitors occupy the shallow (MMP-7) or deep (MMP-3) S1' binding pocket of the respective targets. Interactions at this site of the MMPs have been discussed as a reason for poor selectivity of protease inhibitors.<sup>16,186</sup> Accordingly, it appears likely that the observed inactivity of **C7** toward all tested MMPs can be attributed to a lack of binding to this subsite.

It remains to be said that the selectivity of the mercaptoacetamides was explained based on their interactions with the non-primed edge strand in ColH but not with regard to the complex with LasB. In this case, a primed binding mode was observed, which raises the question why this alternative

orientation of the inhibitor would not lead to MMP inhibition. Assuming absence of the second ligand in a hypothetical MMP-thiol complex, one could conclude that again the non-occupation of the S1' pocket and the lack of edge strand interactions is the reason for the inactivity toward MMPs. Contrary to other studies about bacterial protease inhibitors (see chapter 1.4.3 and 1.5.3), which focused mostly on only a few antitargets, this work describes the *N*-aryl mercaptoacetamides to be selective toward a broad range of six MMPs. The selection of representative enzymes differing in the S1' site might allow conclusions about the inhibition of other structurally related MMPs which were not tested. Presumably, the compounds described herein are also highly selective towards further MMPs because of the abovementioned non-occupation of the S1' pocket and the inability to interact with the non-primed edge strand.

Along with their low cytotoxicity toward selected human cell lines, these results constitute an important prerequisite for the potential application of these protease inhibitors for the treatment of infections with Clostridia or *P. aeruginosa*.

## 4.5 Biological Evaluation of the Impact of LasB Inhibition

Having in hand inhibitors with promising *in vitro* activity on LasB, it was of high interest to analyze the impact of LasB inhibition by these compounds in more complex assay systems. To this end, the potential to restore the effect of the AMP LL-37 was investigated. Furthermore, effects on biofilm formation and on the biofilm component eDNA were analyzed. As outlined in the introduction, these effects represent important resistance mechanisms of *P. aeruginosa*. The most advanced assay performed in this study is an early *in vivo* infection model using *G. mellonella*.

### 4.5.1 LL-37 Rescue

LL-37 is a human  $\alpha$ -helical cathelicidin peptide with antimicrobial activity against various bacteria, including *P. aeruginosa*.<sup>209</sup> It contributes to the innate defense system and is upregulated in CF patients, with concentrations correlating to disease severity.<sup>210,211</sup> Apart from its antimicrobial properties due to membrane permeabilization,<sup>209</sup> LL-37 is known to inhibit the formation of *P. aeruginosa* biofilms and to destruct existing biofilms, exerting synergistic effects in combination with classical antibiotics.<sup>212–214</sup> This is caused partly by QS-mediated downregulation of several genes, e.g. *lasB*.<sup>213</sup> Schmidtchen et al. reported proteases from various bacterial species, including *P. aeruginosa* LasB, to degrade LL-37 for the purpose of immune evasion.<sup>118</sup> These findings and the fact that LL-37 cleavage can be prevented with ilomastat<sup>118</sup> prompted us to analyze the impact of our hydroxamate-based inhibitor on this immune evasive process.

As described in chapter C, we found only a weak effect of LL-37 on the growth of PA14 at 25  $\mu\text{g/mL}$ . This is in line with reported MIC values towards *P. aeruginosa* strains of  $>32 \mu\text{g/mL}$ .<sup>212-214</sup> In order to exclude growth inhibition by **C7**, its potential antibacterial properties were investigated, revealing only a weak effect at high concentrations ( $p < 0.05$  at 250  $\mu\text{M}$ ). Remarkably, bacterial growth was significantly decreased in a concentration-dependent manner when PA14 cultures supplemented with LL-37 were treated with hydroxamate **C7**. This demonstrates that LasB inhibition has the potential to restore the innate defense system of the host which is otherwise impaired by *P. aeruginosa*. Hence, in an infectious disease state, apart from the reduced invasiveness caused by LasB inhibition, the rescue of LL-37 could be of additional benefit for the patient, because of the recovered antimicrobial activity and its anti-biofilm effect.<sup>212,213</sup>

#### 4.5.2 Effects on Biofilm Formation and eDNA Release

As mentioned earlier, the biofilm is a central element favoring resistance of *P. aeruginosa* whose formation is also dependent on LasB.<sup>121,122</sup> Inhibition of LasB has been demonstrated to lead to reduced biofilm formation.<sup>128</sup> Thus, it was of great interest whether on top of strengthening the host, hydroxamate **C7** could also further weaken *P. aeruginosa* by interfering with a key resistance mechanism.

The assay revealed a dose-dependent reduction of the total biofilm volume by **C7**. In addition to that, a significant effect on the release of the major biofilm component eDNA was observed. As discussed above, we found a direct effect of **C7** on the activity of LL-37. Indirectly, the reduction of eDNA should boost the activity of this AMP as well, as it is known to lead to resistance toward LL-37.<sup>71</sup> Similarly, the biofilm reduction could lead to an increased activity of conventional antibiotics.<sup>69,72,215</sup> In case of  $\beta$ -lactams, this could further be achieved by direct inhibition of metallo- $\beta$ -lactamases.<sup>216,217</sup> *In vitro* activity on IMP-7, an enzyme of this class isolated from clinical strains of *P. aeruginosa*, by thiol inhibitor **B36** is an encouraging first result toward the end of an additional restoration effect on penicillin and related antibiotics.

#### 4.5.3 *In Vivo* Efficacy in *Galleria mellonella*

The *G. mellonella* infection experiment is a potent *in vivo* model, with substantial advantages over murine models in terms of expenses, required instruments and ethical constraints.<sup>218</sup> For *P. aeruginosa*, pathogenicity has been shown to highly correlate with mouse models.<sup>219</sup> In the Hartmann group, this model has been employed to demonstrate *in vivo* efficacy of PqsR inhibitors<sup>83</sup> and dual inhibitors of PqsR and PqsD.<sup>215</sup>

*P. aeruginosa* has been reported to produce LasB after infection of *G. mellonella*.<sup>220</sup> The protease itself is toxic for the larvae and stimulates an immune response at concentrations below the lethal

dosis.<sup>221</sup> LasB has further been discussed to evade the *G. mellonella* immune response by degrading antimicrobial peptides of the insect.<sup>222</sup>

The *in vivo* effect of LasB inhibition by thiol **B36** and its prodrug **B27** was investigated. To this end, larvae were challenged with a bacterial load corresponding to two CFUs, which is two times the LD<sub>50</sub> determined by Jander et al.<sup>219</sup> As pointed out in chapter B, the survival rate of the larvae was increased significantly from 43% for the untreated larvae to 72% for larvae receiving 2.5 nmol of **B36**. The ineffectiveness of prodrug **B27** could be due to insufficient activation in the *G. mellonella* hemolymph. *In vivo* efficacy of structurally related LasB inhibitors has been proven by Zhu et al. using a *Caenorhabditis elegans* model.<sup>132</sup> The lifetime of the worms was significantly prolonged when treated with the LasB inhibitors, however, contrary to our results, the overall survival was not affected.<sup>132</sup> Hence, in our assay, inhibition of the virulence factor LasB did not only decelerate disease progression, but importantly reduced the pathogenicity so much so that less larvae were killed.

Taken together, these biological results highlight how the *in vitro* activity of our LasB inhibitors could be translated into significant effects in more complex systems. Using cellular assays, we were able to demonstrate reduction of biofilm formation and eDNA release, as well as a restoration effect on the activity of the AMP LL-37. Finally, we proved *in vivo* efficacy for a thiol inhibitor in *Galleria mellonella*. These findings reflect the various implications of LasB in the pathogenicity of *P. aeruginosa* (chapter 1.4.2) and clearly underline the potential of this extracellular protease as a drug target toward the development of novel, urgently needed anti-infectives.

## 4.6 Outlook

The results described in this work regarding the potent and selective broad-spectrum inhibition of secreted bacterial collagenases pave the way for the rational and straightforward development of new antibacterial drugs with novel modes of action.

Potential further steps in these projects include the following:

- Further analysis of the inhibition of clostridial collagenases other than ColH, including dose-dependent measurements.
- Analysis of the impact of collagenase inhibition on the cleavage of the natural substrate collagen.
- Establishment of an *in vivo* model using *Clostridium* strains expressing the targeted proteases to assess the impact of collagenase inhibition in a more advanced setting.
- Structure-based optimization of the inhibitors based on the here presented X-ray co-crystals. This could aim at (i) replacement of the bridging water molecule between ColH and **A13** to increase affinity; (ii) development of a thiol inhibitor of LasB capable of leading to a closure of the active site cleft by engaging in more interactions with the binding site; (iii) replacement of the zinc-binding group of the thiols by alternative (e.g. heterocyclic) zinc chelators
- Extension of the chemical space of LasB/ColH inhibitors by screening alternative compound libraries.
- Analysis of the impact of LasB inhibition on the activity of antibiotics or LL-37 in biofilm or eDNA assays.
- Determination of selected pharmacokinetic properties to obtain further information regarding a potential application in humans. This would be followed by additional modification of the compounds toward e.g. increased absorption or reduced metabolism when necessary.
- Extension of the selectivity tests to further metalloproteases like HDAC or ACE.

## 5 References

- 1 Barrett, A. J.; Rawlings, N. D.; Woessner, J. F. (2004) *Handbook of proteolytic enzymes. Aspartic and metallo peptidases*, 2. ed., Elsevier, Amsterdam.
- 2 Turk, B. (2006) Targeting proteases. Successes, failures and future prospects. *Nat. Rev. Drug Discov.* 5, 785–799. DOI: 10.1038/nrd2092.
- 3 Schechter, I.; Berger, A. (1967) On the size of the active site in proteases. I. Papain. *Biochem. Biophys. Res. Commun.* 27, 157–162.
- 4 Rawlings, N. D.; Barrett, A. J.; Bateman, A. (2010) MEROPS. The peptidase database. *Nucleic Acids Res.* 38, D227–33. DOI: 10.1093/nar/gkp971.
- 5 Abbenante, G.; Fairlie, D. P. (2005) Protease inhibitors in the Clinic. *Med. Chem.* 1, 71–104.
- 6 Drag, M.; Salvesen, G. S. (2010) Emerging principles in protease-based drug discovery. *Nat. Rev. Drug Discov.* 9, 690–701. DOI: 10.1038/nrd3053.
- 7 Jensen, C.; Herold, P.; Brunner, H. R. (2008) Aliskiren. The first renin inhibitor for clinical treatment. *Nat. Rev. Drug Discov.* 7, 399–410. DOI: 10.1038/nrd2550.
- 8 Smyth, T. P. (2004) Substrate variants versus transition state analogues as noncovalent reversible enzyme inhibitors. *Bioorg. Med. Chem.* 12, 4081–4088. DOI: 10.1016/j.bmc.2004.05.041.
- 9 Fischer, E. (1894) Einfluss der Configuration auf die Wirkung der Enzyme. *Ber. Dtsch. Chem. Ges.* 27, 2985–2993. DOI: 10.1002/cber.18940270364.
- 10 Holden, H. M.; Tronrud, D. E.; Monzingo, A. F.; Weaver, L. H.; Matthews, B. W. (2002) Slow- and fast-binding inhibitors of thermolysin display different modes of binding. Crystallographic analysis of extended phosphoramidate transition-state analogs. *Biochemistry.* 26, 8542–8553. DOI: 10.1021/bi00400a008.
- 11 Glenn, M. P.; Pattenden, L. K.; Reid, R. C.; Tyssen, D. P.; Tyndall, J. D. A.; Birch, C. J.; Fairlie, D. P. (2002)  $\beta$ -Strand Mimicking Macrocyclic Amino Acids. Templates for Protease Inhibitors with Antiviral Activity. *J. Med. Chem.* 45, 371–381. DOI: 10.1021/jm010414i.
- 12 Johnson, S. L.; Pellicchia, M. (2006) Structure- and fragment-based approaches to protease inhibition. *Curr. Top. Med. Chem.* 6, 317–329.
- 13 Powers, J. C.; Asgjan, J. L.; Ekici, Ö. D.; James, K. E. (2002) Irreversible Inhibitors of Serine, Cysteine, and Threonine Proteases. *Chem. Rev.* 102, 4639–4750. DOI: 10.1021/cr010182v.
- 14 Jacobsen, J. A.; Major Jourden, J. L.; Miller, M. T.; Cohen, S. M. (2010) To bind zinc or not to bind zinc. An examination of innovative approaches to improved metalloproteinase inhibition. *Biochim. Biophys. Acta.* 1803, 72–94. DOI: 10.1016/j.bbamcr.2009.08.006.
- 15 Vandenbroucke, R. E.; Libert, C. (2014) Is there new hope for therapeutic matrix metalloproteinase inhibition? *Nat. Rev. Drug Discov.* 13, 904–927. DOI: 10.1038/nrd4390.
- 16 Overall, C. M.; Kleifeld, O. (2006) Towards third generation matrix metalloproteinase inhibitors for cancer therapy. *Br. J. Cancer.* 94, 941–946. DOI: 10.1038/sj.bjc.6603043.
- 17 Coussens, L. M.; Fingleton, B.; Matrisian, L. M. (2002) Matrix metalloproteinase inhibitors and cancer. Trials and tribulations. *Science.* 295, 2387–2392. DOI: 10.1126/science.1067100.
- 18 Fisher, J. F.; Mobashery, S. (2006) Recent advances in MMP inhibitor design. *Cancer Metastasis Rev.* 25, 115–136. DOI: 10.1007/s10555-006-7894-9.
- 19 Cathcart, J.; Pulkoski-Gross, A.; Cao, J. (2015) Targeting Matrix Metalloproteinases in Cancer. Bringing New Life to Old Ideas. *Genes Dis.* 2, 26–34. DOI: 10.1016/j.gendis.2014.12.002.
- 20 Hardy, J. A.; Lam, J.; Nguyen, J. T.; O'Brien, T.; Wells, J. A. (2004) Discovery of an allosteric site in the caspases. *Proc. Natl. Acad. Sci. U S A.* 101, 12461–12466. DOI: 10.1073/pnas.0404781101.
- 21 Marks, P. A.; Breslow, R. (2007) Dimethyl sulfoxide to vorinostat. Development of this histone deacetylase inhibitor as an anticancer drug. *Nat. Biotechnol.* 25, 84–90. DOI: 10.1038/nbt1272.
- 22 Maeda, H. (1996) Role of Microbial Proteases in Pathogenesis. *Microbiol. Immunol.* 40, 685–699. DOI: 10.1111/j.1348-0421.1996.tb01129.x.
- 23 Agbowuro, A. A.; Huston, W. M.; Gamble, A. B.; Tyndall, J. D. A. (2017) Proteases and protease inhibitors in infectious diseases. *Med. Res. Rev.* DOI: 10.1002/med.21475.
- 24 Culp, E.; Wright, G. D. (2017) Bacterial proteases, untapped antimicrobial drug targets. *J. Antibiot.* 70, 366–377. DOI: 10.1038/ja.2016.138.
- 25 Travis, J.; Potempa, J. (2000) Bacterial proteinases as targets for the development of second-generation antibiotics. *Biochim. Biophys. Acta.* 1477, 35–50.

- 26 Raju, R. M.; Goldberg, A. L.; Rubin, E. J. (2012) Bacterial proteolytic complexes as therapeutic targets. *Nat. Rev. Drug Discov.* *11*, 777–789. DOI: 10.1038/nrd3846.
- 27 Supuran, C. T.; Scozzafava, A.; Mastrolorenzo, A. (2005) Bacterial proteases. Current therapeutic use and future prospects for the development of new antibiotics. *Expert Opin. Ther. Pat.* *11*, 221–259. DOI: 10.1517/13543776.11.2.221.
- 28 Davies, J.; Davies, D. (2010) Origins and evolution of antibiotic resistance. *Microbiol. Mol. Biol. Rev.* *74*, 417–433. DOI: 10.1128/MMBR.00016-10.
- 29 Lewis, K. (2013) Platforms for antibiotic discovery. *Nat. Rev. Drug Discov.* *12*, 371–387. DOI: 10.1038/nrd3975.
- 30 Spellberg, B. (2008) Dr. William H. Stewart. Mistaken or maligned? *Clin. Infect. Dis.* *47*, 294. DOI: 10.1086/589579.
- 31 Spellberg, B.; Taylor-Blake, B. (2013) On the exoneration of Dr. William H. Stewart. Debunking an urban legend. *Infect. Dis. Poverty.* *2*, 3. DOI: 10.1186/2049-9957-2-3.
- 32 World Health Organization (2014) *Antimicrobial resistance. Global report on surveillance, 2014*, World Health Organization, Geneva.
- 33 Clatworthy, A. E.; Pierson, E.; Hung, D. T. (2007) Targeting virulence. A new paradigm for antimicrobial therapy. *Nat. Chem. Biol.* *3*, 541–548. DOI: 10.1038/nchembio.2007.24.
- 34 Abraham, E. P.; Chain, E. (1988) An enzyme from bacteria able to destroy penicillin. 1940. *Rev. Infect. Dis.* *10*, 677–678.
- 35 Sir Alexander Fleming Nobel Lecture. [http://www.nobelprize.org/nobel\\_prizes/medicine/laureates/1945/fleming-lecture.html](http://www.nobelprize.org/nobel_prizes/medicine/laureates/1945/fleming-lecture.html).
- 36 World Health Organization (2012) *The Evolving Threat of Antimicrobial Resistance. Options for Action*, World Health Organization, Geneva.
- 37 Bartlett, J. G.; Gilbert, D. N.; Spellberg, B. (2013) Seven ways to preserve the miracle of antibiotics. *Clin. Infect. Dis.* *56*, 1445–1450. DOI: 10.1093/cid/cit070.
- 38 Rice, L. B. (2008) Federal funding for the study of antimicrobial resistance in nosocomial pathogens. No ESKAPE. *J. Infect. Dis.* *197*, 1079–1081. DOI: 10.1086/533452.
- 39 World Health Organization (2017) *Antibacterial Agents in Clinical Development. An analysis of the antibacterial clinical development pipeline, including tuberculosis.*, World Health Organization, Geneva.
- 40 Silver, L. L. (2016) A Gestalt approach to Gram-negative entry. *Bioorg. Med. Chem.* *24*, 6379–6389. DOI: 10.1016/j.bmc.2016.06.044.
- 41 Cooper, M. A.; Shlaes, D. (2011) Fix the antibiotics pipeline. *Nature.* *472*, 32. DOI: 10.1038/472032a.
- 42 Moellering, R. C. (2011) Discovering new antimicrobial agents. *Int. J. Antimicrob. Agents.* *37*, 2–9. DOI: 10.1016/j.ijantimicag.2010.08.018.
- 43 Conly, J.; Johnston, B. (2005) Where are all the new antibiotics? The new antibiotic paradox. *Can. J. Infect. Dis. Med. Microbiol.* *16*, 159–160.
- 44 Lyddiard, D.; Jones, G. L.; Greatrex, B. W. (2016) Keeping it simple. Lessons from the golden era of antibiotic discovery. *FEMS Microbiol. Lett.* *363*. DOI: 10.1093/femsle/fnw084.
- 45 Lipsitch, M.; Samore, M. H. (2002) Antimicrobial use and antimicrobial resistance. A population perspective. *Emerging Infect. Dis.* *8*, 347–354. DOI: 10.3201/eid0804.010312.
- 46 Ling, L. L.; Schneider, T.; Peoples, A. J.; Spoering, A. L.; Engels, I.; Conlon, B. P.; Mueller, A.; Schäberle, T. F.; Hughes, D. E.; Epstein, S.; Jones, M.; Lazarides, L.; Steadman, V. A.; Cohen, D. R.; Felix, C. R.; Fetterman, K. A.; Millett, W. P.; Nitti, A. G.; Zullo, A. M.; Chen, C.; Lewis, K. (2015) A new antibiotic kills pathogens without detectable resistance. *Nature.* *517*, 455–459. DOI: 10.1038/nature14098.
- 47 Kling, A.; Lukat, P.; Almeida, D. V.; Bauer, A.; Fontaine, E.; Sordello, S.; Zaburanyi, N.; Herrmann, J.; Wenzel, S. C.; König, C.; Ammerman, N. C.; Barrio, M. B.; Borchers, K.; Bordon-Pallier, F.; Brönstrup, M.; Courtemanche, G.; Gerlitz, M.; Geslin, M.; Hammann, P.; Heinz, D. W.; Hoffmann, H.; Klieber, S.; Kohlmann, M.; Kurz, M.; Lair, C.; Matter, H.; Nuermberger, E.; Tyagi, S.; Fraise, L.; Grosset, J. H.; Lagrange, S.; Müller, R. (2015) Antibiotics. Targeting DnaN for tuberculosis therapy using novel griselimycins. *Science.* *348*, 1106–1112. DOI: 10.1126/science.aaa4690.
- 48 Pirofski, L.-a.; Casadevall, A. (2012) Q and A. What is a pathogen? A question that begs the point. *BMC Biol.* *10*, 6. DOI: 10.1186/1741-7007-10-6.
- 49 Finlay, B. B.; Falkow, S. (1997) Common themes in microbial pathogenicity revisited. *Microbiol. Mol. Biol. Rev.* *61*, 136–169.

- 50 Heras, B.; Scanlon, M. J.; Martin, J. L. (2015) Targeting virulence not viability in the search for future antibacterials. *Br. J. Clin. Pharmacol.* 79, 208–215. DOI: 10.1111/bcp.12356.
- 51 Rasko, D. A.; Sperandio, V. (2010) Anti-virulence strategies to combat bacteria-mediated disease. *Nat. Rev. Drug Discov.* 9, 117–128. DOI: 10.1038/nrd3013.
- 52 Dickey, S. W.; Cheung, G. Y. C.; Otto, M. (2017) Different drugs for bad bugs. Antivirulence strategies in the age of antibiotic resistance. *Nat. Rev. Drug Discov.* 16, 457–471. DOI: 10.1038/nrd.2017.23.
- 53 Miller, M. B.; Bassler, B. L. (2001) Quorum sensing in bacteria. *Annu. Rev. Microbiol.* 55, 165–199. DOI: 10.1146/annurev.micro.55.1.165.
- 54 Taubes, G. (2008) The bacteria fight back. *Science.* 321, 356–361. DOI: 10.1126/science.321.5887.356.
- 55 Wagner, S.; Sommer, R.; Hinsberger, S.; Lu, C.; Hartmann, R. W.; Empting, M.; Titz, A. (2016) Novel Strategies for the Treatment of Pseudomonas aeruginosa Infections. *J. Med. Chem.* 59, 5929–5969. DOI: 10.1021/acs.jmedchem.5b01698.
- 56 Allen, R. C.; Popat, R.; Diggle, S. P.; Brown, S. P. (2014) Targeting virulence. Can we make evolution-proof drugs? *Nat. Rev. Microbiol.* 12, 300–308. DOI: 10.1038/nrmicro3232.
- 57 Hung, D. T.; Shakhnovich, E. A.; Pierson, E.; Mekalanos, J. J. (2005) Small-molecule inhibitor of Vibrio cholerae virulence and intestinal colonization. *Science.* 310, 670–674. DOI: 10.1126/science.1116739.
- 58 García-Contreras, R.; Martínez-Vázquez, M.; Velázquez Guadarrama, N.; Villegas Pañeda, A. G.; Hashimoto, T.; Maeda, T.; Quezada, H.; Wood, T. K. (2013) Resistance to the quorum-quenching compounds brominated furanone C-30 and 5-fluorouracil in Pseudomonas aeruginosa clinical isolates. *Pathog. Dis.* 68, 8–11. DOI: 10.1111/2049-632X.12039.
- 59 Eibergen, N. R.; Moore, J. D.; Mattmann, M. E.; Blackwell, H. E. (2015) Potent and Selective Modulation of the RhlR Quorum Sensing Receptor by Using Non-native Ligands. An Emerging Target for Virulence Control in Pseudomonas aeruginosa. *Chembiochem.* 16, 2348–2356. DOI: 10.1002/cbic.201500357.
- 60 Hentzer, M.; Wu, H.; Andersen, J. B.; Riedel, K.; Rasmussen, T. B.; Bagge, N.; Kumar, N.; Schembri, M. A.; Song, Z.; Kristoffersen, P.; Manefield, M.; Costerton, J. W.; Molin, S.; Eberl, L.; Steinberg, P.; Kjelleberg, S.; Høiby, N.; Givskov, M. (2003) Attenuation of Pseudomonas aeruginosa virulence by quorum sensing inhibitors. *EMBO J.* 22, 3803–3815. DOI: 10.1093/emboj/cdg366.
- 61 Stover, C. K.; Pham, X. Q.; Erwin, A. L.; Mizoguchi, S. D.; Warren, P.; Hickey, M. J.; Brinkman, F. S.; Hufnagle, W. O.; Kowalik, D. J.; Lagrou, M.; Garber, R. L.; Goltry, L.; Tolentino, E.; Westbrook-Wadman, S.; Yuan, Y.; Brody, L. L.; Coulter, S. N.; Folger, K. R.; Kas, A.; Larbig, K.; Lim, R.; Smith, K.; Spencer, D.; Wong, G. K.; Wu, Z.; Paulsen, I. T.; Reizer, J.; Saier, M. H.; Hancock, R. E.; Lory, S.; Olson, M. V. (2000) Complete genome sequence of Pseudomonas aeruginosa PAO1, an opportunistic pathogen. *Nature.* 406, 959–964. DOI: 10.1038/35023079.
- 62 Sordé, R.; Pahissa, A.; Rello, J. (2011) Management of refractory Pseudomonas aeruginosa infection in cystic fibrosis. *Infect. Drug. Resist.* 4, 31–41. DOI: 10.2147/IDR.S16263.
- 63 Koch, C.; Høiby, N. (1993) Pathogenesis of cystic fibrosis. *Lancet.* 341, 1065–1069.
- 64 Cystic Fibrosis Foundation Patient Registry 2016 Annual Data Report. <https://www.cff.org/Research/Researcher-Resources/Patient-Registry/2016-Patient-Registry-Annual-Data-Report.pdf>.
- 65 Bodey, G. P.; Bolivar, R.; Fainstein, V.; Jadeja, L. (1983) Infections caused by Pseudomonas aeruginosa. *Rev. Infect. Dis.* 5, 279–313.
- 66 Lambert, P. A. (2002) Mechanisms of antibiotic resistance in Pseudomonas aeruginosa. *J. R. Soc. Med.* 95 Suppl 41, 22–26.
- 67 Hancock, R. E. (1998) Resistance mechanisms in Pseudomonas aeruginosa and other nonfermentative gram-negative bacteria. *Clin. Infect. Dis.* 27 Suppl 1, S93-9.
- 68 Flemming, H.-C.; Wingender, J. (2010) The biofilm matrix. *Nat. Rev. Microbiol.* 8, 623–633. DOI: 10.1038/nrmicro2415.
- 69 Høiby, N.; Bjarnsholt, T.; Givskov, M.; Molin, S.; Ciofu, O. (2010) Antibiotic resistance of bacterial biofilms. *Int. J. Antimicrob. Agents.* 35, 322–332. DOI: 10.1016/j.ijantimicag.2009.12.011.
- 70 Whitchurch, C. B.; Tolker-Nielsen, T.; Ragas, P. C.; Mattick, J. S. (2002) Extracellular DNA required for bacterial biofilm formation. *Science.* 295, 1487. DOI: 10.1126/science.295.5559.1487.
- 71 Lewenza, S. (2013) Extracellular DNA-induced antimicrobial peptide resistance mechanisms in Pseudomonas aeruginosa. *Front. Microbiol.* 4, 21. DOI: 10.3389/fmicb.2013.00021.

- 72 Wilton, M.; Charron-Mazenod, L.; Moore, R.; Lewenza, S. (2015) Extracellular DNA Acidifies Biofilms and Induces Aminoglycoside Resistance in *Pseudomonas aeruginosa*. *Antimicrob. Agents. Chemother.* *60*, 544–553. DOI: 10.1128/AAC.01650-15.
- 73 Lynch, A. S.; Robertson, G. T. (2008) Bacterial and fungal biofilm infections. *Annu. Rev. Med.* *59*, 415–428. DOI: 10.1146/annurev.med.59.110106.132000.
- 74 Mittal, R.; Aggarwal, S.; Sharma, S.; Chhibber, S.; Harjai, K. (2009) Urinary tract infections caused by *Pseudomonas aeruginosa*. A minireview. *J. Infect. Public Health.* *2*, 101–111. DOI: 10.1016/j.jiph.2009.08.003.
- 75 Kamal, A. A. M.; Maurer, C. K.; Allegretta, G.; Hauptenthal, J.; Empting, M.; Hartmann, R. W. Quorum Sensing Inhibitors as Pathoblockers for *Pseudomonas aeruginosa* Infections: A New Concept in Anti-Infective Drug Discovery. In *Topics in Medicinal Chemistry*. pp 1-26, Springer, Berlin, Heidelberg.
- 76 Strateva, T.; Mitov, I. (2011) Contribution of an arsenal of virulence factors to pathogenesis of *Pseudomonas aeruginosa* infections. *Ann. Microbiol.* *61*, 717–732. DOI: 10.1007/s13213-011-0273-y.
- 77 van Delden, C.; Iglewski, B. H. (1998) Cell-to-cell signaling and *Pseudomonas aeruginosa* infections. *Emerging Infect. Dis.* *4*, 551–560. DOI: 10.3201/eid0404.980405.
- 78 Nova, A.; Eierhoff, T.; Topin, J.; Varrot, A.; Barluenga, S.; Imberty, A.; Römer, W.; Winssinger, N. (2014) A LecA ligand identified from a galactoside-conjugate array inhibits host cell invasion by *Pseudomonas aeruginosa*. *Angew. Chem. Int. Ed. Engl.* *53*, 8885–8889. DOI: 10.1002/anie.201402831.
- 79 Sommer, R.; Wagner, S.; Rox, K.; Varrot, A.; Hauck, D.; Wamhoff, E.-C.; Schreiber, J.; Ryckmans, T.; Brunner, T.; Rademacher, C.; Hartmann, R. W.; Brönstrup, M.; Imberty, A.; Titz, A. (2017) Glycomimetic, orally bioavailable LecB inhibitors block biofilm formation of *Pseudomonas aeruginosa*. *J. Am. Chem. Soc.* DOI: 10.1021/jacs.7b11133.
- 80 Liu, P. V. (1974) Extracellular toxins of *Pseudomonas aeruginosa*. *J. Infect. Dis.* *130 Suppl*, S94-9.
- 81 Rumbaugh, K. P.; Griswold, J. A.; Hamood, A. N. (2000) The role of quorum sensing in the in vivo virulence of *Pseudomonas aeruginosa*. *Microbes Infect.* *2*, 1721–1731.
- 82 Starkey, M.; Lepine, F.; Maura, D.; Bandyopadhyaya, A.; Lesic, B.; He, J.; Kitao, T.; Righi, V.; Milot, S.; Tzika, A.; Rahme, L. (2014) Identification of anti-virulence compounds that disrupt quorum-sensing regulated acute and persistent pathogenicity. *PLoS Pathog.* *10*, e1004321. DOI: 10.1371/journal.ppat.1004321.
- 83 Lu, C.; Maurer, C. K.; Kirsch, B.; Steinbach, A.; Hartmann, R. W. (2014) Overcoming the unexpected functional inversion of a PqsR antagonist in *Pseudomonas aeruginosa*. An in vivo potent antivirulence agent targeting pqs quorum sensing. *Angew. Chem. Int. Ed. Engl.* *53*, 1109–1112. DOI: 10.1002/anie.201307547.
- 84 Storz, M. P.; Maurer, C. K.; Zimmer, C.; Wagner, N.; Brengel, C.; Jong, J. C. de; Lucas, S.; Müsken, M.; Häussler, S.; Steinbach, A.; Hartmann, R. W. (2012) Validation of PqsD as an anti-biofilm target in *Pseudomonas aeruginosa* by development of small-molecule inhibitors. *J. Am. Chem. Soc.* *134*, 16143–16146. DOI: 10.1021/ja3072397.
- 85 Payne, D. J.; Gwynn, M. N.; Holmes, D. J.; Pompliano, D. L. (2007) Drugs for bad bugs. Confronting the challenges of antibacterial discovery. *Nat. Rev. Drug Discov.* *6*, 29–40. DOI: 10.1038/nrd2201.
- 86 Wretling, B.; Pavlovskis, O. R. (1983) *Pseudomonas aeruginosa* elastase and its role in *Pseudomonas* infections. *Rev. Infect. Dis.* *5 Suppl 5*, S998-1004.
- 87 Morihara, K.; Tsuzuki, H.; Oka, T.; Inoue, H.; Ebata, M. (1965) *Pseudomonas aeruginosa* elastase: isolation, crystallization, and preliminary characterization. *J. Biol. Chem.* *240*, 3295–3304.
- 88 Kessler, E.; Safrin, M.; Gustin, J. K.; Ohman, D. E. (1998) Elastase and the LasA protease of *Pseudomonas aeruginosa* are secreted with their propeptides. *J. Biol. Chem.* *273*, 30225–30231.
- 89 McIver, K.; Kessler, E.; Ohman, D. E. (1991) Substitution of active-site His-223 in *Pseudomonas aeruginosa* elastase and expression of the mutated lasB alleles in *Escherichia coli* show evidence for autoproteolytic processing of proelastase. *J. Bacteriol.* *173*, 7781–7789.
- 90 Kessler, E.; Safrin, M. (1988) Synthesis, processing, and transport of *Pseudomonas aeruginosa* elastase. *J. Bacteriol.* *170*, 5241–5247.
- 91 Thayer, M. M.; Flaherty, K. M.; McKay, D. B. (1991) Three-dimensional structure of the elastase of *Pseudomonas aeruginosa* at 1.5-Å resolution. *J. Biol. Chem.* *266*, 2864–2871.
- 92 Adekoya, O. A.; Sylte, I. (2009) The thermolysin family (M4) of enzymes. Therapeutic and biotechnological potential. *Chem. Biol. Drug Des.* *73*, 7–16. DOI: 10.1111/j.1747-0285.2008.00757.x.

- 93 Heck, L. W.; Morihara, K.; McRae, W. B.; Miller, E. J. (1986) Specific cleavage of human type III and IV collagens by *Pseudomonas aeruginosa* elastase. *Infect. Immun.* *51*, 115–118.
- 94 Heck, L. W.; Morihara, K.; Abrahamson, D. R. (1986) Degradation of soluble laminin and depletion of tissue-associated basement membrane laminin by *Pseudomonas aeruginosa* elastase and alkaline protease. *Infect. Immun.* *54*, 149–153.
- 95 Morihara, K.; Tsuzuki, H. (1966) Proteolytic substrate specificity and some elastolytic properties of a thermostable bacterial proteinase. *Biochim. Biophys. Acta.* *118*, 215–218.
- 96 Gomis-Rüth, F. X.; Botelho, T. O.; Bode, W. (2012) A standard orientation for metallopeptidases. *Biochim. Biophys. Acta.* *1824*, 157–163. DOI: 10.1016/j.bbapap.2011.04.014.
- 97 Kessler, E.; Safrin, M. (2014) Elastinolytic and proteolytic enzymes. *Methods Mol. Biol.* *1149*, 135–169. DOI: 10.1007/978-1-4939-0473-0\_13.
- 98 Wallach, J. (2004) Aeruginolysin. In *Handbook of proteolytic enzymes. Aspartic and metallo peptidases*, 2. ed. pp 582–584, Elsevier, Amsterdam.
- 99 Kessler, E.; Safrin, M.; Olson, J. C.; Ohman, D. E. (1993) Secreted LasA of *Pseudomonas aeruginosa* is a staphylolytic protease. *J. Biol. Chem.* *268*, 7503–7508.
- 100 Kessler, E.; Safrin, M.; Abrams, W. R.; Rosenbloom, J.; Ohman, D. E. (1997) Inhibitors and specificity of *Pseudomonas aeruginosa* LasA. *J. Biol. Chem.* *272*, 9884–9889.
- 101 Malloy, J. L.; Veldhuizen, R. A. W.; Thibodeaux, B. A.; O'Callaghan, R. J.; Wright, J. R. (2005) *Pseudomonas aeruginosa* protease IV degrades surfactant proteins and inhibits surfactant host defense and biophysical functions. *Am. J. Physiol. Lung Cell Mol. Physiol.* *288*, L409–18. DOI: 10.1152/ajplung.00322.2004.
- 102 Tamura, Y.; Suzuki, S.; Kijima, M.; Takahashi, T.; Nakamura, M. (1992) Effect of proteolytic enzyme on experimental infection of mice with *Pseudomonas aeruginosa*. *J. Vet. Med. Sci.* *54*, 597–599.
- 103 Wretling, B.; Wadström, T. (1977) Purification and properties of a protease with elastase activity from *Pseudomonas aeruginosa*. *J. Gen. Microbiol.* *103*, 319–327. DOI: 10.1099/00221287-103-2-319.
- 104 Suter, S.; Schaad, U. B.; Roux, L.; Nydegger, U. E.; Waldvogel, F. A. (1984) Granulocyte neutral proteases and *Pseudomonas* elastase as possible causes of airway damage in patients with cystic fibrosis. *J. Infect. Dis.* *149*, 523–531.
- 105 Kessler, E.; Spierer, A.; Blumberg, S. (1983) Specific inhibition of *Pseudomonas aeruginosa* elastase injected intracorneally in rabbit eyes. *Invest. Ophthalmol. Vis. Sci.* *24*, 1093–1097.
- 106 Azghani, A. O. (1996) *Pseudomonas aeruginosa* and epithelial permeability. Role of virulence factors elastase and exotoxin A. *Am. J. Respir. Cell. Mol. Biol.* *15*, 132–140. DOI: 10.1165/ajrcmb.15.1.8679217.
- 107 Golovkine, G.; Faudry, E.; Bouillot, S.; Voulhoux, R.; Attrée, I.; Huber, P. (2014) VE-cadherin cleavage by LasB protease from *Pseudomonas aeruginosa* facilitates type III secretion system toxicity in endothelial cells. *PLoS Pathog.* *10*, e1003939. DOI: 10.1371/journal.ppat.1003939.
- 108 Parmely, M.; Gale, A.; Clabaugh, M.; Horvat, R.; Zhou, W. W. (1990) Proteolytic inactivation of cytokines by *Pseudomonas aeruginosa*. *Infect. Immun.* *58*, 3009–3014.
- 109 Schultz, D. R.; Miller, K. D. (1974) Elastase of *Pseudomonas aeruginosa*. Inactivation of complement components and complement-derived chemotactic and phagocytic factors. *Infect. Immun.* *10*, 128–135.
- 110 Holder, I. A.; Wheeler, R. (1984) Experimental studies of the pathogenesis of infections owing to *Pseudomonas aeruginosa*. Elastase, an IgG protease. *Can. J. Microbiol.* *30*, 1118–1124.
- 111 Mariencheck, W. I.; Alcorn, J. F.; Palmer, S. M.; Wright, J. R. (2003) *Pseudomonas aeruginosa* elastase degrades surfactant proteins A and D. *Am. J. Respir. Cell. Mol. Biol.* *28*, 528–537. DOI: 10.1165/rcmb.2002-0141OC.
- 112 Kuang, Z.; Hao, Y.; Walling, B. E.; Jeffries, J. L.; Ohman, D. E.; Lau, G. W. (2011) *Pseudomonas aeruginosa* elastase provides an escape from phagocytosis by degrading the pulmonary surfactant protein-A. *PLoS ONE.* *6*, e27091. DOI: 10.1371/journal.pone.0027091.
- 113 Saint-Criq, V.; Villeret, B.; Bastaert, F.; Kheir, S.; Hatton, A.; Cazes, A.; Xing, Z.; Sermet-Gaudelus, I.; Garcia-Verdugo, I.; Edelman, A.; Sallenave, J.-M. (2018) *Pseudomonas aeruginosa* LasB protease impairs innate immunity in mice and humans by targeting a lung epithelial cystic fibrosis transmembrane regulator-IL-6-antimicrobial-repair pathway. *Thorax.* *73*, 49–61. DOI: 10.1136/thoraxjnl-2017-210298.
- 114 Dulon, S.; Leduc, D.; Cottrell, G. S.; D'Alayer, J.; Hansen, K. K.; Bunnett, N. W.; Hollenberg, M. D.; Pidard, D.; Chignard, M. (2005) *Pseudomonas aeruginosa* elastase disables proteinase-activated

- receptor 2 in respiratory epithelial cells. *Am. J. Respir. Cell. Mol. Biol.* 32, 411–419. DOI: 10.1165/rcmb.2004-0274OC.
- 115 Schmidtchen, A.; Holst, E.; Tapper, H.; Björck, L. (2003) Elastase-producing *Pseudomonas aeruginosa* degrade plasma proteins and extracellular products of human skin and fibroblasts, and inhibit fibroblast growth. *Microb. Pathog.* 34, 47–55. DOI: 10.1016/S0882-4010(02)00197-3.
- 116 Casilag, F.; Lorenz, A.; Krueger, J.; Klawonn, F.; Weiss, S.; Häussler, S. (2015) The LasB Elastase of *Pseudomonas aeruginosa* Acts in Concert with Alkaline Protease AprA To Prevent Flagellin-Mediated Immune Recognition. *Infect. Immun.* 84, 162–171. DOI: 10.1128/IAI.00939-15.
- 117 van der Plas, M. J. A.; Bhongir, R. K. V.; Kjellström, S.; Siller, H.; Kasetty, G.; Mörgelin, M.; Schmidtchen, A. (2016) *Pseudomonas aeruginosa* elastase cleaves a C-terminal peptide from human thrombin that inhibits host inflammatory responses. *Nat. Commun.* 7, 11567. DOI: 10.1038/ncomms11567.
- 118 Schmidtchen, A.; Frick, I.-M.; Andersson, E.; Tapper, H.; Björck, L. (2002) Proteinases of common pathogenic bacteria degrade and inactivate the antibacterial peptide LL-37. *Mol. Microbiol.* 46, 157–168.
- 119 Tielen, P.; Rosenau, F.; Wilhelm, S.; Jaeger, K.-E.; Flemming, H.-C.; Wingender, J. (2010) Extracellular enzymes affect biofilm formation of mucoid *Pseudomonas aeruginosa*. *Microbiology (Reading, Engl.)* 156, 2239–2252. DOI: 10.1099/mic.0.037036-0.
- 120 Sundin, G. W.; Shankar, S.; Chugani, S. A.; Chopade, B. A.; Kavanaugh-Black, A.; Chakrabarty, A. M. (1996) Nucleoside diphosphate kinase from *Pseudomonas aeruginosa*. Characterization of the gene and its role in cellular growth and exopolysaccharide alginate synthesis. *Mol. Microbiol.* 20, 965–979.
- 121 Kamath, S.; Kapatral, V.; Chakrabarty, A. M. (1998) Cellular function of elastase in *Pseudomonas aeruginosa*. Role in the cleavage of nucleoside diphosphate kinase and in alginate synthesis. *Mol. Microbiol.* 30, 933–941.
- 122 Yu, H.; He, X.; Xie, W.; Xiong, J.; Sheng, H.; Guo, S.; Huang, C.; Di Zhang; Zhang, K. (2014) Elastase LasB of *Pseudomonas aeruginosa* promotes biofilm formation partly through rhamnolipid-mediated regulation. *Can. J. Microbiol.* 60, 227–235. DOI: 10.1139/cjm-2013-0667.
- 123 Suleman, L. (2016) Extracellular Bacterial Proteases in Chronic Wounds. A Potential Therapeutic Target? *Adv. Wound Care (New Rochelle)*. 5, 455–463. DOI: 10.1089/wound.2015.0673.
- 124 Burns, F. R.; Paterson, C. A.; Gray, R. D.; Wells, J. T. (1990) Inhibition of *Pseudomonas aeruginosa* elastase and *Pseudomonas keratitis* using a thiol-based peptide. *Antimicrob. Agents. Chemother.* 34, 2065–2069.
- 125 Kessler, E.; Israel, M.; Landshman, N.; Chechick, A.; Blumberg, S. (1982) In vitro inhibition of *Pseudomonas aeruginosa* elastase by metal-chelating peptide derivatives. *Infect. Immun.* 38, 716–723.
- 126 Grobelny, D.; Poncz, L.; Galaray, R. E. (2002) Inhibition of human skin fibroblast collagenase, thermolysin, and *Pseudomonas aeruginosa* elastase by peptide hydroxamic acids. *Biochemistry*. 31, 7152–7154. DOI: 10.1021/bi00146a017.
- 127 Cathcart, G. R.; Gilmore, B. F.; Greer, B.; Harriott, P.; Walker, B. (2009) Inhibitor profiling of the *Pseudomonas aeruginosa* virulence factor LasB using N-alpha mercaptoamide template-based inhibitors. *Bioorg. Med. Chem. Lett.* 19, 6230–6232. DOI: 10.1016/j.bmcl.2009.08.099.
- 128 Cathcart, G. R. A.; Quinn, D.; Greer, B.; Harriott, P.; Lynas, J. F.; Gilmore, B. F.; Walker, B. (2011) Novel inhibitors of the *Pseudomonas aeruginosa* virulence factor LasB. A potential therapeutic approach for the attenuation of virulence mechanisms in pseudomonal infection. *Antimicrob. Agents. Chemother.* 55, 2670–2678. DOI: 10.1128/AAC.00776-10.
- 129 Garner, A. L.; Struss, A. K.; Fullagar, J. L.; Agrawal, A.; Moreno, A. Y.; Cohen, S. M.; Janda, K. D. (2012) 3-Hydroxy-1-alkyl-2-methylpyridine-4(1H)-thiones. Inhibition of the *Pseudomonas aeruginosa* Virulence Factor LasB. *ACS Med. Chem. Lett.* 3, 668–672. DOI: 10.1021/ml300128f.
- 130 Fullagar, J. L.; Garner, A. L.; Struss, A. K.; Day, J. A.; Martin, D. P.; Yu, J.; Cai, X.; Janda, K. D.; Cohen, S. M. (2013) Antagonism of a zinc metalloprotease using a unique metal-chelating scaffold. Tropolones as inhibitors of *P. aeruginosa* elastase. *Chem. Commun. (Camb.)* 49, 3197–3199. DOI: 10.1039/c3cc41191e.
- 131 Szamosvári, D.; Reichle, V. F.; Jureschi, M.; Böttcher, T. (2016) Synthetic quinolone signal analogues inhibiting the virulence factor elastase of *Pseudomonas aeruginosa*. *Chem. Commun. (Camb.)* 52, 13440–13443. DOI: 10.1039/c6cc06295d.
- 132 Zhu, J.; Cai, X.; Harris, T. L.; Gooyit, M.; Wood, M.; Lardy, M.; Janda, K. D. (2015) Disarming *Pseudomonas aeruginosa* virulence factor LasB by leveraging a *Caenorhabditis elegans* infection model. *Chem. Biol.* 22, 483–491. DOI: 10.1016/j.chembiol.2015.03.012.

- 133 Yokota, S.; Ohtsuka, H.; Noguchi, H. (1992) Monoclonal antibodies against *Pseudomonas aeruginosa* elastase. A neutralizing antibody which recognizes a conformational epitope related to an active site of elastase. *Eur. J. Biochem.* *206*, 587–593.
- 134 Morihara, K.; Tsuzuki, H. (1978) Phosphoramidon as an inhibitor of elastase from *Pseudomonas aeruginosa*. *Jpn. J. Exp. Med.* *48*, 81–84.
- 135 Nishino, N.; Powers, J. C. (1980) *Pseudomonas aeruginosa* elastase. Development of a new substrate, inhibitors, and an affinity ligand. *J. Biol. Chem.* *255*, 3482–3486.
- 136 Adekoya, O. A.; Sjøli, S.; Wuxiuer, Y.; Bילו, I.; Marques, S. M.; Santos, M. A.; Nuti, E.; Cercignani, G.; Rossello, A.; Winberg, J.-O.; Sylte, I. (2015) Inhibition of pseudolysin and thermolysin by hydroxamate-based MMP inhibitors. *Eur. J. Med. Chem.* *89*, 340–348. DOI: 10.1016/j.ejmech.2014.10.009.
- 137 Sjøli, S.; Nuti, E.; Camodeca, C.; Bילו, I.; Rossello, A.; Winberg, J.-O.; Sylte, I.; Adekoya, O. A. (2016) Synthesis, experimental evaluation and molecular modelling of hydroxamate derivatives as zinc metalloproteinase inhibitors. *Eur. J. Med. Chem.* *108*, 141–153. DOI: 10.1016/j.ejmech.2015.11.019.
- 138 Lopetuso, L. R.; Scaldaferrri, F.; Petito, V.; Gasbarrini, A. (2013) Commensal Clostridia. Leading players in the maintenance of gut homeostasis. *Gut pathogens.* *5*, 23. DOI: 10.1186/1757-4749-5-23.
- 139 Hatheway, C. L. (1990) Toxigenic clostridia. *Clin. Microbiol. Rev.* *3*, 66–98.
- 140 Stevens, D. L.; Aldape, M. J.; Bryant, A. E. (2012) Life-threatening clostridial infections. *Anaerobe.* *18*, 254–259. DOI: 10.1016/j.anaerobe.2011.11.001.
- 141 Stevens, D. L.; Bryant, A. E. (2002) The role of clostridial toxins in the pathogenesis of gas gangrene. *Clin. Infect. Dis.* *35*, S93-S100. DOI: 10.1086/341928.
- 142 Spigaglia, P. (2016) Recent advances in the understanding of antibiotic resistance in *Clostridium difficile* infection. *Ther. Adv. Infect. Dis.* *3*, 23–42. DOI: 10.1177/2049936115622891.
- 143 Huang, H.; Weintraub, A.; Fang, H.; Nord, C. E. (2009) Antimicrobial resistance in *Clostridium difficile*. *Int. J. Antimicrob. Agents.* *34*, 516–522. DOI: 10.1016/j.ijantimicag.2009.09.012.
- 144 Alexander, C. J.; Citron, D. M.; Brazier, J. S.; Goldstein, E. J. (1995) Identification and antimicrobial resistance patterns of clinical isolates of *Clostridium clostridioforme*, *Clostridium innocuum*, and *Clostridium ramosum* compared with those of clinical isolates of *Clostridium perfringens*. *J. Clin. Microbiol.* *33*, 3209–3215.
- 145 Matsushita, O.; Okabe, A. (2001) Clostridial hydrolytic enzymes degrading extracellular components. *Toxicon.* *39*, 1769–1780.
- 146 Berger, T.; Eisenkraft, A.; Bar-Haim, E.; Kassirer, M.; Aran, A. A.; Fogel, I. (2016) Toxins as biological weapons for terror-characteristics, challenges and medical countermeasures. A mini-review. *Disaster Mil. Med.* *2*, 7. DOI: 10.1186/s40696-016-0017-4.
- 147 Bond, M. D.; van Wart, H. E. (1984) Characterization of the individual collagenases from *Clostridium histolyticum*. *Biochemistry.* *23*, 3085–3091.
- 148 Awad, M. M.; Ellemor, D. M.; Bryant, A. E.; Matsushita, O.; Boyd, R. L.; Stevens, D. L.; Emmins, J. J.; Rood, J. I. (2000) Construction and virulence testing of a collagenase mutant of *Clostridium perfringens*. *Microb. Pathog.* *28*, 107–117. DOI: 10.1006/mpat.1999.0328.
- 149 Kassegne, K.; Hu, W.; Ojcius, D. M.; Sun, D.; Ge, Y.; Zhao, J.; Yang, X. F.; Li, L.; Yan, J. (2014) Identification of collagenase as a critical virulence factor for invasiveness and transmission of pathogenic *Leptospira* species. *J. Infect. Dis.* *209*, 1105–1115. DOI: 10.1093/infdis/jit659.
- 150 Bond, M. D.; van Wart, H. E. (1984) Purification and separation of individual collagenases of *Clostridium histolyticum* using red dye ligand chromatography. *Biochemistry.* *23*, 3077–3085.
- 151 Matsushita, O.; Jung, C. M.; Katayama, S.; Minami, J.; Takahashi, Y.; Okabe, A. (1999) Gene duplication and multiplicity of collagenases in *Clostridium histolyticum*. *J. Bacteriol.* *181*, 923–933.
- 152 Jung, W.; Winter, H. (1998) Considerations for the Use of Clostridial Collagenase in Clinical Practice. *Clin. Drug Invest.* *15*, 245–252. DOI: 10.2165/00044011-199815030-00009.
- 153 Eckhard, U.; Huesgen, P. F.; Brandstetter, H.; Overall, C. M. (2014) Proteomic protease specificity profiling of clostridial collagenases reveals their intrinsic nature as dedicated degraders of collagen. *J. Proteomics.* *100*, 102–114. DOI: 10.1016/j.jprot.2013.10.004.
- 154 Ramshaw, J. A.; Shah, N. K.; Brodsky, B. (1998) Gly-X-Y tripeptide frequencies in collagen. A context for host-guest triple-helical peptides. *J. Struct. Biol.* *122*, 86–91. DOI: 10.1006/jsbi.1998.3977.

- 155 Duarte, A. S.; Correia, A.; Esteves, A. C. (2016) Bacterial collagenases - A review. *Crit. Rev. Microbiol.* *42*, 106–126. DOI: 10.3109/1040841X.2014.904270.
- 156 Jung, C. M.; Matsushita, O.; Katayama, S.; Minami, J.; Sakurai, J.; Okabe, A. (1999) Identification of metal ligands in the Clostridium histolyticum ColH collagenase. *J. Bacteriol.* *181*, 2816–2822.
- 157 Matsushita, O.; Jung, C. M.; Minami, J.; Katayama, S.; Nishi, N.; Okabe, A. (1998) A study of the collagen-binding domain of a 116-kDa Clostridium histolyticum collagenase. *J. Biol. Chem.* *273*, 3643–3648.
- 158 Eckhard, U.; Schönauer, E.; Brandstetter, H. (2013) Structural basis for activity regulation and substrate preference of clostridial collagenases G, H, and T. *J. Biol. Chem.* *288*, 20184–20194. DOI: 10.1074/jbc.M112.448548.
- 159 Eckhard, U.; Schönauer, E.; Nüss, D.; Brandstetter, H. (2011) Structure of collagenase G reveals a chew-and-digest mechanism of bacterial collagenolysis. *Nat. Struct. Mol. Biol.* *18*, 1109–1114. DOI: 10.1038/nsmb.2127.
- 160 Eckhard, U.; Schönauer, E.; Ducka, P.; Briza, P.; Nüss, D.; Brandstetter, H. (2009) Biochemical characterization of the catalytic domains of three different Clostridial collagenases. *Biol. Chem.* *390*, 11–18. DOI: 10.1515/BC.2009.004.
- 161 Hurst, L. C.; Badalamente, M. A.; Hentz, V. R.; Hotchkiss, R. N.; Kaplan, F. T. D.; Meals, R. A.; Smith, T. M.; Rodzvilla, J. (2009) Injectable collagenase clostridium histolyticum for Dupuytren's contracture. *N. Engl. J. Med.* *361*, 968–979. DOI: 10.1056/NEJMoa0810866.
- 162 Murrell, G. A.; Francis, M. J.; Bromley, L. (1991) The collagen changes of Dupuytren's contracture. *J. Hand Surg. Br.* *16*, 263–266.
- 163 Dhillon, S. (2015) Collagenase Clostridium Histolyticum. A Review in Peyronie's Disease. *Drugs.* *75*, 1405–1412. DOI: 10.1007/s40265-015-0441-7.
- 164 Shi, L.; Carson, D. (2009) Collagenase Santyl ointment. A selective agent for wound debridement. *J. Wound Ostomy Continence Nurs.* *36*, S12-6. DOI: 10.1097/WON.0b013e3181bfdd1a.
- 165 Breite, A. G.; McCarthy, R. C.; Dwulet, F. E. (2011) Characterization and functional assessment of Clostridium histolyticum class I (C1) collagenases and the synergistic degradation of native collagen in enzyme mixtures containing class II (C2) collagenase. *Transplant. Proc.* *43*, 3171–3175. DOI: 10.1016/j.transproceed.2011.09.059.
- 166 Yiotakis, A.; Hatgiyannacou, A.; Dive, V.; Toma, F. (1988) New thiol inhibitors of Clostridium histolyticum collagenase. Importance of the P3' position. *Eur. J. Biochem.* *172*, 761–766.
- 167 Galardy, R. E.; Grobelny, D. (1983) Inhibition of collagenase from Clostridium histolyticum by phosphoric and phosphonic amides. *Biochemistry.* *22*, 4556–4561.
- 168 Dive, V.; Yiotakis, A.; Nicolaou, A.; Toma, F. (1990) Inhibition of Clostridium histolyticum collagenases by phosphonamide peptide inhibitors. *Eur. J. Biochem.* *191*, 685–693.
- 169 Grobelny, D.; Galardy, R. E. (1985) Aldehyde and ketone substrate analogues inhibit the collagenase of Clostridium histolyticum. *Biochemistry.* *24*, 6145–6152.
- 170 Angleton, E. L.; van Wart, H. E. (2002) Preparation and reconstitution with divalent metal ions of class I and class II Clostridium histolyticum apocollagenases. *Biochemistry.* *27*, 7406–7412. DOI: 10.1021/bi00419a035.
- 171 Oshima, N.; Narukawa, Y.; Takeda, T.; Kiuchi, F. (2013) Collagenase inhibitors from Viola yedoensis. *J. Nat. Med.* *67*, 240–245. DOI: 10.1007/s11418-012-0665-8.
- 172 Supuran, C. T.; Scozzafava, A. (2000) Protease inhibitors. Part 7. Inhibition of Clostridium histolyticum collagenase with sulfonylated derivatives of L-valine hydroxamate. *Eur. J. Pharm. Sci.* *10*, 67–76.
- 173 Scozzafava, A.; Supuran, C. T. (2000) Protease inhibitors - part 5. Alkyl/arylsulfonyl- and arylsulfonylureido-/arylureido- glycine hydroxamate inhibitors of Clostridium histolyticum collagenase. *Eur. J. Med. Chem.* *35*, 299–307.
- 174 Clare, B. W.; Scozzafava, A.; Supuran, C. T. (2001) Protease inhibitors. Synthesis of a series of bacterial collagenase inhibitors of the sulfonyl amino acyl hydroxamate type. *J. Med. Chem.* *44*, 2253–2258.
- 175 Ilies, M.; Banciu, M. D.; Scozzafava, A.; Ilies, M. A.; Caproiu, M. T.; Supuran, C. T. (2003) Protease inhibitors. Synthesis of bacterial collagenase and matrix metalloproteinase inhibitors incorporating arylsulfonylureido and 5-dibenzo-suberenyl/suberyl moieties. *Bioorg. Med. Chem.* *11*, 2227–2239. DOI: 10.1016/S0968-0896(03)00113-5.

- 176 Scozzafava, A.; Supuran, C. T. (2002) Protease inhibitors. Synthesis of matrix metalloproteinase and bacterial collagenase inhibitors incorporating 5-amino-2-mercapto-1,3,4-thiadiazole zinc binding functions. *Bioorg. Med. Chem. Lett.* *12*, 2667–2672.
- 177 Santos, M. A.; Marques, S.; Gil, M.; Tegoni, M.; Scozzafava, A.; Supuran, C. T. (2003) Protease inhibitors. Synthesis of bacterial collagenase and matrix metalloproteinase inhibitors incorporating succinyl hydroxamate and iminodiacetic acid hydroxamate moieties. *J. Enzyme Inhib. Med. Chem.* *18*, 233–242. DOI: 10.1080/1475636031000081134.
- 178 Sbardella, D.; Fasciglione, G. F.; Gioia, M.; Ciaccio, C.; Tundo, G. R.; Marini, S.; Coletta, M. (2012) Human matrix metalloproteinases. An ubiquitous class of enzymes involved in several pathological processes. *Mol. Aspects Med.* *33*, 119–208. DOI: 10.1016/j.mam.2011.10.015.
- 179 Nagase, H.; Visse, R.; Murphy, G. (2006) Structure and function of matrix metalloproteinases and TIMPs. *Cardiovasc. Res.* *69*, 562–573. DOI: 10.1016/j.cardiores.2005.12.002.
- 180 Jobin, P. G.; Butler, G. S.; Overall, C. M. (2017) New intracellular activities of matrix metalloproteinases shine in the moonlight. *Biochim. Biophys. Acta.* *1864*, 2043–2055. DOI: 10.1016/j.bbamcr.2017.05.013.
- 181 Nagase, H.; Woessner, J. F. (1999) Matrix metalloproteinases. *J. Biol. Chem.* *274*, 21491–21494.
- 182 Klein, T.; Bischoff, R. (2011) Physiology and pathophysiology of matrix metalloproteases. *Amino Acids.* *41*, 271–290. DOI: 10.1007/s00726-010-0689-x.
- 183 Roy, R.; Yang, J.; Moses, M. A. (2009) Matrix metalloproteinases as novel biomarkers and potential therapeutic targets in human cancer. *J. Clin. Oncol.* *27*, 5287–5297. DOI: 10.1200/JCO.2009.23.5556.
- 184 Park, H. I.; Jin, Y.; Hurst, D. R.; Monroe, C. A.; Lee, S.; Schwartz, M. A.; Sang, Q.-X. A. (2003) The intermediate S1' pocket of the endometase/matrixlysin-2 active site revealed by enzyme inhibition kinetic studies, protein sequence analyses, and homology modeling. *J. Biol. Chem.* *278*, 51646–51653. DOI: 10.1074/jbc.M310109200.
- 185 Dufour, A.; Overall, C. M. (2013) Missing the target. Matrix metalloproteinase antitargets in inflammation and cancer. *Trends Pharmacol. Sci.* *34*, 233–242. DOI: 10.1016/j.tips.2013.02.004.
- 186 Overall, C. M.; Kleinfeld, O. (2006) Tumour microenvironment - opinion. Validating matrix metalloproteinases as drug targets and anti-targets for cancer therapy. *Nat. Rev. Cancer.* *6*, 227–239. DOI: 10.1038/nrc1821.
- 187 Schönauer, E.; Kany, A. M.; Hauptenthal, J.; Hüsecken, K.; Hoppe, I. J.; Voos, K.; Yahiaoui, S.; Elsässer, B.; Ducho, C.; Brandstetter, H.; Hartmann, R. W. (2017) Discovery of a Potent Inhibitor Class with High Selectivity toward Clostridial Collagenases. *J. Am. Chem. Soc.* *139*, 12696–12703. DOI: 10.1021/jacs.7b06935.
- 188 Kany, A. M.; Sikandar, A.; Hauptenthal, J.; Yahiaoui, S.; Maurer, C. K.; Proschak, E.; Köhnke, J.; Hartmann, R. W. (2018) Binding Mode Characterization and Early in Vivo Evaluation of Fragment-Like Thiols as Inhibitors of the Virulence Factor LasB from *Pseudomonas aeruginosa*. *ACS Infect. Dis.* DOI: 10.1021/acinfecdis.8b00010.
- 189 Congreve, M.; Carr, R.; Murray, C.; Jhoti, H. (2003) A 'rule of three' for fragment-based lead discovery? *Drug Discov. Today.* *8*, 876–877.
- 190 Murray, C. W.; Rees, D. C. (2009) The rise of fragment-based drug discovery. *Nat. Chem.* *1*, 187–192. DOI: 10.1038/nchem.217.
- 191 Albert, A. (1958) Chemical aspects of selective toxicity. *Nature.* *182*, 421–422.
- 192 Stella, V. J.; Charman, W. N.; Naringrekar, V. H. (1985) Prodrugs. Do they have advantages in clinical practice? *Drugs.* *29*, 455–473.
- 193 Jana, S.; Mandlekar, S.; Marathe, P. (2010) Prodrug design to improve pharmacokinetic and drug delivery properties. Challenges to the discovery scientists. *Curr. Med. Chem.* *17*, 3874–3908.
- 194 Pereillo, J.-M.; Maftouh, M.; Andrieu, A.; Uzabiaga, M.-F.; Fedeli, O.; Savi, P.; Pascal, M.; Herbert, J.-M.; Maffrand, J.-P.; Picard, C. (2002) Structure and stereochemistry of the active metabolite of clopidogrel. *Drug Metab. Dispos.* *30*, 1288–1295.
- 195 Matheson, A. J.; Noble, S. (2000) Racecadotril. *Drugs.* *59*, 829-35; discussion 836-7.
- 196 Fériz, J. M.; Vinsová, J. (2010) Prodrug design of phenolic drugs. *Curr. Pharm. Des.* *16*, 2033–2052.
- 197 Ghosh, A. K.; Brindisi, M. (2015) Organic carbamates in drug design and medicinal chemistry. *J. Med. Chem.* *58*, 2895–2940. DOI: 10.1021/jm501371s.
- 198 Pramari, Y.; Das Gupta, V.; Bethea, C. (1992) Stability of captopril in some aqueous systems. *J. Clin. Pharm. Ther.* *17*, 185–189.

- 199 Kirschbaum, J.; Perlman, S. (1984) Analysis of Captopril and Hydrochlorothiazide Combination Tablet Formulations by Liquid Chromatography. *J. Pharm. Sci.* *73*, 686–687. DOI: 10.1002/jps.2600730524.
- 200 Cushman, D. W.; Ondetti, M. A. (1991) History of the design of captopril and related inhibitors of angiotensin converting enzyme. *Hypertension.* *17*, 589–592. DOI: 10.1161/01.HYP.17.4.589.
- 201 Vertes, V.; Haynie, R. (1992) Comparative pharmacokinetics of captopril, enalapril, and quinapril. *Am. J. Cardiol.* *69*, 8C-16C.
- 202 Holland, D. R.; Tronrud, D. E.; Pley, H. W.; Flaherty, K. M.; Stark, W.; Jansonius, J. N.; McKay, D. B.; Matthews, B. W. (1992) Structural comparison suggests that thermolysin and related neutral proteases undergo hinge-bending motion during catalysis. *Biochemistry.* *31*, 11310–11316.
- 203 Bitto, E.; McKay, D. B. (2004) Elastase of *Pseudomonas aeruginosa* with an inhibitor. DOI: 10.2210/pdb1u4g/pdb.
- 204 McKay, D. B.; Overgaard, M. T. (2009) *Pseudomonas aeruginosa* elastase with phosphoramidon. DOI: 10.2210/pdb3dbk/pdb.
- 205 Browner, M. F.; Smith, W. W.; Castelano, A. L. (1995) Matrilysin-inhibitor complexes. Common themes among metalloproteases. *Biochemistry.* *34*, 6602–6610.
- 206 Belviso, B. D.; Caliandro, R.; Siliqi, D.; Calderone, V.; Arnesano, F.; Natile, G. (2013) Structure of matrix metalloproteinase-3 with a platinum-based inhibitor. *Chem. Commun. (Camb).* *49*, 5492–5494. DOI: 10.1039/c3cc41278d.
- 207 Holmes, M. A.; Matthews, B. W. (1981) Binding of hydroxamic acid inhibitors to crystalline thermolysin suggests a pentacoordinate zinc intermediate in catalysis. *Biochemistry.* *20*, 6912–6920.
- 208 Verma, R. P. (2012) Hydroxamic acids as matrix metalloproteinase inhibitors. *EXS.* *103*, 137–176. DOI: 10.1007/978-3-0348-0364-9\_5.
- 209 Dürr, U. H. N.; Sudheendra, U. S.; Ramamoorthy, A. (2006) LL-37, the only human member of the cathelicidin family of antimicrobial peptides. *Biochim. Biophys. Acta.* *1758*, 1408–1425. DOI: 10.1016/j.bbame.2006.03.030.
- 210 Bals, R.; Weiner, D. J.; Meegalla, R. L.; Wilson, J. M. (1999) Transfer of a cathelicidin peptide antibiotic gene restores bacterial killing in a cystic fibrosis xenograft model. *J. Clin. Invest.* *103*, 1113–1117. DOI: 10.1172/JCI6570.
- 211 Chen, C. I.-U.; Schaller-Bals, S.; Paul, K. P.; Wahn, U.; Bals, R. (2004) Beta-defensins and LL-37 in bronchoalveolar lavage fluid of patients with cystic fibrosis. *J. Cyst. Fibros.* *3*, 45–50. DOI: 10.1016/j.jcf.2003.12.008.
- 212 Dosler, S.; Karaaslan, E. (2014) Inhibition and destruction of *Pseudomonas aeruginosa* biofilms by antibiotics and antimicrobial peptides. *Peptides.* *62*, 32–37. DOI: 10.1016/j.peptides.2014.09.021.
- 213 Overhage, J.; Campisano, A.; Bains, M.; Torfs, E. C. W.; Rehm, B. H. A.; Hancock, R. E. W. (2008) Human host defense peptide LL-37 prevents bacterial biofilm formation. *Infect. Immun.* *76*, 4176–4182. DOI: 10.1128/IAI.00318-08.
- 214 Pompilio, A.; Scocchi, M.; Pomponio, S.; Guida, F.; Di Primio, A.; Fiscarelli, E.; Gennaro, R.; Di Bonaventura, G. (2011) Antibacterial and anti-biofilm effects of cathelicidin peptides against pathogens isolated from cystic fibrosis patients. *Peptides.* *32*, 1807–1814. DOI: 10.1016/j.peptides.2011.08.002.
- 215 Thomann, A.; Mello Martins, A. G. G. de; Brengel, C.; Empting, M.; Hartmann, R. W. (2016) Application of Dual Inhibition Concept within Looped Autoregulatory Systems toward Antivirulence Agents against *Pseudomonas aeruginosa* Infections. *ACS Chem. Biol.* *11*, 1279–1286. DOI: 10.1021/acscchembio.6b00117.
- 216 Tehrani, K. H. M. E.; Martin, N. I. (2017) Thiol-Containing Metallo- $\beta$ -Lactamase Inhibitors Resensitize Resistant Gram-Negative Bacteria to Meropenem. *ACS Infect. Dis.* *3*, 711–717. DOI: 10.1021/acsinfectdis.7b00094.
- 217 Klingler, F.-M.; Wichelhaus, T. A.; Frank, D.; Cuesta-Bernal, J.; El-Delik, J.; Müller, H. F.; Sjuts, H.; Göttig, S.; Koenigs, A.; Pos, K. M.; Pogoryelov, D.; Proschak, E. (2015) Approved Drugs Containing Thiols as Inhibitors of Metallo- $\beta$ -lactamases. Strategy To Combat Multidrug-Resistant Bacteria. *J. Med. Chem.* *58*, 3626–3630. DOI: 10.1021/jm501844d.
- 218 Tsai, C. J.-Y.; Loh, J. M. S.; Proft, T. (2016) *Galleria mellonella* infection models for the study of bacterial diseases and for antimicrobial drug testing. *Virulence.* *7*, 214–229. DOI: 10.1080/21505594.2015.1135289.
- 219 Jander, G.; Rahme, L. G.; Ausubel, F. M. (2000) Positive correlation between virulence of *Pseudomonas aeruginosa* mutants in mice and insects. *J. Bacteriol.* *182*, 3843–3845.

- 220 Andrejko, M.; Zdybicka-Barabas, A.; Cytryńska, M. (2014) Diverse effects of *Galleria mellonella* infection with entomopathogenic and clinical strains of *Pseudomonas aeruginosa*. *J. Invertebr. Pathol.* *115*, 14–25. DOI: 10.1016/j.jip.2013.10.006.
- 221 Andrejko, M.; Mizerska-Dudka, M. (2011) Elastase B of *Pseudomonas aeruginosa* stimulates the humoral immune response in the greater wax moth, *Galleria mellonella*. *J. Invertebr. Pathol.* *107*, 16–26. DOI: 10.1016/j.jip.2010.12.015.
- 222 Andrejko, M.; Mizerska-Dudka, M.; Jakubowicz, T. (2009) Antibacterial activity in vivo and in vitro in the hemolymph of *Galleria mellonella* infected with *Pseudomonas aeruginosa*. *Comp. Biochem. Physiol. B.* *152*, 118–123. DOI: 10.1016/j.cbpb.2008.10.008.

## 6 Appendix: Conference Contributions

**Topic: “Development of Novel Inhibitors Targeting Elastase (LasB) from *Pseudomonas aeruginosa*”**

Oral presentations:

Kany, A.M., Haupenthal, J., Eberhard, J., Hartmann R.W. 33<sup>rd</sup> Winter School on Proteinases and Their Inhibitors, February 2016, Tiers, Italy

Kany, A.M., Sikandar, A., de Mello Martins, A.G.G., Haupenthal, J., Köhnke, J., Hartmann R.W. 34<sup>rd</sup> Winter School on Proteinases and Their Inhibitors, March 2017, Tiers, Italy

Poster presentations:

Kany, A.M., Haupenthal, J., Eberhard, J., Hamed, M., Hartmann R.W. 6<sup>th</sup> International HIPS Symposium, June 2016, Saarbrücken, Germany

Kany, A.M., Sikandar, A., de Mello Martins, A.G.G., Eberhard, J., Hamed, M., Haupenthal, J., Köhnke, J., Hartmann, R.W. DPhG Jahrestagung, October 2016, München, Germany

Kany, A.M., Sikandar, A., de Mello Martins, A.G.G., Eberhard, J., Hamed, M., Haupenthal, J., Köhnke, J., Hartmann, R.W. Frontiers in Medicinal Chemistry, February 2017, Bern, Switzerland

**Topic: “Discovery of a Potent Inhibitor Class with High Selectivity towards Clostridial Collagenases”**

Oral presentation:

Schönauer, E.; Kany, A.M.; Haupenthal, J.; Hüsecken, K.; Hoppe, I.J.; Voos, K.; Yahiaoui, S.; Elsässer, B.; Ducho, C.; Brandstetter, H.; Hartmann, R.W. Sommersymposium der Graduiertenschule Naturstoffforschung, August 2017, Saarbrücken, Germany

**Topic: “Development of Inhibitors Targeting Elastase (LasB) from *Pseudomonas aeruginosa* and Collagenase H (ColH) from *Clostridium histolyticum*”**

Poster presentations:

Kany, A.M., Schönauer, E., Sikandar, A., Hauptenthal, J., Maurer, C.K., Yahiaoui, S., Hüsecken, K., Voos, K., Ducho, C., Köhnke, J., Brandstetter, H., Hartmann, R.W. 7<sup>th</sup> International HIPS Symposium, June 2017, Saarbrücken, Germany

Kany, A.M., Schönauer, E., Sikandar, A., Hauptenthal, J., Maurer, C.K., Yahiaoui, S., Hüsecken, K., Hoppe, I.J., Voos, K., Ducho, C., Köhnke, J., Brandstetter, H., Hartmann, R.W. DPhG Jahrestagung, September 2017, Saarbrücken, Germany

Kany, A.M., Schönauer, E., Sikandar, A., Hauptenthal, J., Maurer, C.K., Yahiaoui, S., Hüsecken, K., Hoppe, I.J., Voos, K., Ducho, C., Köhnke, J., Brandstetter, H., Hartmann, R.W. DPhG Doktorandentagung, March 2018, Bad Dürkheim, Germany